

**THE RELATIONSHIP BETWEEN
TROPOSPHERIC OZONE
AND ATMOSPHERIC CIRCULATION
IN TAIWAN**

I-CHIEN LAI

A dissertation submitted for the degree of
Doctor of Philosophy



Climatic Research Unit
School of Environmental Sciences
University of East Anglia

June 2010

© This copy of the thesis has been supplied on condition that anyone who consults it is understood to recognise that its copyright rests with the author and that no quotation from the dissertation, nor any information derived therefrom, may be published without the author's prior, written consent.

Abstract

The aim of the study is to investigate the relationship between variability in tropospheric ozone in Taiwan and the regional atmospheric circulation, paying particular attention to the influence of long-range transport on ozone pollution levels. The study period is 1994 to 2004. The data used in this study include air pollution data from the Taiwan Air Quality Monitoring Network and NCEP/NCAR reanalysis data. The spatial and temporal variations in weather types have been characterised using an objective circulation classification scheme and relationships with episodes of high ozone levels over Taiwan have been determined. The signature of the large-scale atmospheric circulation associated with high ozone pollution and the connection with long-range transport of ozone precursors and ozone have been identified using spatial composites and back-trajectory analysis. Trajectories were calculated using the Hybrid Single-Particle Integrated Trajectory model.

The air pollution data analysis shows that Taiwan experiences a seasonal cycle in ozone levels, with maxima in spring and autumn and a minimum in summer. The spatial composite and back trajectory analyses indicate that long-range transport does play a role in increasing high ozone episodes in Taiwan. A link with the seasonal variation of the monsoon circulations at different times is shown, with a weaker summer monsoon and a stronger winter monsoon circulation associated with enhanced ozone levels over Taiwan. The characteristics of atmospheric circulation for ozone pollution episodes include enhanced north and northeasterly flows, originating from nearby polluted areas and suggest that mainland China, Korea and Japan are source regions of ozone and its precursors for Taiwan. Moreover, the transport pathways at the high level of 2000m show that the southern China is also prominent source region, which is a previously

unidentified distant source of ozone pollution in Taiwan. It is suggested that the increase of ozone pollution in summer found in this study is caused by a weaker summer monsoon circulation in recent years. While it is emphasised that variability in long-range transport is the only factor affecting ozone pollution levels over Taiwan, the influence of global warming on the Asian monsoon circulation and, hence, long-range transport of ozone and its precursors warrants serious consideration.

Acknowledgements

I would like to express my sincere appreciation and thank to Peter Brimblecombe and Mick Kelly for supervising this work throughout the course of this work enabled me to develop an understanding of the subject.

It is a pleasure to thank Ian Harris, Clare Goodess and Phil Jones for giving guidance and advice in the part of this project.

Many thanks to Mike Salmon for providing excellent computing support service and being patient to ameliorate my computer whenever it does not functioning well.

Special thanks to Ching-Wen Huang for helping me on thesis works, support and encouragement throughout my studies at UEA. Grateful appreciation is extended to my former roommates Maribel de la Fuente and Karen Lin provide good company endless hours of entertainment during the course of this work.

I am grateful to Sarah Granich for her kindness and consideration for my health, which is warm support during my study period.

Lastly, thanks to my family, especially to my sister, for putting up with my complaints when times were difficult, and financial support.

Contents

Abstract	ii
Acknowledgements	iv
List of Figures	viii
List of Tables	xv

Chapter 1: Introduction	1
1.1 Tropospheric Ozone Pollution, the Atmospheric Circulation and Taiwan	1
1.2 Aims	5
1.3 Thesis Structure and Contents	6
Chapter 2: Atmospheric Circulation Variability and Tropospheric Ozone Pollution	9
2.1 Introduction	9
2.2 Tropospheric Ozone Variability and Trends	9
2.2.1 The Basic Mechanism of Tropospheric Ozone Formation	9
2.2.2 Trend Analysis	13
2.2.3 Tropospheric Ozone over Taiwan	16
2.3 Local Weather Conditions and the Large-Scale Atmospheric Circulation	22
2.3.1 Local Weather Patterns and the Seasonal Circulation	22
2.3.2 The Large-Scale Atmospheric Circulation and Long-Range Transport	27
2.4 Conclusion	33
Chapter 3: Project Design, Data and Statistical Methods	35
3.1 Introduction	35
3.2 Project Design	35
3.3 Air Pollution Data	41
3.3.1 Data Source	41
3.3.2 Quality Control	42
3.3.3 The Definition of High Ozone Pollution Indices	42

3.4	Gridded Observational Atmospheric Circulation Data	46
3.4.1	NCEP/NCAR Reanalysis Data	46
3.4.2	Quality Control	48
3.4.3	Problems and Known Errors	49
3.4.4	Inter-Comparisons	50
3.4.5	Diagnostic Variables	54
3.5	Objective Circulation Classification Scheme	55
3.5.1	Introduction	55
3.5.2	Methodology	57
3.6	Back Trajectory Analysis	63
3.7	Spatial Compositing	68
Chapter 4: Observed Annual and Seasonal Trends of Ozone		72
4.1	Introduction	72
4.2	Annual Trend of Ozone Pollution	72
4.2.1	Selection of High Ozone Episodes and High Pollution Zones	72
4.2.2	Annual Distribution of High Ozone Episodes	73
4.2.3	Annual Trend in Five High Ozone Pollution Zones	77
4.3	Seasonal Distribution of High Ozone Days (HOD)	81
4.3.1	The Possible Effect of ENSO on Tropospheric Ozone Seasonal Distribution	85
4.4	Conclusions	91
Chapter 5: The Objective Scheme of Circulation Types and Circulation-Ozone Links		93
5.1	Introduction	93
5.2	Frequency and Climatological Analysis	93
5.2.1	Long-Term Trend Analysis in Circulation Type	99
5.2.2	Seasonal Characteristics of Sea Level Pressure Circulation Types Composites	103
5.3	Relationships between Ozone Pollution and Circulation Weather Types	117

5.3.1	Frequency Analysis of Ozone Pollution Circulation Types	118
5.3.2	Evaluation of Ozone Pollution and Circulation Types Relationship	123
5.3.3	Discussion	132
5.4	The Analysis of Large-Scale Atmospheric Circulation Links with HOD ₃	134
5.5	Summary	143
Chapter 6: Trajectory Analysis		145
6.1	Introduction	145
6.2	Back Trajectory Analysis	145
6.3	Framework for Long-Range Transport	169
6.4	Summary	174
6.5	Conclusion	175
Chapter 7: Conclusions		177
7.1	Introduction	177
7.2	Summary of Findings	178
7.3	Limitations of the Study	180
7.4	Recommendations for Further Research	182
7.5	Wider Implications	184
References		185
Appendix		

List of Figures

Figure 1.1	Geographical location of Taiwan in East/Southeast Asia.	3
Figure 2.1	Ozone isopleth plot, contour plot of maximum ozone concentrations based on initial of VOC and NO _x concentration.	12
Figure 2.2	Long-term evolution of ozone at the mid-latitudes of the Northern Hemisphere	15
Figure 2.3	Severn air quality zones of monitoring network system in Taiwan.	17
Figure 2.4	Air monitoring network stations distribution map in Taiwan.	18
Figure 2.5	Example of high ozone episodes in April, thick line is the air quality standard of 8-hour average in Taiwan.	21
Figure 2.6	Percentages of hourly ozone concentration over 8-hour average standard in Taiwan area.	21
Figure 2.7	Seasonal variation of ozone concentration in North and South cities.	24
Figure 2.8	Mean Geopotential Height at 850hpa for 1948 to 2006 during Spring (A) and Autumn (B). The green circle is the location of Taiwan.	25
Figure 2.9	Depiction of local scale and large-scale. Dotted-line rectangle shows local scale, and solid-line rectangle represents the regional scale.	27
Figure 3.1	A schematic research framework.	40
Figure 3.2	Frequency of high ozone episodes (HOEs) in the 22 districts of Taiwan, geographical information of 22 districts sees Figure 2.4.	44
Figure 3.3	The distribution of 53 air monitoring network stations used in this study	45

Figure 3.4	Grid used in the objective circulation-typing scheme (Local Area).	58
Figure 3.5	Grid used in the objective circulation-typing scheme (Regional Area).	58
Figure 4.1	The trend of high ozone days (HOD), based on the 53 station network, from 1994-2004.	74
Figure 4.2	The annual trend of HOD_3 (days). The solid line is associated trend line between 1994 and 2004 obtained by the least-square regression method, and the dashed lines are the trend lines with upper and lower 95% confidence interval. The open circle indicates high ozone days in year 2000, and the diamonds indicate high ozone days of years.	76
Figure 4.3	The annual trend of HOD in five high ozone pollution zones from 1994-2004.	79
Figure 4.4	The annual mean of ozone concentrations in five zones from 1994-2004.	79
Figure 4.5	Seasonal distribution of HOD in five high ozone pollution zones.	83
Figure 4.6	HOD climatology for winter (thin green line), spring (thick red line), summer (thin red line) and autumn (thick green line) for the period 1994-2004.	83
Figure 4.7	Monthly trend of HOD for four seasons (a) winter, (b) spring, (c) summer and (d) autumn for the period 1994-2004.	84
Figure 4.8	Monthly HOD distribution and SST anomaly over Niño 3.4 region (120w-170w, 5N-5S) for the period of 1994 to 2004. The red line presents warm phase of ENSO, the blue line presents cold phase of ENSO and the green line presents normal phase. The triangle indicates strong El Niño period and open triangles indicate strong La Niña. The star symbols show the period with positive correlation between HOD and ENSO. The open circles indicate high ozone days in spring over study period.	87

Figure 5.1	Mean monthly percentage frequency (%days) of the 14 circulation types for each month of two periods 1958-2004 and 1994-2004. (a) and (b) represent local scale and (c) and (d) represent regional scale.	96
Figure 5.2	Annual frequencies of NE, S and SW circulation types for the period 1958-2004, (a) local scale, and (b) regional scale.	102
Figure 5.3	Mean seasonal SLP (hPa) for the regional window for the period 1958-2004.	103
Figure 5.4	(a) Seasonal mean sea level pressure (hPa) map for the representative circulation types in winter.	105
Figure 5.5	(b) Seasonal mean sea level pressure (hPa) map for the representative circulation types in spring.	107
Figure 5.6	(c) Seasonal mean sea level pressure (hPa) map for the representative circulation types in summer	109
Figure 5.7	(d) Seasonal mean sea level pressure (hPa) map for the representative circulation types in autumn.	111
Figure 5.8	Seasonal mean sea level pressure (hPa) map of selected days for fourteen circulation types at the local scale.	113
Figure 5.9	Seasonal mean sea level pressure (hPa) map of selected days for fourteen circulation types at the regional scale.	115
Figure 5.10	The mean annual frequency (shown as the percentage of all days) of thirteen circulation types and twelve circulation types (solid bar), for the local and regional scale, respectively; and their relation with the annual frequency of ozone pollution days (shown as the percentage of total annual HOD3) for ozone pollution days (P), the day prior to the ozone pollution day (P-1 Day), and the two days prior to the ozone pollution days of both scales.	120

Figure 5.11	The mean seasonal frequency (shown as the percentage of all days) of twelve circulation types (solid bar); and their relation with the seasonal frequency of ozone pollution days (shown as the percentage of total seasonal HOD3) for pollution days (P), the day prior to the ozone pollution day (P-1 Day), and the two days prior to the ozone pollution days at the local scale.	121
Figure 5.12	The mean seasonal frequency (shown as the percentage of all days) of thirteen circulation types (solid bar); and their relation with the seasonal frequency of ozone pollution days (shown as the percentage of total seasonal HOD3) for pollution days (P), the day prior to the ozone pollution day (P-1 Day), and the two days prior to the ozone pollution days at the regional scale.	122
Figure 5.13	Standardised ratios $PROP_{ct}/PROP_{tot}$ of year for ozone days (P-Day, P-1 Day and P-2 Day) at the local and regional scale.	127
Figure 5.14	Standardised ratios $PROP_{ct}/PROP_{tot}$ for spring, summer and autumn for ozone days (P-Day, P-1 Day and P-2 Day) at the local scale.	128
Figure 5.15	Standardised ratios $PROP_{ct}/PROP_{tot}$ for spring, summer and autumn for ozone days (P-Day, P-1 Day and P-2 Day) at the regional scale.	129
Figure 5.16	Seasonal mean sea level pressure (hPa) map of selected circulation types for ozone days at both local and regional scales.	130
Figure 5.17	High ozone pollution (left) and Non-pollution (right) days average geopotential height at 850hPa (a) and SLP (hPa) (b) absolute (upper) and anomalies (lower) values for April. Anomalies significant at the 5% level are shaded.	137
Figure 5.18	High ozone pollution (left) and Non-pollution (right) days average geopotential height at 850hPa (a) and SLP (hPa) (b) absolute (upper) and anomalies (lower) values for May. Anomalies significant at the 5% level are shaded.	138

Figure 5.19	High ozone pollution (left) and Non-pollution (right) days average geopotential height at 850hPa (a) and SLP (hPa) (b) absolute (upper) and anomalies (lower) values for June. Anomalies significant at the 5% level are shaded.	139
Figure 5.20	High ozone pollution (left) and Non-pollution (right) days average geopotential height at 850hPa (a) and SLP (hPa) (b) absolute (upper) and anomalies (lower) values for September. Anomalies significant at the 5% level are shaded.	140
Figure 5.21	High ozone pollution (left) and Non-pollution (right) days average geopotential height at 850hPa (a) and SLP (hPa) (b) absolute (upper) and anomalies (lower) values for October. Anomalies significant at the 5% level are shaded.	141
Figure 5.22	High ozone pollution (left) and Non-pollution (right) days average geopotential height at 850hPa (a) and SLP (hPa) (b) absolute (upper) and anomalies (lower) values for November. Anomalies significant at the 5% level are shaded	142
Figure 6.1	(a) Three-day trajectories in April, North site on left column and South site on right column, at the level 100m, 500m and 2000m.	147
Figure 6.1	(b) Three-day trajectories in May, North site on left column and South site on right column, at the level 100m, 500m and 2000m.	148

Figure 6.1	(c) Three-day trajectories in June, North site on left column and South site on right column, at the level 100m, 500m and 2000m.	149
Figure 6.1	(d) Three-day trajectories in September, North site on left column and South site on right column, at the level 100m, 500m and 2000m.	150
Figure 6.1	(e) Three-day trajectories in October, North site on left column and South site on right column, at the level 100m, 500m and 2000m.	151
Figure 6.1	(f) Three-day trajectories in November, North site on left column and South site on right column, at the level 100m, 500m and 2000m.	152
Figure 6.2	The difference of back trajectories at the north and south sites.	153
Figure 6.3	(a) Three-day back trajectories in April, Pollution days on left column and Non-pollution days on right column, at the level 100m, 500m and 2000m, for the north site.	157
Figure 6.3	(b) Three-day back trajectories in May, Pollution days on left column and Non-pollution days on right column, at the level 100m, 500m and 2000m, for the north site.	158
Figure 6.3	(c) Three-day back trajectories in June, Pollution days on left column and Non-pollution days on right column, at the level 100m, 500m and 2000m, for the north site.	159
Figure 6.3	(d) Three-day back trajectories in September, Pollution days on left column and Non-pollution days on right column, at the level 100m, 500m and 2000m, for the north site.	160
Figure 6.3	(e) Three-day back trajectories in October, Pollution days on left column and Non-pollution days on right column, at the level 100m, 500m and 2000m, for the north site.	161

Figure 6.3	(f) Three-day back trajectories in November, Pollution days on left column and Non-pollution days on right column, at the level 100m, 500m and 2000m, for the north site.	162
Figure 6.4	(a) Three-day back trajectories in April, Pollution days on left column and Non-pollution days on right column, at the level 100m, 500m and 2000m, for the south site.	163
Figure 6.4	(b) Three-day back trajectories in May, Pollution days on left column and Non-pollution days on right column, at the level 100m, 500m and 2000m, for the south site.	164
Figure 6.4	(c) Three-day back trajectories in June, Pollution days on left column and Non-pollution days on right column, at the level 100m, 500m and 2000m, for the south site.	165
Figure 6.4	(d) Three-day back trajectories in September, Pollution days on left column and Non-pollution days on right column, at the level 100m, 500m and 2000m, for the south site.	166
Figure 6.4	(e) Three-day back trajectories in October, Pollution days on left column and Non-pollution days on right column, at the level 100m, 500m and 2000m, for the south site.	167
Figure 6.4	(f) Three-day back trajectories in November, Pollution days on left column and Non-pollution days on right column, at the level 100m, 500m and 2000m, for the south site.	168

List of Tables

Table 3.1	Air quality standards for various countries: definition of high ozone episodes.	44
Table 3.2	The 27 weather types from Lamb's weather category.	62
Table 3.3	The 14 weather types from Lamb's weather category.	62
Table 3.4	The implementation of HYSPLIT_4	66
Table 3.5	The population and sample size for non-pollution days' selection in high ozone pollution months for the period 1994-2004.	69
Table 3.6	Summary of Research Design.	71
Table 4.1	The statistical result of HOEs, HOD and HOD ₃ from 53 network stations for the period 1994-2004. The fifth row is high ozone day (HOD) occurrence frequency of per year.	73
Table 4.2	The trend line slope, standard errors (SEs), and coefficient of determination (R ²) estimated using linear regression for high ozone days (HOD) from 1994 to 2004.	78
Table 4.3	The trend line slope, standard errors (SEs), and coefficient of determination (R ²) estimated using linear regression for annual average ozone concentrations from 1994 to 2004.	78
Table 4.4	Significant Pearson correlation coefficients (at the 95% confidence interval level) identified between ENSO and high ozone days for three episodes.	87
Table 5.1	Mean annual and seasonal circulation type frequencies (%days) for the periods 1958-2004 at the local and regional scales.	97

Table 5.2	Mean annual and seasonal circulation type frequencies (%days) for the periods 1958-2004 at the local and regional scales.	98
Table 5.3	The direction of long-term trends of fourteen circulation types for the period 1958-2004 at the local scale.	100
Table 5.4	The direction of long-term trends of fourteen circulation types for the period 1958-2004 at the regional scale.	101
Table 5.5	The distribution of ozone pollution days (P), the day prior to the ozone pollution day (P-1 Day), and the two days prior to the ozone pollution days under thirteen circulation-type at both scales.	117

Chapter 1: Introduction

1.1 Tropospheric ozone pollution, the atmospheric circulation and Taiwan

The subject of this study is the relationship between the atmospheric circulation and tropospheric ozone concentrations over Taiwan (Republic of China). In this chapter, the key issues and the content of the thesis are introduced.

Tropospheric ozone, which is the most important oxidant in the atmosphere, is formed through *in-situ* photochemical reactions involving nitrogen oxides and volatile organic compounds (Crutzen, 1974; Brimblecombe, 1996; Finlayson-Pitts and Pitts, 2000; Wayne, 2000). Enhanced levels of tropospheric ozone are a serious concern because of effects on human health, (Burnett *et al.*, 1997; Tsai *et al.*, 2003a, b; WHO, 2003; Lee *et al.*, 2006) crops, ecosystems, building materials (Brimblecombe, 1996; Aunan *et al.*, 2000; Krupa *et al.*, 2001; Penkett *et al.*, 2003; Wang and Mauzerall, 2004) and, hence, the economy (Holland and King, 1998; Holland *et al.*, 2002; Reilly *et al.*, 2004, 2007; Ashmore, 2005).

For example, numerous epidemiological studies have verified that extreme tropospheric ozone concentrations affect human mortality and respiratory morbidity in Europe and North America (Burnett, *et al.*, 1997; WHO, 2003; Bell *et al.*, 2006). In East Asia, the investigation of adverse health effects shows an association with cardiovascular diseases and asthma (Chang, *et al.*, 2005; Zhang, *et al.*, 2006). The damage to agricultural crops

is a critical issue for Asia where there is high economic dependence upon agriculture and a more rapidly increasing population than other regions of the world. According to Wang and Mauzerall (2004), the economic cost of grain loss related to tropospheric ozone was about US\$1.2 billion in 1990 and could rise to US\$1.6 billion in 2020 for Japan. With a similar sectoral composition of GDP to Japan, adjusting for the difference in GDP, Taiwan might expect losses of US\$25 million by 2020 according to these results.

A widespread increase in tropospheric ozone concentrations has been observed over the Northern Hemisphere over the past few decades (Logan, 1985; Bojkov, 1986; Bojkov *et al.*, 1994; Low *et al.*, 1990, 1992; Sunwoo *et al.*, 1994; Nolle *et al.*, 2002, 2005; Carslaw, 2005). Observations of tropospheric ozone concentrations over Europe and North America show no significant response to decreasing emissions of primary pollutants after the mid-1980s (Guicherit and Roemer, 2000). Further analysis by Fiala *et al.* (2003) shows tropospheric ozone concentrations frequently exceed the information threshold value ($180\mu\text{g}/\text{m}^3$) of the ozone directive in Europe over the period 1995-2002, even though the main precursors, nitrogen oxides (NOx) and non-methane volatile organic compounds, have reduced by about 30% during the 1990s.

For Europe and North America, the effect of ambient average levels of tropospheric ozone has moderated since the 1990s, as efficient emission control of the main precursors; therefore, the concern of tropospheric ozone is focusing on frequently occurrence of extreme ozone concentrations in recently. Trends in ambient average levels, however, for Asia (e.g. China, Japan, South Korea and Taiwan) are still on the increase. For example, both NOx emissions at $3.9\% \text{ y}^{-1}$ and ozone concentrations at $2.5\% \text{ y}^{-1}$ have risen over the period 1989-1997 (Guicherit and Roemer, 2000). The

growth in NO_x emissions is moving from North America and Europe to Asia (Prather *et al.*, 2001). With the rapid economic development of China and India, predictions of tropospheric chemistry models suggest large increases of tropospheric ozone concentrations over Asia in the near future (Lelieveld and Dentener, 2000; Brasseur *et al.*, 2001; Prather *et al.*, 2001; Dentener *et al.*, 2005). Tropospheric ozone pollution is an important issue for Asia countries now and increasingly in the future.

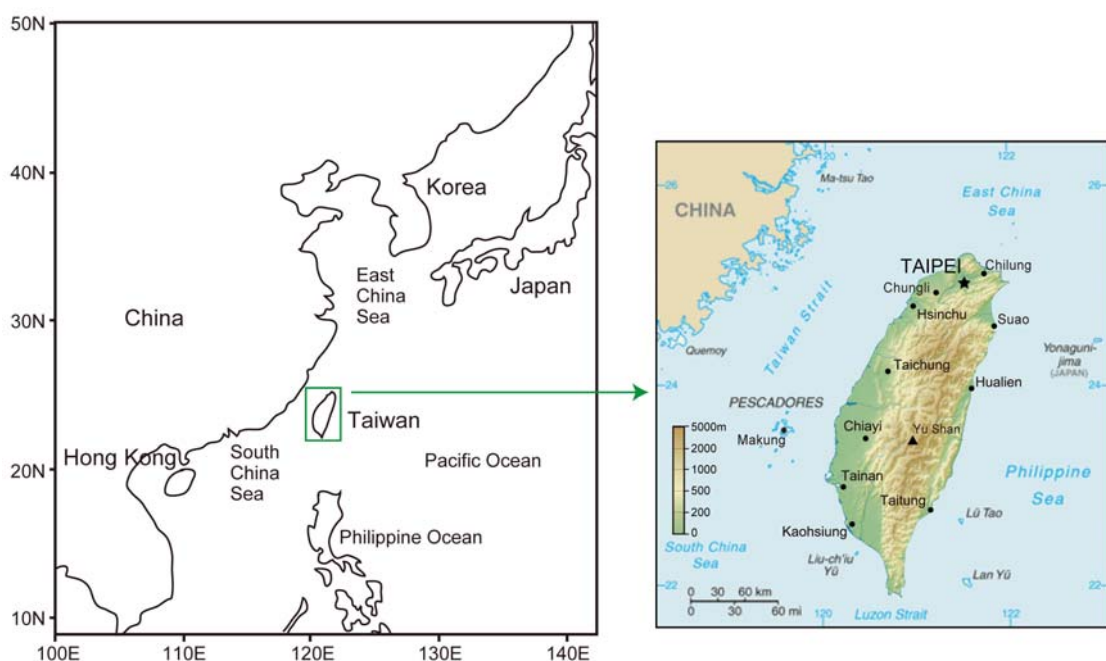


Figure 1.1: Geographical location of Taiwan in Southeast/East Asia.

(Source: Central Intelligence Agency, 2010)

Taiwan is an archipelago in East Asia (Figure 1.1). The position of Taiwan is between 21.3'50"°N and 25.8'20"°N and between 120.1'00"°E and 121.9'15"°E. The islands lie in the west of the Pacific Ocean and the east of China; Japan, South Korea and the East China Sea are located in the north of Taiwan, South China Sea, Philippine Sea and Philippines are in the south. The countries in the neighbourhood of Taiwan include: Japan, South Korea, China and Philippines. According to the Human Development

report (UNDP, 2009), Japan and South Korea are classified as developed countries, and China and Philippines are developing countries. The development of economy for these countries is based on various industries, such as electronics, automobile, textiles and food processing. One of these countries, China, is a rapid growth industrial country.

Taiwan is bounded on the east by the Pacific Ocean and is located along the southeast coast of the Asian continent; the climate is generally oceanic and greatly affected by the Eurasian continent, Pacific Ocean circulation. In addition, local topography features are also influenced the climate in Taiwan. For instance, the most important topographic feature, which can affect the movement of air masses, is the central range with the maximum height of 3952m. The central range extends from Su-ao in the north to Eluanbi in the south. The interaction between the air masses from the Asian continent and the Pacific Ocean, and the effect of local topography divide the climate in two different zones: subtropical and tropical zones for the north and south Taiwan, respectively. The climatic difference between the north and south Taiwan results in uneven seasonal distribution of precipitation in Taiwan, especially for southern Taiwan, the rainfall generally concentrates on the period from May to June.

In Taiwan, tropospheric ozone is a more recent concern than PM₁₀ since ozone has become the major air pollution standard index (PSI) in 2001. A 2005 air quality and long-term trends analysis study by the Taiwanese Environmental Protection Administration (EPA) concludes that nearly all pollutants show significant reductions in ambient levels over the past decade, resulting from the achievements of air quality control strategies. The exception is ozone, which shows an increasing trend of annual mean concentration, about 38% for the period of 1994-2003 (EPA Taiwan, 2004, 2005). This indicates that more factors than simply precursor concentrations contribute to

ozone trends (Davies *et al.*, 1992; Liu *et al.*, 1994; Lelieveld and Dentener, 2000; Dueas *et al.*, 2002).

Tropospheric ozone has a complicated production mechanism, which involves precursors, chemical processes and meteorological conditions (Finlayson-Pitts and Pitts, 2000; Dueas *et al.*, 2002; Penkett *et al.*, 2003; Snyder and Strawbridge, 2004). This makes it difficult to predict trends based on a single process, such as regulation of a single pollutant. Furthermore, there is observational evidence, for example, that interannual variability in tropospheric ozone concentrations in Europe is associated with atmospheric circulation changes (Low *et al.*, 1990, 1992). In the future, ozone trends may be affected by global warming as this could be a contributing factor in altering the frequency of weather conditions favouring ozone formation (Davies *et al.*, 1987). The link between variability and trends in the atmospheric circulation and tropospheric ozone concentrations has not been examined in depth for Taiwan and is the subject of this thesis.

1.2 Aims

The aim of this project is to investigate the correlation between the occurrence of high ozone pollution days over Taiwan and the regional atmospheric circulation in order to identify mechanisms, such as long-range transport. The differential role of the local and the regional scale circulations for high ozone pollution days is an issue that will be addressed. The long-range transport mechanisms identified in this study might provide the basis for projecting potential effects of global warming on future tropospheric ozone in Taiwan.

Key questions to be considered in the context of the thesis include:

- What characteristics of the regional atmospheric circulation are associated with high ozone pollution days?
- Is there evidence that long-range transport is contributing to high ozone levels over Taiwan?
- Is there any link with the dominant monsoonal circulation of the region?

In addressing these questions, three main analyses are undertaken: (1) a weather type classification scheme is developed for Taiwan and the links between climate and ozone concentrations are determined. (2) Back trajectory analysis is used to identify patterns of long-range transport of precursors or pollutants. (3) As a basis for projecting global warming effects, the role of variability in the monsoonal circulation is considered using pressure anomaly composites.

1.3 Thesis structure and contents

In Chapter 2, a detailed review of the previous studies relevant to this project is described. The content provides background of regional atmospheric circulation influence, local weather conditions and mechanism of tropospheric ozone formation. The long-range intercontinental transport of precursor pollutants over Europe and North America is discussed in this chapter. The overall content of this chapter is to give a scientific background of physical and chemical factors of tropospheric ozone pollution and to identify the issues of this study and for project design.

In Chapter 3, an overall project design and the methodology for this research is developed. The content includes the description of datasets collection and selection, statistical analyses used in this study. Data quality control and limitation issues of observation data sources that include tropospheric ozone concentration data from Taiwanese EPA, NCEP/NCAR reanalysis data. The research methods used to identify the mechanism of long-range transport involve automatic circulation type scheme, spatial compositing and back trajectory model for this project are discussed.

In Chapter 4, the analysis of tropospheric ozone trends in Taiwan based on the network observations of ozone concentration is described. The definition of high ozone pollution events is given including the three processes used to select the indices (HOD_3) of high ozone pollution days employed in this research. The discussion of ozone trend analysis consists of the seasonal and spatial variability and interannual trends result. The selected indices (HOD_3) are used to investigate the features of composite atmospheric pattern and categorised by season.

In Chapter 5, weather type classification based on an automatic scheme is used to investigate the effects of local and regional scale circulation on HOD_3 . The results of the weather type classification are used to depict the frequency of specific weather types during high ozone pollution occurrence and provide long-term weather type frequency information in Taiwan. In this chapter, the results describe the characteristic of the atmospheric circulation patterns, which are linked with pollution days, from both the objective scheme and observational field. Additionally, the important discussion is on the effects from local and regional circulation with seasonal variability as related to the identification of the relationship between large-scale circulation and long-range transport.

In Chapter 6, a supporting investigation of the pollutants/precursors long-range transport in Chapter five is undertaken through back trajectory analysis. The analysis involves two metropolitan cities and three different vertical levels to give the information of airflow pathway for long-range transport and compares these with the features of atmospheric circulation patterns of high ozone pollution. Furthermore, the contrasting, results are compared to clarify pathway discrepancies between non-pollution and pollution days.

In Chapter 7, the focus is to conclude the findings from this study and to assess the weaknesses such as how the methodology presented in this thesis could be improved and further refinement and development of the strengths introduced. Aspects of possible future work to extend this study are also proposed in this chapter.

Chapter 2: Atmospheric Circulation Variability and Tropospheric Ozone Pollution

2.1 Introduction

In this chapter, the role of atmospheric circulation variability in determining levels of tropospheric ozone, especially in terms of long-range transport, is discussed. The literature review considers previous research on Europe and North America and then focuses on the East Asia region, in particular, Taiwan. The understanding that is gained is applied to the project design for the study region in the following chapter.

2.2 Tropospheric Ozone Variability and Trends

2.2.1 The Basic Mechanism of Tropospheric Ozone Formation

Ozone exists both in the stratosphere and the troposphere. About 90% of the total ozone is present in the stratosphere, and this plays an important role in protecting the biosphere on the earth. In contrast, tropospheric ozone causes adverse human health effects (Burnett *et al.*, 1997; Tsai *et al.*, 2003a, b; WHO, 2003; Chang *et al.*, 2005; Lee *et al.*, 2006) and results in crop yield reduction (Aunan *et al.*, 2000; Holland *et al.*, 2002; Reilly *et al.*, 2004, 2007) and damage to forest growth and other aspects of ecosystem health and building materials (Brimblecombe, 1996; Krupa *et al.*, 2001; Penkett *et al.*, 2003; Ashmore, 2005). Additionally, tropospheric ozone is the third most important

greenhouse gas after carbon dioxide and methane (Guicherit and Roemer, 2000; Prather *et al.*, 2001; Ehhalt, 2001); hence, the increasing trend in tropospheric ozone is influencing both the chemical composition of the atmosphere and global climate (Brasseur *et al.*, 2001; Akimoto, 2003).

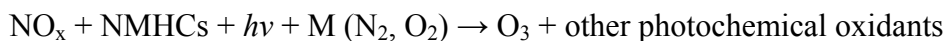
Ozone is a secondary photochemical pollutant (Stern, 1968; Finlayson-Pitts and Pitts, 2000). The main sources of ozone in the troposphere are:

1. incursion from the stratosphere (Oltmans, 1981; Levy II *et al.*, 1985)
2. reactions involving precursors that come from biogenic volatile organic compounds (VOC) (Wayne, 2000); and,
3. photochemical reactions with the precursors, nitrogen oxides ($\text{NO}_x = \text{NO} + \text{NO}_2$), carbon monoxide (CO), methane (CH_4) and other organic compounds resulting from anthropogenic activities.

It was thought that tropospheric ozone largely resulted from the processes of stratosphere-troposphere exchange and organic materials deposition at the Earth's surface. In the early 1950's, Professor Haagen-Smith demonstrated that Los Angeles smog could be formed by ultraviolet irradiation on a mixture of hydrocarbon vapours and nitrogen dioxide in the atmosphere (Stern, 1968). Much research has proved these reactions lead to ozone formation, as well as other co-pollutants (for example, peroxyacetyl nitrates, organic hydroperoxides), under specific meteorological conditions of low humidity, high temperature and strong solar radiation (Stern, 1968).

As far as the photochemistry is concerned, the formation mechanism is influenced by the mixing ratio between all the relevant chemical compounds (for example, precursors and oxidants). Otherwise, an important factor related to ozone formation is solar

radiation with a wavelength range of around 320nm to 410nm (Brimblecombe, 1996; Wayne, 2000). A general process of ozone formation at the boundary layer can be written as follows (Cheng, 2001):



(NMHCs = nonmethane hydrocarbons; $h\nu$ = ultraviolet solar radiation, 320nm~410nm; and other terms have been defined above).

A conversion reaction of NO_x should be noted, involving a catalytic cycle of ozone formation and consumption (Crutzen, 1970, 1974; Milford *et al.*, 1994; Brimblecombe, 1996; Wayne, 2000). The cyclic reactions are as follow:

1. $\text{NO}_2 + h\nu \rightarrow \text{O} + \text{NO}$
2. $\text{O} + \text{O}_2 + M \rightarrow \text{O}_3 + M (M = \text{N}_2, \text{O}_2)$
3. $\text{O}_3 + \text{NO} \rightarrow \text{O}_2 + \text{NO}_2$

An ozone isopleth diagram (Figure 2.1) can illustrate the Non-linear relation between precursors and ozone production. The ozone ridge line in Figure 2.1 is used to identify the maximum ozone concentration that can be achieved at a given VOC level with varying NO_x level. It separates the diagram into two regions: the region above the ridge line as “ NO_x saturated”; that below the ridge line is “ NO_x - limited”. In the NO_x saturated region, NO_x reduction can result in an increase in maximum ozone. For the NO_x - limited region, there is no effect on ozone maximum with large reductions in organics (Seinfeld and Pandis, 1998). The controlling of tropospheric ozone, therefore, is more complicated than only taking action to restrict precursor emission amounts.

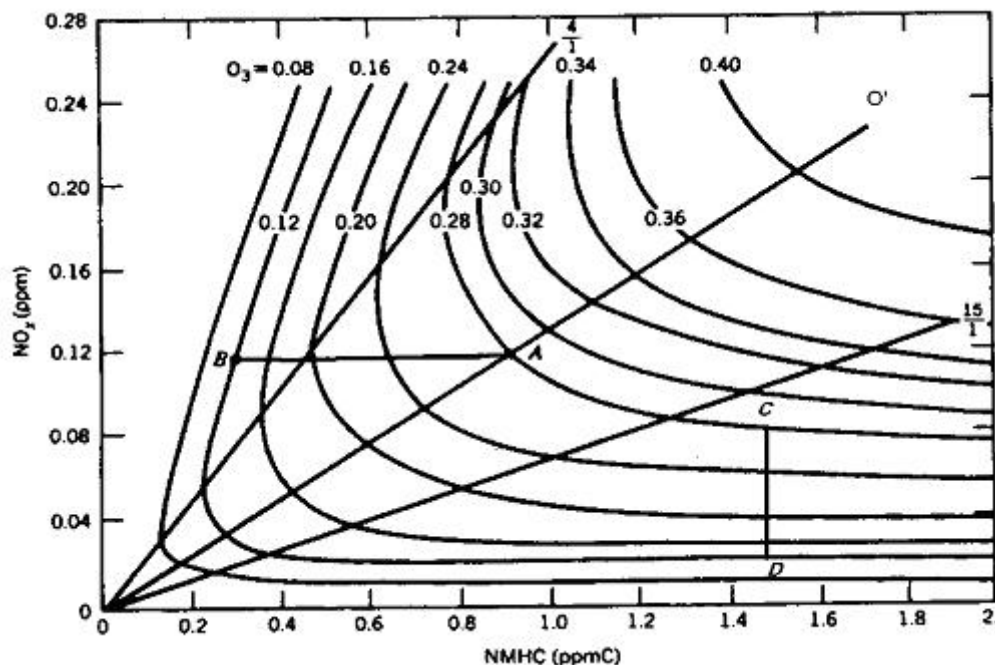


Figure 2.1: Ozone isopleth plot, contour plot of maximum ozone concentrations based on initial of VOC and NO_x concentrations.

(Source: Miflold *et al.*, 1994)

The major physical mechanisms affecting tropospheric ozone formation include local meteorological conditions (such as humidity, temperature, wind speed and direction) (Liu *et al.*, 1994; Seinfeld and Pandis, 1998). For instance, low humidity, low wind speeds, calm weather and cloud-free conditions favour the photochemical reactions. Also important are regional formation mechanisms (for example, large-scale convection) (Luo *et al.*, 2000; Erukhimova and Bowman, 2006) and international and intercontinental long-range transport (associated with frontal systems and large-scale circulation systems) (Penkett *et al.*, 2003). Regional mechanisms and long-range transport, related to ozone formation, become to have an important role in controlling tropospheric ozone (Lelieveld and Dentener, 2000; Brasseur *et al.*, 2001), in particular for those countries which have controlled precursors emission effectively, located in the vicinity with severe pollution. For example, the local sources of primary pollutants are

limited in Taiwan in comparison to many other areas (see Section 2.2.4) but there are a number of substantial source areas within the region. Therefore, the precursors and ozone from the vicinity could bring more serious effects on the air quality of Taiwan than the local sources influence.

2.2.2 Trend Analysis

Historical ozone measurements have been used to identify trends in background ozone concentrations (Bojkov, 1986; Volz and Kley, 1988; Sandroni *et al.*, 1992; Sandroni and Anfossi, 1994; Vingarzan, 2004). World-wide, the trends from observational datasets can be separated into four stages from 1870 to present (Marenco *et al.*, 1994; Guicherit and Roemer, 2000; Vingarzan, 2004). The first period is between 1870 and 1910. During this time, there were more than 300 ozone measurement stations over Europe, North America, Australia and Russia, mostly located in North America and Europe (Bojkov, 1986; Lelieveld *et al.*, 2004; Vingarzan, 2004). Meanwhile, there were some short-term observations in South America and Southeast Asia, (Sandroni and Anfossi, 1994). The second time period is 1930 to 1950. New optical and chemical techniques were used at European locations such as Jungfraujoch (at 3500m in Switzerland) from 1933. The third period is from 1956 to the early 1970s. During this period, there are a number of long-term daily surface ozone records, such as that at Hohenpeissenberg Observatory (Germany) since 1971. As importantly, total ozone measurements were taken from surface stations in this period. The final stage is from 1970 to the present. A number of surface “background” stations (including some of the aforementioned observatories) operated systematically from the beginning of the 1970s, and then satellite data (for example, Total ozone Mapping Spectrometer, TOMS) have

been added to the tropospheric ozone record, resulting in much-improved coverage globally. Although the spatial representativeness of ozone measurement has been improved at higher resolutions in present, the accurate measurement of tropospheric ozone difficulties remain, as the short lifetime of ozone.

The long-term trend analysis of tropospheric ozone observational data, primarily based on European and North American records, indicates a continuous increase at mid-latitudes of the Northern Hemisphere, with a particularly marked rise during the 1970s and early 1980s (Figure 2.2) (Low *et al.*, 1992; Marenco *et al.*, 1994; Vingarzan, 2004; Carslaw, 2005). Changing data quality has been suspected as a contributing factor to the trend due to improvement in techniques. A similar upward trend has been observed in Japan (Lee *et al.*, 1998). The most recent records show that ambient ozone levels over Europe and North America have increased only slightly or not increased at all since the mid-1980s (Fiore *et al.*, 1998; Lee *et al.*, 1998; Guicherit and Roemer, 2000; Fiala *et al.*, 2003). In contrast, trends for Northeast Asia (China, Japan, South Korea and Taiwan) are still notably positive for the period 1989-1997 (Lee *et al.*, 1998; Guicherit and Roemer, 2000). Changing patterns of NO_x emissions, in response, for example, to earlier legislation in Europe and North America, have been held partially responsible for these differing trends (Prather *et al.*, 2001).

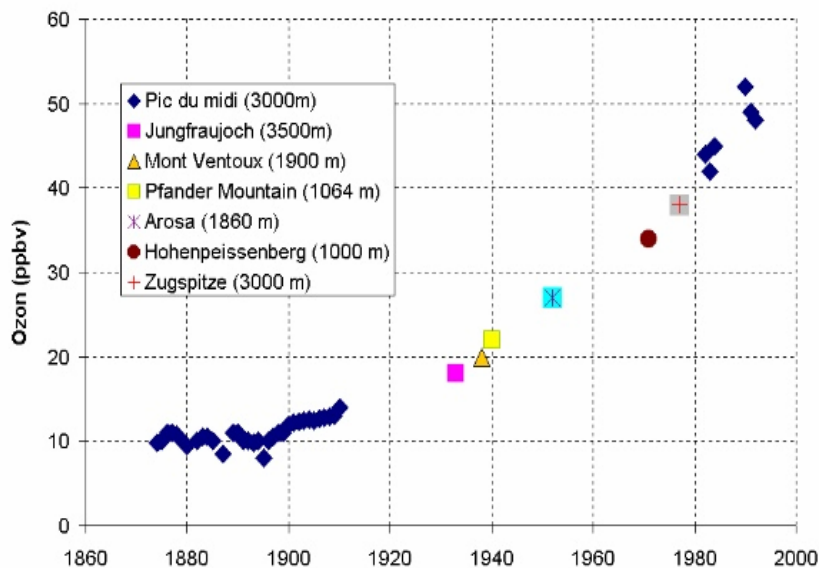


Figure 2.2: Long-term evolution of ozone at the mid-latitudes of the Northern Hemisphere.

(Source: Gros, 2007)

Sources of ozone precursors, such as non-methane hydrocarbons (NMHCs) and nitrogen oxides (NO_x), are predominantly related to fossil fuel consumption. The source categories include motor vehicles, power plants and the petroleum industry (Kley *et al.*, 1994). In parts of the Southern Hemisphere and many tropical areas, ozone formation is also strongly related to biomass burning (Chandra, *et al.*, 2002; Lelieveld *et al.*, 2004). In the developed nations, legislation is limiting future emissions growth (Guicherit and Roemer, 2000; Prather *et al.*, 2001; Fiala *et al.*, 2003), but East Asia is considered to be a major growth region for pollutant sources for coming decades (Wild *et al.*, 2004). For example, China and India have become substantial emitters of pollutants over the past decade due to industrialization, the increase in population growth and related trends such as automobile ownership. East Asia, NO_x emissions for 2020 will be more than double the emissions of 1995 (Street and Waldhoff, 2000; Richter *et al.*, 2005, Ohara *et al.*, 2007).

Multiple three-dimensional chemical transport models (for example, GEOS-CHEM and MOZART) have been developed to simulate tropospheric ozone concentrations based on emissions trends since the 1970s (Brasseur *et al.*, 1998; Hauglustaine *et al.*, 1998). The results can be compared and/or combined with past observation data and used to predict future situation. According to Ehhalt (2001), the simulated results that incorporate limited observations from the late 19th and early 20th centuries suggest that tropospheric ozone has increased from a global mean value¹ of 25 DU to a value of 34 DU. The predictions indicate no marked increase over western Europe and North America over the next few decades but large increases over eastern China, India and Africa as well as Central and South America (Lelieveld and Dentener, 2000; Brasseur *et al.*, 2001; Prather *et al.*, 2001; Stevenson, *et al.*, 2006). The evidence suggests that East Asia will continue to experience an increasing trend in ozone levels, a strong reason to pay greater attention to understanding regional tropospheric ozone variability.

2.2.3 Tropospheric Ozone over Taiwan

In Taiwan, the major air pollutants, which include particulate matter (PM_{10}), sulphur dioxide (SO_2), carbon monoxide (CO), nitrogen oxides (NO_x) and ozone (O_3), have been monitored to assess ambient air quality since 1982 and a systematic monitoring network was established in 1993. Nowadays, the network includes 76 monitoring stations distributed in seven air quality zones (Figures 2.3 and 2.4).

¹ DU: The Dobson Unit 1 DU = $2.687 * 10^{16}$ molecules of O_3 per square centimetre; global mean value 1 DU = 10.9 Tg (O_3) and 1 ppb of tropospheric O_3 = 0.65 DU



Figure 2.3: Seven air quality zones of monitoring network system in Taiwan.

(Source: EPA Taiwan, 2006)

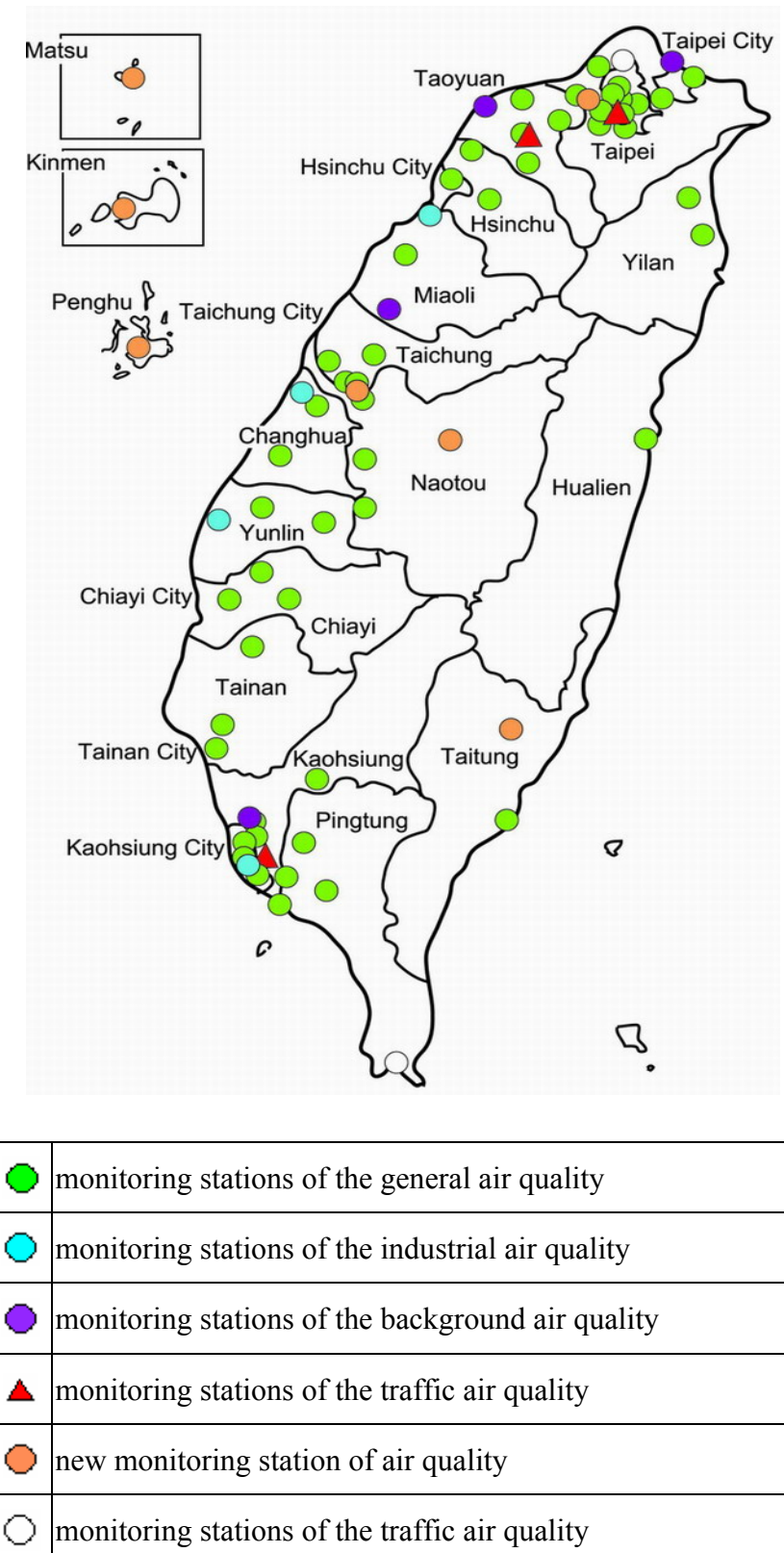


Figure 2.4: Air monitoring network stations distribution map in Taiwan.

(Source: EPA Taiwan, 2006)

It continues to evolve as, for example, stations are re-located due to changing factors (for example, population distribution, sources of pollution, geographical and meteorological features) (EPA Taiwan, 2005). Most stations are installed over the western plain, the most populations' part of Taiwan.

The emission inventory about the turn of the century shows that most PM₁₀ arises from industrial emissions (about 53%). Factory exhaust is the main source for SO₂ (about 86%), and the CO source is mostly vehicles (about 77%). The precursors for ozone formation, NO_x and non-methane hydrocarbons (NMHCs), come mostly from vehicle exhaust (about 60% and 30%, respectively); the other source is industrial emissions (about 40% for NO_x and 46% for NMHCs) (EPA Taiwan, 2004).

A comprehensive analysis, in terms of the Pollution Standard Index (PSI)², indicates that air quality improved during the period 1994 to 2004, though there was a slight increase in ‘unhealthy’ days by about 1.8% in 2004 compared with 2003. Most air pollutants show gradual declines over the period 1994 to 2004, for example, the decreases were 23%, 28%, and 58% for PM₁₀, CO and SO₂, respectively. Nitrogen dioxide also presented a decreased trend of about 23% from 1994-2003. The only exception for this period was ozone, where the trend shows a steady increase totalling

² PSI: a segmented linear function transforms the monitoring concentrations of each pollutant onto a scale from 0 to 500. The transformation value of each pollutant contrasts the influence of human health to convert the secondary indices, and takes the maximum of these secondary indices as the PSI on that day. The index value includes five levels: Level 0~50, 51~100, 101~199, 200~299, over 300 with the influence on health of Good, Moderate, Unhealthy, Very Unhealthy and Hazardous, respectively (EPA Taiwan, 2005).

about 38% in annual mean concentration (8 ppbv). The increase in ozone concentrations has offset the other improvements in Taiwan's air quality for the period of 1994 to 2004 (EPA Taiwan, 2004, 2005). Though lagging behind by about ten years, the analysis of major pollutants trend is similar to the results from Europe and North America over the past few decades (Guicherit and Roemer, 2000; Prather *et al.*, 2001; Fiala *et al.*, 2003). Tropospheric ozone has been substituted for PM₁₀ as the driver of ambient air quality since 2001 (EPA Taiwan, 2005; Chou *et al.*, 2006). This ozone pollution has become the most important issue of air quality control in Taiwan.

Over Taiwan, the seasonal distribution of ozone is characterized by two periods of high concentrations, one is spring and the other one is autumn; the lowest levels occur in summer (EPA Taiwan, 2005). In contrast, ozone concentrations display a summer maximum over the European and North American continents, particularly for rural areas at mid-latitudes. The spring and autumn maxima typical of Taiwan can be observed over the region of East Asia, especially for subtropical areas (Oltmans and Levy II, 1994; Logan, 1985; Wang, *et al.*, 2001). This distinction in seasonal cycle with location is associated with seasonal climatic characteristics, such as the occurrence of high pressure weather types, and the characteristics of the large-scale circulation, which influences tropospheric ozone and precursor transport between continents (Akimoto *et al.*, 1996; Logan *et al.*, 1999; Stohl, 1999; Wild and Akimoto, 2001; Wild *et al.*, 2004). The difference in the characteristics of tropospheric ozone in the Asian region compared with other region underlines the need for greater understanding of regional processes.

In assessing the role of the physical and chemical processes, it is useful to distinguish between slow changes in the mean level of ozone concentrations and the occurrence of

short episodes of greatly elevated concentration, referred to henceforward as high ozone episodes (Figure 2.5). In recent years, the trend over Taiwan is also evident in the changing frequency of high ozone episodes (Figure 2.6). This study focuses on such episodes as the link with prevailing conditions can be clearer in these cases.

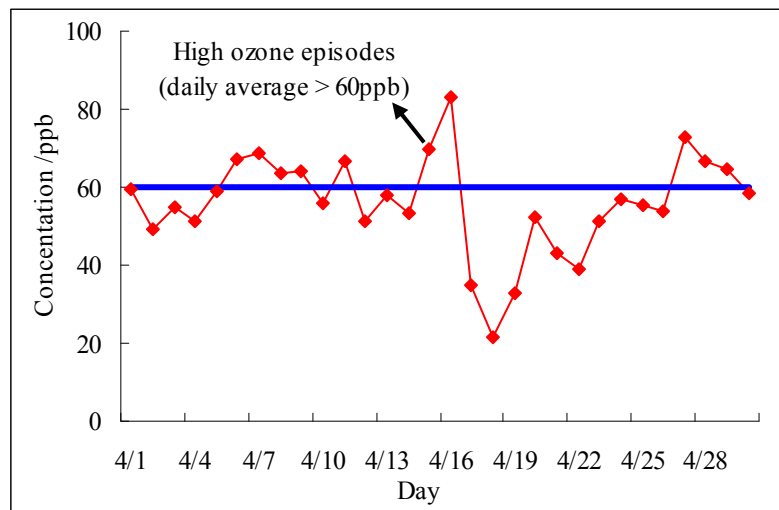


Figure 2.5: Example of high ozone episodes in April, 1999, the thick line is the air quality standard of 8-hour average in Taiwan.

(Data source: EPA Taiwan, 2001)

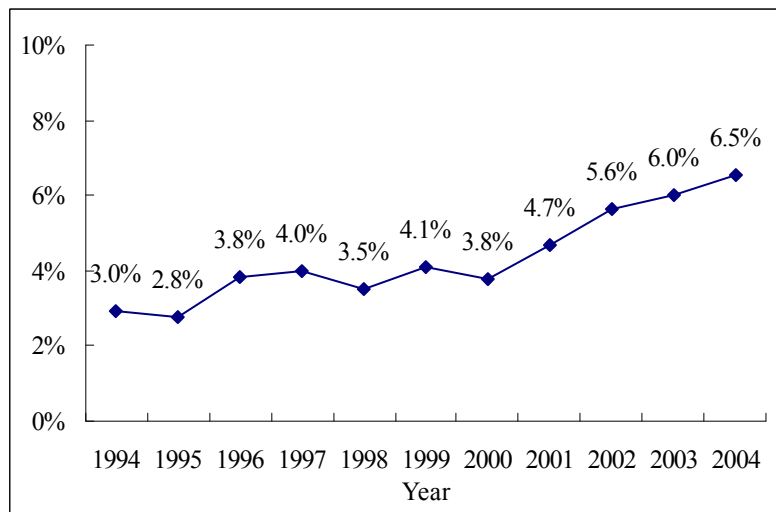


Figure 2.6: Percentages of hourly ozone concentration over 8-hour average standard in Taiwan area.

(Data source: EPA Taiwan, 2005)

2.3 Local Weather Conditions and the Large-Scale Atmospheric Circulation

The interplay between local weather conditions and the large-scale atmospheric circulation is an important mechanism for local and regional tropospheric ozone formation. It relates to the diurnal and seasonal variation of ozone levels. In this section, the effects of local weather conditions, such as the local sea breeze circulation, and the large-scale atmospheric circulation on ozone pollution are discussed.

2.3.1 Local Weather Patterns and the Seasonal Circulation

Much attention has been paid to the relationship between high ozone pollution levels and local weather conditions in previous research, because of the role that various atmospheric parameters play, generally as secondary influences, in ozone formation (see, for example, Liu *et al.*, 1994, 1997, and Cheng, 2001). For Taiwan, observational studies show that important factors include wind speed, the amount and time of precipitation, cloud cover, solar radiation and any local sea breeze circulation connected with topographical features (for example, the basin terrain in Taipei and Taichung and the restriction caused by the central range) (Liu *et al.*, 1994, 1997; Cheng, 2001; Chen *et al.*, 2004). These factors influence, amongst other things, the availability of precursors, pollutant lifetimes and accumulation and dispersal, and the efficiency of photochemical processes (Cheng, 2001).

One of the most influential factors is the land-sea breeze in dispersing or accumulating pollution (Millán *et al.*, 1996; Pont and Fontan, 2000). Because Taiwan is surrounded by the ocean and has pronounced topographical features, the effect of the local sea breeze circulation on pollutant dispersion and accumulation is significant, and correlates with the diurnal variation of tropospheric ozone concentrations (Liu *et al.*, 1994, 1997; Cheng, 2002). The transition period, around 0800-1000 (local time), of the local sea breeze circulation is the key factor for high ozone concentrations. During this period, a weak local circulation and high traffic emissions act with other favourable conditions to enhance ozone formation from precursors. After this transition period, pollutants are accumulated by the sea-to-land circulation in downwind areas, especially in basin terrains, and these show the highest ozone concentrations about midday.

Certain synoptic weather patterns, associated with particular local atmospheric conditions, can be associated with the seasonal variation of tropospheric ozone concentrations, as well as precursor import to Taiwan (Liu *et al.*, 1994, Cheng, 2001). Taiwan is on the boundary between the Eurasian continent and the Pacific Ocean. It is mainly affected by the Siberian cold anticyclone in winter (January, February and December) and by Pacific anticyclones in summer (June, July and August). These two synoptic weather patterns interplay with the local topography and create favourable conditions for tropospheric ozone formation, particularly during the transition periods of the spring (March, April and May) and autumn seasons (September, October and November) (Figure 2.7). During summer, ozone accumulation is limited by the short lifetime of the pollutant under strong incident radiation and, during winter, high wind speeds and the regional circulation result in high dispersal rates (Cheng, 2001; Central Weather Bureau Taiwan, 2006).

Spring weather patterns are generally characterised by stationary synoptic systems and low wind speeds as the winter-time influence of the Siberian anticyclone slowly declines (Figure 2.8 A) (Central Weather Bureau Taiwan, 2006; Tu *et al.*, 2003). These conditions generally favour ozone formation and result in the spring peak in concentrations (Figure 2.7). Later in the season, rain belts form over central or southern mainland China. At this time of year, an increase in the strength of the Pacific anticyclonic influence, or southerly flow with a cyclonic pattern, can relieve ozone pollution in the south of Taiwan. These conditions, though, generate ozone accumulation in the north because of the basin terrain and obstruction by the central mountain range.

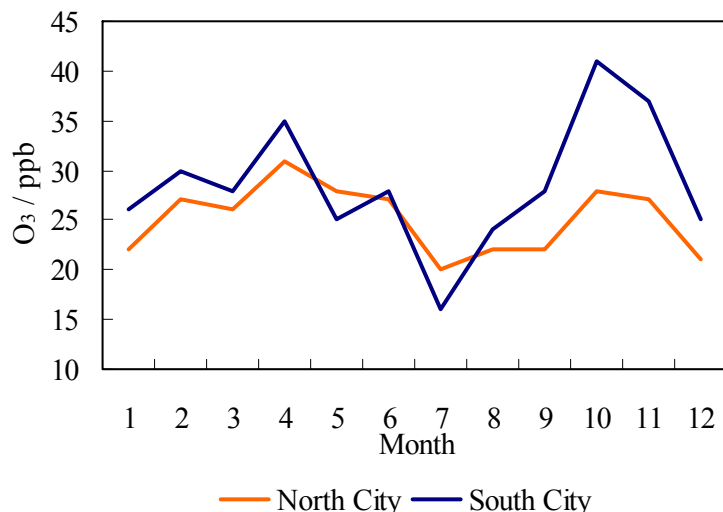
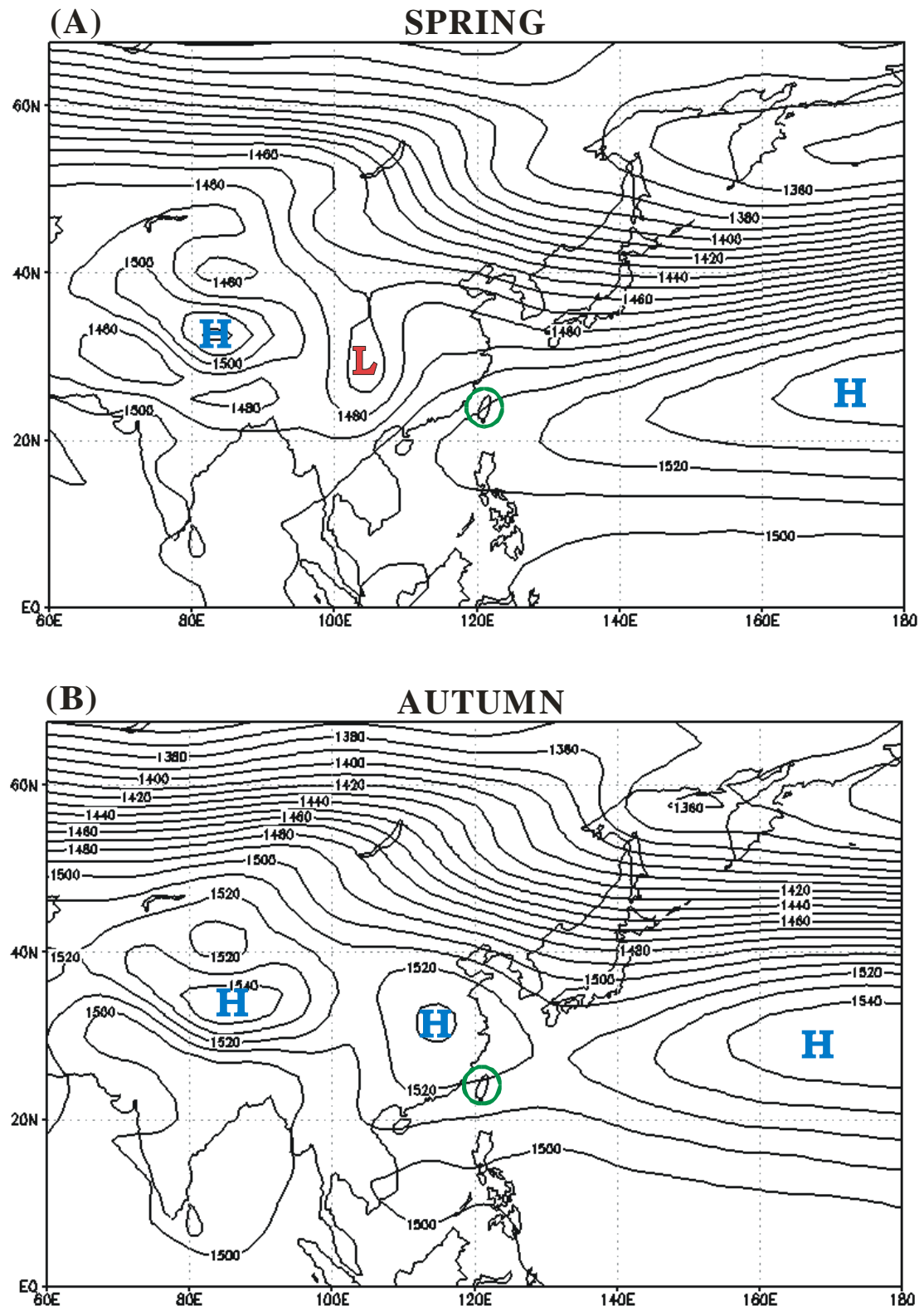


Figure 2.7: Seasonal variation of ozone concentration in North and South cities, grey line is for the north city and black line is for the south city.

(Data source: EPA Taiwan, 2004)



During the autumn months, there is a marked transition period between September and October (Figure 2.8 B). In September, Pacific anticyclones and tropical depressions form the major weather patterns. Siberian anticyclones bring a strong northeast monsoon during October, and these conditions are unfavourable for ozone formation in the north; however, the central and south regions are situated in the lee areas of the central mountain range with low wind speeds and a temperature inversion layer, which provide the opportunity to accumulate pollutants (Cheng, 2001).

Previous studies of the relationship between high ozone pollution episodes and synoptic weather conditions and circulation patterns over Taiwan have shown a clear association (Liu *et al.*, 1997; Cheng 2001; Chen *et al.*, 2004; Wang, 2005; Yu and Chang, 2006). There have been a number of classifications of weather patterns over Taiwan. Lee *et al.* (1998), for example, distinguished 41 weather patterns based on the climatic characteristics for four seasons in Taiwan. Based on these, the 14 synoptic weather patterns associated with high ozone pollution have been subjectively identified (Wu and Chen, 1993). In general, most of these weather patterns are associated with high pressure systems, which are in agreement with other investigations in Europe and North America (Comrie, 1994; Pont and Fontan, 2000; Dueas *et al.*, 2002), and accompanied by northeasterly flow towards Taiwan during the transition seasons.

While a considerable amount of research has been undertaken in recent years on the link between high ozone episodes and local prevailing meteorological conditions over Taiwan, less attention has been paid to the broader context in terms of the large-scale (regional) atmospheric circulation and the long-range transport of pollutants. The local scale meteorology is generally defined as meteorological conditions occurring within

the range from around 5 kilometres to several hundred kilometres horizontal dimensions; and the range for the large-scale is more about 1000 kilometres (Figure 2.9).

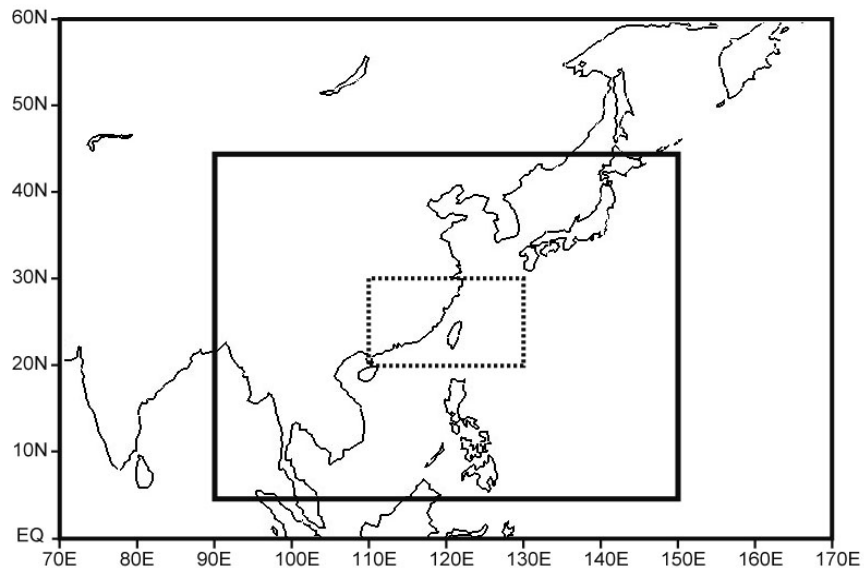


Figure 2.9: Depiction of local scale and large-scale. Dotted-line rectangle shows local scale, and solid-line rectangle represents the regional scale as defined in this study.

2.3.2 The Large-Scale Atmospheric Circulation and Long-Range Transport

Long-range transport is an important influence on trace gas distributions and budgets in the troposphere. It means that pollution sources affect more than the local area, even another continent. In middle latitudes, the lifetime of ozone in the free troposphere is in the order of months, thus ozone or its precursors can, under certain conditions, be transported hundreds of kilometres (Knap, 1989; Crawford *et al.*, 1997; Penkett *et al.*, 2003). A number of dynamic processes, including convection and motion associated with frontal systems and individual synoptic circulations, affect long-range transport (Barry and Chorley, 1998; Penkett *et al.*, 2003).

For example, convection determines vertical exchange through convective updrafts (Knap, 1989; Ehhalt *et al.*, 1992). Precursors or pollutants can be brought to the upper troposphere where they have a longer lifetime, as destructive processes are less effective. Pollutants may then be transported downwards from the upper levels to the planetary boundary layer within frontal systems (Ehhalt *et al.*, 1992; Penkett *et al.*, 2003). Numerous studies have shown that frontal systems (for example, through the “warm conveyor belt”) are important processes in the long-range transport for ozone and its precursors between continents. Using ozone lidar data analysis, Stohl (1999) found elevated ozone levels of the upper troposphere in southern Germany could be attributed to long-range transport involving frontal processes from North America to Europe. Near Taiwan, high pressure systems can be important in accumulating pollution over a wide area of downward motion and then transporting pollutants between regions.

Other evidence of long-range pollutant transport over the North Atlantic and Europe can be observed from aircraft experiments (for example, North Atlantic Regional Experiment) and model simulations, which suggest North America and Asia as substantial tropospheric ozone contributors for Europe (Penkett *et al.*, 2003; Derwent *et al.*, 2004; Auvray and Bey, 2005). Moreover, it has been observed that low ozone concentrations are also associated with the long-range transport of clean air in Europe, for example, from maritime areas (Low *et al.*, 1992). This work also suggests that long-range transport is one of major factors determining the ozone distribution and budget over the Atlantic Ocean.

Over East Asia, the main factors influencing long-range transport are, according to Penkett *et al.* (2003) and Jacob *et al.* (2003), the dominant westerly winds over mid-latitudes and vertical mixing over parts of the continent, as affected by extension

of the continental high pressure from Siberia and the occasional influence of the Pacific High. Orographic forcing over central and eastern China is also a major process responsible for lifting pollution into the free troposphere. The air pollutants from China can be exported from the Asian continent and reach Taiwan and Japan (Naja and Akimoto, 2004; Oltmans *et al.*, 2004).

As far as Taiwan is concerned, outflow of pollution from the Asian continent is a key consideration. To investigate the influence of photochemistry and continental outflow on the tropospheric ozone distribution over the western North Pacific, several international campaigns have taken place over the region. For example, studies have included the Pacific Exploratory Mission-West Phase A and B for different seasons (PEM-West A and B), the Transport and Chemical Evolution over the Pacific Project (TRACE-P), and the International Global Atmospheric Chemistry/East Asia-North Pacific Regional Study (IGAC/APARE) (Crawford *et al.*, 1997; Jacob *et al.*, 2003; Liu *et al.*, 2003; Lam *et al.*, 2004).

According to the analysis of the PEM-West B field experiment (February-March 1994), continental outflow (for example, via the Siberia High) from the west Pacific Rim affects tropospheric ozone levels of both subtropical and mid-latitude ocean areas, and the chemical composition of the outflow reflects anthropogenic emission (Crawford *et al.*, 1997). Crawford et al. (1997) show that the high and low levels of NO_x in the study regions (latitudes of 10°S to 50°N and altitudes of 0-12km) were transported by convective transport from continental regions and tropical marine air masses, respectively. It is interesting to note that net ozone production was evident at both subtropical and mid-latitudes and at all altitudes over the Pacific marine environment, particularly for the boundary layer and the lower free tropospheric altitudes, during this

experiment (Crawford *et al.*, 1997). This suggests that the continental outflow of ozone precursors over the northwestern Pacific basin (for example, over Taiwan and Japan) is a significant factor in generating ozone; this could extend far from the Asian Pacific Rim, especially for the marine boundary layer, during the later winter and early spring seasons.

A later aircraft mission, TRACE-P, was conducted in February-April 2001 over the western North Pacific in the same geographic area as PEM-West B. The data analysis was combined with Measurements of Pollution in the Troposphere (MOPITT) satellite data to investigate transpacific transport from Asian pollution outflow (Jacob *et al.*, 2003). Fuelberg *et al.* (2003) pointed out that the transition from winter to spring and a weak La Niña effect for the later winter period resulted in rapid changes in the atmospheric circulation. The Siberian anticyclone and the frequent development of cyclones at mid-latitudes around the east coast of Asia played a vital role for continental outflow to the North Pacific (Fuelberg *et al.*, 2003; Liu *et al.*, 2003; Wild *et al.*, 2004). The mechanism was the interplay between cold fronts and warm conveyor belts to transport pollution out of Asia to the Pacific in spring (Jacob *et al.*, 2003; Liu *et al.*, 2003).

This study revealed a complex interaction of processes that determined ozone distribution. Ozone production was insignificant in the upper troposphere as a result of unfavourable conditions of formation (Pierce *et al.*, 2003). A weak Siberian anticyclone resulted in highly efficient ozone production but with a short chemical lifetime. An Aleutian cyclone was characterised by low ozone pollution but deep cloud convection took ozone and precursors into the free troposphere where chemical lifetimes are longer (Wild *et al.*, 2004). The interplay between these mechanisms makes a substantial

contribution to the pattern of long-range transport of ozone in the spring (Heald *et al.*, 2003; Wild *et al.*, 2004). Another phenomenon that should be noted was that, over subtropical regions such as north Taiwan, the boundary layer ozone was at high concentrations as the result of outflow from the Asian continent. Hong Kong showed elevated ozone levels in the lower troposphere caused by biomass burning from sources in Southeast Asia at that time of year (Liu *et al.*, 2003; Oltmans *et al.*, 2004; Wild *et al.*, 2004).

Aircraft investigations only provide evidence for a particular time period and cannot help in defining longer-term patterns. In recent years, the Frontier Research Centre for Global Change (FRCGC) has completed Asia-Pacific and Eurasian long-range transport investigations using long-term ozonesonde data and model simulations for East Asia. Although there are a few long-term ozonesonde observation sites, these studies still provide useful and comparable information with other regions, such as Europe or North America, to understand the dynamic processes over the Asian region and Eurasian continent.

Naja and Akimoto (2004) discovered that Eurasian air masses and regionally polluted air masses (from China) were the main long-range transport contributors to ozone levels over Japan over the period 1970-2002. Polluted air masses from China contributed higher ozone concentrations for lower latitude sites (for example, Kagoshima, 31.6°N, 130.6°E, and Naha, 26.2°N, 127.7°E). Ozone concentrations were mainly affected by the Eurasian air masses at mid-latitude observation sites (for example, Sapporo, 43.05°N, 141.3°E) with a smaller contribution. The effects from these air masses resulted in seasonal and interannual ozone variations.

In summary, there is considerable evidence that long-range transport of pollutants can affect ozone levels over the Asia-Pacific rim, including Taiwan. There are, however, a number of mechanisms underlying long-range transport, which vary in effectiveness by source and destination.

2.4 Conclusion

Previous studies of the distribution of tropospheric ozone around the world indicate that long-range transport is a key issue. This is not to reduce in importance the dominant role of local processes, such as photochemistry, in determining ozone levels in most areas. Nevertheless, there is strong evidence that long-range transport can exert an appreciable influence.

Past experience from Europe and North America shows that the physical processes underlying tropospheric ozone formation are particularly important factors for those countries with emission control legislation that limit local sources. The most influential factors are regional formation mechanisms and intercontinental long-range transport. Taiwan is moving into this situation now as legislation is implemented to control local pollution sources. Much research into related processes has been done for Europe and North America but less attention has been paid to the East Asia region, which is likely to be a substantial source of precursor emitters for the coming decades. Moreover, studies of the role of the atmospheric circulation in determining long-range transport have been undertaken for mid-latitude areas of Europe, North America and Japan, but research is lacking over subtropical regions, under different atmospheric circulation conditions. A greater understanding of the effects of atmospheric circulation variability on long-range transport and pollutant distribution in a subtropical region, such as Taiwan, is required.

This literature review, suggests the important points for the design of this study can be summarised as follows.

- Given the episodic nature of extreme ozone concentrations, a daily timescale for

the study is necessary (rather than a focus on long-term changes in mean ozone levels).

- Previous studies have indicated that the episodic variability of ozone levels is affected by synoptic weather patterns, such as the Siberia and the Pacific high pressure systems, which are dominated by the large-scale (regional and intercontinental) atmospheric circulation. The identification of the role of the large-scale atmospheric circulation should be the basis of the study.
- It is useful to distinguish two geographical scales in examining the influences on local ozone levels: the local area of Taiwan and the regional context.
- In the local area of Taiwan, the influence of processes, such as local meteorological conditions, including the sea breeze, is strongly related to pollutant accumulation and dispersion, both for regional and local emission sources, and to diurnal ozone level variation as well.
- On the regional and larger scale, the Asian monsoon system is an important influence on the character of the Asian continental outflow (for example, polluted air masses or clean air masses) on long-range pollutant transport. The variability of the Asian monsoon can be linked to intraseasonal to interannual ozone variation over Asia, in particular for subtropical areas, and this aspect of the general circulation of the atmosphere, as a regional integration, provides a focus for the study.
- The relative contribution of the various regional sources, such as China, Japan and Korea, to local ozone levels is a key concern and directional considerations may permit identification of the role of these different sources in affecting ozone levels over Taiwan.

These conclusions provide a basis for the project design described in the following chapter.

Chapter 3: Project Design, Data and Statistical Methods

3.1 Introduction

On the basis of past research, the previous chapter presented the effects of regional formation mechanisms and intercontinental long-range transport on tropospheric ozone levels, largely for mid-latitudes. A number of issues were identified that form the basis of the project design. The first section of this chapter provides the research framework and definition for the entire project. The second section describes and defines data sources, particularly their specific use in this study. The final section introduces the methodologies that will be applied.

3.2 Project Design

As has been addressed in Chapter One, the aim of this project is to investigate the role of the large-scale atmospheric circulation in the occurrence of high ozone days over Taiwan. It tries to understand the link between long-range transport mechanisms and the regional atmospheric circulation. The project focuses on the identification of atmospheric circulation features related to high ozone pollution days over the period 1994-2004 and the likely climatological explanation of these links. The study of the short period only from 1994 to 2004 is a result of air pollution data availability.

The role of the monsoon, the dominant feature of the circulation of the region, will provide a focus. Taiwan is governed by two prevailing wind systems: one is

characterised by northeasterlies and is called the winter monsoon, and the other by southwesterlies and is called the summer monsoon (Yen and Chen, 2000). The variation of these two monsoonal circulations and the transition between them affects the character of the Asian continental outflow and thus long-range transport. A schematic of the research framework and thesis structure is presented in Figure 3.1. Three key questions must be addressed.

- **What are the characteristics of high ozone pollution episodes and their variability over Taiwan?**
- **Is there evidence that regional atmospheric circulation patterns are linked to the occurrence of high ozone pollution days?**
- **What is the role of long-range transport and other circulation mechanisms, including the dominant monsoonal circulation of the region?**

A brief overview of the analysis associated with each question is given here. A more detailed discussion of the data and techniques, including references to the literature, follows in subsequent sections.

What are the characteristics of high ozone pollution episodes and their variability over Taiwan?

As tropospheric ozone formation mechanisms are dependent on local meteorological conditions and topographic features, ozone pollution exhibits a diversity of regional, seasonal and interannual behaviour. Ground-level ozone concentration is obtained from the Taiwan Air Quality Monitoring Network (TAQMN) for the period 1994 to

2004, provided information on ozone pollution episodes. These daily data are used to identify high ozone pollution episodes, as defined by air quality standard, and analyse the seasonal and interannual trends by various statistical methods. Three indices for analysing long-term trend of ozone pollution are constructed and the high ozone pollution areas in this study are established.

Further details follow in Section 3.3.

Is there evidence that regional atmospheric circulation patterns are linked to the occurrence of high ozone pollution days?

To consider the features of the local synoptic weather patterns and of the regional atmospheric circulation that accompany high ozone pollution days, three main analytical processes are undertaken:

- definition of high ozone pollution days and characteristics of occurrence;
- objective definition of local and regional weather types; and,
- composite analysis of pressure conditions accompanying high ozone pollution days.

Given the seasonal evolution of atmospheric circulation, the analyses are stratified by month.

Long-term synoptic meteorological data are applied to define local and regional atmospheric circulation patterns. The NCEP/NCAR reanalysis dataset of daily geopotential height data (HGT.PRS) from different pressure levels (850hPa and

500hPa) and sea-level pressure (SLP) over the period 1994 to 2004 are used. The GrADS system is utilised to manage and analyse these data, with separate Fortran routines for particular analyses. This system uses a 4-dimensional data environment. The review of likely sources of pollution relevant to Taiwan and the role of long-range transport suggest an analytic domain that covers Asia and the neighbouring Pacific Ocean.

An objective scheme, based on wind strength and direction and vorticity defined from SLP, is used to define daily weather types and to explore in detail the link between atmospheric circulation patterns and high ozone events. The method, developed in middle latitudes, is amended for application in lower latitudes and its strengths and limitations are considered. The daily weather type catalogue is used to define the synoptic conditions on and before high ozone pollution days. Two spatial scales are investigated; local and regional, with the latter providing a link with the next stage of the analysis.

The character of the large-scale atmospheric circulation at the time of each pollution day is examined by averaging the circulation data (geopotential height at different levels) for days with high ozone values and so producing the average pattern of the circulation that is related to high ozone occurrence. This pattern can be viewed as anomalies based on departures from the long-term mean. Statistical significance testing (Cramer test) is used to determine which aspects of the pattern are important. In this way, the important features of the synoptic circulation accompanying of high pollution episodes are identified.

Further details follow in Section 3.4 and 3.5.

What is the role of long-range transport and other circulation mechanisms, including the dominant monsoonal circulation of the region?

In this study, back trajectory analysis is used to investigate further the role of long-range transport, including the importance of different source regions, in high ozone pollution episodes over Taiwan. The transport pathways over the region are calculated by the HYSPLIT (Hybrid Single-Particle Lagrangian Integrated Trajectory) model. The meteorological input is from NCEP reanalysis dataset to model flow paths for consistency with the statistical atmospheric circulation analysis discussed above. The results of the back trajectory analysis are compared with the statistical analysis results of large-scale circulation patterns. In addition, a comparison study is also investigated to explore differences between ‘pollution’ and ‘non-pollution’ episodes’ transport pathways. Seasonal and spatial characteristics are considered and, where appropriate, case studies are used to explore features of particular interest.

The results of this analysis are combined with the results of the previous two sets of analyses to provide an assessment of the role of Asian monsoon variability and other circulation features in influencing high ozone pollution episodes over Taiwan. The relevance of this assessment to determining potential global warming effects on future ozone levels are discussed, as a sample application.

Further details follow in Section 3.6.

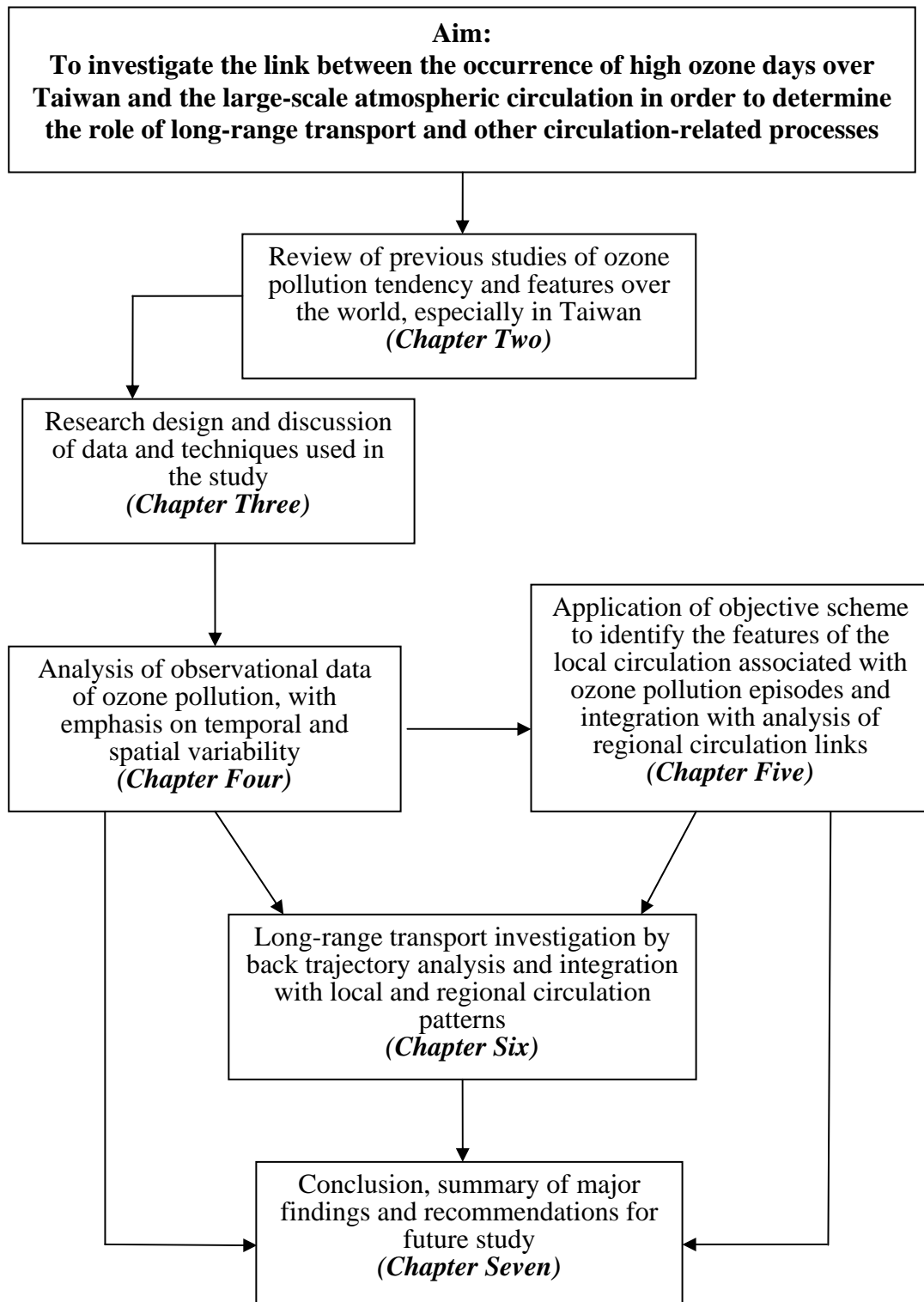


Figure 3.1: A schematic research framework

3.3 Air Pollution Data

3.3.1 Data Source

The present study uses daily mean ozone concentration data from the Taiwan Air Quality Monitoring Network (TAQMN) to define the features of high ozone pollution. The complete TAQMN has been established since late 1993. The network consists of 76 monitoring stations in seven air quality zones (Noth, Chu-Mian, Central, Yun-Chia-Nan, Kao-Ping, Yilan and Hua-Tung) (see Figure 2.4), which are divided by the characteristics of local air pollutants, geography and meteorological conditions. Five types of air quality monitoring station, including background site, ambient site, roadside site, industrial site and national park, serve different purposes. For example, background monitoring stations are installed in the upwind areas of the major urban cities, where there is little immediate influence by anthropogenic pollution, to monitor the long-range transport of pollutants. Roadside sites are located near heavily travelled roadways to assess the emission of motor vehicles and the exposure levels of pedestrians. The priority monitored pollutants include particulate matter (PM_{10}), sulphur dioxide (SO_2), carbon monoxide (CO), nitrogen oxides (NO_x), ozone (O_3) and hydrocarbons (HC_s). In this study, data are selected from only the 64 stations (see Figure 2.4) that had complete ozone data for the study period, 1994-2004.

3.3.2 Quality Control

The Taiwan EPA Data Quality Assurance Procedures (DQAP), which follow those prescribed by the U.S. Environmental Protection Agency (USEPA), have been established since 1991 (the early stage of the monitoring network in Taiwan). The DQAP covers regular system maintenance (for example, daily zero, operating check, biweekly precision check and monthly instrument functions check) and data performance auditing, which is based on a set of standard TAQMN performance audit processes. The ambient ozone monitors are calibrated and audited by ozone concentration standards that are dynamically generated and assayed by UV photometry. Monitoring of inspection instruments, standard gas calibration, and laboratory standard operation processes and other checks have been routinely performed throughout the monitoring network (EPA Taiwan, 2001, 2002; Yang, *et al.*, 2005). The limitation of the air pollution data is that the data are only available for a short period from 1994-2004. The shortness of record may affect some results, particularly when ozone pollution trends are discussed. To reduce the effect of the short data record, a daily analysis period is used and all available stations records are selected to define indices of high ozone pollution days. A valid daily value is considered as only the average of data collected for more than 16 effective hours per day, such that a better representative daily average is obtained.

3.3.3 The Definition of High Ozone Pollution Indices

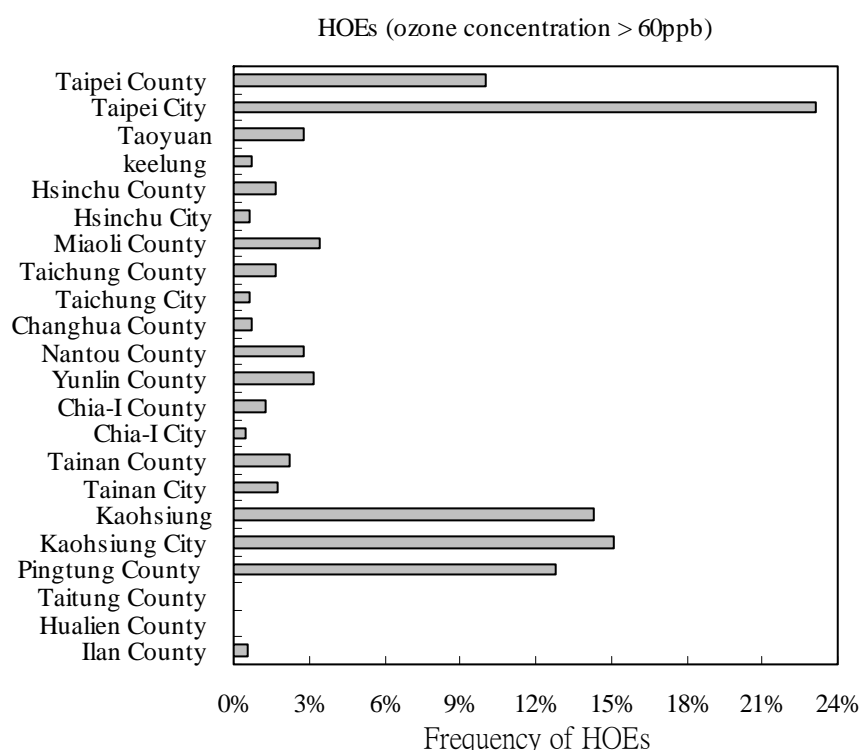
The characteristics of high ozone pollution episodes, indices for the study are established through a series of calculation and statistics processes. Daily mean data are

used to identify high ozone pollution episodes. The procedure is as follows: according to the air quality standard (Table 3.1), there are two definitions of a high ozone pollution episode in Taiwan, one is daily maximum hourly ozone concentration > 120 ppb, and the other one is an eight-hour mean concentration > 60 ppb. In this study, we focus on exceptionally high levels in order to ensure a strong signal from the related data sets; hence, we conservatively define high ozone episodes (HOEs) as those with a daily-mean ozone concentration > 60 ppb. If the condition is met at two stations, for example, on the same day, then this is counted as two episodes in the HOE index.

At some of the stations, only a few high ozone pollution episodes have been observed over the study period. To eliminate these areas from the analysis, stations are dropped if the percentage of HOEs is less than 1% over the eleven-year record (Figure 3.2). This process leaves 53 stations in five air quality zones (Figure 3.3). Using this more limited network, the high ozone day (HOD), a second index, is defined as a day with one station exhibiting average concentration over 60 ppb. As there is a concern that local pollution episodes could result in a high occurrence rate of HOD, a third index, HOD₃, is defined when at least three stations exhibit a daily mean concentration > 60 ppb to investigate the effect of regional pollutants transport on Taiwan's air quality. It is this index that is used in later analyses to define high ozone pollution days for Taiwan as a whole to establish the relationships with atmospheric circulation data.

Table 3.1: Air quality standards for various countries: definition of high ozone episodes.

Pollutant	Averaging Time	Taiwan	U.K.	U.S.	Singapore
O_3	1 Hour	120 ppb		120 ppb	120 ppb
	4 Hours				
	8 Hours	60 ppb	50 ppb	80 ppb	80 ppb
Pollutant	Averaging Time	Australia	Hong Kong	Japan	
O_3	1 Hour	100 ppb	120 ppb	60 ppb	
	4 Hours	80 ppb			
	8 Hours				

**Figure 3.2:** Frequency of high ozone episodes (HOEs) in the 22 districts of Taiwan, geographical information of 22 districts see Figure 2.4.

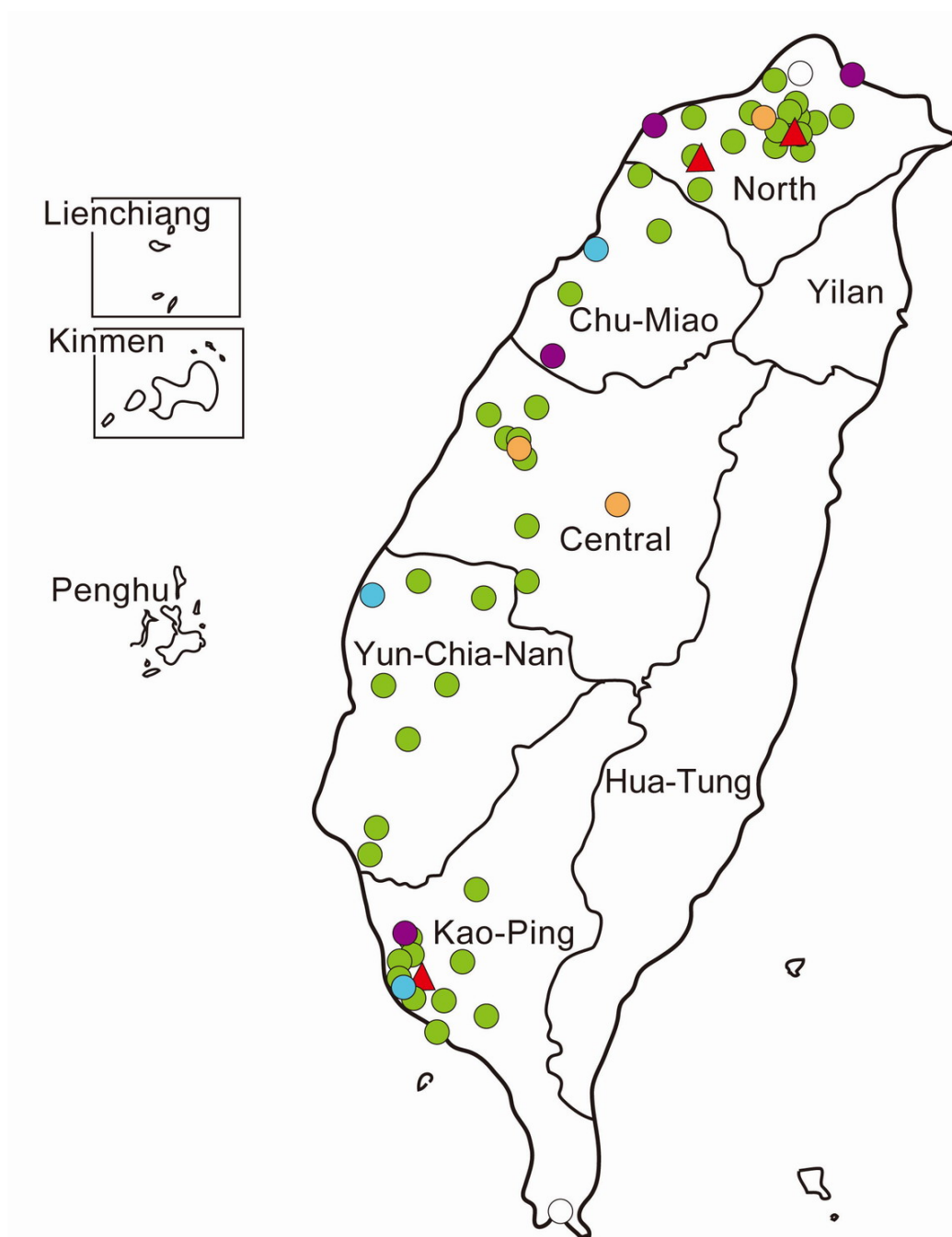


Figure 3.3: The distribution of 53 air monitoring network stations and the five air quality zones used in this study.

3.4 Gridded Observational Atmospheric Circulation Data

Observational meteorological networks on a global scale have existed since 1946. Due to changes in instrumentation and observational methods, there are limitations in the use of these data for investigating climate change and interannual climate variability. These changes can result in temporal and spatial inhomogeneities in the data and the recorders interruption. In order to tackle inhomogeneous data and the discontinuities, a number of climate research centres have attempted to reproduce and assimilate data by a stable, invariant analysis system, through what is called a ‘reanalysis’ project, such as NCEP/NCAR reanalysis Project (Kalnay *et al.*, 1996; Kistler *et al.*, 2001).

The aim of this thesis study is to investigate the characteristics of the local synoptic weather patterns and the large-scale atmospheric circulation related to high ozone pollution occurrence. Daily atmospheric data were obtained from the National Centre for Environmental Prediction (NCEP)/National Center for Atmospheric Research (NCAR) reanalysis project. The following sections will introduce the background of the NCEP/NCAR reanalysis, the quality control process, problems and known errors, inter-comparison results and the diagnostic variables used in this study.

3.4.1 NCEP/NCAR Reanalysis Data

The aim of the NCEP/NCAR reanalysis project is to provide the climate research, monitoring and modelling community with a record of global atmospheric analyses (Kalnay *et al.*, 1996). It began in 1991 as a development of the NMC Climate Data Assimilation System (CDAS) project. The data are currently available from 1948 to

the present. The quality of these re-analyses should be superior to NCEP's original analyses because (Kalnay *et al.*, 1996):

- a frozen state-of-the-art data assimilation system is used;
- more observations are used;
- quality control has been improved;
- consistent model/data assimilation system is used over the entire project;
- many more fields are being saved; and,
- global coverage and a variety of output archives.

The development of reanalysis datasets has recovered land surface, ship, rawinsonde, aircraft, satellite and other fields. In addition, the products include forecasts data file and the binary universal format representation (BUFR) of the atmospheric observations. The complete output data have a horizontal resolution of $2.5^\circ \times 2.5^\circ$ latitude/longitude and vertical resolution up to 17 levels.

Data assimilation theory, models and computers have been improved substantially over the past fifty years. The reanalysis project is, however, still affected by changes in the observing system. The quality of the output variables is related to the evolution of the global observing systems, which can be separated into three major phases: the early period from the 1940s to the International Geophysical Year in 1957, when the first upper-air observations were established; the modern rawinsonde network from 1958 to 1978; and the modern satellite era from 1979 to the present (Kistler *et al.*, 2001).

The output variables have been classified into four classes, depending on the degree to which they are influenced by the observations or the modelling (Kalnay *et al.*, 1996)

Class A: The primary reanalysis data sources are mostly directly observed, and variables of this type are, therefore, in the most reliable class (for example, upper air temperature, geopotential height, sea-level pressure).

Class B: The variable is directly influenced by the observed data as well as model values (for example, moisture variable, divergent wind, surface parameters).

Class C: No observations directly affect the variable. These variables are derived only from the model fields, which are forced by the data assimilation to remain close to the atmosphere (for example, surface fluxes, heating rates, clouds and precipitation).

Class D: A field fixed from climatological values and, therefore, with no dependence on the model (for example, surface roughness).

3.4.2 Quality Control

Data quality has been checked through multiple quality control processes during the reanalysis project. Two major quality control systems are the Complex Quality Control (CQC) and the Optimal Interpolation Quality Control (OIQC) processes.

The Complex Quality Control (CQC) system is used to assess the quality of the rawinsonde heights and temperatures program (Gandin, 1988). The CQC code includes a number of checks used operationally, including a hydrostatic check, increment check and horizontal and vertical interpolation check. A baseline check is used to detect the

changes in the station locations as well as errors in the location. The method of CQC is to compute residuals from several independent checks and then use these residuals with an advance decision making algorithm to accept, reject or correct data (Collins and Gandin, 1990). The performance of CQC for rawinsonde observations detection shows that of the hydrostatically detectable errors about 75% are corrected, while 60% of the baseline errors are corrected (Kalnay *et al.*, 1996).

The role of Optimal Interpolation Quality Control (OIQC) is the final screening for observational data (Woollen *et al.*, 1994). As far as problems caused by instrumental, human or communications processes are concerned, the OIQC is used to detect obvious and unresolved errors and withhold them from assimilation system. In addition, unrepresentative observations are also detected in the OIQC. The OIQC algorithm is based on three approaches: firstly, multivariate three-dimensional statistical interpolation is used to do prescribed area checks for each observation; secondly, use of independent interpolation and other types of checks that when assessed collectively suggests whether errors exist in an observation; and thirdly, use of a non-hierarchical decision making algorithm to monitor the results of various checks and to make final accept/reject decision after all processes are completed.

3.4.3 Problems and Known Errors

Problems resulting from observing systems changes or model deficiencies are inevitable in reanalysis projects. Many problems and errors were corrected over time within the reanalysis process, having been discovered both through internal NCEP monitoring and by external users who had access to early results or the observations

themselves (Kistler *et al.*, 2001). Where problems affect periods more than few months, they cannot be solved by rerunning the reanalysis immediately. These problems have been reported and posted on the project website. For example, data were sometimes omitted in the assimilation system, such as snow cover in February 1997 and TOVS data during May to June in 2003. A problem with regard to TOVS data retrievals affects high-level temperature and geopotential heights through the period from March 1997 to September 2001. More detailed information, with updates, can be obtained from the website: <http://www.cdc.noaa.gov/cdc/reanalysis/problems.shtml>

3.4.4 Inter-Comparisons

It is important to estimate the reliability of reanalysis results by thorough inter-comparisons with other available reanalyses (Kistler *et al.*, 2001). Other reanalysis projects are conducted by the European Centre for Medium-Range Weather Forecasts (ECMWF, ERA) and the National Aeronautics and Space Administration Data Assimilation Office (NASA/DAO). They use nearly the same observations, but apply different assimilation models (Kistler *et al.*, 2001). For example, the reanalysis and assimilation at NCEP/NCAR are done by Spectral triangular 62 (T62), with 28 vertical levels and 209 km horizontal resolution. The grid resolution of T62, about 2x2 degree latitude/longitude, is coarser for topographic analysis than the model used in the ERA. In this section, selected studies that have attempted to compare these datasets and/or satellite observations are discussed, to give an indication of the strengths and weaknesses of the NCEP/NCAR dataset.

As noted above, there are four levels of output variable quality. The comparison of type A variables, such as zonal wind (u component), air temperature and geopotential height at 500hPa, shows good agreement between the NCEP/NCAR and the ECMWF reanalyses, but with significant differences in the tropics, in particular, in the interannual scale comparison (Kistler *et al.*, 2001; Covey *et al.*, 2002). A number of comparisons focus on type C variables, less affected by observations, for instance, cloudiness, surface fluxes and precipitation. In this case, these variables are compared with observations, mostly “direct” observations such as satellite observations. Covey *et al.* (2002) pointed out that cloudiness from the NCEP/NCAR reanalysis, compared with International Satellite Cloud Climatology Project (ISCPP) (Rossow *et al.*, 1991), is underestimated, and the ERA exhibits better agreement than the NCEP/NCAR for the period of 1984-1990.

For energy fluxes, the comparison of solar radiation at the top of the atmosphere shows that, overall, the net shortwave radiation of the NECP/NCAR reanalysis is less than Earth Radiation Balance Experiment (ERBE) observations (Barkstrom *et al.*, 1989). The NCEP/NCAR outgoing-longwave-radiation, compared with the ERA and Goddard Earth Observing System (GEOS) data, is closest to ERBE for 1985-1989. The ERA is overestimated and GEOS is too low in the tropics, but too high out of the tropics (Kistler *et al.*, 2001; Covey *et al.*, 2002).

Comparisons of zonal mean precipitation (another Type C variable) have been made between three reanalyses and two independent estimates from the Climate Prediction Centre merged analysis (CMAP, Xie and Arkin, 1996) and by the Global Precipitation Climatology Project (GPCP) over land and ocean. Of the three reanalyses, comparison with the CMAP, shows that NCEP/NCAR and GEOS underestimate variability over

the tropical oceans and the ERA substantially overestimates it (Kistler *et al.*, 2001). This result is consistent with the comparisons with the GPCP. In addition, NCEP, ECMWF and GPCP show the same pattern of the spatial mean as well as seasonal cycles in most regions (Quarly *et al.*, 2007). Precipitation in the NCEP/NCAR reanalysis more closely follows the observations in the tropics and the ERA presents better agreement over the Northern Hemisphere continents and the extratropical oceans.

In terms of zonal mean temperature, Trenberth *et al.* (2001) indicated that the NCEP/NCAR and the Microwave Sound Unit (MSU) agree quite well with each other over the tropics. In contrast, the ERA reanalysis exhibits large difference with these two datasets (Covey *et al.*, 2002). The lack of accuracy of ERA over the tropics is related to spurious fluctuations in tropospheric temperatures and moisture on several time scales as well as two discontinuities in late 1986 and early 1989 (Trenberth *et al.*, 2001). For temperature anomalies at 850hPa, the NCEP/NCAR anomalies showed fairly good agreement with the NASA/DAO (Kistler *et al.*, 2001). Overall, analysts conclude that the NCEP/NCAR reanalysis presents more reliable quality than the ECMWF reanalysis, in particular for the tropics.

A comparison of the reanalysis datasets with observed sea level pressure (SLP) climatologies (Trenberth and Paolino, 1980) indicated that the monthly SLP data of NCEP/NCAR exhibits an unusually strong annual cycle over southeastern Russia, Mongolia and northern China before 1967 (Yang *et al.*, 2002). This result is also found by Inoue and Matsumoto (2004), who reported an evidently increase SLP of NCEP/NCAR between the two periods, one is in the mid-1960s and the other one occurred in the mid-1970s. The first increase could result from the earlier (1948 to

1967) data conversion process (Kistler *et al.*, 2001). However, it is not recognised in the ERA and other observational datasets (for example, Climatic Research Unit of University of East Anglia, CRU-UEA) used in their study. This suggests that the SLP of ERA over East Eurasia (40°N-60°N) and its vicinity before the 1970s is more reliable than the NCEP/NCAR reanalysis. Although the data quality of SLP from NCEP/NCAR, before 1968, is arguable, the period of the current study from 1994 to 2004 is quite consistent with other reanalyses.

For the Southern Hemisphere, climate analysis is limited through the sparse station network, especially for the high and middle latitudes. Bromwich and Fogt (2004) have carried out a comparison of the NCEP/NCAR and ERA data with Antarctic and mid-to high latitude station observations for the period 1958 to 2001. They found large discrepancies between NCEP and ERA due to the different assimilation schemes. The NCEP/NCAR reanalysis is constrained by the station observational network, whereas the ERA is more strongly constrained by the satellite data. Therefore, ERA shows better agreement with the observations than the NCEP/NCAR reanalysis, in particular after the start of the modern satellite era (post 1978). The quality of both reanalyses is less before 1970 (the pre-satellite era), due to the lack of data sources (Sterl, 2004).

Some comparisons indicate that the ERA data set is more accurate, in particular for land surface regions, because its high resolution is better at simulating topographic influences (Annamalai *et al.*, 1999). The results suggest, though, that the NCEP/NCAR reanalysis data present a better potential for tropical studies, due to the better depiction of variability in these regions. Otherwise, all data sets cover the core period for this study, defined by ozone data availability, but the NCEP/NCAR data cover the longest period (which can be used to place the representativeness of the study period in

context). Despite the advantages of NCEP/NCAR reanalysis for tropical studies, there are, as noted, potential deficiencies that must be borne in mind. In particular, the quality of the reanalysis data for those regions with sparse observational networks may be strongly affected by the model simulation and this could affect ocean regions of the Asia-Pacific study area.

3.4.5 Diagnostic Variables

Two central diagnostic variables from the NCEP/NCAR reanalysis have been chosen for the present study to clarify the effect of atmospheric circulation variability on tropospheric ozone pollution. Sea level pressure is used to classify the features of local and regional weather types associated with tropospheric ozone occurrence and to investigate the influence of local circulation. The other variable is geopotential height, an upper-air variable, for investigating the large-scale circulation associated with long-range precursors/pollutants transport. Geopotential height is a vertical coordinate referenced to the mean sea level. The two pressure levels, 850hPa and 500hPa, are considered. Both sea level pressure and geopotential height data from the NCEP/NCAR reanalysis are designated as Class A variables. This means that both variables are highly influenced by the observations, and hence they are in the most reliable class (Kalnay *et al.*, 1996), though the potential errors discussed in the previous section with regard to pressure over northeast Asia must be borne in mind.

3.5 Objective Circulation Classification Scheme

3.5.1 Introduction

Synoptic weather typing has been used in various studies, such as on the effects of atmospheric circulation on weather elements (Yarnal, 1985; Jones *et al.*, 1993) and the correlation between synoptic weather type and air pollutants (Lennartson and Schwartz, 1999; Schwarzhoff and Reid, 2000; Cheng *et al.*, 2001). Synoptic weather typing development can be divided into : subjective (manual) approaches and objective (automated) approaches (El-kadi and Smithson, 1992). In this study, an objective scheme, developed by Jenkinson and Collison (1977), is used to classify daily weather types for the local and regional circulation over Taiwan for the period 1994 to 2004. This objective scheme is based on numerical values of flow and vorticity calculated from gridded sea-level pressure (SLP) data (Jenkinson and Collison, 1977). The results from the weather type classification are utilized to assess the correlation between the character of the local and regional circulation over Taiwan and Northeast Asia during high ozone events.

Barry and Perry (1973) argued that atmospheric circulation pattern classification and assessment of the relationship between atmospheric circulation patterns and local weather elements are two important procedures within synoptic climatology research. Perhaps the most famous subjective classification scheme was developed by Lamb (1950), who identified seven kinds of atmospheric circulation patterns for the British Isles and later expanded this to 27 types (Lamb, 1972). These 27 weather types consist of an unclassified type, two types defined by geostrophic vorticity (anticyclonic and cyclonic), eight directional types and 16 hybrid types (Table 3.2). Many applications

have demonstrated the value of Lamb's synoptic classification approach in a variety of weather analyses (for example, Murray and Lewis, 1966; Jones and Kelly, 1982; Briffa *et al.*, 1990).

Despite its proven value, subjective classification may be affected by bias, lack of precision and other potential errors. Objective (automated) schemes using numerical and statistical techniques can lead to the improvement of precision and errors and certainly are more efficient in terms of time and labour during the classification processes (Yarnal and White, 1987). The earliest objective weather type classification procedure was developed by Lund (1963), who applied statistical methods to group patterns on weather maps. The objective scheme used in this study, demonstrated that wind flow and vorticity parameters could be used to define the direction and type of surface flow for the British Isles related to the subjective Lamb Weather Type Catalogue (Jenkinson and Collison, 1977). Jones *et al.* (1993) have shown that this objective scheme can be used to reproduce Lamb's daily catalogue successfully for the British Isles. The scheme has been used for the validation of general circulation model output (Hulme *et al.*, 1993). More recently, Goodess and Palutikof (1998), Spellman (2000), Trigo and DaCamara (2000) and Tomás *et al.* (2004) used the scheme to study the Mediterranean area, which displays a different climate regime, showing that it could provide suitable indices for precipitation research and other meteorological conditions. Although objective schemes have been used with in many applications successfully, the inherent subjectivity, such as grid spacing, operator decision on thresholds, remains to be considered (Yarnal, 1984; Spellman, 2000; Tomás *et al.*, 2004).

3.5.2 Methodology

The Lamb Weather Type (LWT) objective scheme was initially developed using a 16-point grid centred on 55° N with a resolution of 5° latitude by 10° longitude (Jenkinson and Collison, 1977), reflecting the resolution of the underlying UK Meteorological Office pressure data (Jones *et al.*, 1993). In the objective scheme, the daily circulation is classified according to categories and thresholds of a set of indices associated with vorticity and air flow, which are calculated from daily grid point sea-level pressure data. The flow and vorticity parameters provide information about wind strength and direction and circulation type, such as cyclonic and anticyclonic. In this study, the daily gridded sea-level pressure data are taken from the NCEP/NCAR reanalysis dataset. Because interest is in both the local and regional scales, two different ‘window sizes’ are classified. For the small (local) window, the area covered is from 17.5° N to 32.5° N and from 110° E to 130° E with a resolution of 2.5° latitude by 5° longitude (Figure 3.4). The larger (regional) window covers the area defined from 0° N to 50° N and from 80 ° E to 160° E with a resolution of 10° latitude by 20° longitude (Figure 3.5). Both areas are represented by a 16-point grid within the window, centred on 23.75° N, Taiwan, and the primary analysis period is from January 1994 to December 2004. In addition, the analysis of the long-term trend covers the period from 1958 to 2004.

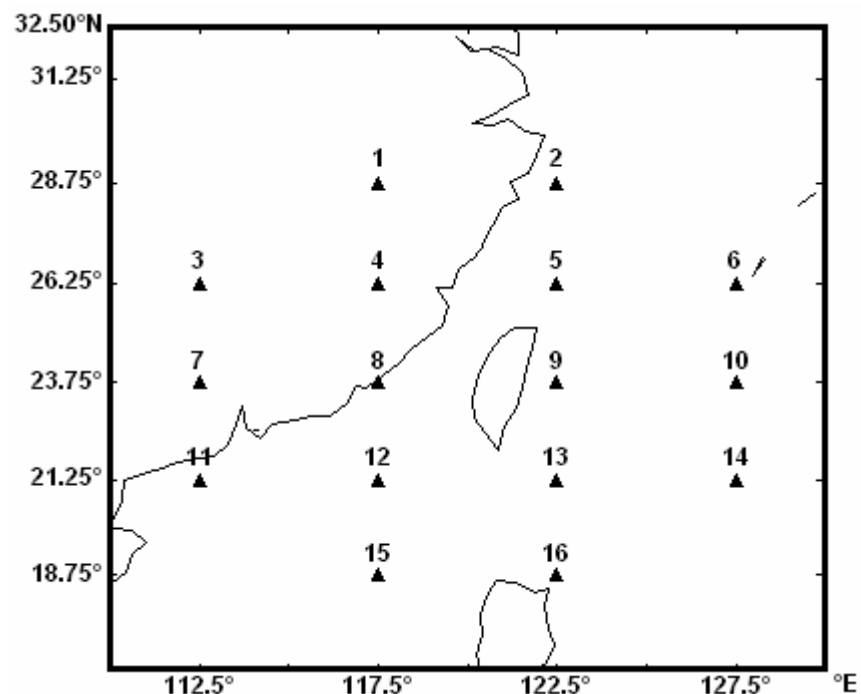


Figure 3.4: Grid used in the objective circulation-typing scheme (Local Area).

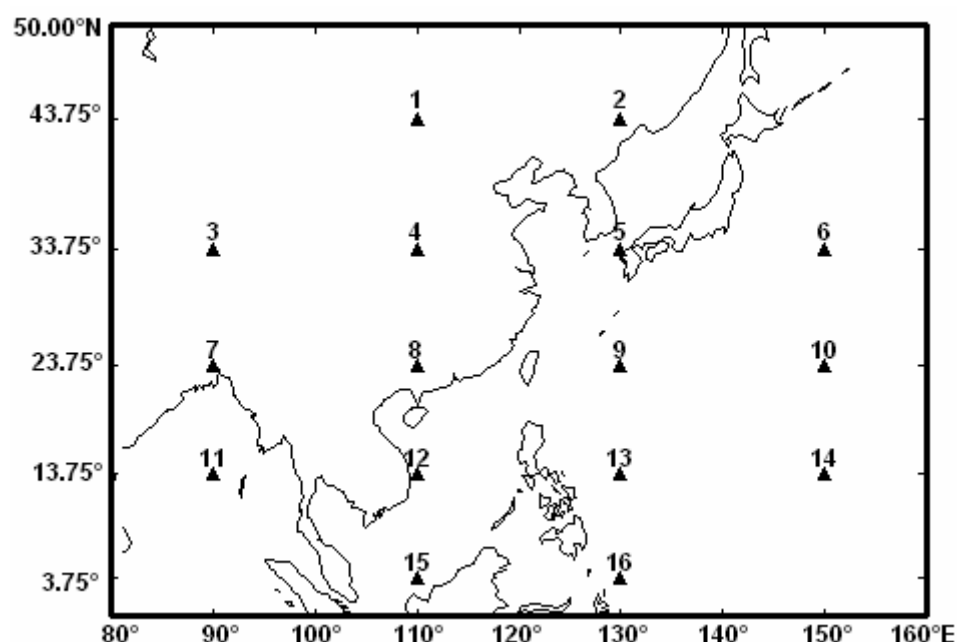


Figure 3.5: Grid used in the objective circulation-typing scheme (Regional Area).

The calculation of the flow and vorticity parameters for the grid is shown in this example below for the local area (Figure 3.4) and the calculation for the regional area is shown in Appendix one:

- westerly flow (W): the westerly component of geostrophic surface wind calculated from the pressure gradient between 21.25° N and 26.25° N;
- southerly flow (S): the southerly component of geostrophic surface wind calculated from the pressure gradient between 117.5° E and 122.5° E;
- resultant flow (F): total resultant westerly and southerly flow;
- direction (dir): in degree (0 to 360 °) of the resultant surface wind obtained from w and s , the directional category is calculated on a eight-point compass with a resolution of 45 ° (e.g. NE occurs between 22.5 ° and 67.5 °);
- westerly shear vorticity (ZW): difference of the westerly flow between 18.75° N and 23.75° N minus that between 23.75° N and 28.75° N;
- southerly shear vorticity (ZS): difference of the southerly flow between 23.75° N and 127.5° E minus that between 23.75° N and 112.5° E;
- total shear vorticity (Z): the sum of westerly and southerly shear vorticity.

All the indices, listed above, are calculated from the grid-point values using the following equations (adapted from Jenkinson and Collison, 1997; Jones *et al.*, 1993):

$$W = 0.5(12+13)-0.5(4+5) \quad (3.1)$$

$$S = 1.09 [0.25(5+2x9+13)-0.25(2+2x8+12)] \quad (3.2)$$

$$F = (S^2 + W^2)^{1/2} \quad (3.3)$$

$$ZW = 1.11 [0.5(15+16)-0.5(8+9)]-0.91[0.5(8+9)-0.5(1+2)] \quad (3.4)$$

$$\mathbf{ZS} = 0.6 [0.25(6+2x10+14)-0.25(5+2x9+13)-$$

$$0.25(4+2x8+12) +0.25(3+2x7+11)] \quad (3.5)$$

$$\mathbf{Z} = \mathbf{ZW} + \mathbf{ZS} \quad (3.6)$$

The classification scheme is based on values of total shear vorticity \mathbf{Z} , the resultant flow strength \mathbf{F} , and direction. The numbers 1-16 refer to the grid-points shown in Figure 3.2 and 3.3. The geostrophic flow and vorticity units are expressed as hPa per 10° latitude at the central latitude (23.75° N). The constants (1.09, 1.11, 0.91, and 0.60) for local area, calculated following the method of Dessouky and Jenkinson (1975), reflect the relative differences between the grid-point spacing in the north-south and east-west direction used here. The multipliers (0.5 and 0.25) reflect the number of grid points used here.

The rules to identify the Lamb Weather Types are based on the definition of Jenkinson and Collison (1977), as follows:

1. The direction of flow is $\tan^{-1} (W/S)$. Add 180 degrees, if W is positive.
2. If $|\mathbf{Z}|$ is less than \mathbf{F} , flow is essentially straight and corresponds to a Lamb pure directional type.
3. If $|\mathbf{Z}|$ is greater than $2\mathbf{F}$, then the pattern is strongly cyclonic ($\mathbf{Z} > 0$) or anticyclonic ($\mathbf{Z} < 0$). This corresponds to Lamb's pure cyclonic and anticyclonic type.
4. If $|\mathbf{Z}|$ lies between \mathbf{F} and $2\mathbf{F}$ then the flow is partly (anti-) cyclonic and corresponds to one of Lamb's synoptic/direction hybrid types, e.g. AE.
5. If \mathbf{F} is less than threshold and $|\mathbf{Z}|$ is less than threshold, there is light indeterminate flow, corresponding to Lamb's unclassified type, U.

In this study, 27 different weather types, following Lamb's classification, were initially identified (Table 3.2). The \mathbf{F} and \mathbf{Z} threshold values, used to define the unclassified type (U type), were modified in light of the features of the lower-latitude zone under analysis. The original threshold value of LWT scheme for British Isles is six. The

threshold values for this study were selected by comparison with experience in other mostly middle-latitude regions, modified after experimentation for use in this lower latitude region. In experimenting with different thresholds, the key concern was to define an appropriate range of weather types without too many undefined days. The main difficulty here lay in the consistency and, in the case of undefined days, low wind speeds, of the Taiwanese weather patterns. A threshold for U was determined on the basis of an acceptable number of undefined days, ensuring that the categorisation was realistic through consideration of the actual weather patterns. Therefore, the thresholds for the local and regional scale selected were 1.5 and 3.5, respectively.

The monthly frequencies of the 27 circulation weather types show that certain weather types, particularly for the northwesterly type and its hybrid types, are relatively infrequent over the study areas. Given that small sample sizes are unsuitable for trend analysis and other statistical analyses, these infrequently occurring types, whose relative frequencies are less than 2% at both scales, were eliminated. However, this process may cause the elimination of any high ozone days (HOD_3) related to infrequently occurring types. To avoid analytical bias in the investigation of the link between ozone pollution and circulation type, one more type, which is the CNE type, is retained, though its relative frequency is less than 2%. Thus, there are 14 circulation types (Table 3.3) retained for occurrence frequency analysis and the investigation of the relationship between circulation type and ozone pollution.

Table 3.2: The original 27 weather types from Lamb's weather category.

Anticyclonic types	Cyclonic types	Directional types	Unclassified
A	C	NE	U
ANE	CNE	E	
AE	CE	SE	
ASE	CSE	S	
AS	CS	SW	
ASW	CSW	W	
AW	CW	NW	
ANW	CNW	N	
AN	CN		

Table 3.3: The 14 weather types from Lamb's weather category

Anticyclonic types	Cyclonic types	Directional types	Unclassified
A	C	NE	U
ANE	CNE	E	
AE	CE	SE	
ASE		S	
ASW		SW	

3.6 Back Trajectory Analysis

Trajectories are defined as the paths traced by moving particles of air (Dutton, 1976). Back trajectories describe where an air parcel came from and forward trajectories indicate where it will go. Air trajectory models have been used to study dynamical processes in the atmosphere for several decades but developed into numerical methods more recently (Draxler and Hess, 1997, 1998; Stohl, 1998; Abdulkogith and Harrison, 2005). The applications vary from synoptic meteorology to climatology and the environmental sciences, for instance, to determine the potential source regions of measured airborne pollutants (Draxler, 1996; Stohl, 1998). During the early stage of development, trajectory models were based on simple advection schemes to calculate the prior position of an air parcel by using estimated wind speed and direction, for the time period, of a particular monitoring site (Stohl, 1998; Kleiman and Marin, 2002). The present study uses the Hybrid Single-Particle Lagrangian Integrated Trajectory (HYSPLIT_4) model an improved version of the earlier models (Draxler and Hess, 1997, 1998) to study long-range transport pathways of pollutants/precursors from potential emission source regions to Taiwan. The model results are compared with the weather type classification results and regional circulation patterns to investigate the relationship between long-range transport and high ozone pollution episodes in Taiwan. In this study, the model was run through the Real-time Environmental Applications and Display sYstem (READY) via the website (Draxler and Rolph, 2010).

The Hybrid Single-Particle Lagrangian Integrate Trajectory (HYSPLIT) model was designed by the NOAA Air Resources Laboratory (ARL) to support a wide range of simulations related to the long-range transport, dispersion and deposition of pollutants using previously gridded meteorological data (Draxler and Hess, 1997, 1998). It can be

applied to respond to atmospheric emergencies (accidental radiological releases or volcanic ash eruptions), routine air quality assessment and climatological analysis. The evolution of the HYSPLIT model has been through several stages over the past decades. The initial version (1982) used only rawinsonde observations and only with uniform daytime mixing of the dispersion calculation. In the next revision (1988), a temporally and spatially varying diffusivity profile was introduced for variable strength mixing. In the HYSPLIT_3 version (1992), input data were replaced by gridded meteorological data from either analyses or short-term forecasts. In the current version (HYSPLIT_4), the advection algorithms have been substantially improved with updated stability and dispersion equations (Draxler and Hess, 1997). The computation of dispersion rate is from the vertical diffusivity profile, wind shear and horizontal deformation of the wind field. A three-dimensional particle dispersion routine has been added to compute air concentrations from the dispersal of an initial fixed number of particles.

Atmospheric dispersion modelling is usually divided into Eulerian and Lagrangian models (Dutton, 1976; Draxler and Hess, 1998). Eulerian models solve the advection-diffusion equation on a fixed grid, especially when complex emission scenarios are considered, requiring solutions at all grid points. The advection and diffusion components calculation of Lagrangian models is handled independently. These models can be used to tackle the cases of single-point-source emissions with restriction of a few grid points' computations. The calculation method of HYSPLIT_4 is a hybrid between the Eulerian and Lagrangian approaches. It is based on a Lagrangian framework of advection and diffusion calculations, while concentrations are calculated on a fixed grid. This method results in short calculation time advantages. The approach of HYSPLIT_4 is to combine both puff and particle methods by

assuming a puff distribution in the horizontal and particle dispersion in the vertical direction. Based on the dispersion calculation of Lagrangian model computed following the particle or puff method, the advection of a single pollutant particle is computed independently in the HYSPLIT_4 model.

The procedures of trajectory calculation consist of meteorological data pre-processing and advection calculations. Data pre-processing is necessary to maintain a larger degree of flexibility within HYSPLIT's internal structure so that meteorological data from different sources with, for example, different resolutions can be used. Meteorological data fields may be provided on one of four different vertical coordinate systems: pressure-sigma, pressure-absolute, terrain-sigma, or a hybrid absolute-pressure-sigma. The input parameters can vary by different sources of meteorological data. The time integrated advection of each particle can be viewed as a simple trajectory. It is computed from the average of the three-dimensional velocity vectors, which are linearly interpolated in both space and time. Position (P) computed from average velocity (V) at the initial position $P(t)$ and the first-guess position $P'(t+dt)$ is

$$P'(t+dt) = P(t) + V(P,t) dt \quad (3.7)$$

The final estimated position is

$$P(t+dt) = P(t) + 0.5 [V(P,t) + V(P',t+dt)] dt \quad (3.8)$$

The integration time step (dt) can vary. However, the limitation is that the advection distance per time-step should be less than 0.75 of the meteorological grid spacing. The input data and parameters used in this study are shown in Table 3.4.

Table 3.4: The implementation of HYSPLIT_4.

Model	HYSPLIT version 4
Vertical coordinate system	Pressure-sigma
Meteorological data source	NCEP/NCAR reanalysis dataset
Input parameters	U,V wind components, Temperature, Height, Pressure, the Pressure at the surface, Relative Humidity

The current version of HYSPLIT model has been improved since the first version of the model was designed in 1982. The evolution includes the revision of the algorithms and equations based upon the more recent literature. The advantages of HYSPLIT_4 model in present study are as follows:

- Execution with multiple nested input data grids: Data Assimilation System data, Global Data Assimilation System data and NCEP/NCAR reanalysis data.
- Forecasts and archives meteorological data are available, such as produced by the NCEP/NCAR data.
- Trajectory ensemble option using meteorological variations.
- Single or multiple simultaneous trajectories.
- Option grid of initial starting locations.
- Graphics displayed both Postscript files and illustration formate, such as GIF.

However, the accuracy of trajectory calculations is considered to be affected by the temporal and spatial resolution of the meteorological input (for example, interpolation errors), measurement errors, analysis error, receptor location and from any

assumptions (for example, vertical wind component) used in the trajectory model (Draxler, 1991; Stohl, 1998; Harris *et al.*, 2005). Trajectories and air concentration accuracy of the HYSPLIT_4 model have been evaluated by Chemical tracer gases (Across North America Tracer Experiment) and balloon trajectories (Aerosol Characterization Experiment) (Draxler, 1991; Stunder, 1996; Draxler and Hess, 1998). These studies showed that trajectory error ranged from 10 to 30 per cent of the total transport distance. The range of error percentage is affected by travel time, the strength of wind flow and vertical height. Therefore, model results are sensitive to the vertical atmospheric structure, when near ground-level, as strong wind gradients and direction can result in a high inaccuracy for the trajectory simulations (Draxler and Hess, 1997, 1998). Given the meteorological character of the study area in this study, in particular, the generally stable, low wind speed conditions, these factors are not considered as serious weaknesses but should be borne in mind.

For this study, the main benefit of using the HYSPLIT_4 model is that one of the input meteorological data options, NCEP/NCAR reanalysis data, is the same data source used for the weather type classification and regional scale atmospheric circulation analysis in this thesis. This ensures consistency in data sources across the study. Other advantages are the short execution time, easily accessible user interface and a comprehensive quality evaluation system.

In estimating back trajectories in this study, the following conditions apply:

1. the trajectory is calculated 72 hours back in time with a six-hour timestep from 04:00 UTC¹ of the high ozone pollution day; and ,
2. the locations of Taiwan are tracked both in the north (25°N , 121.3°E) and south (22.5°N , 120.5°E).

The initial starting time is set by the local peak ozone concentration. The atmosphere is divided into three layers above ground level: 100m, 500m, and 2000m. The level selection is to observe how the pollutant transport varies from the surface to higher altitudes.

3.7 Spatial Compositing

Spatial compositing techniques have been used in various applications in meteorology and climatology (Barry and Perry, 1973). In this application, it confirms the interpretation of the weather types and also adds broader spatial information to aid the definition of the behaviors of the large-scale atmospheric circulation. In this study, the spatial compositing approach can reveal the main features of large-scale atmospheric circulation common to high ozone pollution events, reducing random features or noise. The spatial composite maps are derived from the diagnostic variables from the NCEP/NCAR reanalysis data (for example, geopotential height). The main series of

¹ The setting up of start time from 04:00 UTC is concerned that the local time is eight hours ahead of universal time. The setting is based on the occurrence of high ozone concentration at local time.

composite maps are determined by averaging the geopotential height during a set of high ozone pollution days (HOD₃) (Appendix two). The results are displayed as the absolute values and as the difference between the means for the high ozone pollution days and the long-term pattern for the relevant time of year. Composites are also calculated for non-pollution days as a control. The selection of non-pollution days consists of two procedures: (1) total number of days (N_{total}) in each month of eleven years (1994-2004) minus the days with high ozone concentration over 60 ppb defined as HOD (see section 3.3.3) in each month of eleven years, (2) non-pollution days are selected from the rest of days (N_{rest}), without HOD, of each month by using random sampling method of Excel software. The number of non-pollution days (N_{non-p}) is equal to the number of pollution days defined as HOD₃ (see Section 3.3.3) in each high ozone pollution month which is April, May, June, September, October and November (Table 3.5).

Table 3.5: The sample sizes for non-pollution days' selection in high ozone pollution months for the period 1994-2004.

Month	N_{total}	HOD	N_{rest}	HOD ₃	N_{non-p}
April	330	92	238	22	22
May	341	117	224	29	29
June	330	41	289	10	10
September	330	92	238	19	19
October	341	119	222	32	32
November	330	67	263	10	10

The statistical significance of the difference between the mean fields is assessed by Cramer's test. Cramer's test is similar to Student's *t*-test and tests significance when a small sample of events is drawn as a subset from a longer period of data (Mitchell *et al.*, 1966). The null hypothesis used for all tests is that 'the anomaly is not significantly different from zero, i.e. that the control and perturbation variable samples being considered have the same mean. If the null hypothesis is correct, the test statistic has a *t* distribution. A rejection of the hypothesis at a level of 5% means there is only a 5% probability that the difference in the mean is a result of chance, i.e. there is 95% probability that there is an 'actual' difference. The 5% level will be used throughout this study for significance testing. The Cramer's test is computed as:

$$t_c = T_c * [\{ n(N-2) \} / N - n(1 + T_c^2)]^{1/2} \quad (3.9)$$

$$\text{where: } T_c = (m_2 - M_1) / S \quad (3.10)$$

there are $(N-2)$ degrees of freedom

S is the standard deviation of the entire record of N values

M_1 is the mean of the entire record of N values

m_2 is the mean of the sub-period of n values

In this study, the sub-periods will be the number of high ozone pollution days, which are categorised by months, and the whole period is taken to be the 1994-2004 period.

Table 3.6: Summary of research design

	Analysis	Method	Data
1. What are the characteristics of high ozone pollution episodes and their variability over Taiwan?	Define high ozone pollution events	Define high ozone pollution indices based on air quality standards.	Taiwan Air Quality Monitoring Network (TAQMN) data cover the period from 1994 to 2004.
	High ozone pollution areas and seasonal variation analysis	Descriptive statistics	
2. Is there evidence that regional and large-scale atmospheric circulation patterns are linked to the occurrence of high ozone pollution days?	The features of local synoptic weather type patterns during high ozone pollution occurrence	Objective circulation classification scheme	Sea Level Pressure data
	Large-scale atmospheric circulation and anomaly patterns of high ozone pollution days	Spatial compositing and Cramer's test	Geopotential Height data at 850hPa and 500 hPa levels
3. What is the role of long-range transport and other circulation mechanisms, including the dominant monsoonal circulation of the region?	Potential pollutants source region investigation.	Back trajectory analysis (HYSPLIT Model)	Input meteorological data for back trajectory analysis based on NCEP/NCAR Reanalysis data

Chapter 4: Observed Annual and Seasonal Trends of Ozone

4.1 Introduction

This chapter presents annual and seasonal variations in ozone pollution from 1994 to 2004. The occurrence of high ozone episodes, the overall seasonal cycle and interannual variability and trends are linked to changes in atmospheric circulation features over Taiwan in order to define a framework for the later analysis of links between ozone trends and the large-scale atmospheric circulation.

4.2 Annual Trend of Ozone Pollution

4.2.1 Selection of High Ozone Episodes and High Pollution Zones

The definition of high ozone episodes (HOEs) is daily eight-hour average ozone concentration ≥ 60 ppb. In the 64 stations of the network, there are a few stations with a low frequency of high ozone episodes, less than 1% in the eleven-year record. The elimination of these stations has made it easier to distinguish high ozone pollution areas and low ozone pollution areas. This process leaves 53 stations in ten administrative areas of five air quality zones (North, Chu-Miao, Central, Yun-Chia-Nan, and Kao-Ping); all five air quality zones are distributed around the western plain, from north to south Taiwan (see Figure 3.3). The second index (HOD) used in this study is to examine whether or not the high ozone episodes identified at each station are geographically isolated episodes. In addition, the third index (HOD_3) is defined to

eliminate the influence from localized pollution episodes. The definition of each index (HOEs, HOD and HOD₃) has been presented in the previous chapter (see Section 3.3.3).

4.2.2 Annual Distribution of High Ozone Episodes

Table 4.1 statistically summarizes the annual number of HOEs, HOD and HOD₃ in the high ozone pollution areas from 1994 to 2004. The table shows that there are 1,334 HOEs (from 273,020 records) in 53 monitoring network stations. Although these high ozone episodes only occupy a small proportion in the total record, the occurrence of episodes has increased dramatically, by seven-fold from 1994 to 2004, with values of 30 episodes in 1994 and 209 episodes in 2004 (Figure 4.1).

Table 4.1: The statistical result of HOEs, HOD and HOD₃ from 53 network stations for the period 1994-2004. The fifth row is high ozone day (HOD) occurrence frequency of per year.

Year	1994	1995	1996	1997	1998	1999	2000	2001	2002	2003	2004
HOEs (days)	30	31	64	56	133	129	86	149	181	266	209
HOD (days)	24	28	40	42	52	61	63	71	76	77	105
HOD ₃ (days)	1	1	8	4	13	18	4	14	22	20	22
HOD/year	7%	8%	11%	12%	14%	17%	17%	19%	21%	21%	29%

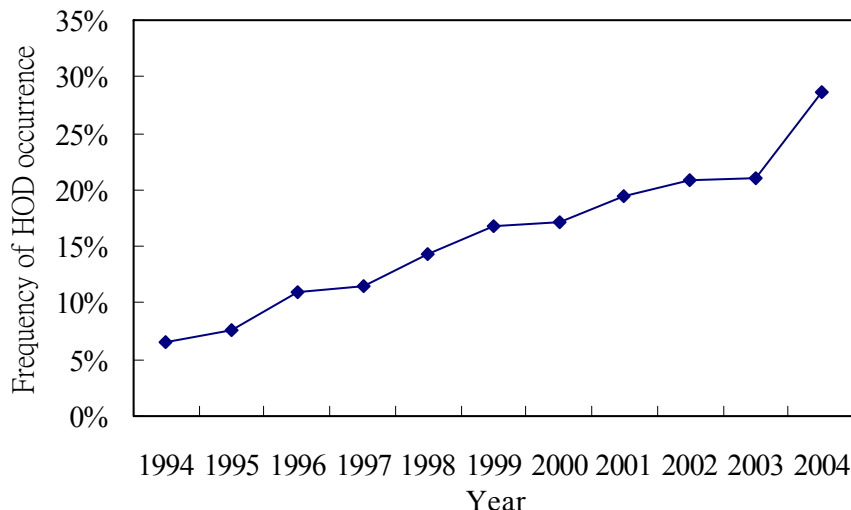


Figure 4.1: The frequency of high ozone days (HOD) occurrence, based on the 53 station network, from 1994-2004.

It is noted that about half of high ozone episodes occurred in the period 2002 - 2004, as did the cases of HOD and HOD₃. The result is consistent with Chang and Lee (2007) who indicated that the occurrence of moderately high ozone concentrations (ozone concentration ≤ 60 ppb, 8-hr average) showed an upward trend in recent years, particularly in northern Taiwan. From daily ozone concentration data analysis, there are three network stations, Matsu, Kinmen and Penhu,¹ located in the Taiwan Strait (see Figure 2.4) which is a low local emission region without heavy industry, which also show a great number of high ozone episodes in 2002-2004. The data of Matsu, Kinmen and Penhu stations suggest that long-range transport of ozone or its precursors

¹ The Matsu, Kinmen and Penhu stations were established to monitor air pollutants' concentration as reference stations in 2001, 2002 and 2003, respectively. Because of their location and low local emissions (the economy of these areas is based on tourism without industries), the data of these stations are favourable to identify long-range transport of air pollutants from mainland China, though there are only a few years data available (EPA Taiwan, 2004).

from mainland China might be the reason for the sharp increase in frequency of high ozone episodes in 2002 – 2004, however, the source of ozone and its precursors may vary with seasons.

Notably, there is a distinctive drop in the number of HOEs in the year 2000, compared with the eleven-year upward trend of ozone (Figure 4.2). The most probable explanation of this dramatic decrease of high ozone episodes in the year 2000 seems to be associated with variation of the large-scale circulation. Wang (2005) quantified the airstreams over the East Asia region and indicated that the airstreams from northern China increased about 20-23% in frequency during the 2000 spring. The characteristic of the airstreams shows a spatial distribution from close to the Gobi desert area which is one of the major sources of dust storms (Sun *et al.*, 2001; Kurosaki and Mikami, 2003; Wang *et al.*, 2008) to the East Asian continent and low latitudes (Wang, 2005). These kind of airstreams follow a cold front and usually transport a significant amount of dust material entrained from the Gobi area and through the Asian continent southeastward to Taiwan with the prevailing wind, particularly in spring and winter (Lin, 2001; Lin *et al.*, 2005; Liu *et al.*, 2006; Hsu *et al.*, 2008). The impact of dust storms on Taiwan is mainly in the northern area (Liu *et al.*, 2006), which is also the major location of high ozone pollution episodes in spring.

In spring 2000, a significant peak value of PM₁₀ was observed in Taiwan compared with a downward trend in PM₁₀ concentration over a nine-year period (1994-2002) (Wang, 2005). The anomalously high PM₁₀ concentration was caused by severe dust events. About 12 dust events were observed in 2000 spring (Lin, 2001; Liu *et al.*, 2006). The airstreams not only enhanced PM₁₀ concentrations during the period of dust storms, but also brought cold temperature and high wind speeds which blew local

pollutants away, as there was no obvious diurnal cycle of air pollutants during the period of dust storms (Lin *et al.*, 2004, 2007; Xie *et al.*, 2005; Liu *et al.*, 2006). Lin *et al.*, (2004) found that air pollutants and dust are usually transported in different air parcels associated with the transport paths and atmospheric boundary conditions.

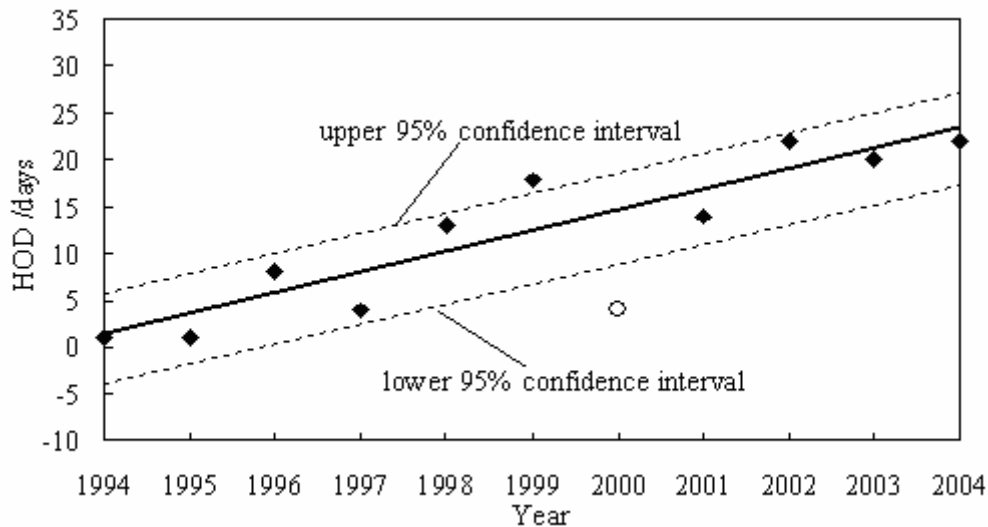


Figure 4.2: The annual trend of HOD₃ (days). The solid line is associated trend line between 1994 and 2004 obtained by the least-square regression method, and the dashed lines are the trend lines with upper and lower 95% confidence interval. The open circle indicates high ozone days in year 2000, and the diamonds indicate high ozone days of other years.

This means that ozone or its precursors are probably not transported to Taiwan simultaneously during severe dust storms. Although some of the stations where dust fall was first detected observed increasing ozone concentrations along with PM₁₀ (Lin *et al.*, 2004; Liu *et al.*, 2006), the meteorological conditions along with airstreams are not favourable for the accumulation of ozone. Furthermore, the effects of dust aerosols, such as increased aerosol optical depth, reduction of visibility and solar radiation, and surface temperature cooling (Charlson *et al.*, 1992; Husar *et al.*, 2001; Ogunjobi *et al.*, 2004; Eck *et al.*, 2005; Huang *et al.*, 2006) also influence ozone formation processes. It is concluded that there are two reasons that may have resulted in low high ozone

episodes in spring 2000: (1) the limitation of ozone and its precursors' sources (both local and regional). (2) both the meteorological features of the airstreams and the influence of dust aerosols suppressed photochemical activity for ozone formation.

In spite of the exception of 2000, the annual frequency of high ozone pollution shows positive trends in three indices (HOEs, HOD and HOD₃) during the period 1994 to 2004. The explanation of these upward trends of high ozone pollution needs to consider the emission variation of ozone precursors both in local and regional areas and long-range transport of ozone and its precursors from vicinity areas.

4.2.3 Annual Trend in Five High Ozone Pollution Zones

Based on the abovementioned pollution area selection, there are five air quality zones (North, Chu-Miao, Central, Yun-Chia-Nan, and Kao-Ping zones) identified as high ozone pollution zones (see Figure 3.3). The annual trends for high ozone days (HOD) and ozone concentrations are evaluated by linear regression analyses. The values of trend line slope, standard errors (SEs), and coefficient of determination (R^2) for HOD and annual average ozone concentrations are shown in Tables 4.2 and 4.3, respectively. The standard error is used to calculate the interval of the confidence level of slope with the significance level of 5%. The R^2 value is used to identify the reliability of slope. When the value of R^2 approaches one, the calculation of trend line slope has high reliability. In the five air quality zones, the annual number of HOD all show an increasing tendency. The annual increasing trends of HOD in the North and Kao-Ping (South) zones are obviously higher than in the other three zones (Table 4.2 and Figure 4.3). For the eleven-year period, the annual number of HOD has increased by about

12% relative to 1994 in the North and Kao-Ping zones; for the other three zones, the annual number of HOD has only increased about 4% (Figure 4.3). In regard to analyses of the annual average ozone concentrations for the five air quality zones, the results indicate that the annual ozone concentrations gradually increase about 2% year by year (Table 4.3 and Figure 4.4). The magnitude of the increase of the annual average concentration is from about 0.70 to 0.82 ppb year⁻¹. The results of trend analyses suggest that there may be more moderate ozone pollution (ozone concentration \leq 60 ppb, 8-hr average) in the North and Kao-Ping zones than extreme high ozone pollution, as there is a slight increase in the annual average ozone concentrations with an apparent larger increase in the annual number of HOD over the period 1994-2004.

Table 4.2: The trend line slope, standard errors (SEs), and coefficient of determination (R^2) estimated using linear regression for high ozone days (HOD) from 1994 to 2004.

	North	Chu-Miao	Central	Y-C-N	Kao-Ping
Slope	4.95	0.84	1.32	1.21	3.66
SE	0.91	0.66	0.72	0.56	0.88
R^2	0.86	0.34	0.60	0.66	0.63

Table 4.3: The trend line slope, standard errors (SEs), and coefficient of determination (R^2) estimated using linear regression for annual average ozone concentrations.

	North	Chu-Miao	Central	Y-C-N	Kao-Ping
Slope	0.77	0.80	0.70	0.82	0.74
SE	0.05	0.09	0.07	0.09	0.06
R^2	0.93	0.70	0.70	0.84	0.85

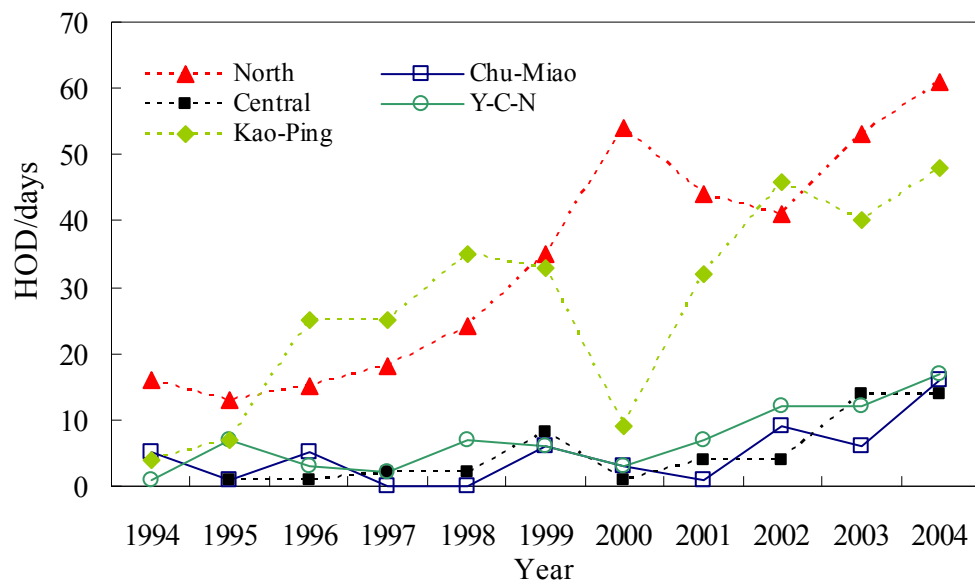


Figure 4.3: The annual trends of HOD in five high ozone pollution zones from 1994-2004.

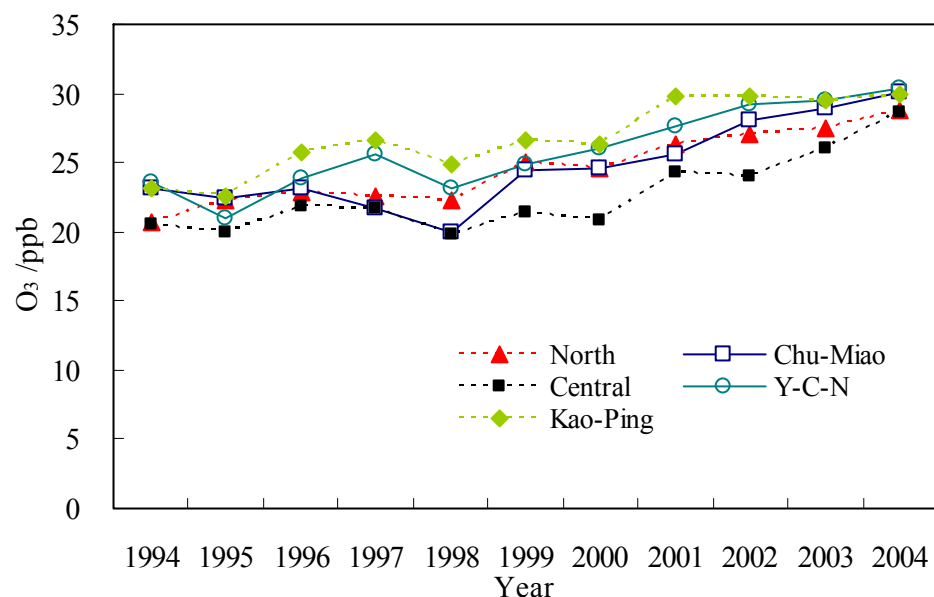


Figure 4.4: The annual average of ozone concentrations in five zones from 1994-2004.

A dramatic difference in the number of HOD between the North zone and the Kao-Ping zone can be seen for year 2000. There are about 53 HOD in the North zone, compared with nine days in the Kao-Ping zone in 2000. The reduction in HOD in the Kao-Ping zone is caused by the decrease of total high ozone episodes (HOEs) in 2000 (Table 4.1), as the reduction in the other three zones presents less influence. A further investigation of each high ozone episode shows that most HOEs occurred at one station (Yangming station) in the North zone. Because the height of Yangming station (25.10'57"°N and 121.31'46"°E) is more than above 850m of the sea level, Yangming station is overlain by stratus clouds and moist air from the northeastlies most time of year. The topography and climatic features of Yangming station are favourable for particle deposition during dust storms as they arrive at Taiwan (Liu *et al.*, 2006). Thus, a sudden escalation of PM₁₀ at this station was not paralleled by an increase in ozone concentrations during spring of 2000. In addition to the particle deposition, the effect of NO_x destruction on ozone formation processes (see Section 2.2.1) at Yangming station should be considered, as Yangming station is a background station in the monitoring network.

4.3 Seasonal Distribution of High Ozone Days (HOD)

Vukovich (1994) pointed out that meteorological change is one of the factors that causes year-to-year variation of tropospheric ozone. The changes in tropospheric ozone may, for example, be associated with variations in synoptic patterns or an increase in the stagnation of circulation (Davies *et al.*, 1992; Comrie, 1994; Liu *et al.*, 1994; Lelieveld and Dentener, 2000). Liu *et al.* (1994) indicated there was no significant linear relationship between meteorological variables and ozone pollution in Taiwan, however, the effect of synoptic patterns on the variation of ozone pollution was well-founded. Cheng (2001) also found that ozone concentrations over central Taiwan were strongly affected by synoptic patterns and with an evident seasonal cycle.

Considering the conditions of ozone formation and weather conditions in Taiwan, a seasonal pattern in the occurrence of high ozone pollution episodes is to be expected. In this study, the conventional meteorological classification of four seasons in a year is adopted, namely, spring consists of March, April, and May (MAM); summer consists of June, July, and August (JJA); autumn consists of September, October, and November (SON); and winter consists of December, January, and February (DJF) (see Section 2.3.1). Figures 4.5 and 4.6 present the seasonal variation of HOD from 1994 to 2004; most HODs occur in spring and autumn (transition seasons). The seasonal distribution of HOD corresponds with results from studies of the seasonal behaviour of ozone concentrations in East Asia (Chan *et al.*, 1998; Tanimoto *et al.*, 2002; Chen *et al.*, 2004; Oltmans *et al.*, 2006; Yamaji *et al.*, 2006; Yu and Chang, 2006).

Figure 4.5 depicts the seasonal distribution of HOD in the five air quality zones. Two peaks of high ozone days show in the transition seasons, spring and autumn, in Taiwan.

In the five air quality zones, the variation of seasonal distribution is clearly to be observed in the North zone and the Kao-Ping zone. For the North zone, the first peak period with a high frequency of high ozone days appears in spring (172 days), and the second peak appears in autumn (121 days), while the lowest frequency occurs in summer (38 days). In contrast, the Kao-Ping zone displays opposite distribution, the first peak period shows in autumn (154 days), the second peak shows in spring (109 days), and a similar pattern of a summer minimum (19 days). The data indicate that the effect of ozone pollution on air quality in the North zone in spring is greater than in other seasons and in the Kao-Ping zone in autumn. The discrepancy of seasonal distribution of HOD in both the North and Kao-Ping zones is consistent with the results from studies by Chen, *et al.*, (2004) and Yu and Chang (2006).

In addition to the seasonal variation of high ozone days, Figure 4.6 shows that the occurrence of high ozone days exhibits elevated trends in all seasons. Further investigation of monthly trend during the period 1994 to 2004, a regular increase of high ozone days (HOD) is observed in March, and December (Figures 4.7a and b). Otherwise, February, June and October show marked increases of HOD (Figures 4.7a, c and d). Moreover, high amplitude fluctuations of HOD are observed in high ozone pollution months, for example, April, May, September and October (Figures 4.7b and d). This phenomenon suggests that the short-term variation of synoptic weather patterns, such as monsoon circulation, may result in influence on ozone pollution in Taiwan.

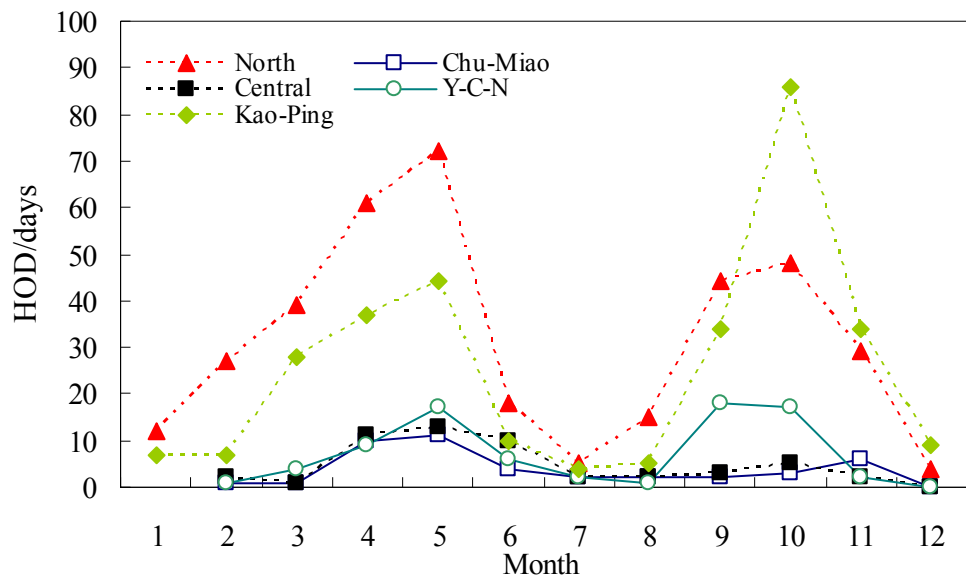


Figure 4.5: Seasonal distribution of HOD in five high ozone pollution zones.

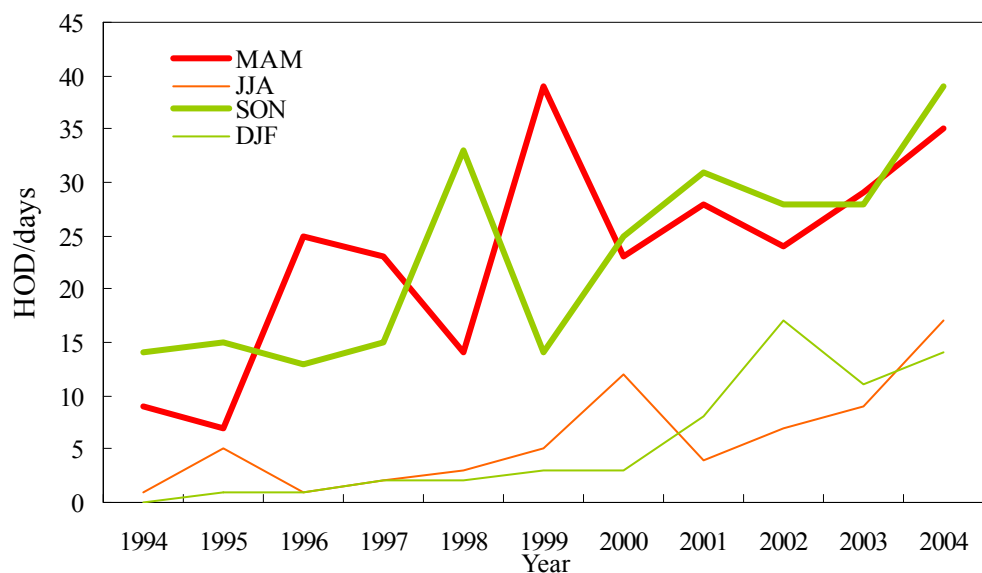


Figure 4.6: HOD climatology for winter (thin green line), spring (thick red line), summer (thin red line) and autumn (thick green line) for the period 1994-2004.

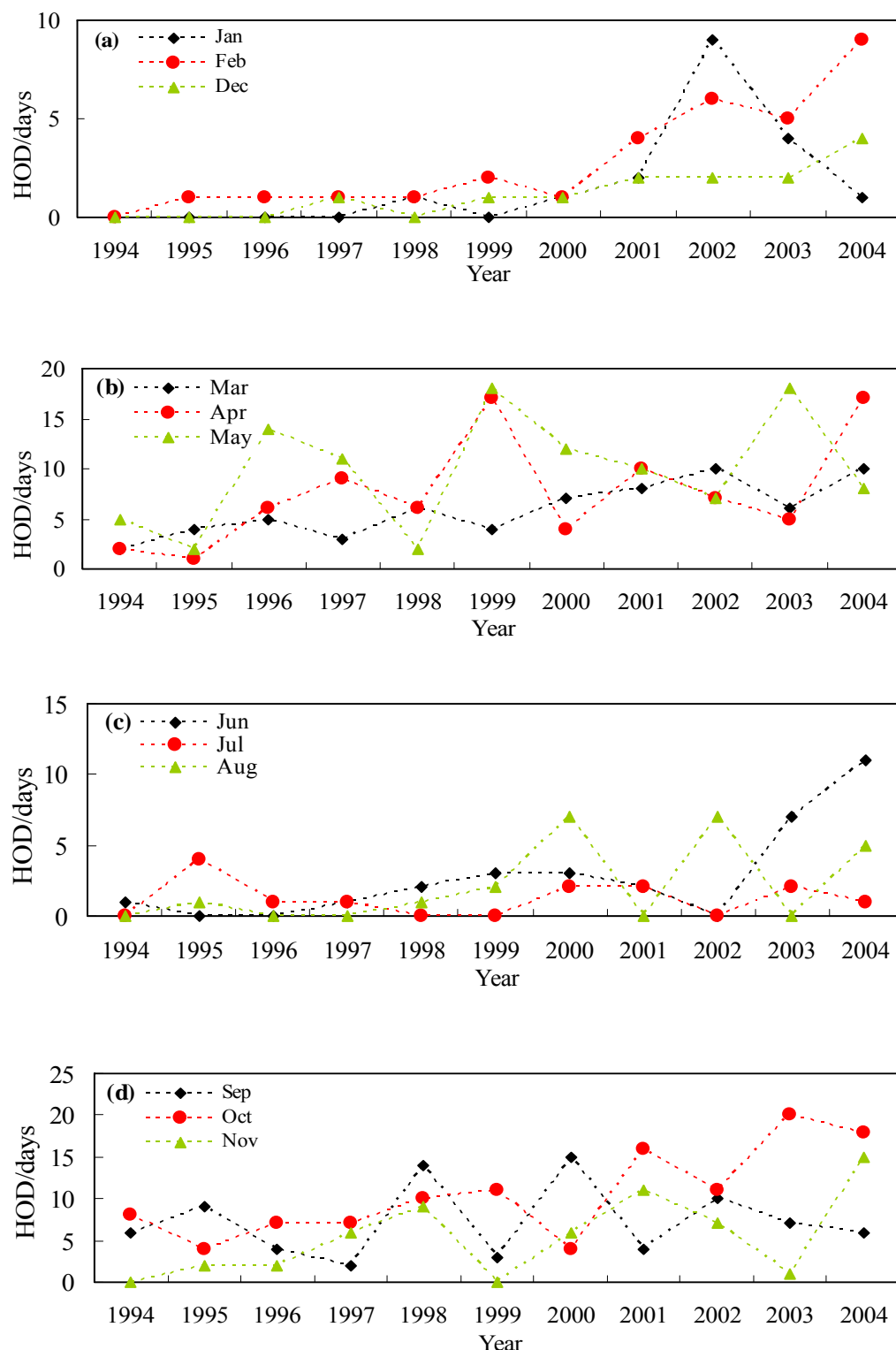


Figure 4.7: Monthly trend of HOD for four seasons (a) winter, (b) spring, (c) summer and (d) autumn for the period 1994-2004.

4.3.1 The Possible Effect of ENSO on Tropospheric Ozone

Seasonal Distribution.

It is important to note that the seasonal distributions show high amplitude fluctuations in 1998 and 1999. An evident decrease (increase) of HOD appeared in 1998 spring (autumn). By contrast, a sharp increase (decrease) of HOD shows in 1999 spring (autumn). The dramatic variation of seasonal distributions of HOD seems to be related to short-term variation of climate that might result from the effect of El Niño Southern Oscillation (ENSO).

McPhaden (1999) indicated that the year 1997-1998 was the strongest El Niño phenomenon on record and followed by an extended La Niña period that began in mid-1998 to the winter of 2000 and slowly decayed from the spring of 2001. In order to understand the correlation between ENSO and high ozone days, the data of ENSO indices anomaly sea surface temperatures (anomaly SST) were collected from the National Climate Data Centre (NCDC) website. Figure 4.8 shows monthly HODs distribution and SST anomaly. The diagram presents three phases (warm, normal and cold phases). The warm phase is defined as anomaly SST $\geq 0^{\circ}\text{C}$ and the cold phase is anomaly SST $\leq -0^{\circ}\text{C}$. There is only one period defined as normal phase (06/2001~01/2002), because of small fluctuation of SST. Based on these definitions, the study period has been separated into seven sub-periods to calculate the correlation between anomaly SST and high ozone days. The result of this analysis is that it is difficult to identify any correlation between ENSO and HOD. Nevertheless, indirect influences of ENSO might be a factor affecting seasonal distribution of ozone pollution in Taiwan. The variability of global climate might be the factor of the anomalous seasonal distribution of HOD observed in 1998 and 1999.

Chandra *et al.* (1998) and Ziemke and Chandra (1999) found that the interannual variations of Total column ozone (TCO) were associated with the shift in tropical convective activities caused by SST changes. During the El Niño period, the enhanced convection results in an increase in rainfall and water vapour which decreases TCO over the eastern Pacific, and a significant increase in TCO over the western Pacific is associated with suppressed convection and downward motion (Chandra *et al.*, 1998; Ziemke and Chandra, 1999; Sudo and Takahashi; 2001; Wang *et al.*, 2000; Chandra *et al.*, 2007).

In the western Pacific region, the interaction between suppressed convection and downward motion is the factor causing ozone in the lower-middle troposphere to increase. Otherwise, one more factor caused the increase of TCO over the western Pacific was forest fires in the Indonesia region during the 1997-1998 El Niño period, in particular in autumn and winter for 1997. There is, however, no apparent increase of tropospheric ozone in the later year of 1997 observed in Taiwan (Figure 4.7). According to Tie *et al.* (2007), there was less effect of forest fire in the Indonesia region on tropospheric ozone in East Asia compared with the contribution from industrial emission during the 1997 El Niño period. Moreover, the interaction among anomalous Pacific circulations results in different impact of synoptic weather patterns (i.e. rainy seasons) over East Asia on tropospheric ozone during the ENSO period (Wang *et al.*, 2000). Therefore, the variations of tropospheric ozone in Taiwan may be very different from the equatorial region of western Pacific.

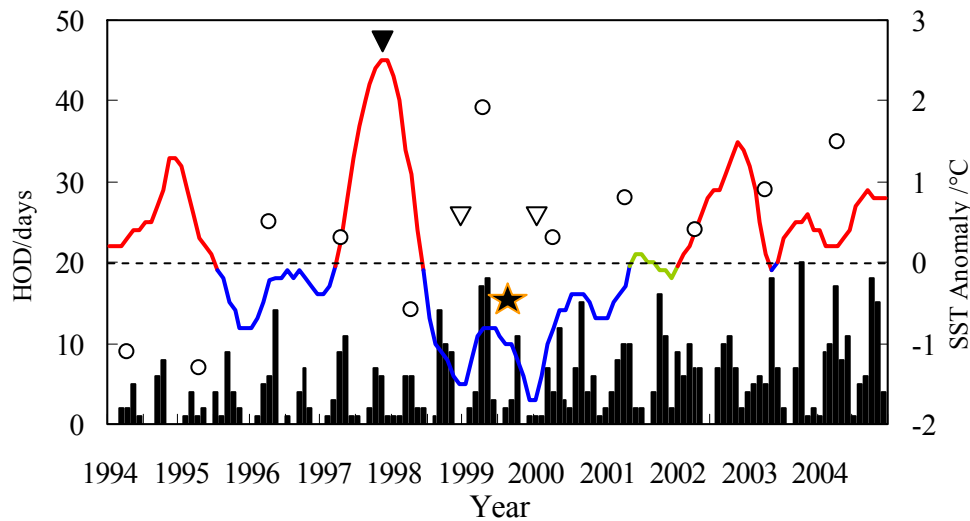


Figure 4.8: Monthly HOD distribution and SST anomaly over Niño 3.4 region (120W-170W, 5N-5S) for the period of 1994 to 2004. The red line represents warm phase of ENSO, the blue line represents cold phase of ENSO and the green line represents a normal phase. The triangle indicates a strong El Niño period and open triangles indicate a strong La Niña. The star symbols show the period with positive correlation between HOD and ENSO. The open circles indicate high ozone days in spring over study period.

Table 4.4: Significant Pearson correlation coefficients (at the 95% confidence interval level) identified between ENSO and high ozone days for three episodes.

Warm phases	Period	01/1994~06/1995	04/1997~05/1998	02/2002~05/2003	06/2003~12/2004
	r	0.04	-0.43	-0.36	-0.004
Normal phase	Period	06/2001~01/2002			
	r		-0.41		
Cold phases	Period	07/1995~03/1997	06/1998~05/2001		
	r	0.22	0.29		

The interplay between the Asian winter monsoon and ENSO plays an influential role in East Asian climate. The linkage between the climate of East Asia and ENSO has been found, for example, a weaker East Asian winter monsoon along the East Asian coast occurs during the mature phase of ENSO (Tomita and Yasunari, 1996; Zhang *et al.*, 1996; Wang *et al.*, 2000; Lu, 2006) and the relationship between the rainfall patterns and ENSO (Huang *et al.*, 2002; Chen *et al.*, 2003; Jiang *et al.*, 2003). Nevertheless, the effects of La Niña on climate show a reverse situation, especially in equatorial region (Glantz, 2002).

For the case of 1997 winter, in addition to the reduced effect of Indonesia forest fire on tropospheric ozone, the air-sea interaction in the western Pacific is a possible factor. During the 1997 El Niño period (October to December), the SST anomaly over the East Asian coast was warmer than normal winter (Kuo and Ho, 2004). In winter, the cold northeasterly winter monsoon moves through a warm ocean surface and creates vertical mixing in the boundary layer which is favourable for pollution dispersion to the upper-troposphere (Wang *et al.*, 2000), though the strength of the winter monsoon is weak. Therefore, there was less tropospheric ozone pollution observed in 1997 winter, as well as in autumn.

Chen *et al.* (2003) indicated that 1998 is the second wettest spring in Taiwan over the study period. The apparent decrease of HOD in 1998 spring (Figure 4.7 and 4.8 (B)) may be in response to heavy rainfall resulting from the El Niño effect on the East Asian climate, as the wet weather is favourable to dilute the concentrations of air pollutants. The correlation between spring rainfall and the Niño 3 SST has been proved and shows a positive correlation in Taiwan (Chen *et al.*, 2003; Jiang *et al.*, 2003). Some of the studies indicated that the variations and interactions of atmospheric convection over the

western Pacific, East Asia and Southeast Asia region are the major effects on extreme summer rainfall in East Asia during ENSO period (Zhang *et al.*, 1996; Tanaka, 1997; Wang *et al.*, 2000; Chen *et al.*, 2003; Jiang *et al.*, 2003; Lu, 2004; Yim *et al.*, 2008). In Taiwan, the synoptic circulation feature shows a seasonal cycle: it is mainly southwesterly in summer and northeasterly in the other seasons, and the strength varies with seasons (Kuo and Ho, 2004). There a strong southwesterly produced by the interaction between the circulations in the western North Pacific and Southeast Asia over Taiwan and northern South China Sea with heavy rain observed during El Niño (1998 spring) period (Wang *et al.*, 2000; Huang *et al.*, 2002; Chen *et al.*, 2003; Jiang *et al.*, 2003). Thus, the interaction of convection resulting from ENSO which brings heavy rainfall for Taiwan is the factor of dramatic decreasing HODs in spring for 1998.

In contrast to the influence of El Niño phenomenon, La Niña phenomenon presents a different seasonal influence on the East Asian climate. During the mature phase of La Niña, Taiwan is affected by a strong western North Pacific monsoon and dominated by a cyclone in the lower troposphere; the interaction between these two synoptic circulations caused an enhanced convection which increases the rainfall during the summer and autumn (Tanaka, 1997; Wang *et al.*, 2000; Chou *et al.*, 2003). Therefore, low high ozone days in autumns were observed in 1996 and 1999. There is, however, in the decaying of El Niño in the autumn of 1998 and the onset of La Niña in the spring of 1999, the interaction between the western North Pacific monsoon and Taiwan shows an opposition situation, a weak western North Pacific monsoon and anticyclone over Taiwan establish a suppressed convection, which is unfavourable to ozone pollution dispersion in Taiwan. In addition, the strength shift of northeasterly winter monsoon and the SST in the Taiwan Strait may result in the apparent number of high ozone days in 1998 autumn.

Consequently, the variability of climate resulting from the influences of ENSO, such as precipitation distribution, strong convection activity and the strength of monsoon circulations, might be the factors for the anomalous seasonal distribution of HOD in 1998 and 1999. Nevertheless, there is a need to further investigate the relationship between ENSO and ozone pollution through other ENSO index (i.e. Southern Oscillation Index) and climate factors (i.e. rainfall anomaly).

4.4 Conclusions

Based on an eleven-year ozone concentration data series, the annual trends of high ozone days (HOD), annual average ozone concentrations, seasonal cycle and geographical differences of ozone pollution have been obtained; however, the effect of the short record of daily ozone concentration data on the reliability and robustness of ozone pollution trend analyses should be noted.

The annual trends of HOD and annual average ozone concentrations in five air quality zones show obviously increasing trends, particularly for the North and Kao-Ping zones, for the period from 1994 to 2004. The seasonal cycle shows maxima in spring and autumn, in addition, a minimum season is observed in summer. In the North zone, the first peak season appears in spring, however, the maximum in the Kao-Ping zone is autumn. The seasonal cycle and geographical difference of ozone pollution may be affected by the onset and descent of monsoon circulation; however, the influences may vary with seasons.

Given the ozone pollution in Taiwan shows a clear seasonal cycle, an identification of the relationship between synoptic weather patterns and ozone pollution is necessary. The relevant studies which have been done in Taiwan are usually based on the results of subjective weather type classification. The identification of weather patterns related to high ozone episodes is subject to researchers' experience. Therefore, development of an objective classification scheme is necessary to improve the accuracy of synoptic weather patterns classification and the identification of its relationship with ozone pollution.

Based on the results obtained in this chapter, the high ozone days of HOD₃, an objective classification scheme is used to investigate the relationship between synoptic weather patterns and ozone pollution in chapter five. Also, a spatial composite analysis of geopotential height at 850hpa is used to identify the features of atmospheric circulation of high ozone pollution.

Chapter 5: The Objective Scheme of Circulation Types and Circulation – Ozone Links

5.1 Introduction

In this chapter, an identification of the relationship between ozone days and circulation types is performed, both at the local and regional scales. The main emphasis is on the circulation types characteristics of days with high ozone concentrations and on differences between the seasons. The analyses comprise frequency analyses of circulation types both over the long-term period and on ozone days. In addition, a complementary spatial compositing analysis of the atmospheric circulation at sea level pressure and 850hpa during ozone episodes is discussed.

5.2 Frequency and Climatological Analysis

The daily circulation is classified according to categories and thresholds of a set of indices associated to the vorticity and air flow, which are calculated from daily grid point sea level pressure (SLP) data (Jenkinson and Collison, 1977) (see Section 3.5). In order to investigate the influence of local and regional circulations on ozone pollution, two resolutions are used in this study for Taiwan daily circulation classification. One is for a local area window covering the area 17.5° N to 32.5° N and 110° E to 130° E, and the other one is for a regional area covering the area 0° N to 50° N and 80° E to 160° E, both centred on 23.75° N and the resolutions, for local and regional area, are 2.5° latitude by 5° longitude and 10° latitude by 20° longitude, respectively.

The relative frequencies (number of days with respect to the total) of each circulation type for every month of the year over two periods (1958-2004 and 1994-2004) for the two scales are shown in Figure 5.1 and Tables 5.1 and 5.2. The classification results covering the period from 1958 to 2004 are used to analyse the long-term trends in the annual, seasonal and monthly frequencies of circulation types; in addition, the period of 1994-2004 is used to analyse the links between ozone pollution days (HOD_3) (see Section 3.3.3) and circulation types.

The frequencies at the local scale show the most frequent circulation pattern throughout the year is the E type, followed by the northeasterly type (NE), which shows similar seasonal distribution with a winter maximum and a summer minimum (Figure 5.1a and Table 5.1). In the annual frequency, the U type also shows a high frequency. In the case of spring and summer, the U and A types are the most frequent weather types, as the synoptic circulation is mainly dominated by the Pacific anticyclone in this season (Tu *et al.*, 2003). The other two most common circulation types observed in summer are the southwesterly type (SW) and the cyclonic type (C), whereas the frequencies of these circulation types at the local scale are lower than the regional scale. The results of annual frequency analysis suggest that the main circulation types at the local scale are the E, NE, U and A types. In contrast to the local scale, the circulation types at the regional scale show large temporal variability (Figures 5.1c and d). The group of cyclonic and southerly types (including C, S and SW types) have a stronger seasonal cycle than the local scale, though the same peak season is summer (Table 5.1). Moreover, the anticyclonic type (A) shows lower frequency in autumn and maximum frequency in spring. The E and NE types are also the most frequent circulation types in the annual frequency, as the same as the cases at the local scale.

In terms of both local and regional scales, the fourteen circulation types display significant seasonal characteristics. The main circulation patterns of both scales show a similarity throughout the months, although the frequencies of circulation patterns can differ. The easterly type (E) is the most frequent circulation type on both scales; a hybrid type anticyclonic northeasterly (ANE) is the least frequent circulation type at the local scale; and the cyclonic northeasterly (CNE) type is the least frequent type at the regional scale (Figure 5.1a and c). Despite the key influence of the E and NE types for most seasons, the comparison between the local scale and regional scale indicates that the local scale has high frequencies of unclassified type (U) and anticyclonic type (A) in summer (Figure 5.1a and b). With a grid size of 17.5°N - 32.5°N x 110°E - 130°E being classified as local, this result is expected, because: (1) The climate in Taiwan is divided into subtropical and tropical climate zones, with long-period of low wind speed and warm weather characteristics, (2) the dominant synoptic weather type in Taiwan is usually represented by the Pacific anticyclone in summer. However, the regional scale shows that the cyclonic type (C) and the southerly group (the S, SE and SW types) is appearing to have significant influence in summer (Figure 5.1c and d). The dramatic difference of circulation types between the two scales suggests that the synoptic circulation in Taiwan is influenced by the interaction of a number of circulations, such as the Pacific anticyclone, the C type and southerly group in summer. Further discussions on the difference of dominant circulation types between the local scale and regional scale follow in Section 5.2.2.

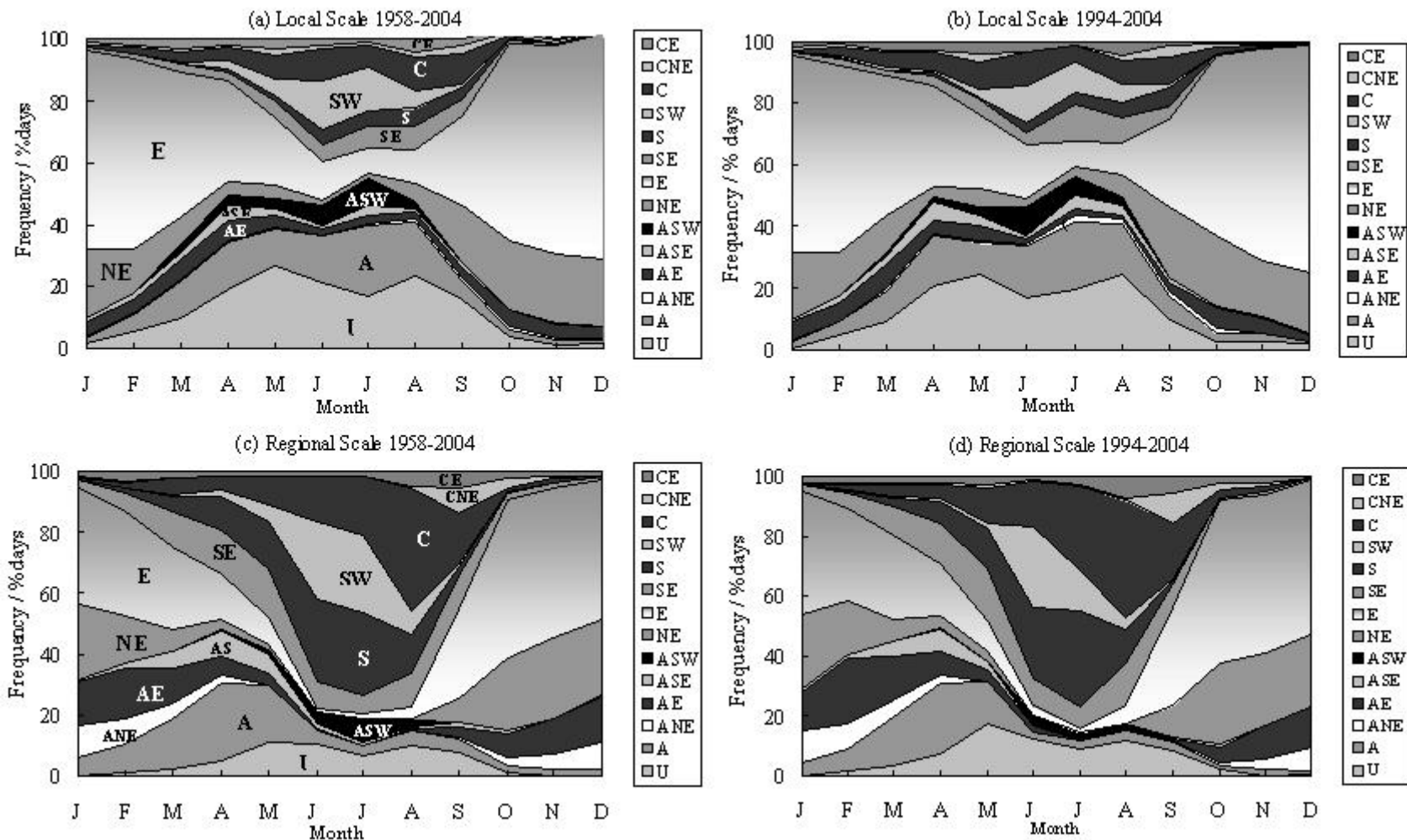


Figure 5.1: Mean monthly percentage frequency (% days) of the 14 circulation types for each month of two periods 1958-2004 and 1994-2004 (a) and (b) represent the local scale, and (c) and (d) represent the regional scale.

Table 5.1: Mean annual and seasonal circulation type frequencies (% days) for the periods 1958-2004 at the local and regional scales.

Local Scale						Regional Scale					
CT	Annual	Winter	Spring	Summer	Autumn	CT	Annual	Winter	Spring	Summer	Autumn
U	11.3	2.8	17.2	18.3	6.6	U	4.1	0.4	5.6	7.4	3.0
A	8.7	2.5	11.8	17.1	3.1	A	7.4	5.5	17.6	3.7	2.6
ANE	0.5	0.3	0.4	0.5	0.7	ANE	3.6	9.5	2.5	0	2.6
AE	4.0	4.4	5.4	1.9	4.4	AE	7.5	15	7.3	0.3	7.5
ASE	1.7	1.0	3.0	1.9	0.7	ASE	2.2	0.9	5.8	0.9	1.0
ASW	1.7	0.1	2.4	4.2	0.1	ASW	1.2	0	0.7	3.8	0.1
NE	11.8	19.3	5.6	2.5	20.1	NE	11.1	22	3.8	0.2	18.9
E	40.2	65.6	34	9.2	52.8	E	25.4	39.5	16.9	1.9	43.7
SE	2.9	0.8	3.2	5.6	1.8	SE	7.0	2.8	13.1	7.6	4.3
S	1.5	0	1	3.9	1.1	S	7.0	0.3	8.4	18.2	1.0
SW	2.8	0.1	2.3	8.4	0.4	SW	4.8	0	2.3	16.5	0.3
C	4.1	0.9	4.7	7.7	3.1	C	8.2	0.9	5.5	20.6	5.7
CNE	1.1	0.8	1.2	1.0	1.4	CNE	1.1	0.4	0.3	0.2	3.6
CE	1.97	1	2.8	1.9	1.1	CE	2.2	2.1	1.7	2.0	3.1

Table 5.2: Mean annual and seasonal circulation type frequencies (% days) for the periods 1994-2004 at the local and regional scales.

Local Scale						Regional Scale					
CT	Annual	Winter	Spring	Summer	Autumn	CT	Annual	Winter	Spring	Summer	Autumn
U	10.6	2.4	17.1	18.2	4.5	U	5.4	0.5	8.2	9.4	3.4
A	8.7	2.3	10.8	17.4	4.3	A	6.1	4.3	15.9	2.4	1.9
ANE	0.6	0.1	0.5	0.9	1.1	ANE	3.3	9.1	2.8	0.0	1.5
AE	4.1	4.7	5.4	1.8	4.6	AE	7.7	15.9	8.9	0.5	5.6
ASE	2.2	1.1	3.7	3.0	1.0	ASE	1.5	0.7	4.3	0.4	0.5
ASW	1.4	0.0	1.9	3.9	0.0	ASW	0.5	0.0	0.2	1.8	0.0
NE	12.1	18.8	6.6	3.3	21.0	NE	12.0	22.6	4.7	0.2	20.5
E	40.4	65.9	33.9	10.7	52.3	E	27.3	41.5	18.3	3.5	46.3
SE	3.3	1.1	3.1	7.2	1.6	SE	7.0	2.2	12.9	9.5	3.1
S	1.4	0.1	0.4	3.4	1.6	S	6.3	0.2	6.4	18.1	0.3
SW	2.1	0.1	1.4	6.6	0.1	SW	3.2	0.2	0.9	11.4	0.3
C	4.2	1.4	5.9	6.2	3.1	C	9.3	0.7	6.6	22.5	7.3
CNE	1.1	0.8	1.4	0.6	1.6	CNE	1.3	0.3	0.6	0.5	4.0
CE	1.8	1.0	3.3	2.1	1.0	CE	2.4	1.6	2.3	2.7	3.1

5.2.1 Long-Term Trend Analysis in Circulation Type

The long-term trends between 1958 and 2004 for the percentage frequencies of all fourteen weather types were examined using least-squares linear regression. The directions of the trends for the two scales are shown in Tables 5.3 and 5.4.

For the local scale, four types show significant (at the 5% level) trends in the annual frequency. The AE and CNE types show significant increasing trends and the trends for the S and SW types are significant decreasing trends for the study period (Table 5.3 and Figure 5.2). In addition, the long-term trend of the monthly frequencies shows a significant increase of the A type in June and July and the NE type shows a significant increasing trend in March and August. The long-term decreasing trends of the S and SW types in the monthly frequencies are evident in both spring and summer (Table 5.3). For the regional scale, in most cases, the trends observed were significant in the annual frequency, except the ANE, AE, SE and CE types (Table 5.4). In comparing the monthly long-term trends between the local and regional scales, the S and SW types at the regional scale show the same significant decreasing trends as the local scale (Tables 5.3 and 5.4). The NE type also shows a similar long-term trend with the local scale, a significant increasing trend observed in spring and autumn. Moreover, a significant positive change of the U type in the monthly frequency is observed in spring.

The trends in the weather types suggest a link with the summer and winter monsoon, with a weaker summer monsoon associated with reduced S and SW types and a stronger winter monsoon with more frequent NE type. Significant decreasing trends of the S and SW types for both scales suggest a reduction of rainfall, especially in spring and summer, because these two types are strongly associated with the seasonal precipitation distribution in Taiwan (Yeh and Chen, 1998; Chen *et al.*, 1999; Chen and Wang, 2000; Yen and Chen, 2000; Chen and Chen, 2003).

Table 5.3: The direction of long-term trends of fourteen circulation types for the period 1958-2004 at the local scale.

CT	ANNUAL	JAN	FEB	MAR	APR	MAY	JUN	JUL	AUG	SEP	OCT	NOV	DEC
U	-	-	-	-	+	-	-	+	+	-	-	-	-
A	+	+	+	-	-	+	+*	+*	-	+	+	+	-
ANE	+	-	-	+	+	+	+	+	-	-	+	-	+
AE	+*	+	+	+	-	+	+	+	-	+	+	-	+
ASE	+	-	-	-	+	+	-	+	+	+	+	-	-
ASW	-	-	-	-	-*	-	+	-*	-	-	-	-	-
NE	+	+	-	+*	-	+	+	+	+*	+	+	-	-
E	+	+	+	+	+	+	+*	+	-	+	-	+	+
SE	-	-	+	-	-	-	-	+*	-	-	-	-	-
S	-*	-	-	-	-	-	-	-*	-	+	-*	-	-
SW	-*	-	-*	-*	-*	-*	-*	-*	-*	-*	-*	-	-
C	-	-*	+	+	+	+	-	-	-	-	-	-	+
CNE	+*	+	+	+	+	+*	-	-	-	+	+	+	-
CE	+	+	-*	-	+	+	+	+	+	-	-	-	+

Positive and Negative trends indicated by plus and minus signs respectively.

* indicates trend significant at the 5% level

Table 5.4: The direction of long-term trends of fourteen circulation types for the period 1958-2004 at the regional scale.

CT	Annual	JAN	FEB	MAR	APR	MAY	JUN	JUL	AUG	SEP	OCT	NOV	DEC
U	+\$*	-\$*	+	+\$*	+\$*	+\$*	+	+\$*	+	+	-	-	+\$
A	-\$*	-	-	-	-	-\$*	+	+	-	-\$*	-	-	-\$*
ANE	+	-	+	+	+	+				-	-	+	+
AE	-	-	+	+	+	+	+	+	-	-	-\$*	-	-
ASE	-\$*	+	-	-	-	-\$*	-	+	+	-	-	-	-
ASW	-\$*			-	-	-\$*	-	-\$*	-\$*	-\$*	-\$*		
NE	+\$*	+	+	+	+\$*	+\$*	+		+	+	+\$*	+	+
E	+\$*	+	-	+\$*	+	+\$*	+	+	+\$*	+\$*	+	+	+
SE	-	-	-	-	-	+	+	+	+	-	-\$*	-\$*	-\$*
S	-\$*	-	-	-	-\$*	-\$*	-\$*	+	-\$*	-\$*	+		
SW	-\$*		+	-	-	-\$*	-	-\$*	-\$*	-\$*	-\$*		
C	+\$*	-	-	-	+\$*	+	+\$*	+	+\$*	+	+	+	-
CNE	+\$*	+	+	+	+	+\$*	+	+	+\$*	+	+	+	-\$*
CE	+	-	-	+	+	+\$*	+	+	+\$*	+	-	+	-\$*

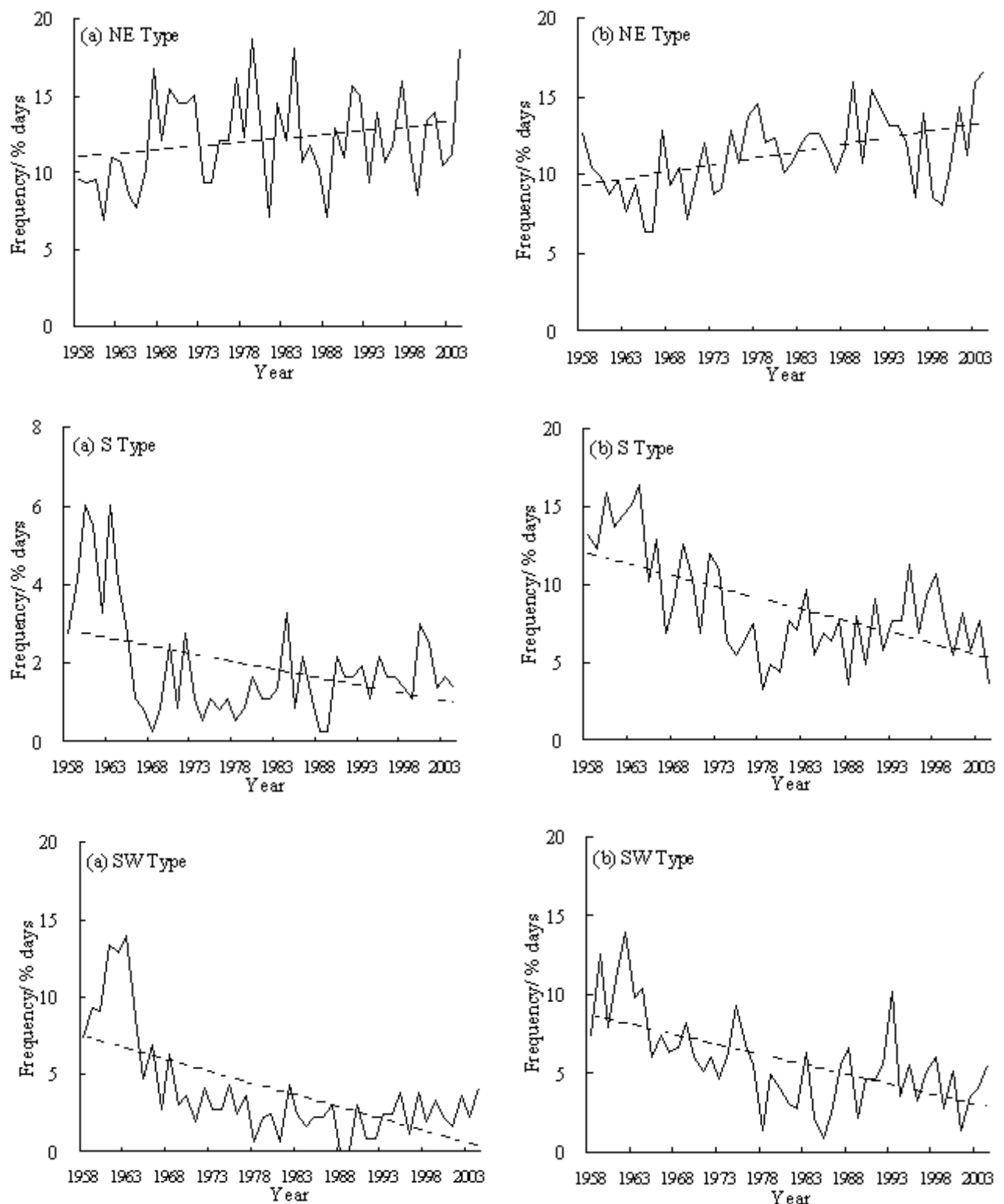


Figure 5.2: Annual frequencies of NE, S and SW circulation types for the period 1958-2004, (a) local scale, and (b) regional scale. Dashed lines are least-squares linear trends.

5.2.2 Seasonal Characteristics of Sea Level Pressure Circulation Types Composites

To clarify the characteristics of circulation types for each season and to further verify that the classified results of circulation types by the objective scheme are meaningful in a lower latitude region; analyses of SLP composites of circulation types for four seasons are presented and discussed in this section. The mean seasonal SLP map is shown in Figure 5.3. The representative monthly circulation type composite maps at both local and regional scales for each season calculated from SLP data for the period 1994-2004 are shown in Figures 5.4 to 5.7, for winter, spring, summer and autumn, respectively. In addition, selected individual days representing each circulation type at both spatial scales are shown in Figures 5.8 and 5.9.

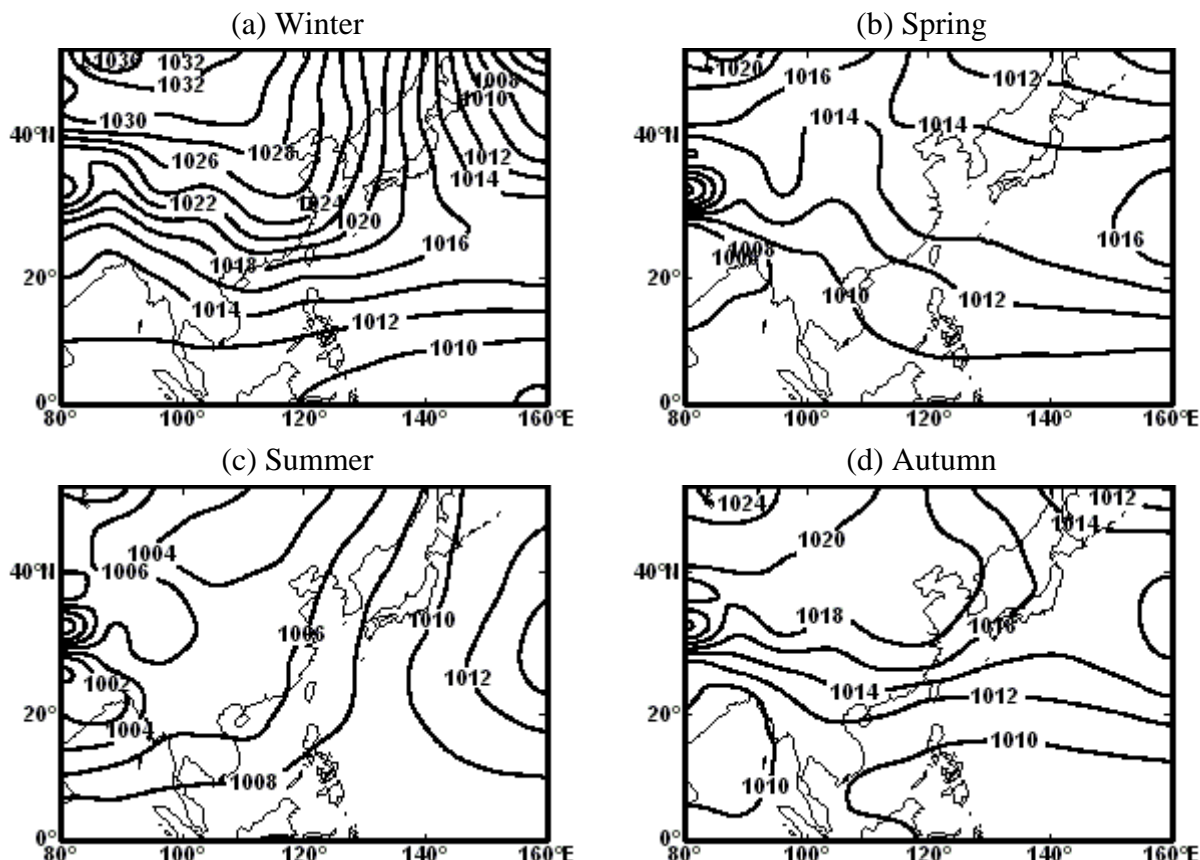


Figure 5.3: Mean seasonal SLP (hPa) for the regional window for the period 1958-2004.

In winter, the representative types, for the local and regional scale, are the E and NE types (Figure 5.4a), and the E, NE, AE and ANE types (Figure 5.4b), respectively. The characteristics of the E and NE types at the local scale are very similar to the patterns at the regional scale (Figures 5.4b-1 and b-2), except that composite of circulation types at the regional scale represent better distribution of synoptic weather systems around Taiwan. All these representative types, for the two spatial scales, are closely related to the East Asian continental high-pressure system. When the East Asian continental high-pressure system (the Siberian anticyclone) moves from northern China southeastward to the West Pacific, its peripheral circulation causes strong easterly and northeasterly flows around Taiwan (Figures 5.4a and 5.4b). These air flows are classified as the E and NE type. A similar flow pattern can be observed for the ANE type (Figure 5.4b-4). However, the high pressure centre is located closer to Taiwan and there is a more extensive northeasterly flow compared to the NE type. The differences among these winter representative types are associated with the relative strength of the high-pressure system and the cyclonic flow from the equator. On the selected days representing the E type for the local scale, and the NE, AE and ANE types for regional scale show clear examples of composite differences of these types (Figures 5.8 and 5.9). In the E and NE cases, the trough from the equatorial cyclone suppresses the southward influence of the anticyclone and generates a more intensive pressure gradient with a greater easterly or northerly flow over Taiwan (for example, the E type in Figure 5.8 and the NE type in Figure 5.9). On the other hand, the pressure centres of the AE and ANE types are close to the east coast of China (Figures 5.4b-3 and b-4) with a weak influence from the equatorial cyclone, which places Taiwan under a stronger anticyclonic effect than for the pure directional types (for example, the AE and ANE types in Figure 5.9).

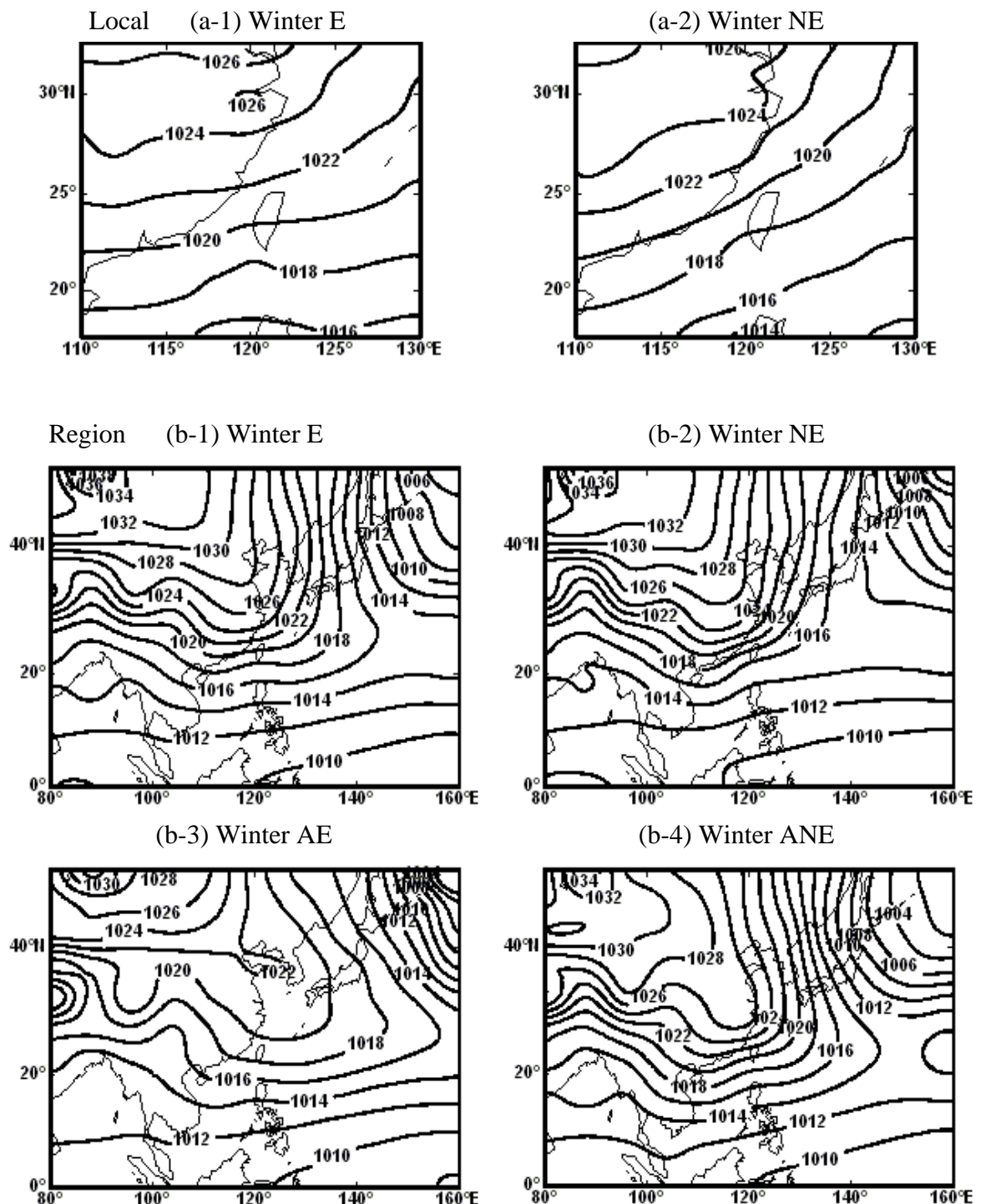


Figure 5.4: Seasonal mean sea level pressure (hPa) map for the representative circulation types in winter (a) local scale; and (b) regional scale.

The more frequent circulation types in spring are the A, E and U types and the A, E and SE types for the local and regional scales, respectively (Figures 5.5a and b). The E flow type, at both the local and regional scales, shows the air flows originating from the East Asian continent (Figures 5.5a-1 and b-1) and a weak anticyclone is observed over the east coast of China and Japan, whereas Taiwan is subject to easterly flow related to the equatorial low pressure (Figure 5.5b-1). In the case of the A-type, the local and regional scales represent Taiwan is affected by two different anticyclonic systems. For the local scale, the composite map shows that Taiwan is under the influence of an anticyclone from the Pacific Ocean (Figure 5.5a-2). There are, however, two high pressure centres associated with the A type at the regional scale, one appears over the East China Sea and the other one is situated over the West Pacific Ocean. Peripheral circulation of the anticyclone over the East China Sea blows clockwise to bring an easterly or northeasterly wind around Taiwan (Figure 5.5b-2). Additionally, the selected composite of the A type at the regional scale shows that Taiwan is also under the influence of an evolving Pacific anticyclone and low pressure from northern China (Figure 5.9). The composite features of the A type suggest that the Siberian anticyclone is declining in this season. With the SE type, the increased strength of anticyclone over the West Pacific Ocean brings the prevailing wind with a southeast direction to Taiwan (Figure 5.5b-3). The U type at the local scale shows no obvious air flow over Taiwan (Figure 5.5a-3).

In spring, the circulation types at both spatial scales are associated with a declining Siberian anticyclone and an evolving Pacific anticyclone with a less intensive pressure gradient, compared with that in winter, around Taiwan. Depending on the location of the high pressure centre and the interaction with the Pacific anticyclone, the prevailing wind may shift from the easterly to the southeasterly. Otherwise, Taiwan is apparently affected

by the high pressure subsidence flow in this season, as high pressure centres move from the East Asian continent toward the East China Sea (Figures 5.5a-1, b-1 and b-2).

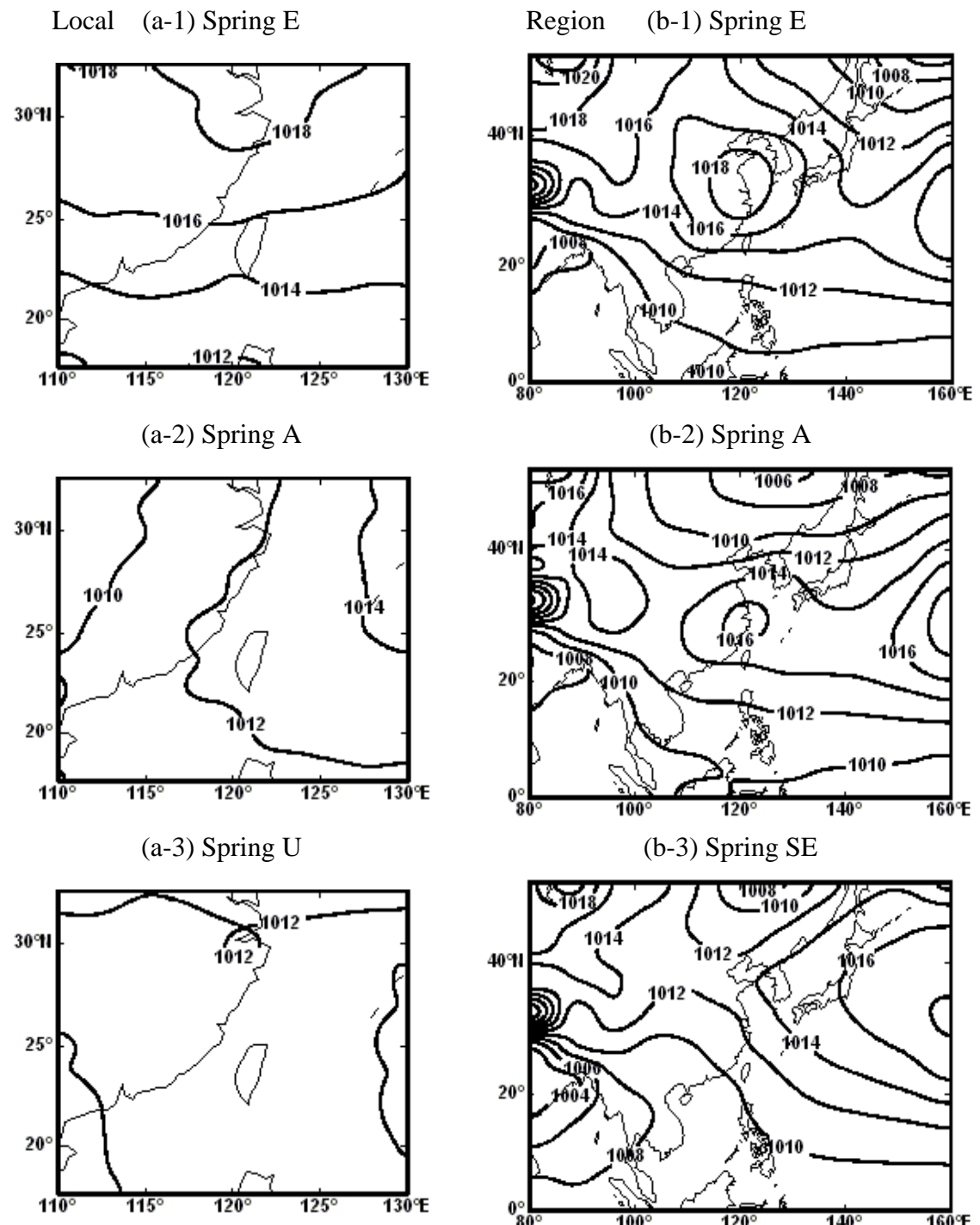


Figure 5.5: Seasonal mean sea level pressure (hPa) map for the representative circulation types in spring (a) local scale; and (b) regional scale.

In summer, the local and regional scales both show that the SW, C and U types are the dominant circulation types (Figures 5.6a and b). In addition, the other representative circulation types are the A and E types, and the S type, for the local and regional scales, respectively. The anticyclonic type (Figure 5.6a-1), at the local scale, is very similar to the A type (Figure 5.5a-2) in spring, and characterised by a strong Pacific high. With the S and SW types, a low pressure appears over central and southern China (Figures 5.6b-1 and b-2). The composite characteristics of the S and SW types of selected days (Figures 5.8 and 5.9) show a good agreement with the mean seasonal composite maps at both local and regional scales (Figure 5.6). In this season, Taiwan is under the influence of the Asian summer monsoon flow and the Pacific anticyclone. The Pacific anticyclone moves westward against the low pressure systems over China and generates strong southwesterly flow which is the typical air flow in this season (Figures 5.6a-2, b-1 b-2, 5.8 and 5.9). The characteristic of the C type is a low pressure centre located over Taiwan (Figure 5.6a-3 and b-3). In the case of the U type, at both spatial scales; weak peripheral circulation occurs around Taiwan, because of the climate characteristics over this subtropical area with no significant weather system affecting the country (Figure 5.6a-4 and b-4). A similar pattern is often observed in late spring as well (Figure 5.5a-3).

Another specific circulation type in summer evident at the local scale is the E type (Figure 5.6a-5). The characteristic of the E type in this season represents a different circulation pattern, compared to other seasons (winter and spring); the air flow direction is from the South China Sea moving northeastward to Taiwan.

In addition to the U type, the representative circulation types (the A, S, SW, C and E types) in summer demonstrate that the air flows over or around Taiwan mainly originate from maritime regions, such as the Pacific Ocean and the South China Sea. The characteristic

features of these circulation types suggest that Taiwan is generally influenced by strong convective activities in summer.

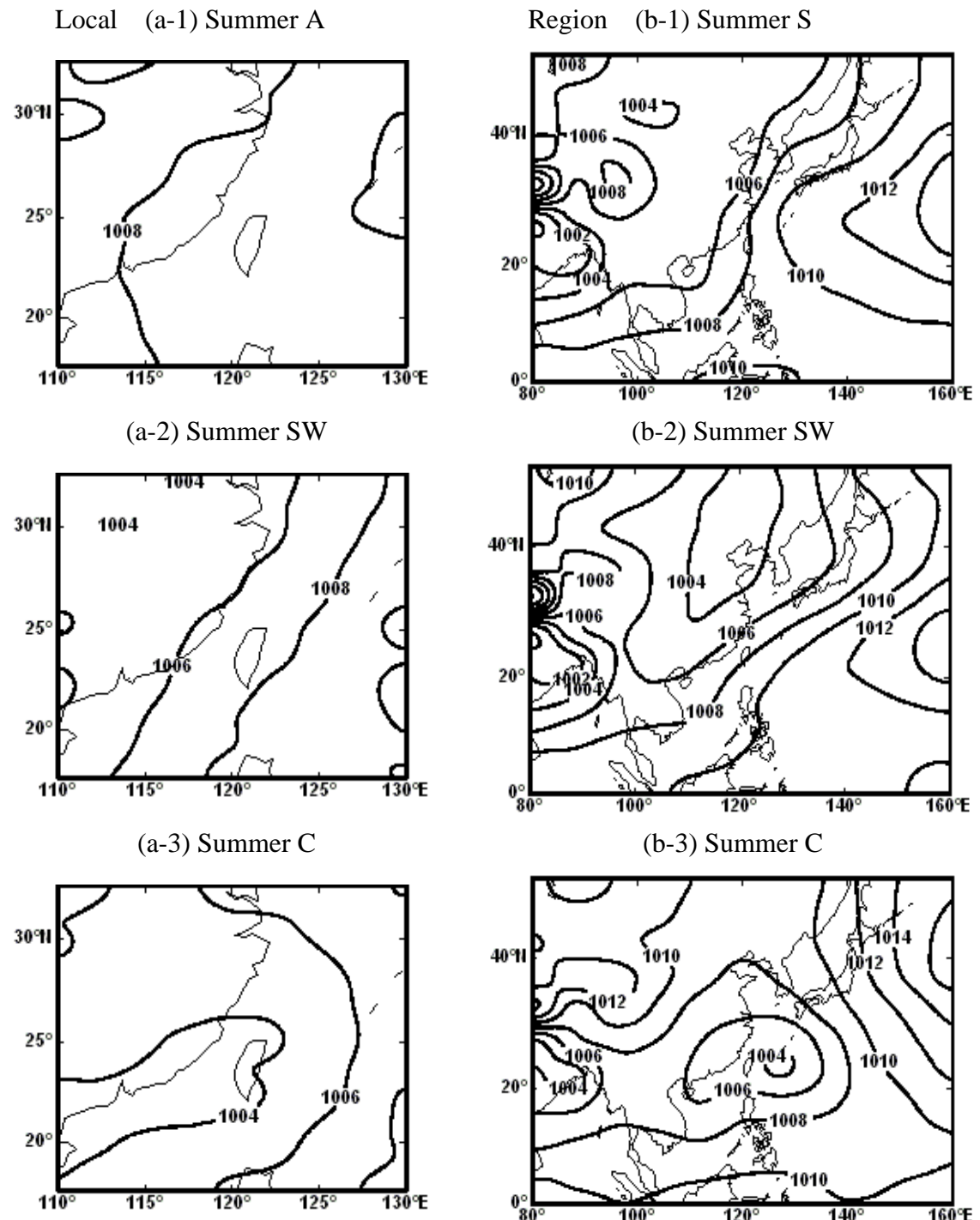
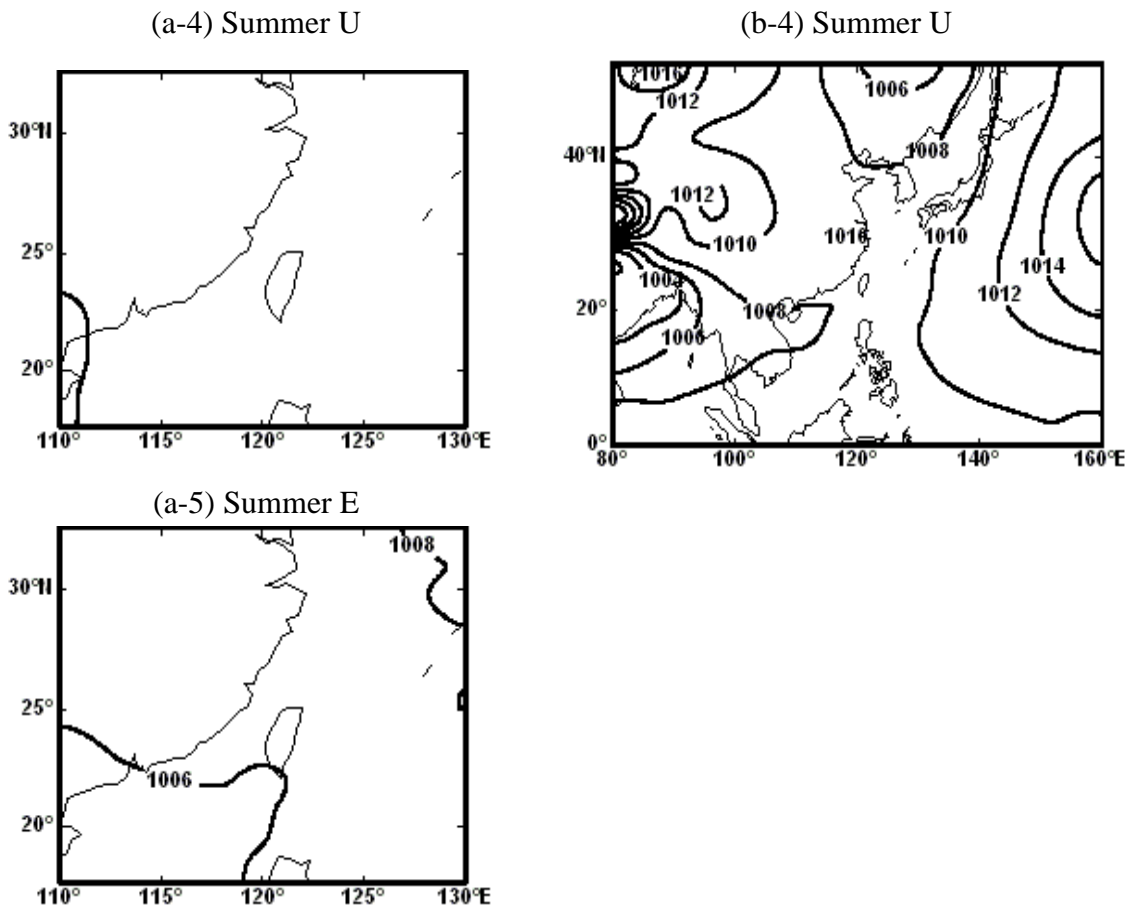


Figure 5.6: Seasonal mean sea level pressure (hPa) map for the representative circulation types in summer (a) local scale; and (b) regional scale.

Figure 5.6



In autumn, the E and NE types are the representative types for both spatial scales. The E and NE types (Figures 5.7a, b-1 and b-2) show similar patterns to the cases in winter (Figures 5.4a, b-1 and b-2), but with smaller pressure gradients. Otherwise, the effect of low pressure from the equator or the South China Sea is more evident in autumn, compared with the E and NE types in winter. The C type, at the regional scale, presents a low pressure centre situated on the east side of Taiwan. The circulation flow embedded within the East Asian winter monsoon flow is so as to give northeast flow over Taiwan.

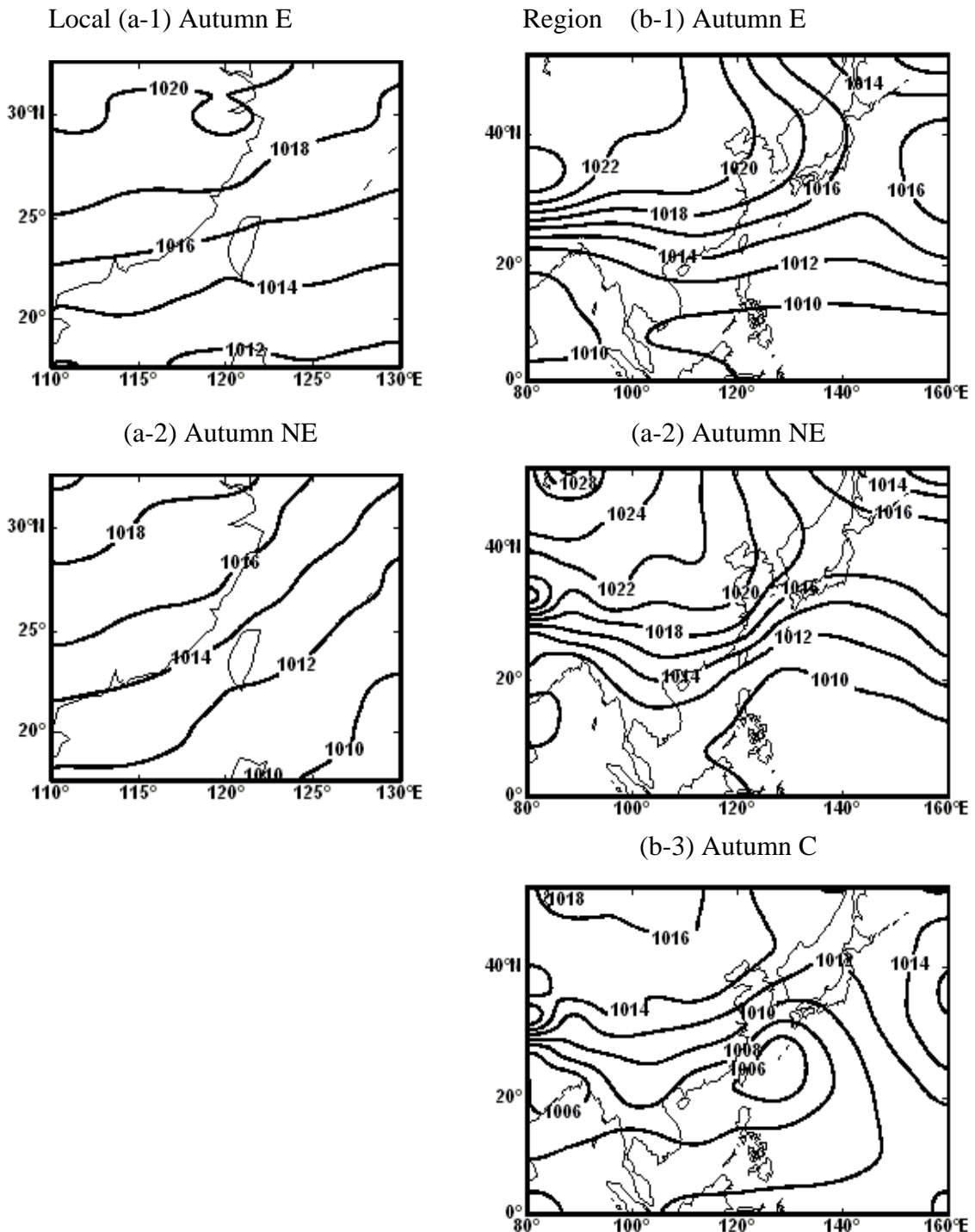


Figure 5.7: Seasonal mean sea level pressure (hPa) map for the representative circulation types in autumn (a) local scale; and (b) regional scale.

On the basis of the characteristics of the SLP composite maps, the representative circulation types are of the expected type for each season with respect to air flow over Taiwan. In terms of the differences between the local and regional scales, the classifications of circulation types at the local scale in each season are more related to the air flow affecting Taiwan on the day; on the other hand, the patterns at the regional scale represent better distribution of synoptic weather systems around Taiwan. The results classified with this objective scheme show a good agreement with the synoptic weather type classification by Wu and Chen (1993). They categorised the climate of Taiwan into 14 synoptic weather patterns. They pointed out that four synoptic weather patterns mainly dominate the climate in Taiwan: the northeasterly winter monsoon in winter, the Pacific high pressure system in summer, southerly flows from southern China and cyclones related to the typhoon seasons in summer and autumn. This agrees with the results of the objective scheme presented here. In addition, the advantages of the objective scheme, apart from its objectivity, are ease of calculation and use in statistical analyses. The results of the objective scheme are, therefore, valid to be used to investigate the relationship between ozone pollution and circulation types.

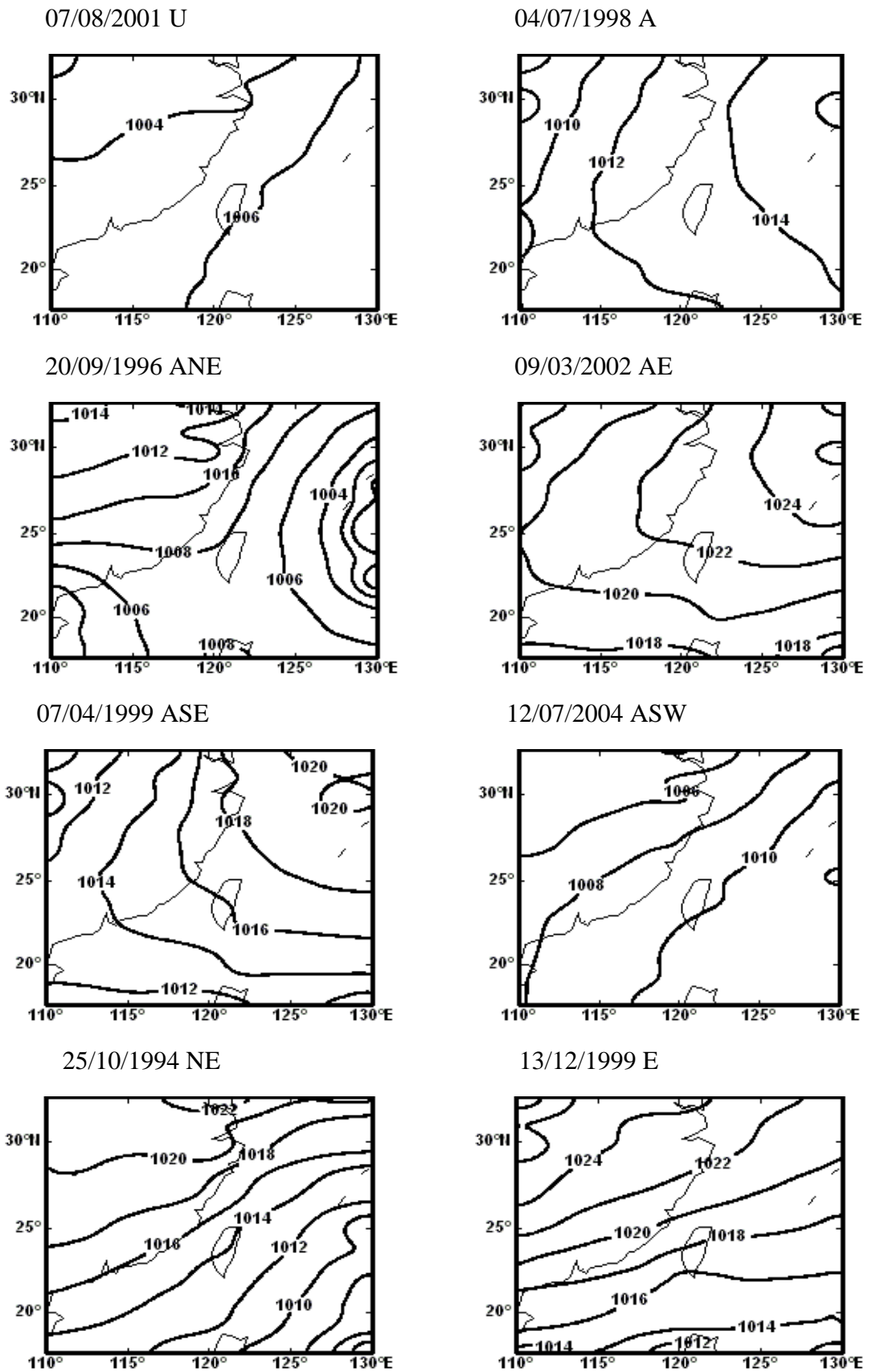
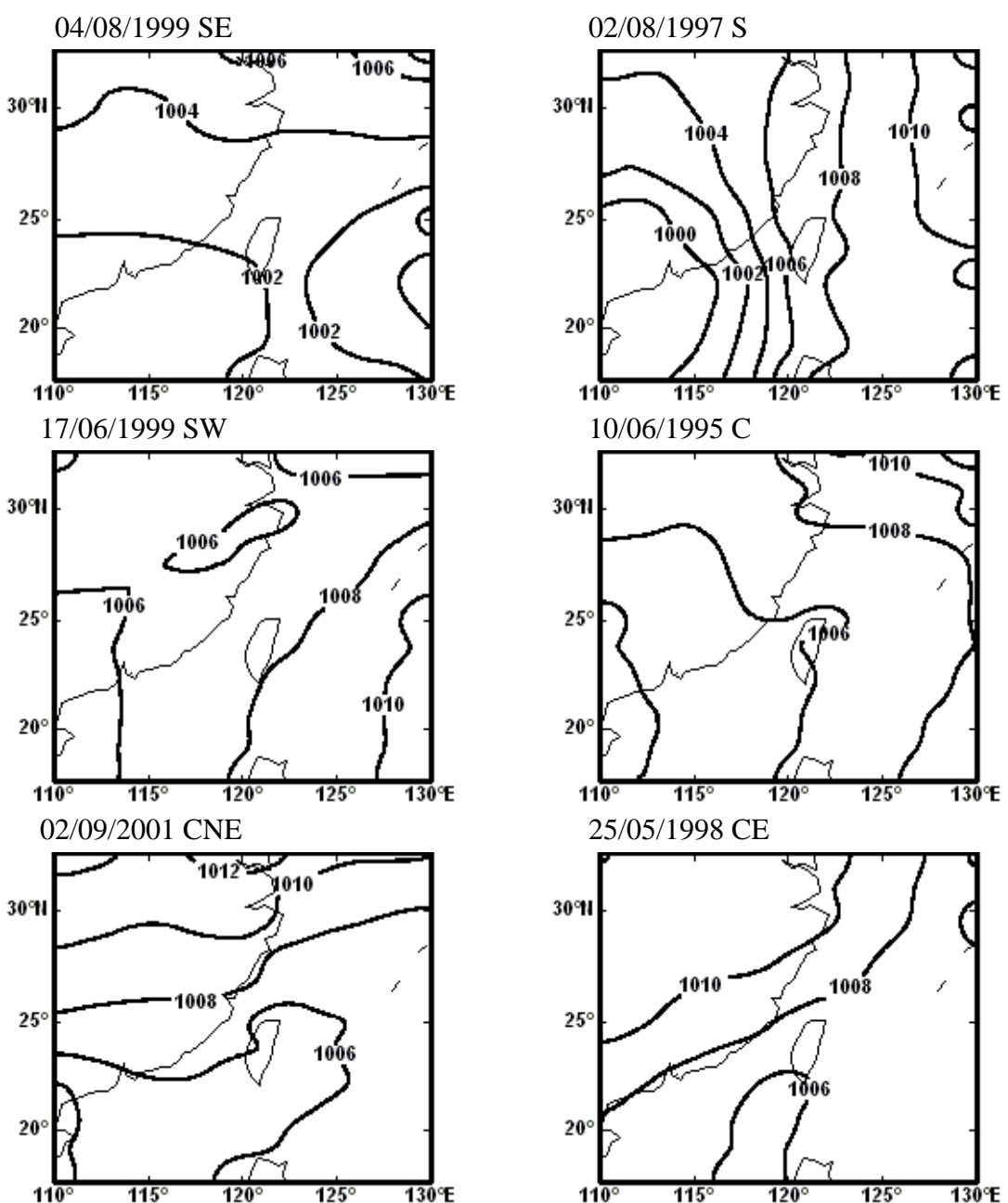


Figure 5.8: Seasonal mean sea level pressure (hPa) map of selected days for fourteen circulation types at the local scale.

Figure 5.8:



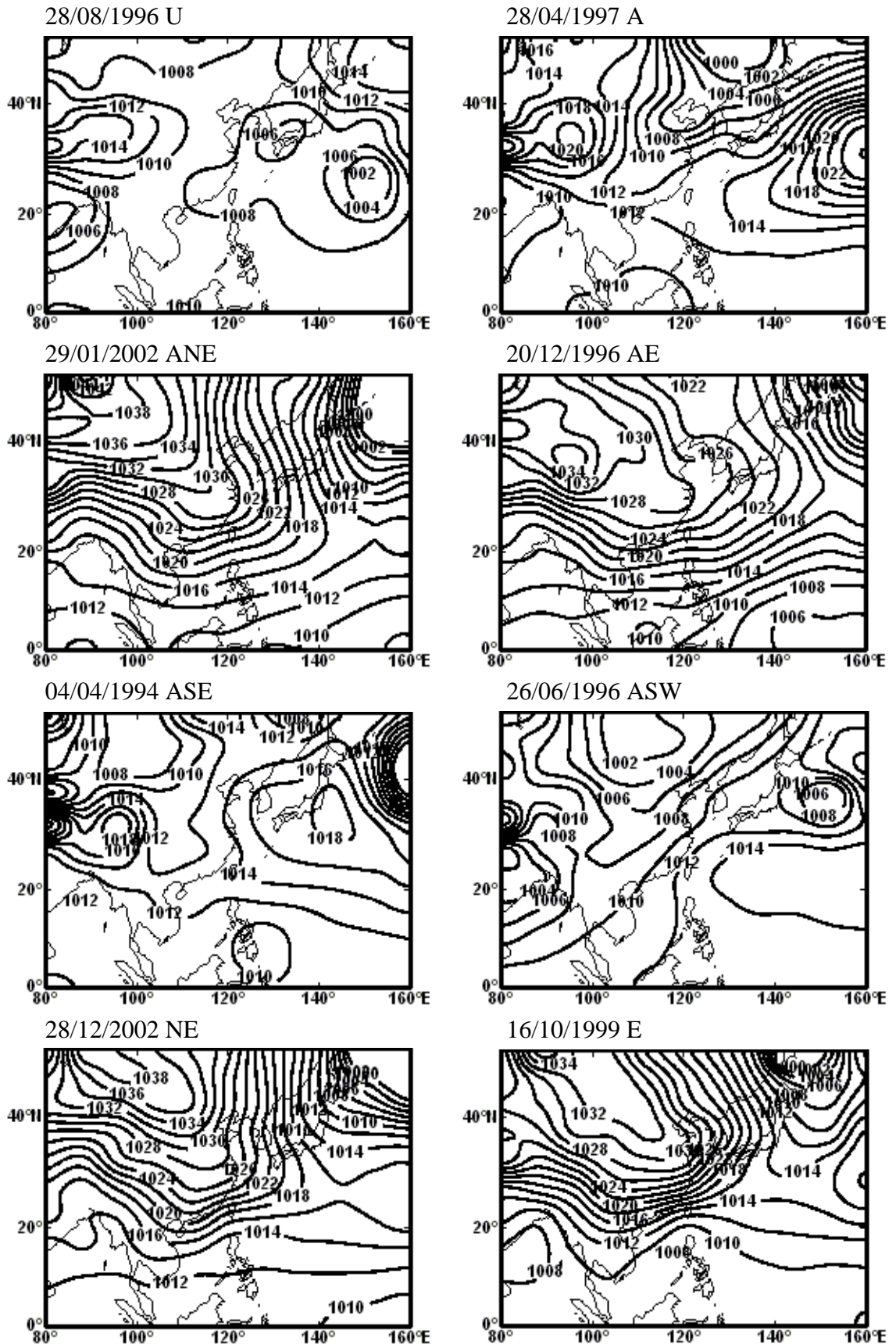
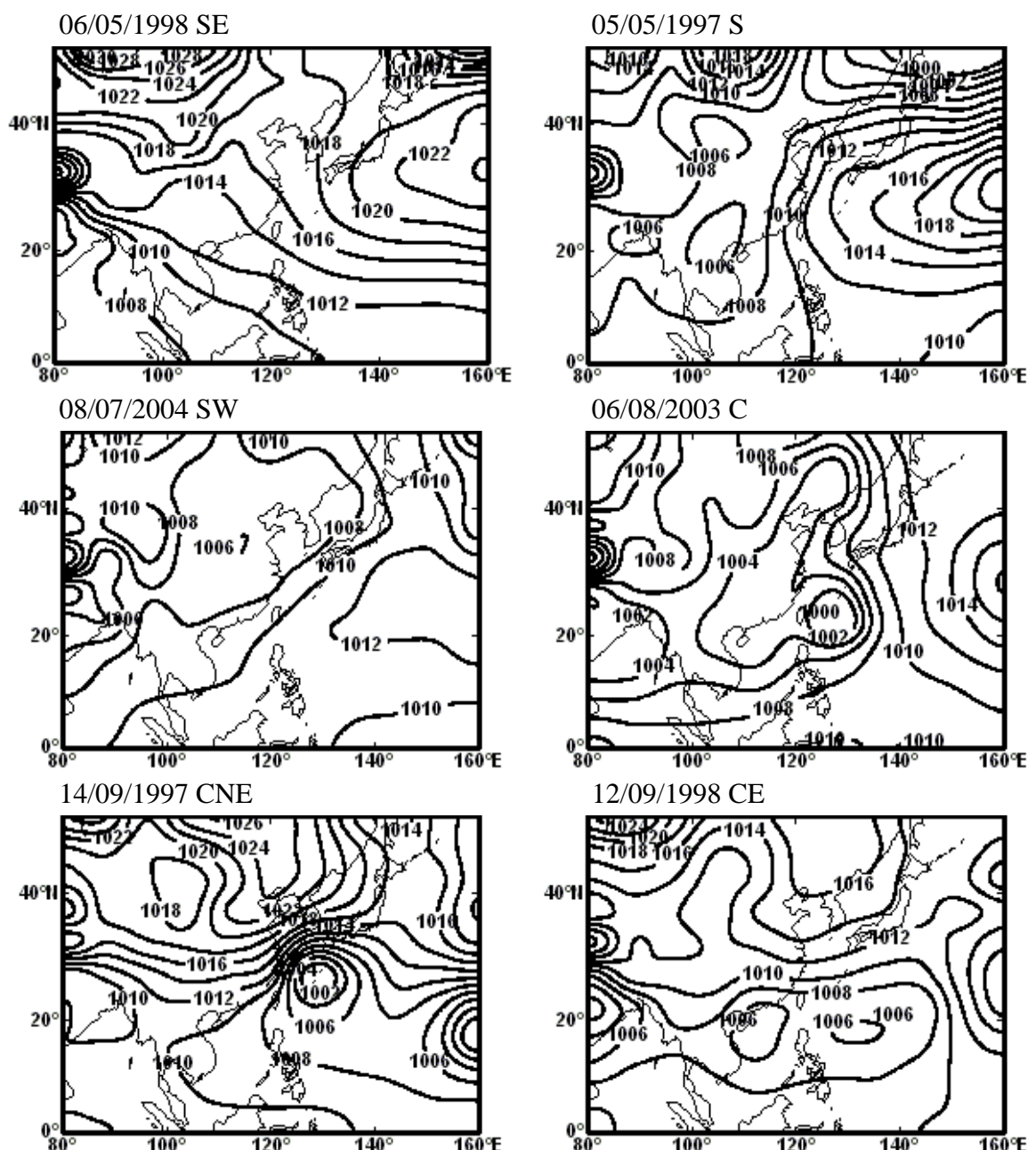


Figure 5.9: Seasonal mean sea level pressure (hPa) map of selected days for fourteen circulation types at the regional scale.

Figure 5.9:



5.3 Relationships between Ozone Pollution and Circulation Weather Types

The classification results of the circulation weather types are now used to investigate the relationship between ozone pollution days defined as the index HOD₃ (see Section 3.3.3) and specific weather types for the period 1994-2004. In order to understand the correlation of long-range transport of ozone pollution in Taiwan, the circulation weather type for the day prior to the ozone pollution day (P-1 Day) and the two days prior to the ozone pollution day (P-2 Day) are investigated as well as the concurrent relationship. Here, the HOD₃ day is defined as pollution day (P-Day). Total ozone pollution days (HOD₃) used in this investigation are 128 days (see Table 4.1) in the eleven-year period. The distribution of the 128 ozone days (P-Day, P-1 Day and P-2 Day) within 13 of the 14 circulation types is shown in Table 5.5, as there is no such case observed for the ASW type. The seasonal distribution of HOD₃ over the study period is 53 days, 12 days, 61 days, and two days for spring, summer, autumn and winter, respectively.

Table 5.5: The distribution of ozone pollution days (P), the day prior to the ozone pollution day (P-1 Day), and the two days prior to the ozone pollution day (P-2 Day) under thirteen circulation-type at both spatial scales.

Local Scale	U	A	ANE	AE	ASE	NE	E	SE	S	SW	C	CNE	CE
P (days)	7	12	4	14	12	13	60	2	2	0	0	2	0
P-1 (days)	6	6	4	21	3	27	54	3	1	0	1	1	1
P-2 (days)	8	4	3	11	0	35	52	2	0	0	7	3	3
Regional Scale													
P (days)	6	10	2	8	7	25	36	8	2	1	16	5	2
P-1 (days)	6	16	2	6	4	30	31	4	0	1	19	5	4
P-2 (days)	4	17	0	11	1	28	25	5	0	1	21	9	6

5.3.1 Frequency Analysis of Ozone Pollution Circulation Types

The annual frequencies of ozone days within the specific circulation types from 1994 to 2004 at both spatial scales are shown in Figure 5.10. The annual frequencies of the ozone days at both spatial scales are with high frequencies of the E and NE types (Figure 5.10). In contrast, the S and SW types are the least frequent types related to the ozone days at both the local and regional scales. Otherwise, the ozone days also show high frequencies within the A and C types at the regional scale.

Figures 5.11 and 5.12 show the seasonal frequencies of ozone days within twelve circulation types (without the ASW and SW types) and thirteen circulation types (without the ASW type) for the local and regional scales, respectively. Seasonal frequencies are not shown for winter because less than 1% of cases of high ozone days are observed in this season. With respect to the seasonal frequencies, the ozone days (P-Day, P-1 Day and P-2 Day) show high frequencies within the E and NE types for both local and regional scales, especially in autumn (Figures 5.11 and 5.12). Apart from the high frequencies of ozone days on the E and NE type days, the frequencies of the ozone days related to specific circulation types vary with seasons.

In spring, the anticyclonic group (the A, AE, ANE and ASE types) also shows high frequency on the P-Day at the local scale (Figure 5.11). The distribution of the P-Day within these types indicates that ozone pollution usually occurs under a high pressure system, as the subsidence of high pressure systems is not favourable for precursors or pollutants dispersion (Figure 5.5). For the regional scale, the ozone days are related to a variety of circulation types. For instance, the P-Day is related to the NE, SE and C types; and the P-1 Day and P-2 Day is associated with the A, NE and C types (Figure 5.12).

These results indicate that the ozone days at the regional scale are related to not only pure directional types but to anticyclonic and cyclonic patterns.

In summer, the E, NE, AE and U types are the most important circulation types for ozone days at the local scale (Figure 5.11). On the other hand, the ozone days, at the regional scale, show high frequencies related to the C, U and E types. In this season, the C type is characterised as a low pressure centre with a small pressure gradient observed over Taiwan (Figures 5.6a-3 and b-3). Otherwise, the high frequency of the U type at both local and regional scales suggests that those ozone days classified as the U type, particularly on the P-Day, may be related to local pollution, as the characteristic of the U type is a weak peripheral circulation around Taiwan (Figures 5.6a-4 and b-4).

In autumn, most of the ozone days are associated with the E and NE types at both the local and regional scales. The characteristics of the E/NE type show that air flow moves from the East Asian continent toward the East China Sea (Figures 5.7a and b). In this season, the frequency of the NE type gradually increases back in time at both spatial scales; higher frequency shows on the P-2 Day than the P-1 Day and P-Day. These results suggest that air flows from the northeasterly direction may play an important role in long-range transport of ozone and its precursors for Taiwan, as the air flows pass through polluted areas such as China, Korea and Japan.

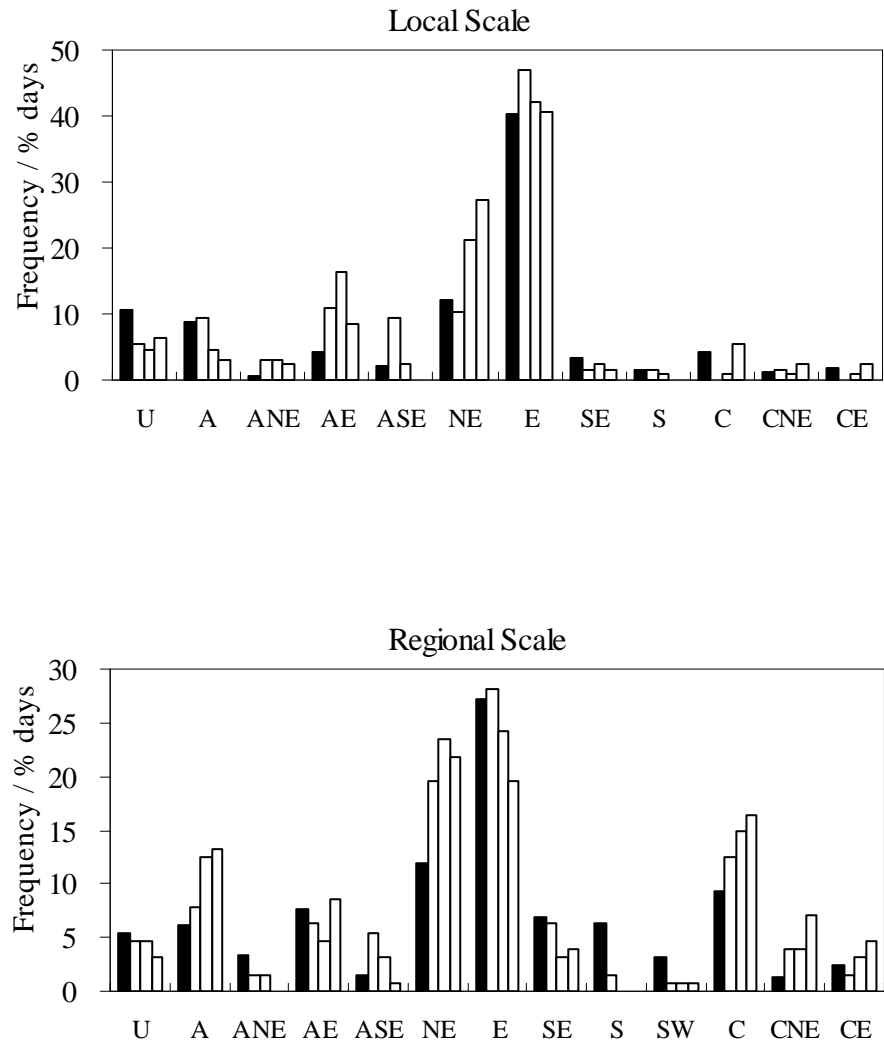


Figure 5.10: The mean annual frequency (shown as the percentage of all days) of twelve circulation types at the local scale and of thirteen circulation types at the regional scale (solid bars); and their relation with the annual frequency of ozone days (shown as the percentage of total annual ozone days) (open bars). The first open bar represents the pollution day (P-Day), the second open bar represents the day prior to the ozone pollution day (P-1 Day) and the third open bar represents the two days prior to the ozone pollution day (P-2 Day).

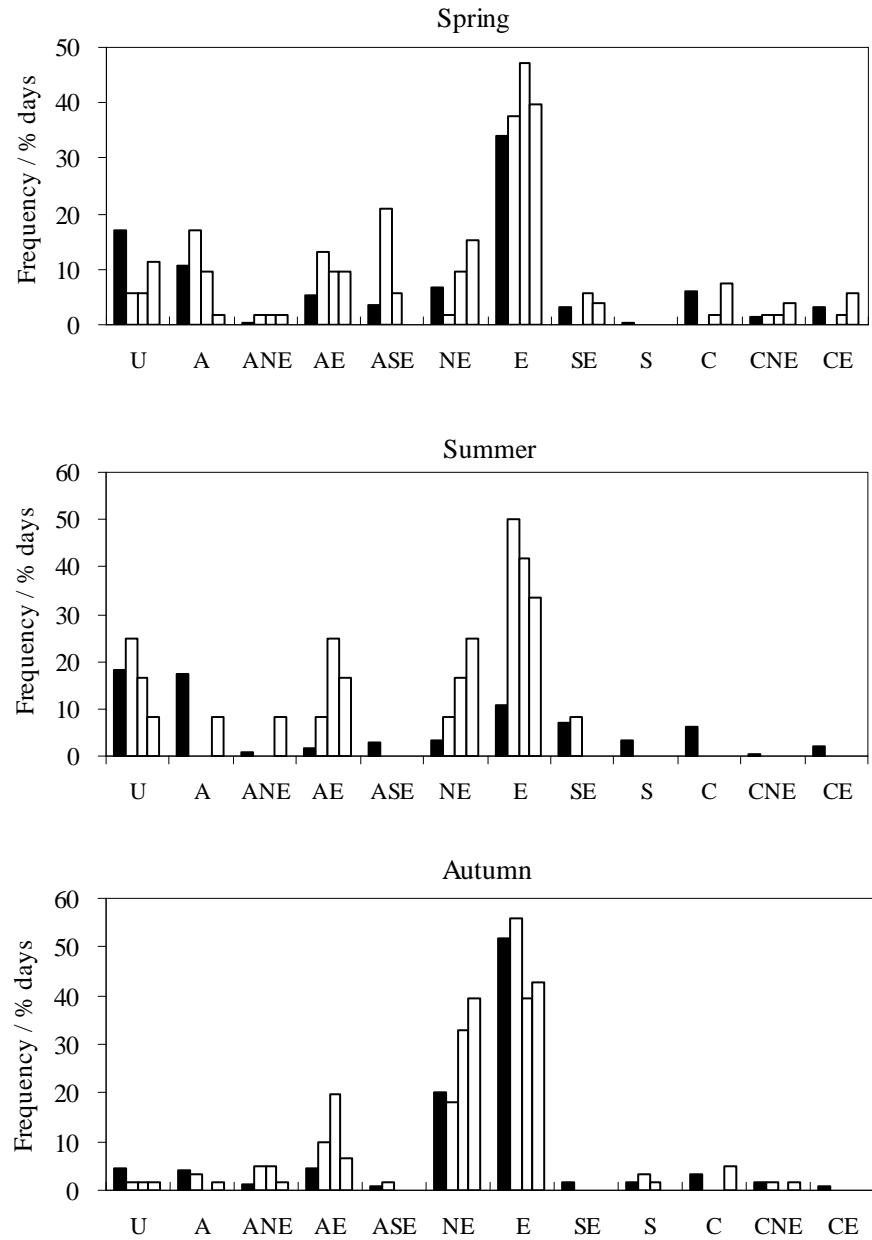


Figure 5.11: The mean seasonal frequency (shown as the percentage of all days) of twelve circulation types at the local scale (solid bars); and their relation with the seasonal frequency of ozone days (shown as the percentage of total seasonal ozone days) (open bars). The first open bar represents the pollution day (P-Day), the second open bar represents the day prior to the ozone pollution day (P-1 Day) and the third open bar represents the two days prior to the ozone pollution day (P-2 Day).

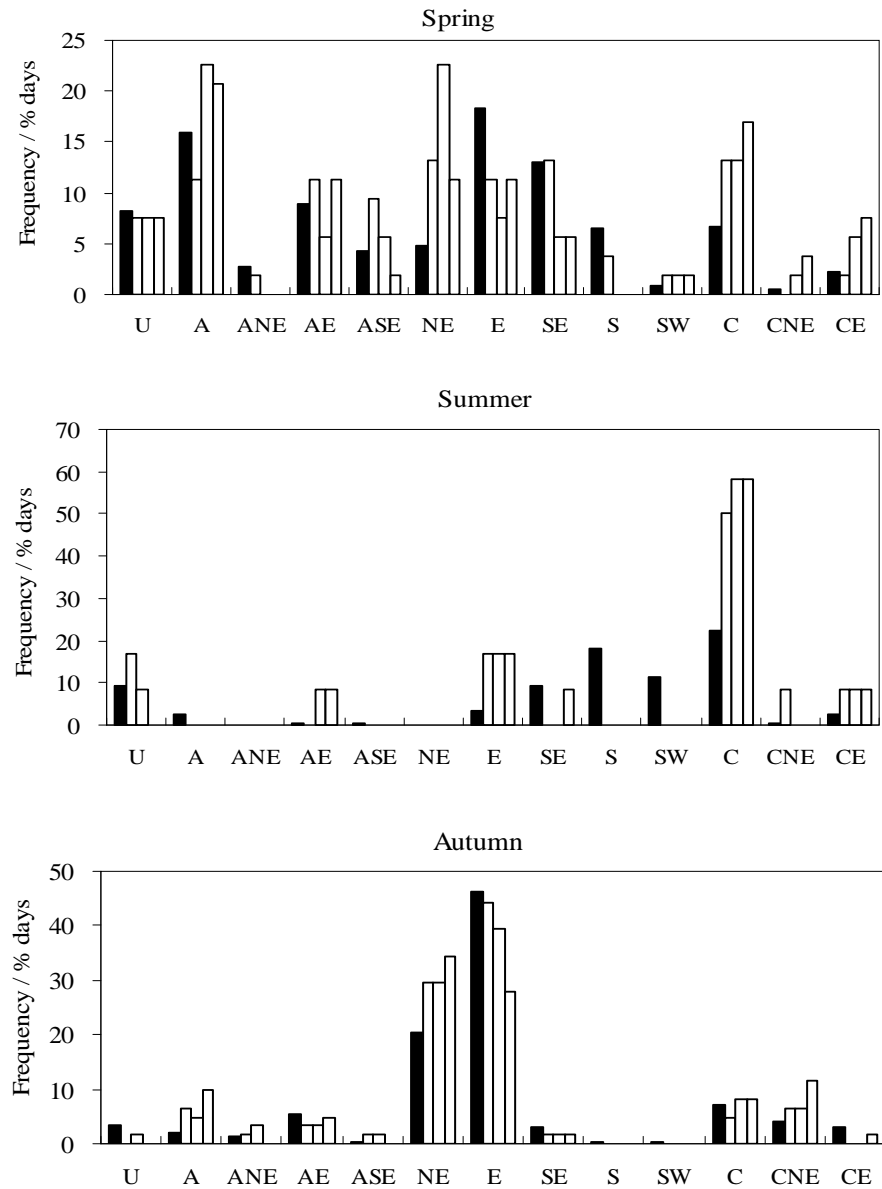


Figure 5.12: The mean seasonal frequency (shown as the percentage of all days) of thirteen circulation types at the regional scale (solid bars); and their relation with the seasonal frequency of ozone days (shown as the percentage of total seasonal ozone days) (open bars). The first open bar represents the pollution day (P-Day), the second open bar represents the day prior to the ozone pollution day (P-1 Day) and the third open bar represents the two days prior to the ozone pollution day (P-2 Day).

5.3.2 Evaluation of Ozone Pollution and Circulation Type Relationships

The frequency analysis presented in the previous section suggests that the ozone days (P-Day, P-1 Day and P-2 Day) are mainly related to the E and NE types, particularly for the local scale (Figures 5.10, 5.11 and 5.12); and that ozone days also correspond with the A and C types at the regional scale (Figure 5.12). The correlation between the ozone days and these circulation types may be because these types are the most frequent circulation types during the study period (1994-2004), for instance, the annual frequency of the E type is 40.44% and 27.25% for the local and regional scales, respectively (Figure 5.10). In order to more rigorously identify the relationship between ozone days and circulation types, a standardised ratio of the ozone days related to circulation type frequency is calculated. The ratio is calculated by $PROP_{ct}/PROP_{tot}$, where $PROP_{ct}$ is the proportion of type days which are ozone days, and $PROP_{tot}$ is the proportion of all days which are ozone days. Annual and seasonal ratios have been calculated for the ozone days (P-Day, P-1 Day and P-2 Day) for both spatial scales (Figures 5.13, 5.14 and 5.15). When the value of the ratio of a specific circulation type is greater than 1.0, the probability of occurrence of the ozone days on that specific circulation type is more likely than the mean frequency of the circulation type. Moreover, selected individual days representing the characteristics of the circulation types related to ozone days at both the local and regional scales are shown in Figure 5.16

The annual and seasonal ratios indicate the variability between the two spatial scales, as well as seasons; however, a number of consistent relationships can be identified. The annual ratios show that the P-Day, at the local scale, is related to the anticyclonic group (the ANE, AE and ASE types), and the P-1 Day and the P-2 Day are mainly related to

the ANE, AE and NE types (Figure 5.13). On the other hand, the cases at the regional scale are associated with the A, NE, C, CNE and CE types (Figures 5.13). Otherwise, the P-2 Day is also related to the cyclonic group (the C, CNE and CE types) at the local scale; though the ratios are lower than for the regional scale. For both the local and regional scales, the ozone days are mainly related to anticyclonic and cyclonic patterns, as well as the NE type. In the annual standardised analysis, the correlation between the ozone days and the S and SW types is in accordance with the result of the frequency analysis. However, the E type, at the two spatial scales, shows much less correlation with ozone days compared to the result of the frequency analysis (Figures 5.10 and 5.13).

In spring, the ozone days (P-1 Day and P-2 Day) are related to a variety of circulation types at the local scale. The P-1 Day is related to the anticyclonic group (the ANE, AE and ASE types) and the NE, E, SE and CNE types (Figure 5.14). Moreover, the ANE, NE and CNE types have a higher relation than expected on the P-2 Day (Figure 5.14). The synoptic circulation characteristics of the ANE, NE and E types are related to air flow originating from the East Asian Continent (Figures 5.5 and 5.8), and the CNE type is related to the cyclone originating from southern China or the South China Sea in this season (Figures 5.16a). The air flows of these types may pass through polluted areas (i.e. China and Japan) and bring northeasterly flow to Taiwan. The results suggest that the ozone days related to these types may be caused by long-range transport. In the cases of the ozone days within the SE and ASE types, the features of the composite maps in Figures 5.5 and 5.8 suggest that ozone days may result from more local pollution, as the air flows of these two types mainly originate from low polluted areas (maritime areas). Otherwise, the P-Day shows a clear relationship within the anticyclonic group (the A,

ANE, AE and ASE types) which is similar with the result of the frequency analysis (Figure 5.14).

For the regional scale, the P-1 Day and P-2 Day ozone days are mainly associated with the cyclonic group (the C, CNE and CE types), which also show at the local scale (Figures 5.14 and 5.15). The synoptic circulation features of the cyclonic type show low pressure over the South China Sea and the air flows pass through South China and Southeast Asia (Figure 5.16a). The characteristics of the cyclonic group suggest that the ozone days may be related to long-range transport and the source region of pollutants may be from south China and Southeast Asia in spring (Figure 5.16a).

In summer, the ozone days (P-1 Day and P-2 Day) correspond with the ANE, AE and NE types at the local and regional scales (Figures 5.14 and 5.15). The high ratios indicate that the occurrence of these types may result in high probability of ozone pollution in this season. These types show that Taiwan is under the influence of air flow from the East Asian continent (Figure 5.16b). The air flows of these types may bring ozone or its precursors from the East Asian continent to Taiwan. In addition, the correlation between the ozone days and the C and CE type, at the regional scale, suggests that ozone pollution may be affected by the air flow from southern China or Japan (Figures 5.6 and 5.9). The E type is associated with ozone days (P-Day, P-1 Day and P-2 Day) at both local and regional scales. The circulation features suggest that ozone pollution within the E type in this season may result from local pollution, as the composite map shows a weak flow over Taiwan (Figure 5.6a-5). In the standardised analysis, there is no obvious correlation between the ozone days and the U type, which is different from the result of the frequency analysis (Figures 5.14 and 5.15).

In autumn, the circulation types of the ozone days, at the local scale, resemble the cases in spring (Figure 5.14). The ozone days (P-Day, P-1 Day and P-2 Day) are associated with the anticyclonic group. In addition, the P-1 Day and P-2 Day ozone days are also related to the NE type (Figure 5.14). The similar circulation patterns on the ozone days in spring and autumn may be because these two seasons are transition seasons for Taiwan; the synoptic weather is affected by the evolution of a Siberian anticyclone and a Pacific anticyclone (Figure 5.16c). For the regional scale, the ozone days are related to the anticyclonic group (the A, ANE, and ASE types), the CNE and NE types (Figure 5.15). In this season, the circulation features show small pressure gradients around Taiwan and air flow from the northeast direction to Taiwan, except for the AE type at the local scale (Figure 5.16c). The characteristics of circulation types (the A, ANE, CNE and NE types) suggest that ozone or its precursors may be transported from polluted areas (i.e. China Korea and Japan) and accumulated in Taiwan, as small pressure gradients occur in this season. Therefore, ozone pollution in this season may be affected by both local pollution and long-range transport (Figure 5.16c). The comparison of the results between standardised analysis and frequency analysis indicates that the relationship between the ozone days and the E type is not that obvious in the standardised analysis in this season, though the E type shows the highest frequency in the frequency analysis. However, the results of the standardised analysis show clearer features of the circulation types associated with ozone pollution compared to the result of frequency analysis, because the standardised analysis reduces the effect of high frequencies types on the identification of the relationship between ozone days and circulation types (for example, the E type in spring and autumn and the U type in summer).

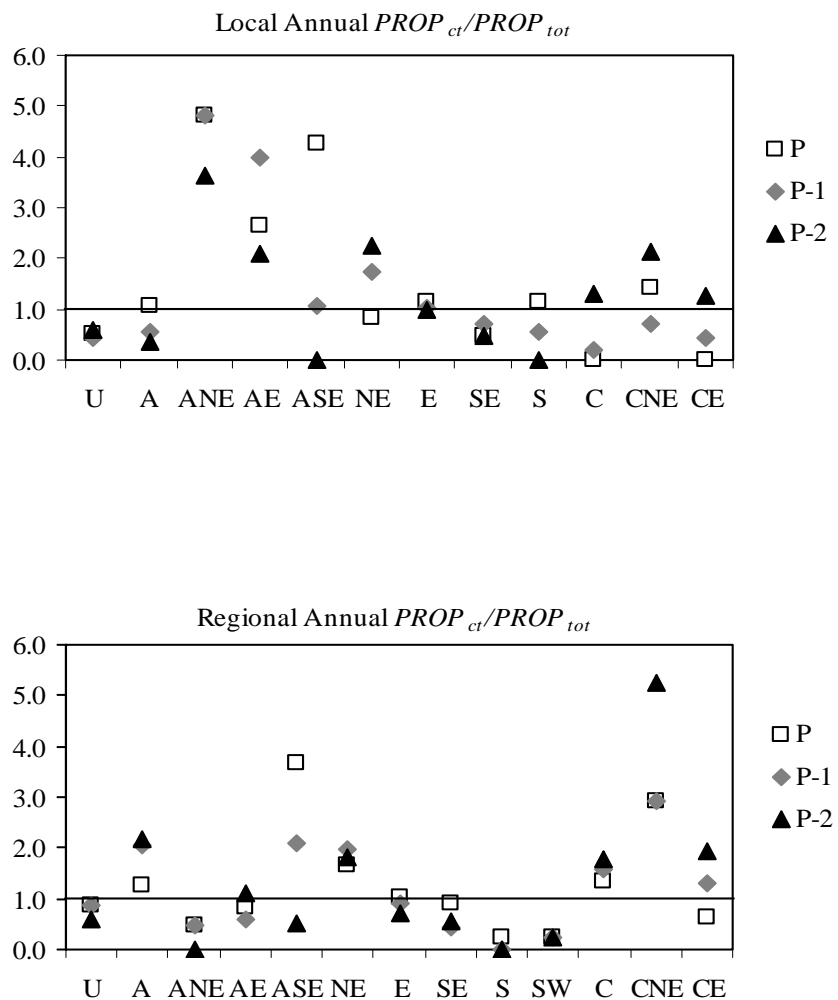


Figure 5.13: Standardised ratios $PROP_{ct}/PROP_{tot}$ of year for ozone days (P-Day, P-1 Day and P-2 Day) at the local and regional scale.

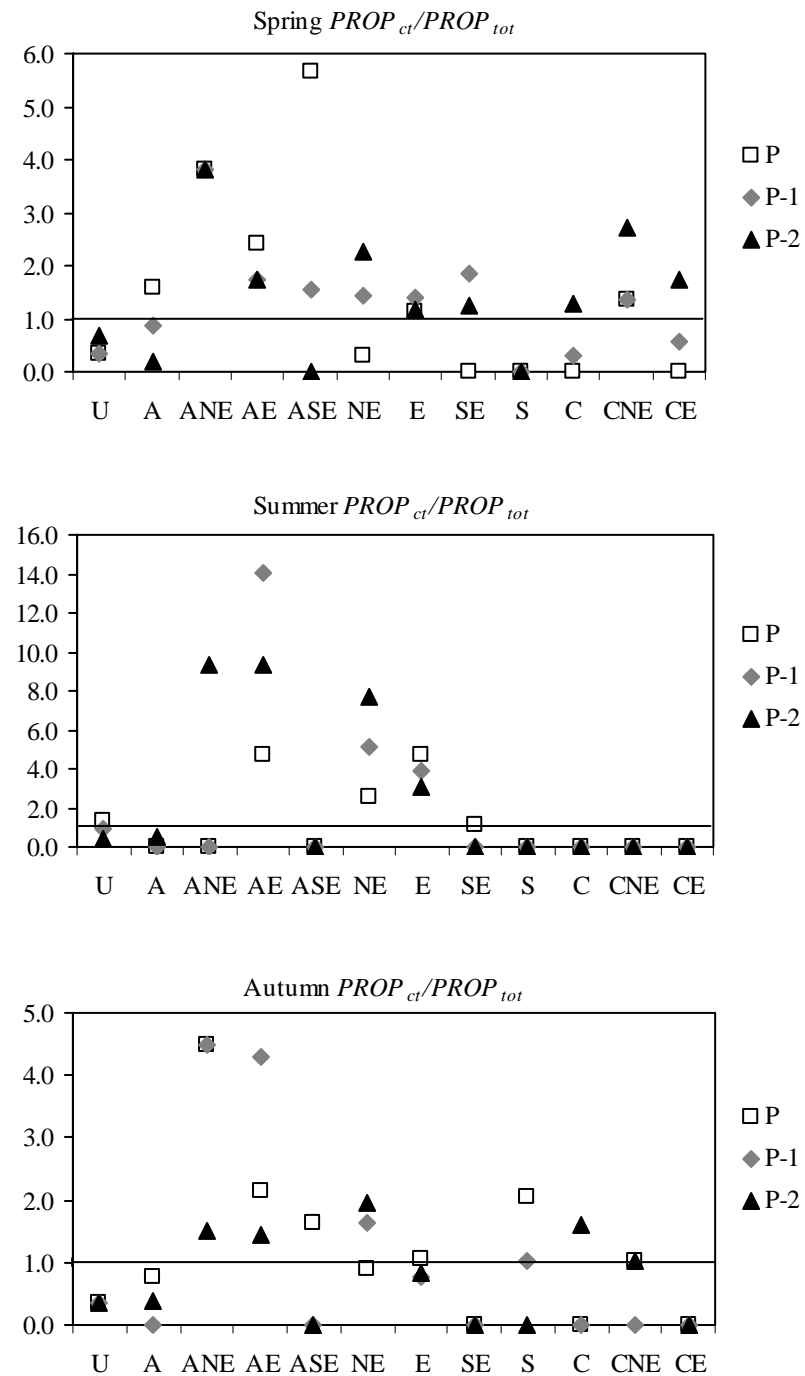


Figure 5.14: Standardised ratios $PROP_{ct}/PROP_{tot}$ for spring, summer and autumn for ozone days (P-Day, P-1 Day and P-2 Day) at the local scale.

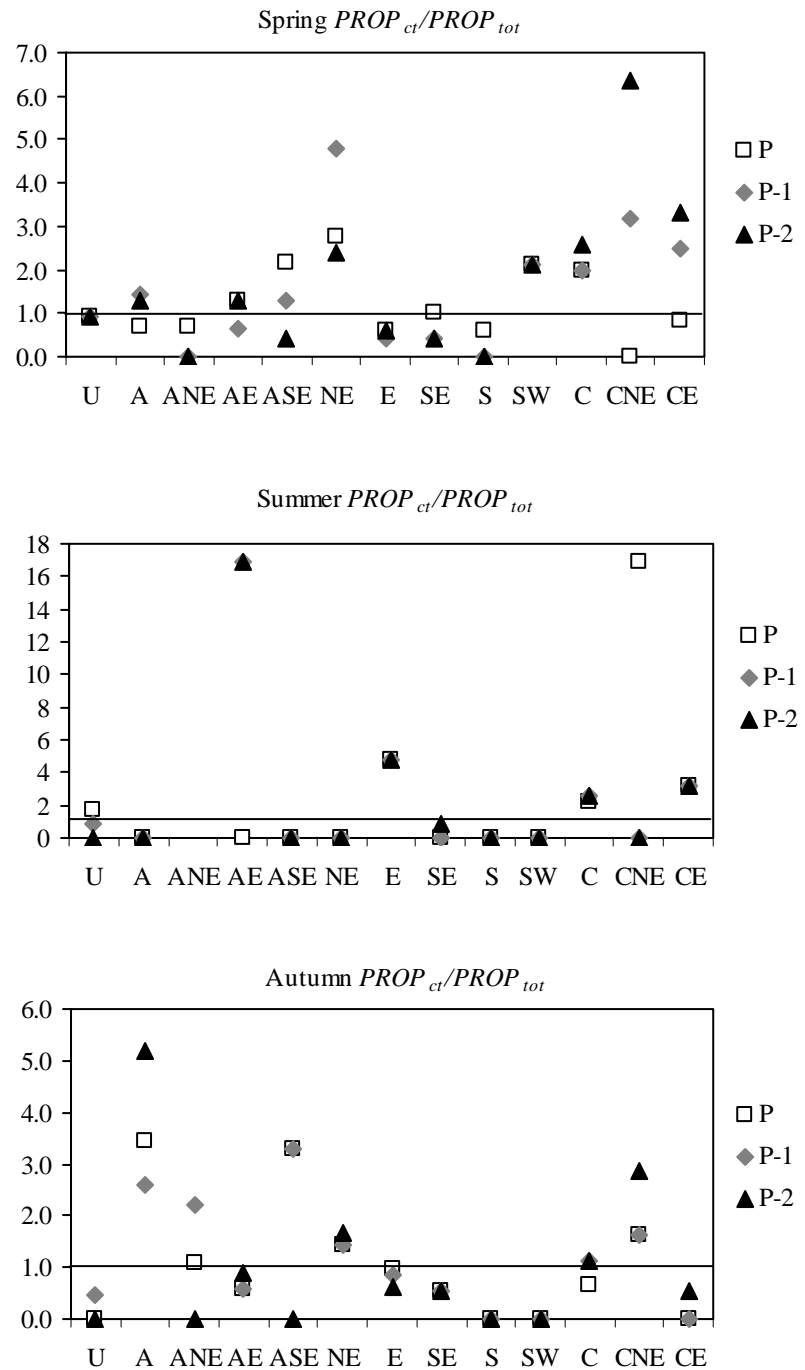


Figure 5.15: Standardised ratios $PROP_{ct}/PROP_{tot}$ for spring, summer and autumn for ozone days (P-Day, P-1 Day and P-2 Day) at the regional scale.

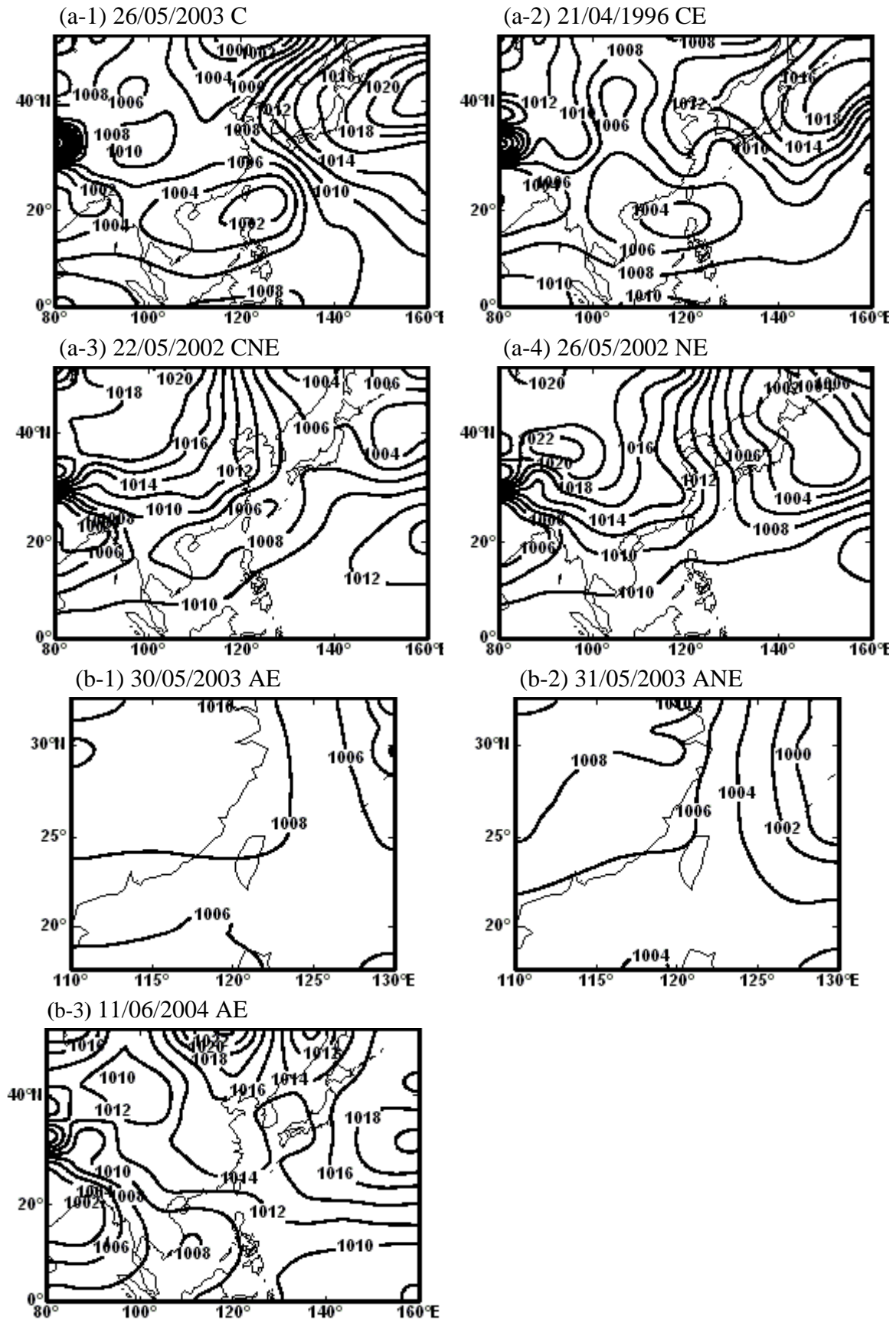
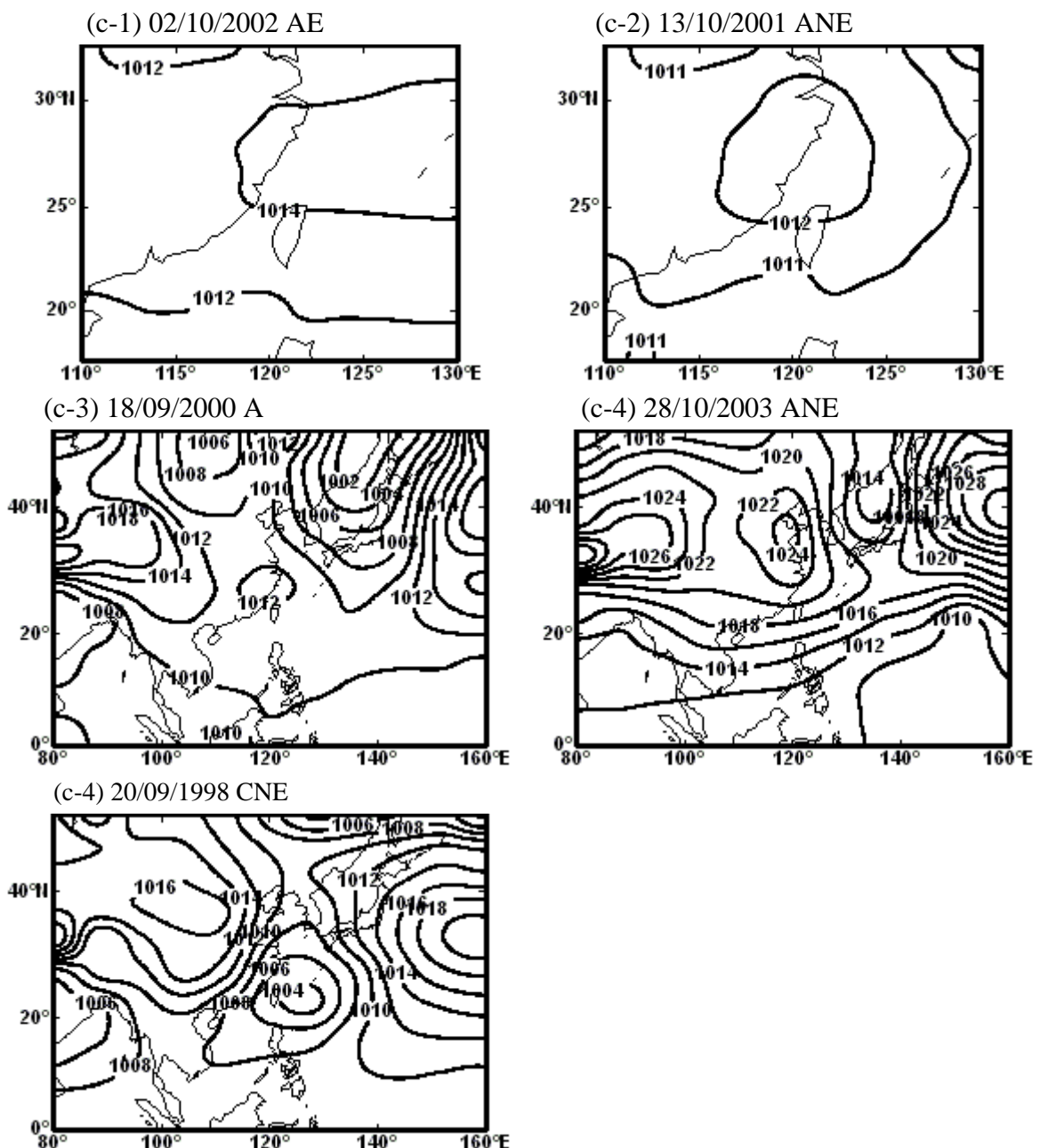


Figure 5.16: Seasonal mean sea level pressure (hPa) map of selected circulation types for ozone days at both local and regional scales.

Figure 5.16:



5.3.3 Discussion

The relationship between ozone days (P-Day, P-1 Day and P-2 Day) and circulation types shows that the ozone days, at the local and regional scale, are mainly associated with anticyclonic types, cyclonic types and the NE type, but vary with season. The P-Day is associated with the anticyclonic types (i.e. the A, ANE, AE and ASE types) in spring and autumn for the local scale and only autumn for the regional scale. The characteristics of the anticyclonic types suggest that subsidence associated with anticyclones may result in ozone pollution occurring under anticyclonic types, as the subsidence of high pressure impedes pollutants' dispersion.

The important circulation types on the days prior to the P-Day (i.e. P-1 Day and P-2 Day) are the types with northeasterly flow, such as the ANE, CNE and NE types, for both the local and regional scales in spring and autumn. The synoptic features of these circulation types show that air flows pass through an area of high pollution (i.e. China, Korean and Japan). Ozone and its precursors may be collected from these areas and transported downward to Taiwan. These results suggest that ozone pollution occurring in these two seasons is very likely related to long-range transport. Otherwise, it is worth noting that the circulation features of the cyclonic types, at the regional scale, suggest that ozone pollution may be contributed to by different source regions in different seasons; the pollutants may be transported from southern China to Taiwan in spring (Figure 5.16a), and northern China, Korea and Japan in autumn (Figure 5.16c). The characteristics of circulation types (i.e. the ANE, AE and NE types) on the P-1 Day and P-2 Day in summer demonstrate that ozone pollution in this season is related to long-range transport, and the east coast of China is a possible source region. Otherwise, the relationship between the C and CE types and the ozone days suggests that southern China and Japan are also possible source regions of ozone and its precursors in summer.

In addition to the contribution of long-range transport to ozone pollution, the features of the SE and ASE types in spring and autumn, and the E type in summer suggest that ozone pollution can also be associated with local pollution events because the air flows of these types are from clean, maritime regions to southeastern Taiwan.

5.4 The analysis of large-scale atmospheric circulation links with HOD₃

In this section, the features of the large-scale atmospheric circulation that accompany high ozone pollution days, as defined by the HOD₃ index, which is defined as a day with three or more stations exhibiting a daily concentration > 60 ppb (see Section 3.3.3), are investigated using sea level pressure (SLP) data and geopotential height data at the 850hpa level (see Section 3.6). Both absolute and anomaly maps are presented to define the characteristics of the large-scale circulation on ozone days to throw light on the role of long range transport, in particular, identified as possibilities in the preceding discussion. Given the seasonal evolution of the atmospheric circulation, the analysis is stratified by month to focus on the analysis of high ozone pollution months. A random selection of non-pollution days (see Section 3.7) is used as a control.

The composite geopotential height anomaly map of the ozone days in April (Figure 5.17a-left) shows a positive pressure centre northwest of Taiwan, which may collect pollution over the underlying source regions, and a strong anomalous airflow from northeast to southwest over Taiwan, suggesting long-range transport from the direction of mainland China, Japan and Korea (Figure 5.17 a-left). In contrast, on the non-pollution days in April (Figure 5.17a-right), the anomalous map shows an interaction between a positive circulation located in the northeast Asia region and negative circulation over the Pacific Ocean (Figure 5.17a-right) bringing pristine air masses from maritime areas. The anomalous SLP maps show a similar pattern of flow to the anomalous map of geopotential height (Figure 5.17a and b left).

For May, the anomaly maps of geopotential height and SLP are similar to the anomaly maps in April but the pattern is much stronger (Figure 5.18a and b left).

In the cases of ozone days in June, Taiwan is affected by a cyclone or the peripheral circulations of a cyclone (Figure 5.19a and b left). Generally, the weather conditions of a cyclone are associated with strong convective activity which is unfavourable for ozone formation. However, the anomalous patterns show a similar pattern to April and May (Figure 5.19a and b lower left) with air flows from the notheasterly direction, though the pattern is weaker than in April and May.

During September, the patterns are quite different. The ozone days are associated with a strengthening of the dominant high pressure belt, particularly the two main centres (Figure 5.20a-left). The anomalous map presents a strong and significant positive pressure centre located over mainland China (Figure 5.20a lower left) and illustrates that Taiwan is under an anomalous air flow along the east coast of China. Otherwise, the composite maps of SLP show a trough from the equator to Japan, enhanced air flow from Japan is observed both in the actual and anomaly maps (Figure 5.20b-left). The results suggest that both mainland China and Japan may be the precursor source of ozone pollution in September. With respect to the non-pollution days, the patterns suggest that Taiwan is affected by a later (delayed end) summer monsoon over southern China which delivers a cleaner air mass from maritime areas to Taiwan.

In October, the geopotential height maps (Figure 5.21a-left) illustrate the influence of the Siberian high and an intensive trough from Japan and a northward displacement of the Pacific anticyclone. In this month, Taiwan is controlled by the Siberian anticyclone (Figure 5.21a and b left). Nevertheless, there is no obviously anomalous air flow affecting

Taiwan, except the circulation near Japan may bring a northeast direction flow towards Taiwan (Figure 5.21a and b lower left), but this is not as marked as in the September case.

The anomalous maps for November show an intensification of the prevailing seasonal circulation, with Taiwan on the fringe of a large negative pressure anomaly area and the peripheral circulation from mainland China passing over the country (Figure 5.22a and b lower left). The composite maps of non-pollution days show Taiwan affected by anomalous easterly flow from low polluted maritime areas (Figure 5.22a and b right). These results strongly suggest a role for long-range transport in the contrast between polluted and non-polluted source areas for the air passing over Taiwan during pollution and non-pollution days, respectively.

To summarise, in spring, the findings suggest that long-range precursor transport from a northeasterly direction may be a factor determining the occurrence of high ozone days with stronger anticyclonic conditions permitting the accumulation of pollutants over source regions and dispersal to the periphery. The suggested pollutant source area in this case is over the region north and northeast of Taiwan. The high ozone pollution observed in May should be considered as the result of interaction between long-range precursors transport and local stable weather conditions. Significantly enhanced northerly or northeasterly flows are also observed in autumn, though the pattern is much stronger in September.

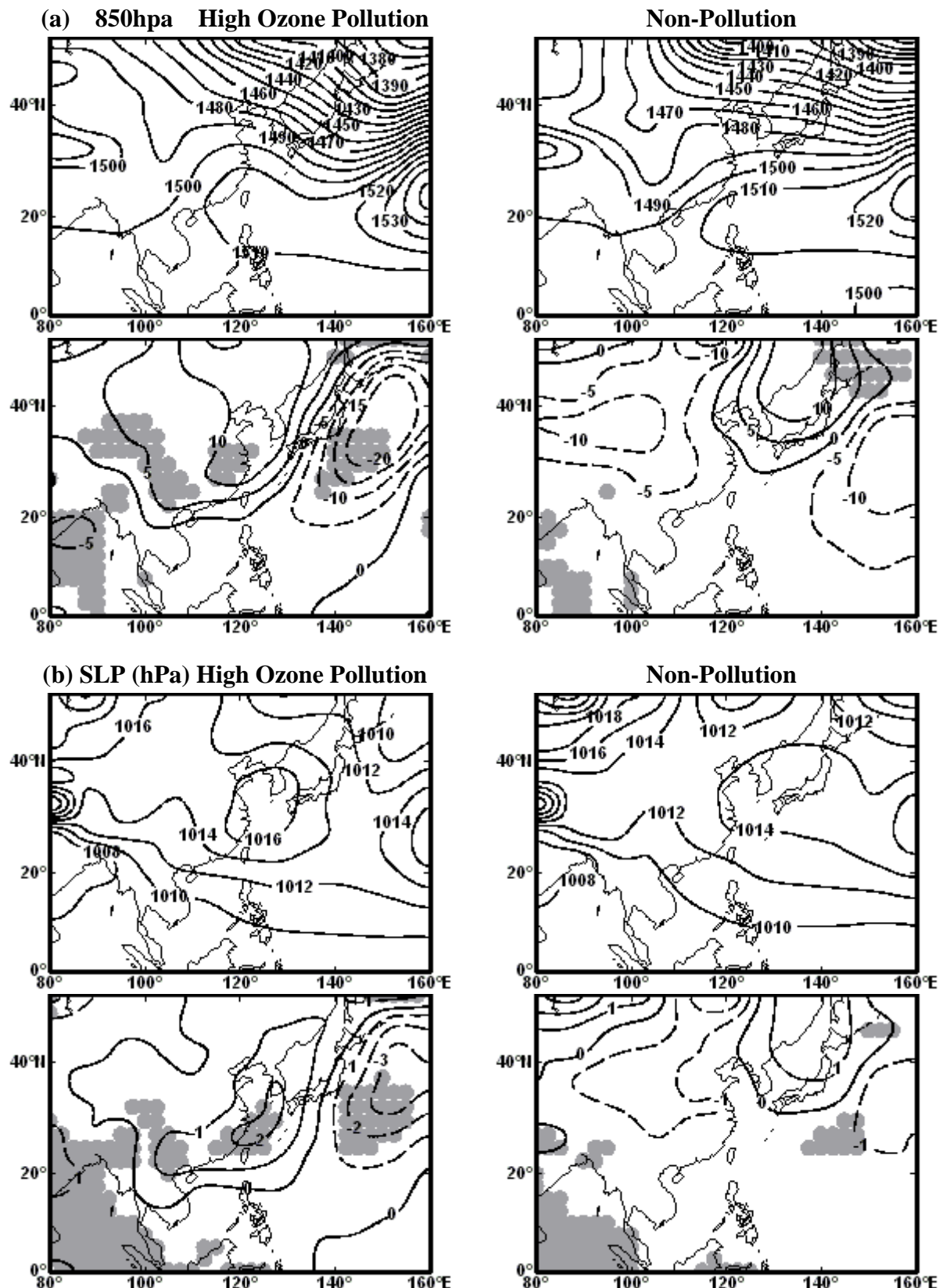


Figure 5.17: High ozone pollution (left) and Non-pollution (right) days average geopotential height at 850hPa (a) and SLP (hPa) (b) absolute (upper) and anomalies (lower) values for April (22 days). Anomalies significant at the 5% level are shaded.

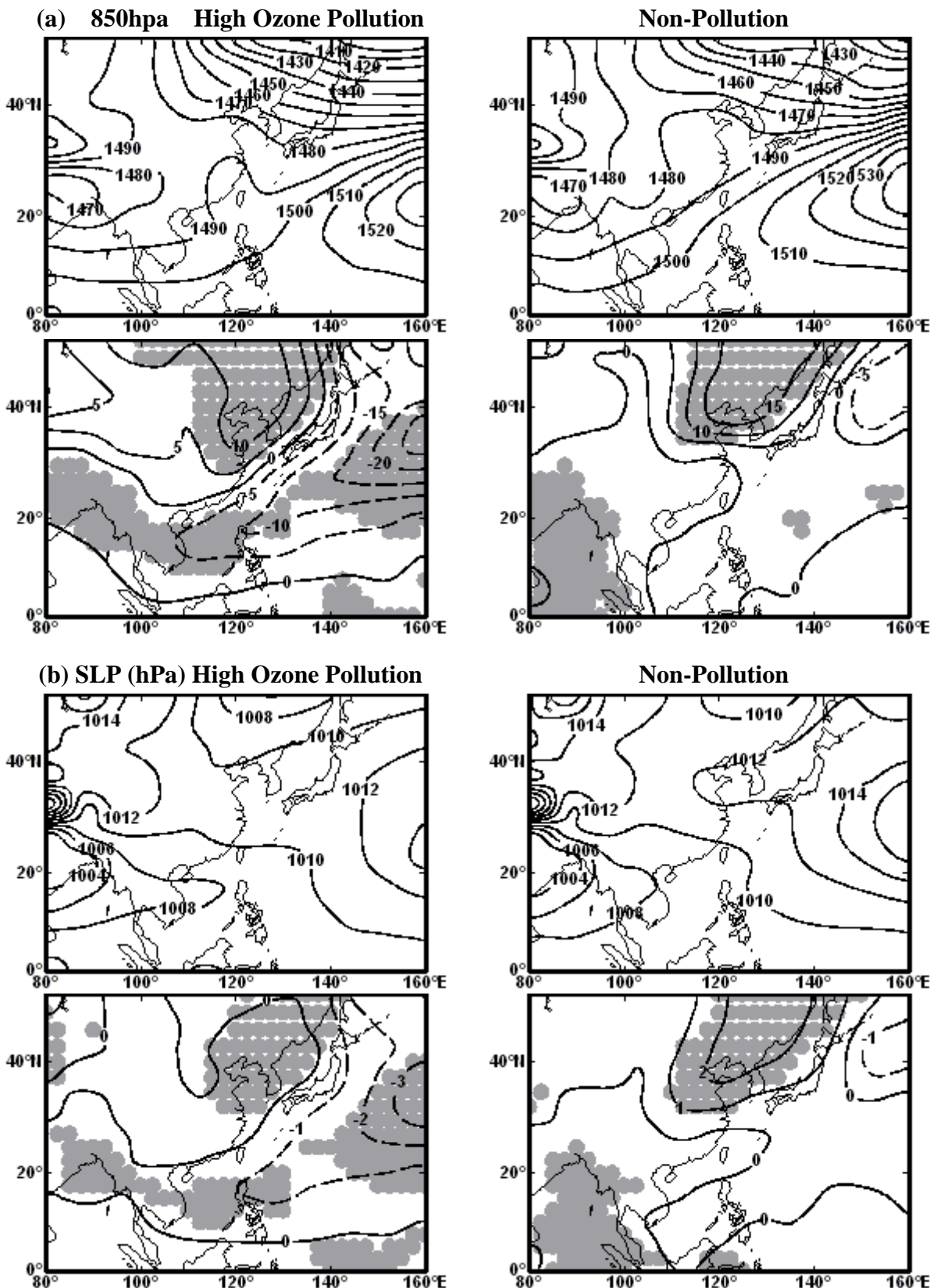


Figure 5.18: High ozone pollution (left) and Non-pollution (right) days average geopotential height at 850hPa (a) and SLP (hPa) (b) absolute (upper) and anomalies (lower) values for May (29 days). Anomalies significant at the 5% level are shaded.

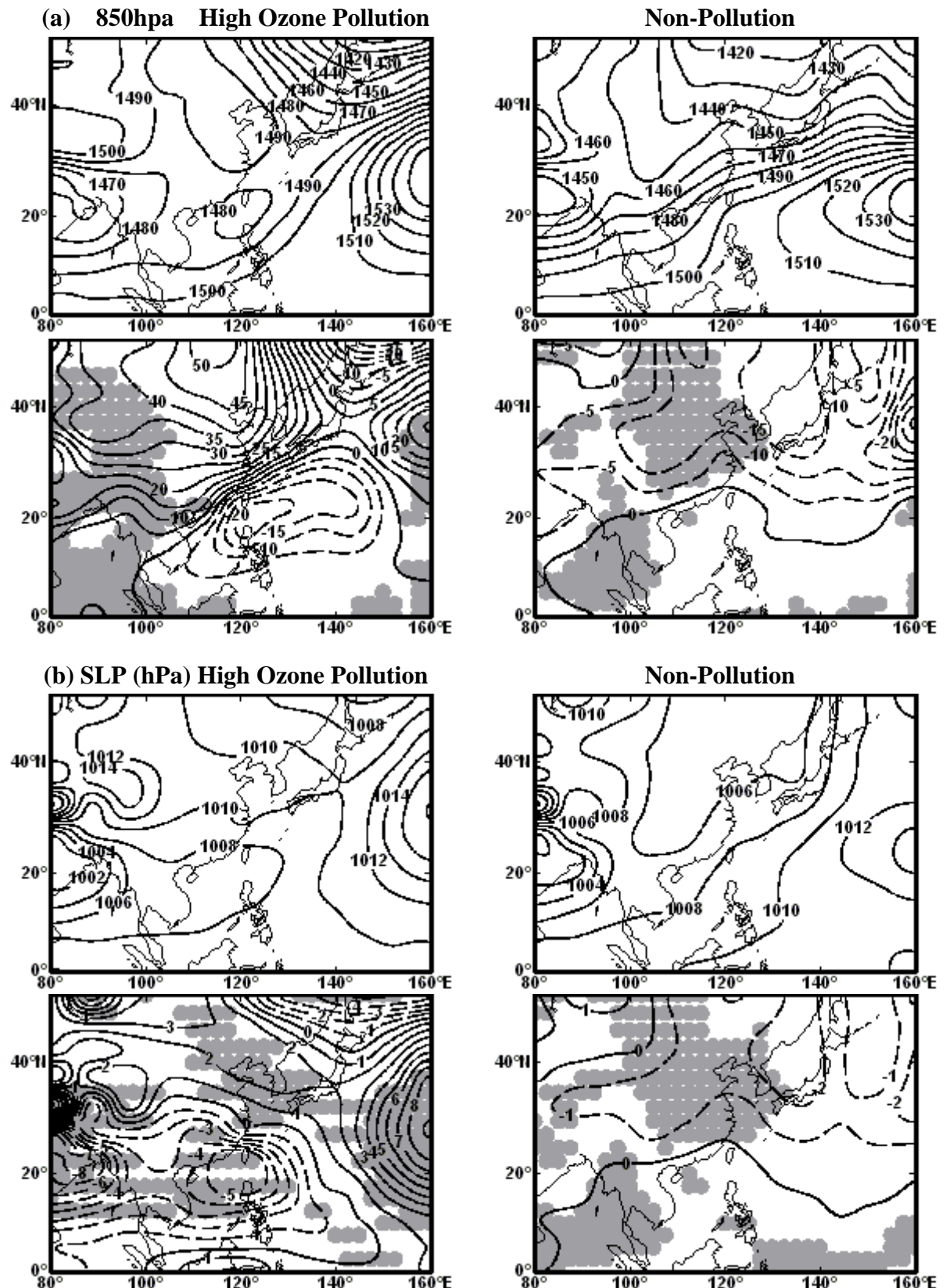


Figure 5.19: High ozone pollution (left) and Non-pollution (right) days average geopotential height at 850hPa (a) and SLP (hPa) (b) absolute (upper) and anomalies (lower) values for June (10 days). Anomalies significant at the 5% level are shaded.

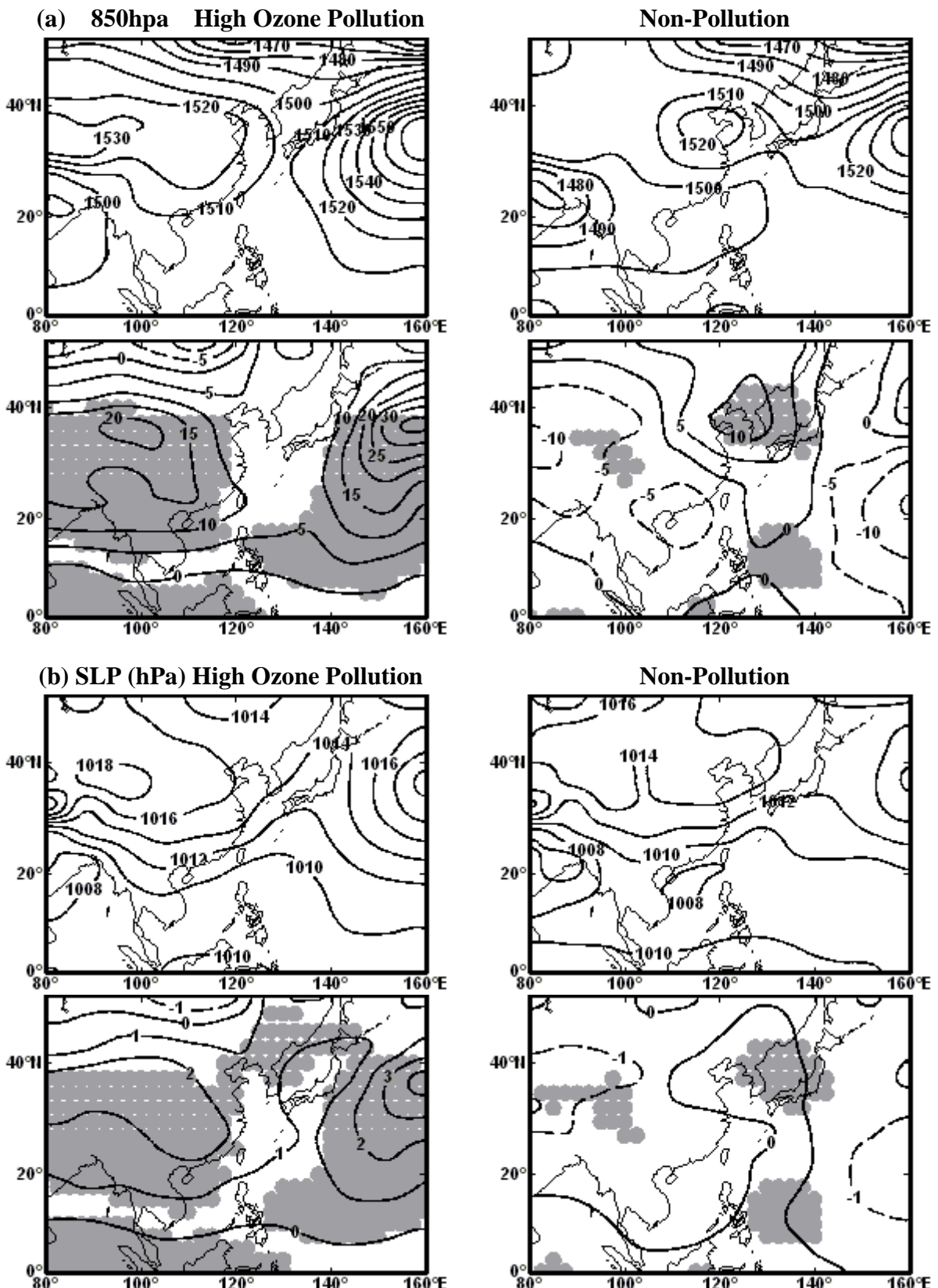


Figure 5.20: High ozone pollution (left) and Non-pollution (right) days average geopotential height at 850hPa (a) and SLP (hPa) (b) absolute (upper) and anomalies (lower) values for September (19days). Anomalies significant at the 5% level are shaded.

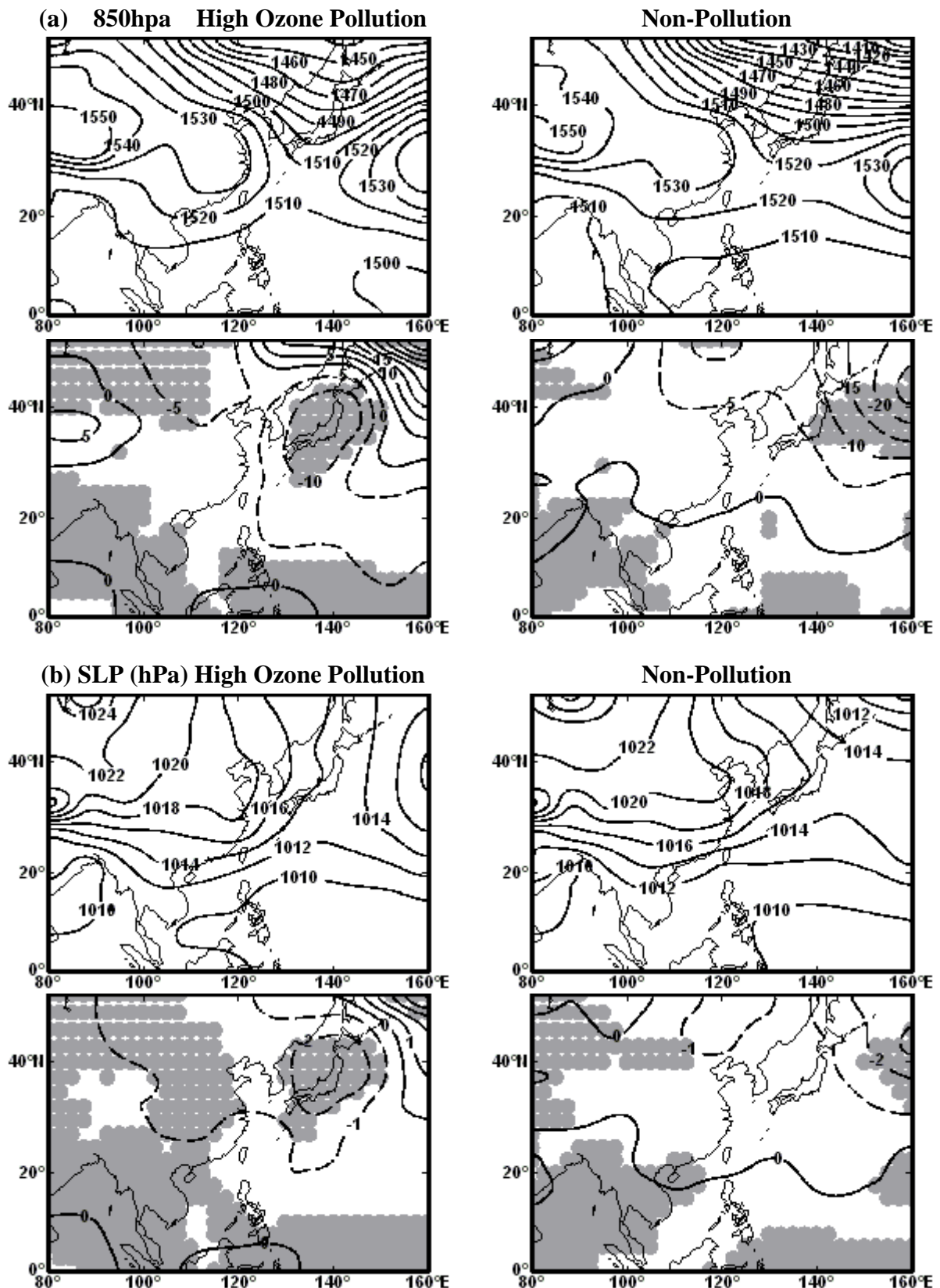


Figure 5.21: High ozone pollution (left) and Non-pollution (right) days average geopotential height at 850hPa (a) and SLP (hPa) (b) absolute (upper) and anomalies (lower) values for October (32 days). Anomalies significant at the 5% level are shaded.

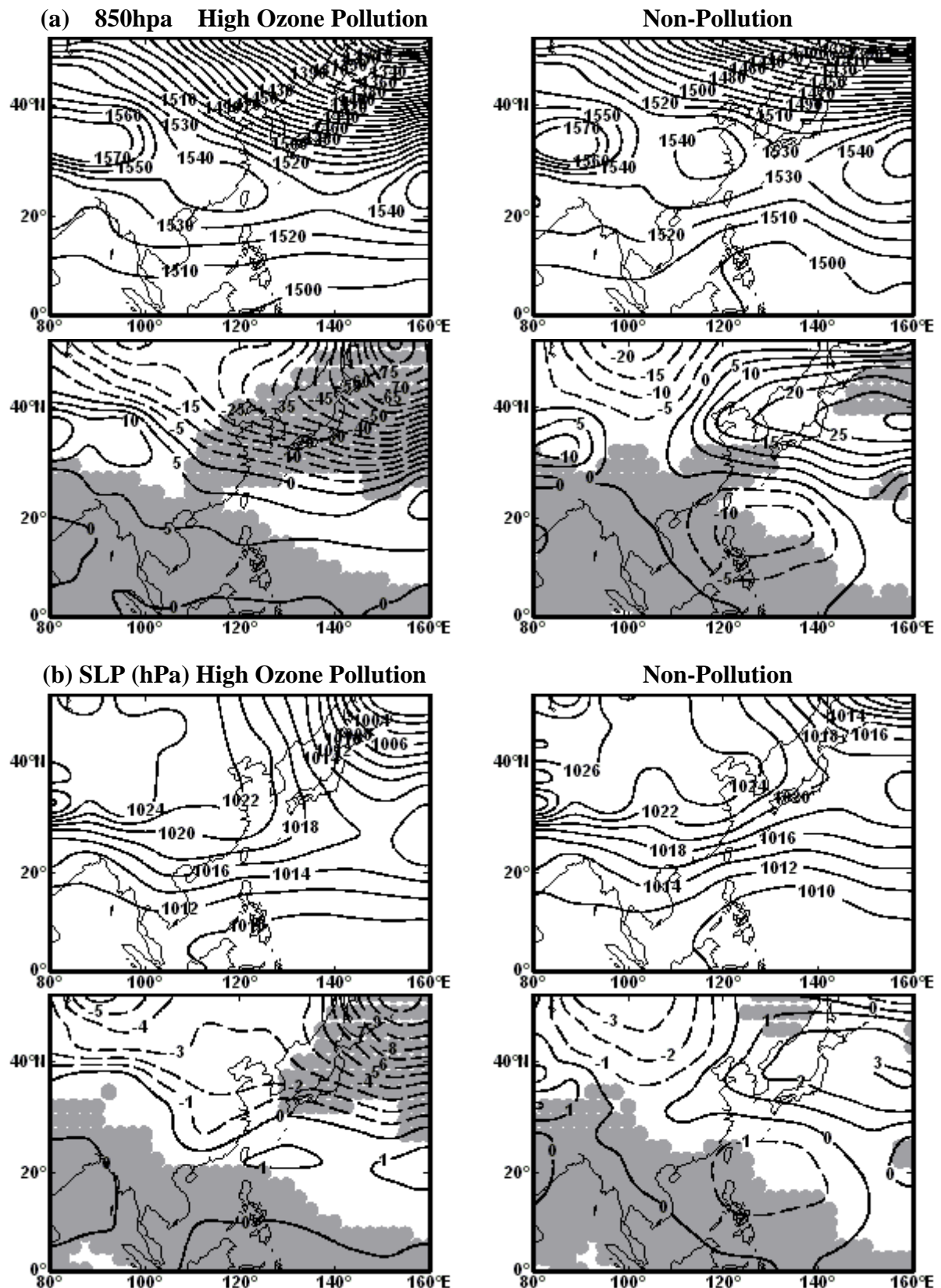


Figure 5.22: High ozone pollution (left) and Non-pollution (right) days average geopotential height at 850hPa (a) and SLP (hPa) (b) absolute (upper) and anomalies (lower) values for November (10 days). Anomalies significant at the 5% level are shaded.

5.5 Summary

The successful results of weather type classification by the objective scheme show seasonal characteristics of circulation weather types in Taiwan at two different scales (local and regional scales). On the basis of the results of the composite SLP and geopotential height analyses, the relationship between the ozone days (P-Day, P-1 Day and P-2 Day) and circulation type is identified for the local and regional scales. Four key findings in this chapter can be summarised as follows:

- Consistent with the climate of Taiwan, the synoptic circulation in Taiwan is mainly classified as the E and NE types; the prevailing winds around Taiwan are usually easterly or northeasterly, except for the circulations in summer, which are related to the C, S and SW types.
- The long-term trends of circulation types indicate that the NE type increases significantly in spring, and while the S and SW types significantly decrease in spring and summer at both spatial scales. Changes of these types may influence the winter and summer monsoon activities in Taiwan.
- Ozone pollution is mainly associated with the types with northeasterly flow (i.e. the ANE, CNE and NE types) in spring, summer and autumn. The air flows of these types suggest that long-range transport from a northeasterly direction may be a factor in high ozone pollution in Taiwan.
- The correlation between ozone pollution and the cyclonic types (i.e. the C, CNE and CE types) suggests that convective activity may also play a role in long-range transport and the source region of pollutants may differ with season; pollutants

may be transported from southern China and Southeast Asia in spring and Northeast Asia in autumn.

The relationships between ozone pollution and synoptic circulation demonstrated in this chapter suggest that ozone days are related to air flows originating from the East Asian continent. However, the source region and the transport pathways of long-range transport need to be further clarified; a back trajectory analysis is used to investigate the source-receptor relationship in chapter six.

Chapter 6: Trajectory Analysis

6.1 Introduction

In the previous chapter, the circulation weather types and spatial compositing analyses showed pronounced airflows from the north or northeast direction towards Taiwan during the ozone days. These air flows may export pollutants from source areas of Northeast Asia to Taiwan. Back trajectory analysis is employed to test the apparent relationship between source-receptor of ozone pollution at the north (25°N , 121.3°E) and south (22.5°N , 120.5°E) sites in Taiwan. The selection of two receptor sites is due to the climatic distinction between the north and south Taiwan. In the south, the climate is mainly affected by tropical monsoon activity. On the other hand, the climate in the north Taiwan is classified as subtropical climate. Three-day back trajectory simulations arriving at three different heights, 100m, 500m and 2000m above ground level are computed with a six-hour timestep from 04:00 UTC. A comparative analysis is investigated to discriminate the difference of transport pathways between pollution and non-pollution days (see Section 3.7). The correlation with atmospheric circulation is discussed as well.

6.2 Back Trajectory Analysis

Back trajectories of high ozone days are calculated by the Hybrid Single-Particle Lagrangian Integrated Trajectory model (HYSPPLIT_4) in this study (see Section 3.6). The ozone days used here for trajectory analysis are the index HOD₃ of high ozone days

to be consistent with the ozone days used in spatial compositing analysis in the previous chapter.

Back trajectory analyses showing transport pathways of HOD₃ for each high ozone pollution month at three altitudes of 100m, 500m and 2000m for the two analytical locations are presented in Figure 6.1. The air parcels at 100m and 500m mostly originate in the industrial areas on the east coast of China or northern China and Korea with a few from Japan. The results confirm the findings derived from the analysis of weather types and pressure patterns that air parcels originating in industrial areas may contribute significant ozone or its precursors. The trajectory pattern is especially marked for April, September and October, less so for June. There is, however, a pronounced discrepancy observed at the level 2000m, where the source region is to the northwest of Taiwan (Figure 6.1). It would appear that the key pollutant transport is at a lower level. For the south site, high frequencies of back trajectories at 2000m are related to clean maritime air flows from the South China Sea and the western Pacific Ocean in spring, whilst back trajectories are largely associated with the continental air masses at the north site (Figure 6.1 and 6.2). An example of discrepancy of back trajectories at the high level (2000m) between the north and south sites is shown in Figure 6.2. The trajectories for the north site are mostly related to continental air flows; however, the trajectories for the south site originating from maritime air flows at the level 2000m. In addition, the trajectories at the south sites represent slower-moving air parcels or stagnant circulations.

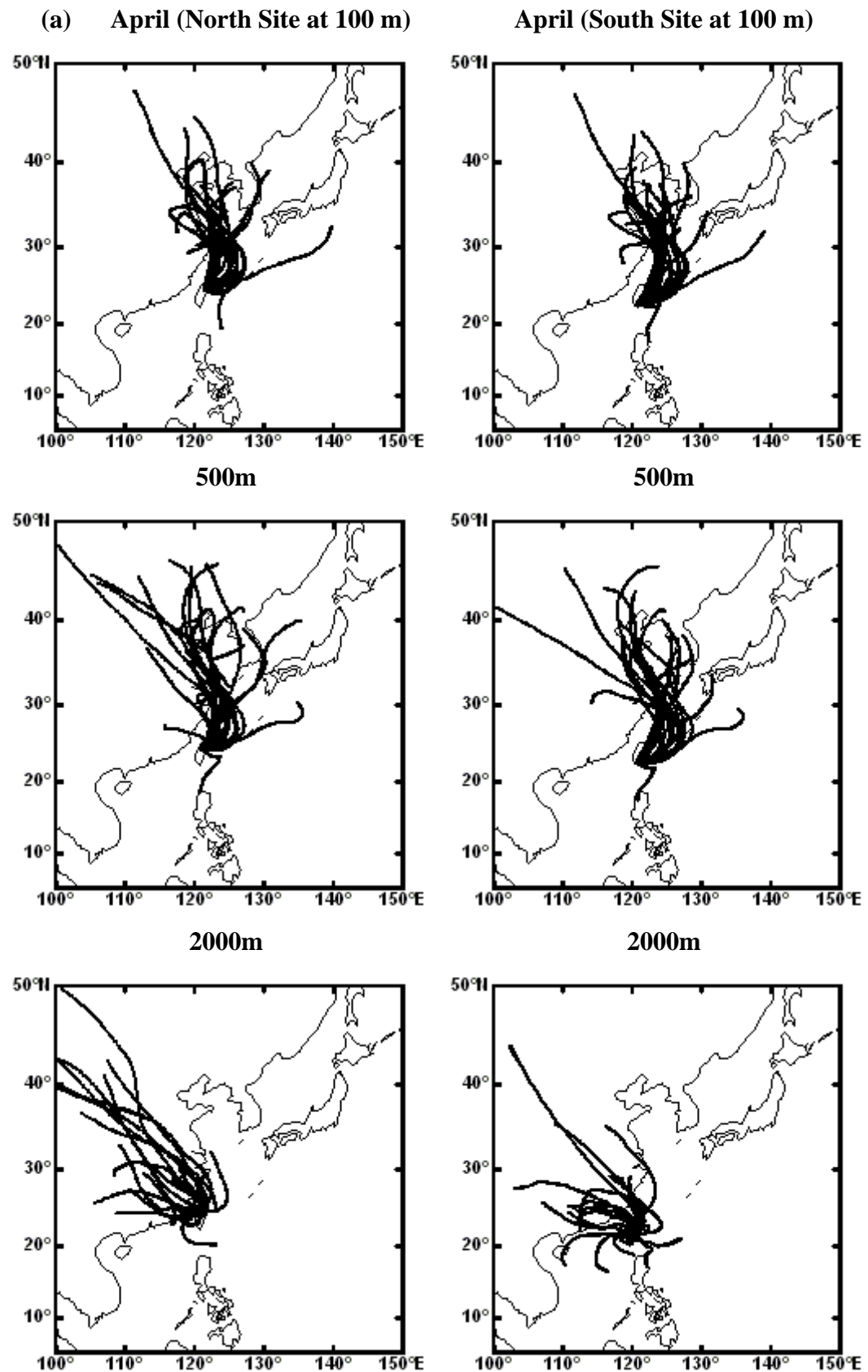


Figure 6.1: Three-day trajectories in April (a), May (b), June (c), September (d), October (e) and November (f), North site in left column and South site ion right column, at the level 100m, 500m and 2000m.

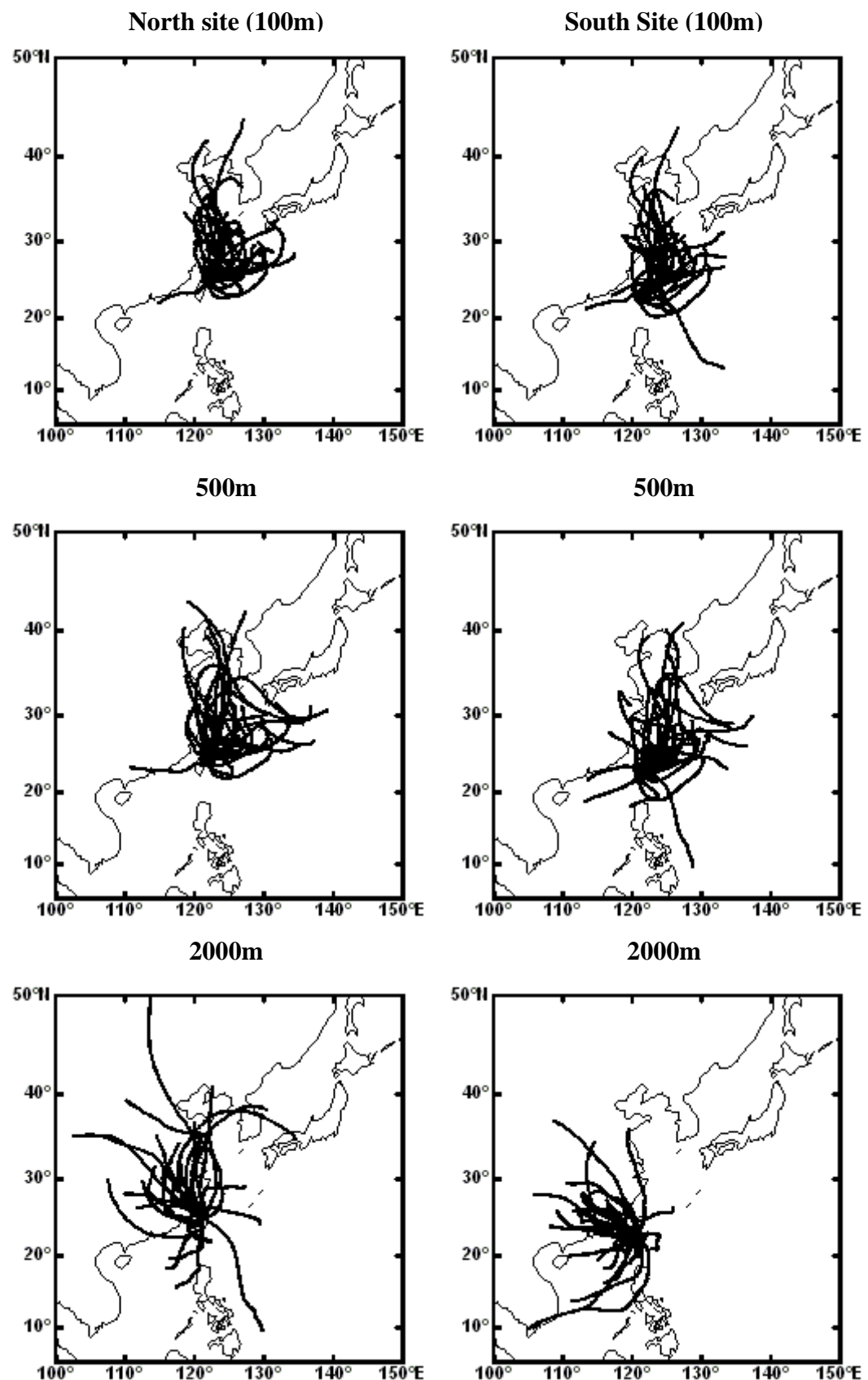
Figure 6.1(b): same as Figure 6.1 (a) but for May

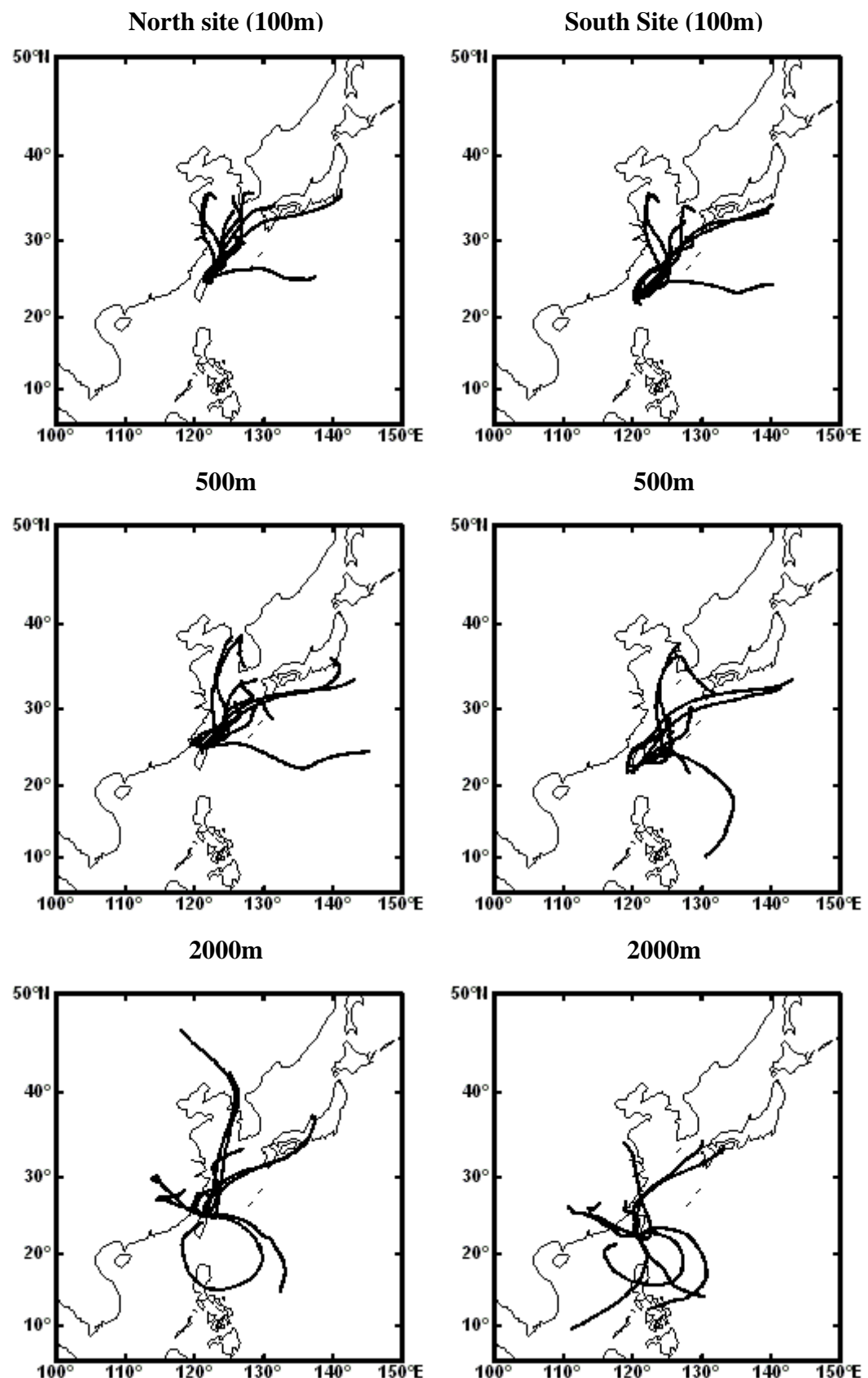
Figure 6.1(c): same as Figure 6.1 (a) but for June

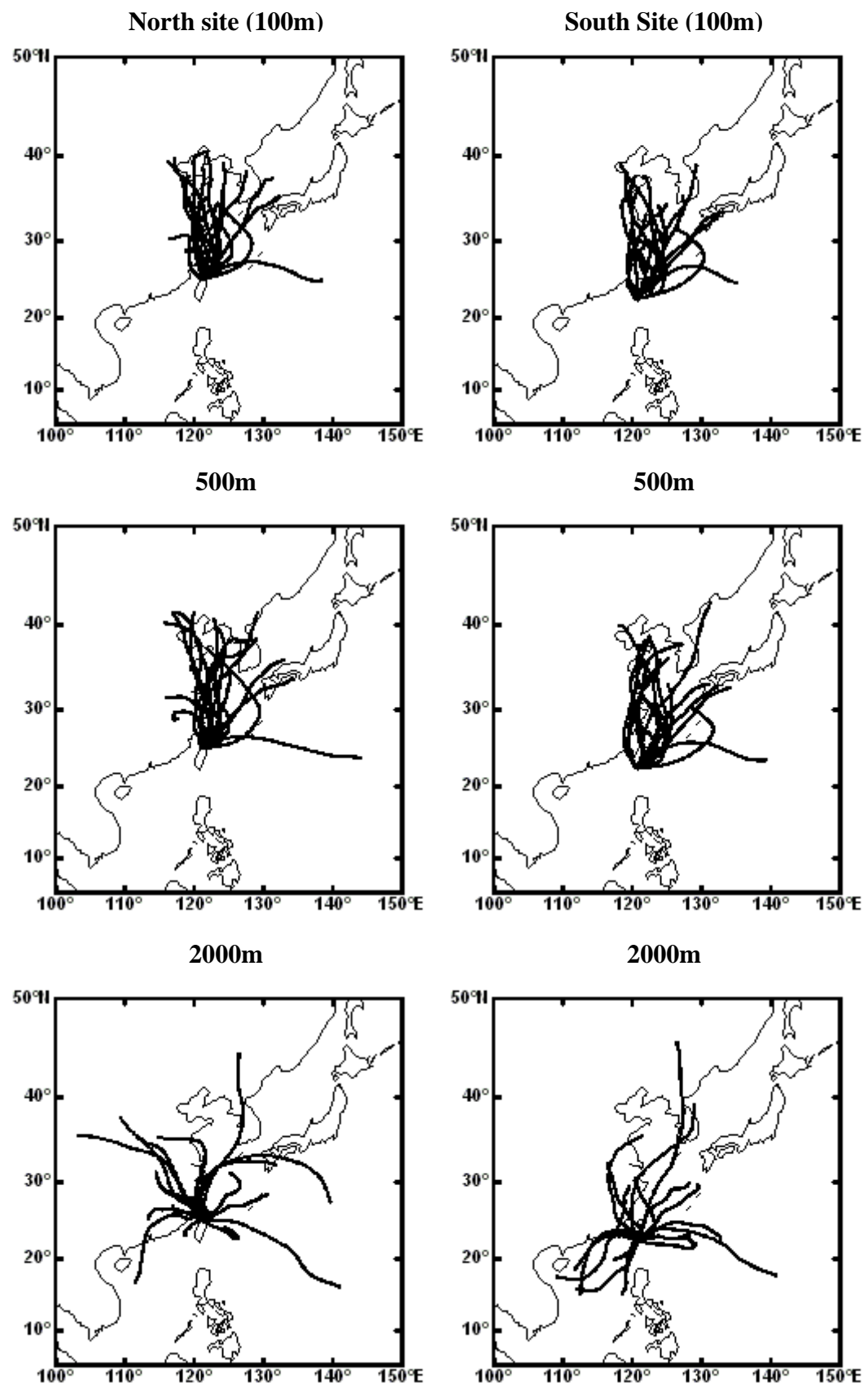
Figure 6.1(d): same as Figure 6.1 (a) but for September

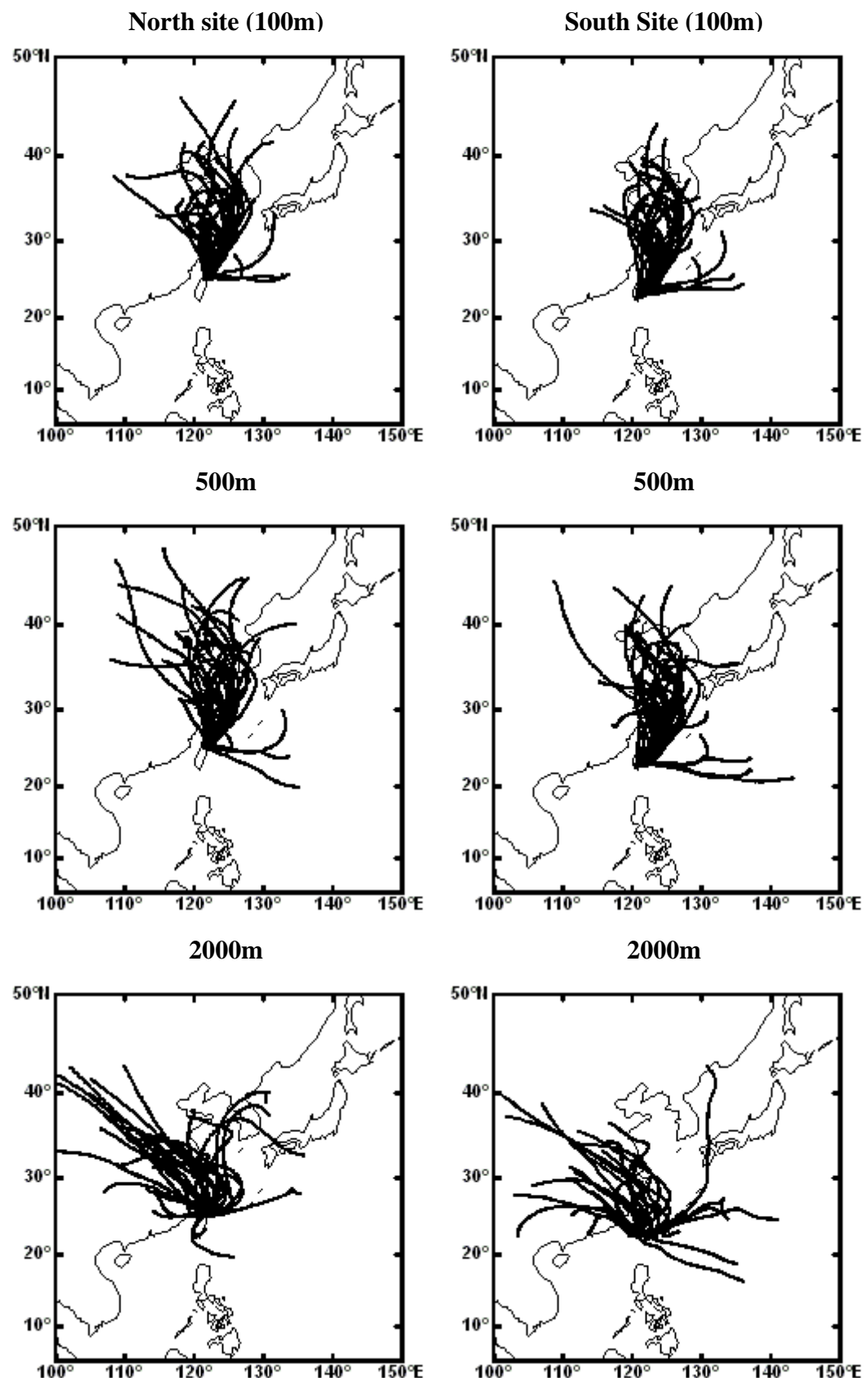
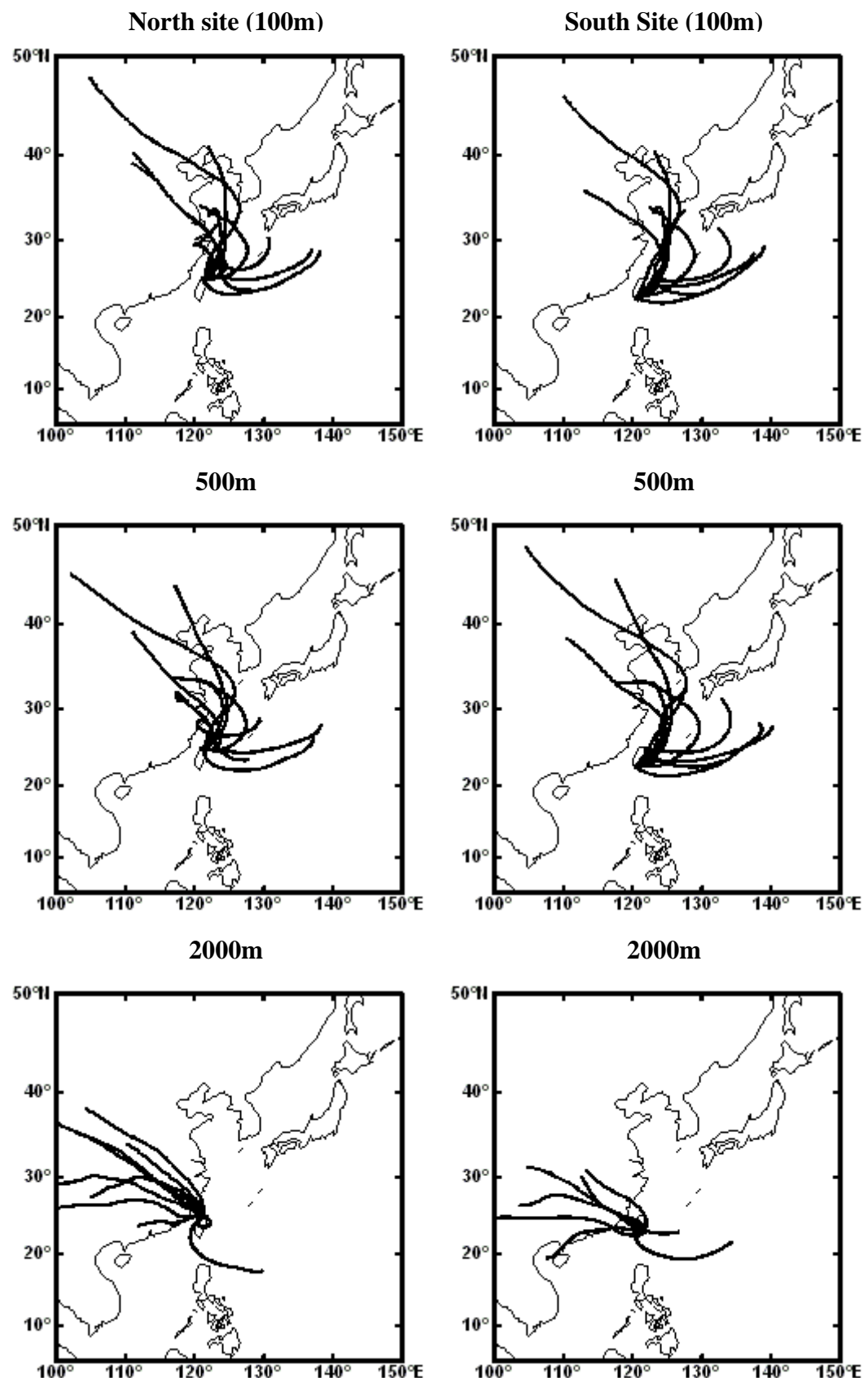
Figure 6.1(e): same as Figure 6.1 (a) but for October

Figure 6.1(f): same as Figure 6.1 (a) but for November

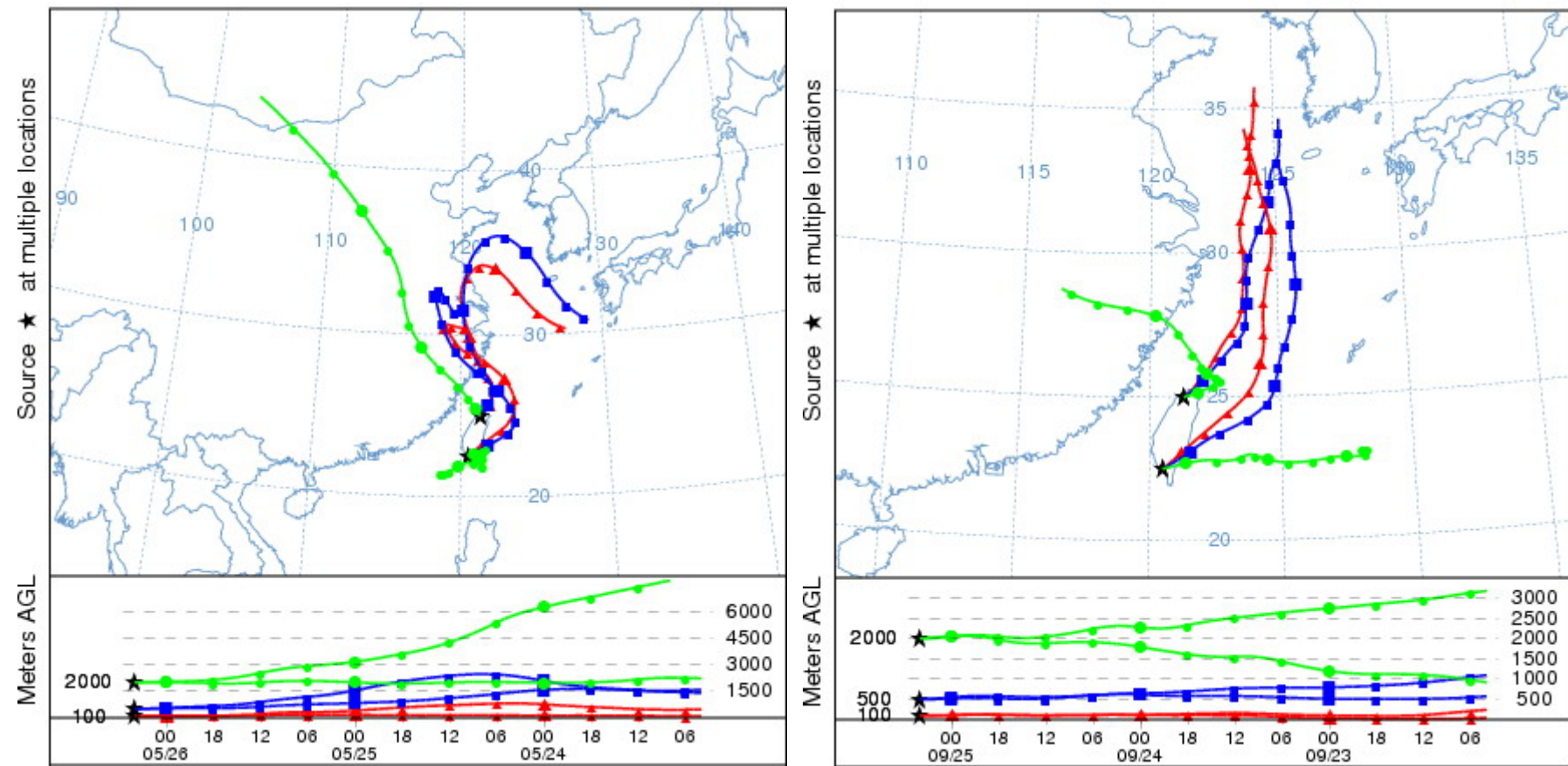


Figure 6.2: The discrepancy of back trajectories at the high level (2000m) for the north and south sites.

To check that the back trajectories for ozone days represent a true characteristic of these days and are not an artefact of the dominant circulation, back trajectory analysis was also performed for a random set of non-pollution days. The results for the pollution and non-pollution days for the north and south are compared in Figures 6.3 and 6.4 and are now discussed in detail. A strong contrast in the trajectories for these two sets of days is clear.

The back trajectory analysis of ozone pollution days in April shows a high proportion of source areas over mainland China and some from Korea at the levels 100m and 500m (Figure 6.3a and 6.4a). However, the investigation of the level 2000m shows that advection changes to mostly a northwest source direction for the north site and west source direction for the south site. In the non-pollution cases for the north site, the back trajectories at the three elevation levels exhibit pathways mainly from low-polluted maritime regions, such as the East China Sea or the South China Sea, and recirculation flows around the Western Pacific region (Figure 6.3a). Although the East China Sea and South China Sea may be affected by air pollutants exported from the Asian continent (Hoell *et al.*, 1996; Jacob *et al.*, 2003), the concentration of pollutants in these regions is still lower than over the Asian continent. The back trajectories of non-pollution days for the south site show that the air parcels originate over the western Pacific Ocean and the South China Sea (Figure 6.4a).

For May, the back trajectory analyses for the pollution days indicate a localised, looping circulation close to Taiwan and the air parcels are mainly from a maritime region at the low levels (100m and 500m), north and northeast from Taiwan (Figures 6.3b and 6.4b). It is suggesting that the circulations at the low levels are associated with stable and stagnant conditions which do not facilitate pollutants dispersion. On the other hand, the

back trajectories at the altitude of 2000m show high frequencies of air parcels originating from over China. The result suggests that ozone or its precursors may be transported by convective activity of cyclone in the South China Sea. The ozone contributed from South China is also observed in Japan (Naja and Akimoto, 2004). The back trajectories of non-pollution days present a quite similar pattern to the cases in April, in spite of less air parcels related to continental air masses (Figures 6.3b and 6.4b).

In the case of June, the trajectories for the pollution days show slow-moving air parcels apparently originating from Korean and Japan, particularly for the north site (Figures 6.3c and 6.4c). At the level of 2000m, the circulation flows around Southeast Asia suggest that Taiwan is under a cyclonic synoptic weather pattern. The trajectory of air parcels for the non-pollution days mostly originate from southern, low-polluted maritime areas (Figures 6.3c and 6.4c).

In September, the trajectories for the pollution days show a similar distribution at low levels (100m and 500m), from the north and over the eastern coastline of China (Figures 6.3d and 6.4d), suggesting again that pollutants are transported at low levels from the east cost of China, Korea and Japan. On the other hand, the non-pollution days are obviously associated with fast-moving air parcels from maritime regions, which deliver clean air masses to Taiwan and may sweep away local pollution resulting in low ozone levels.

The trajectories in October for the pollution days present analogous pathways with the cases in September, a high frequency of air parcels originating from mainland China and Korea at low levels (Figures 6.3e and 6.4e). During this month, though, the strengthening of the Siberian anticyclone brings a prevailing wind from the Asian

continent to Taiwan at the 2000m level and this is evident in the trajectories at this level, especially at the north site. In the case of the non-pollution days, there is again a high frequency of air parcels travelling from low-polluted maritime regions and the strong winds associated with these fast-moving air parcels may facilitate pollutant dispersion.

Finally, in November, the trajectories for both the pollution days and non-pollution days show analogous pathways at the lower levels (Figures 6.3f and 6.4f). There is a contrast, though, at the 2000m level; at that height, the back trajectories for the pollution days show air parcels originating from central and south China.

In summary, this comparison between back trajectories on sets of pollution days and non-pollution days confirms that there is a contrast in the air sources for these two sets of days with, broadly, flow from pollution source areas a characteristic of the pollution days whereas flow from clean, maritime regions a characteristic of the non-pollution days in most months. Moreover, the trajectories for the pollution days are in general agreement with the results of the weather type analysis and the anomalous flow shown by the pressure maps in Chapter 5. A seasonal picture of the varying contribution of long-range transport to ozone levels over Taiwan is now developed.

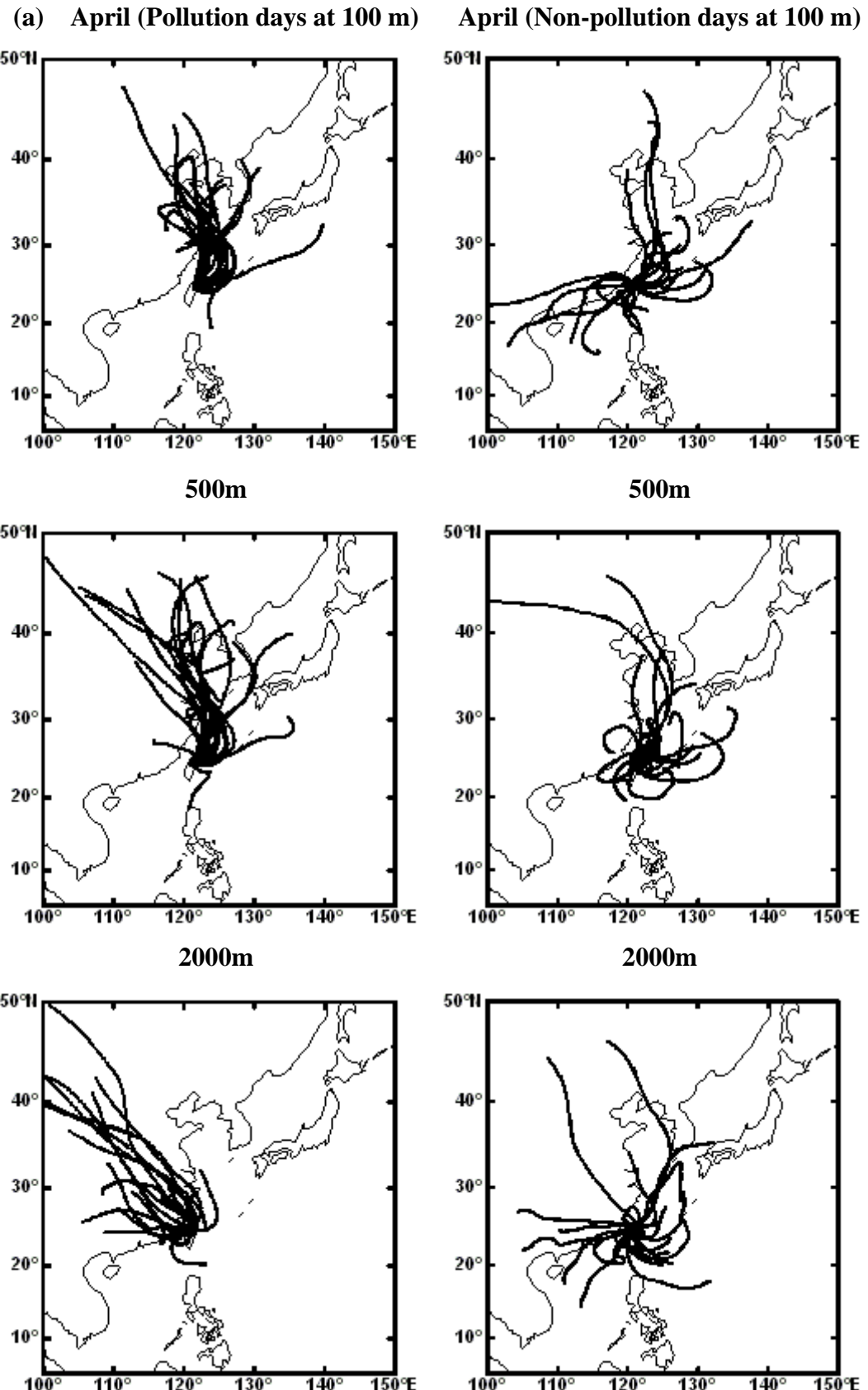


Figure 6.3: Three-day back trajectories in April (a), May (b), June (c), September (d), October (e) and November (f), Pollution days in left column and Non-pollution days in right column, at the level 100m, 500m and 2000m, for the north site.

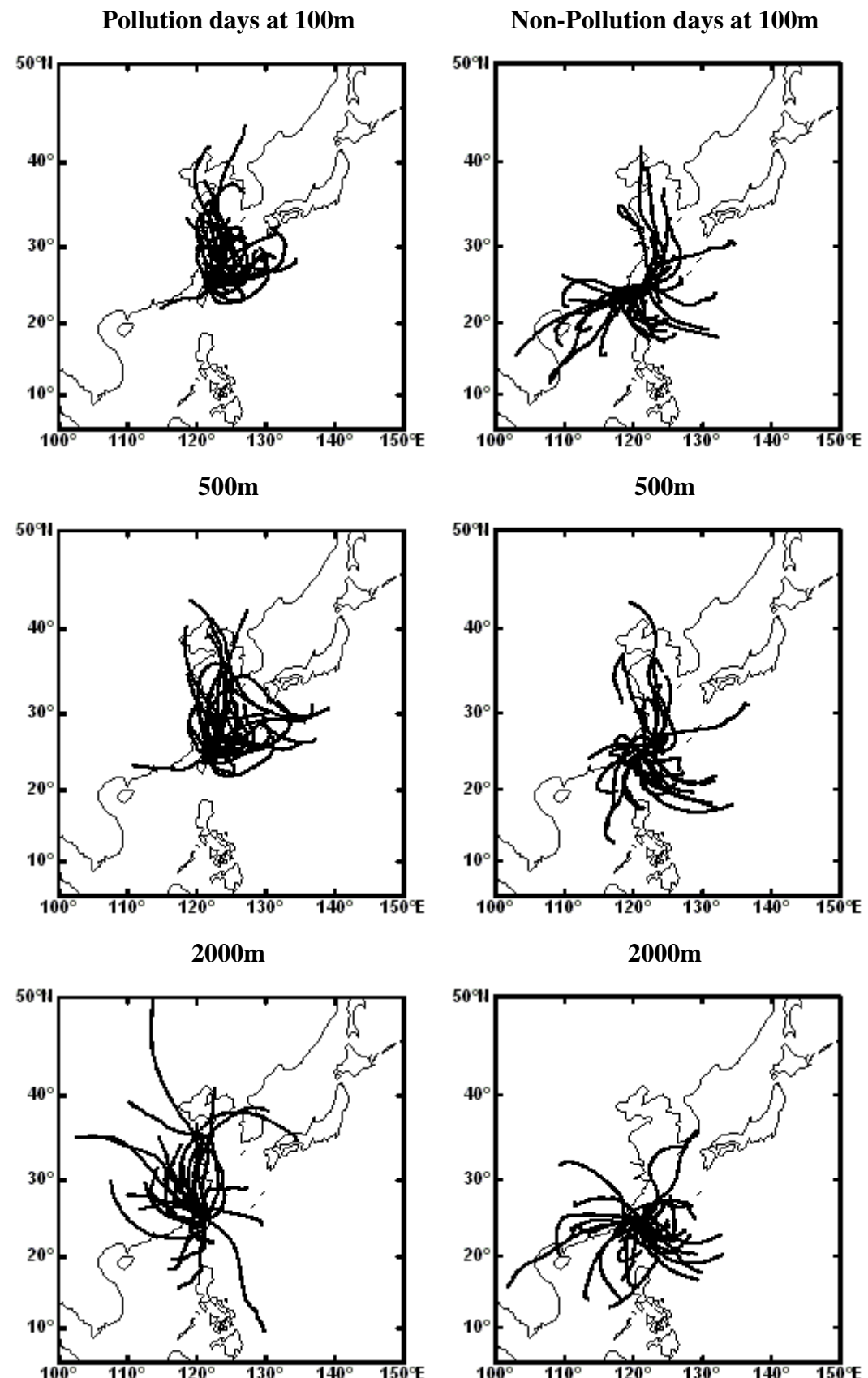
Figure 6.3(b): same as Figure 6.3 (a) but for May.

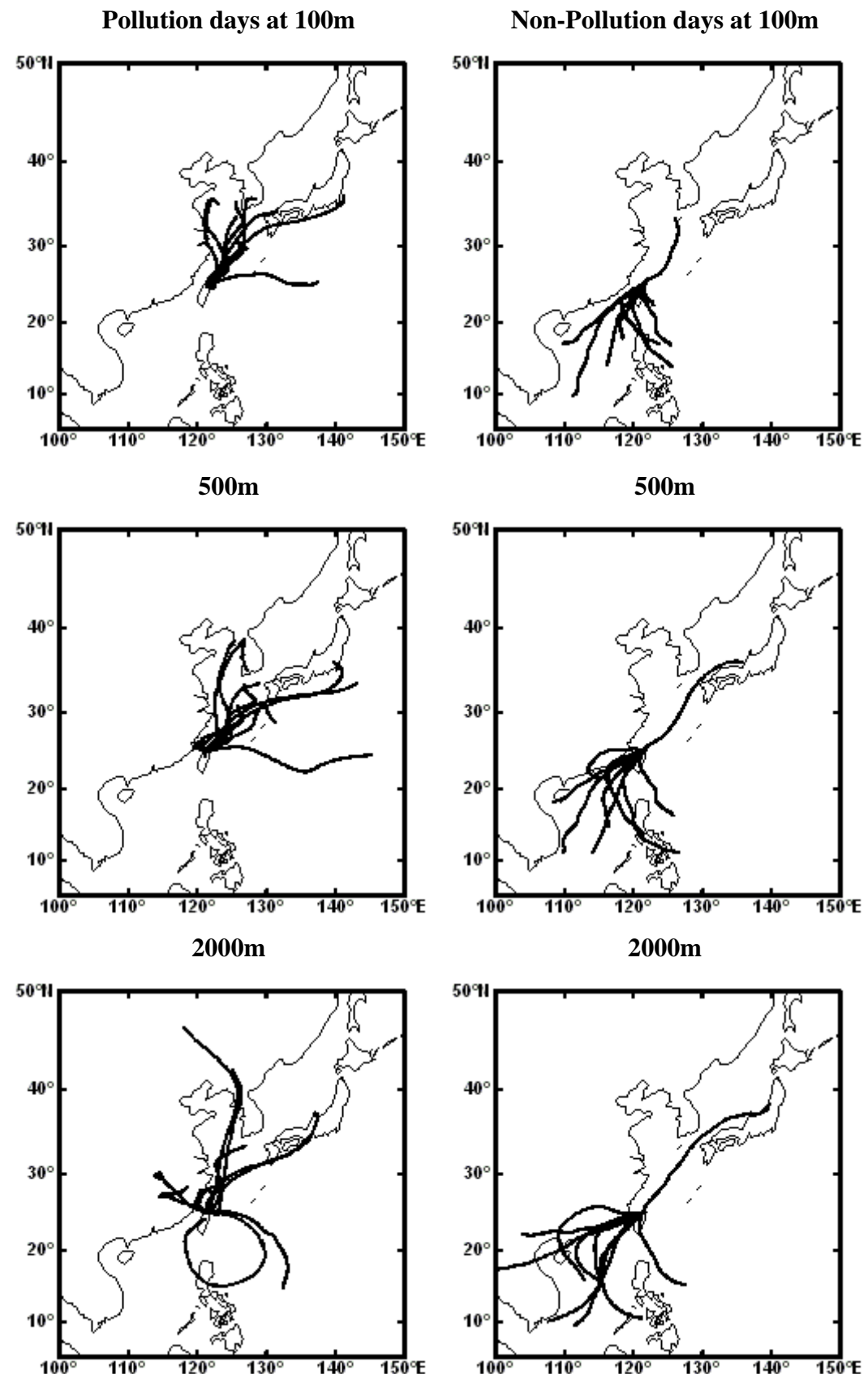
Figure 6.3(c): same as Figure 6.3 (a) but for June.

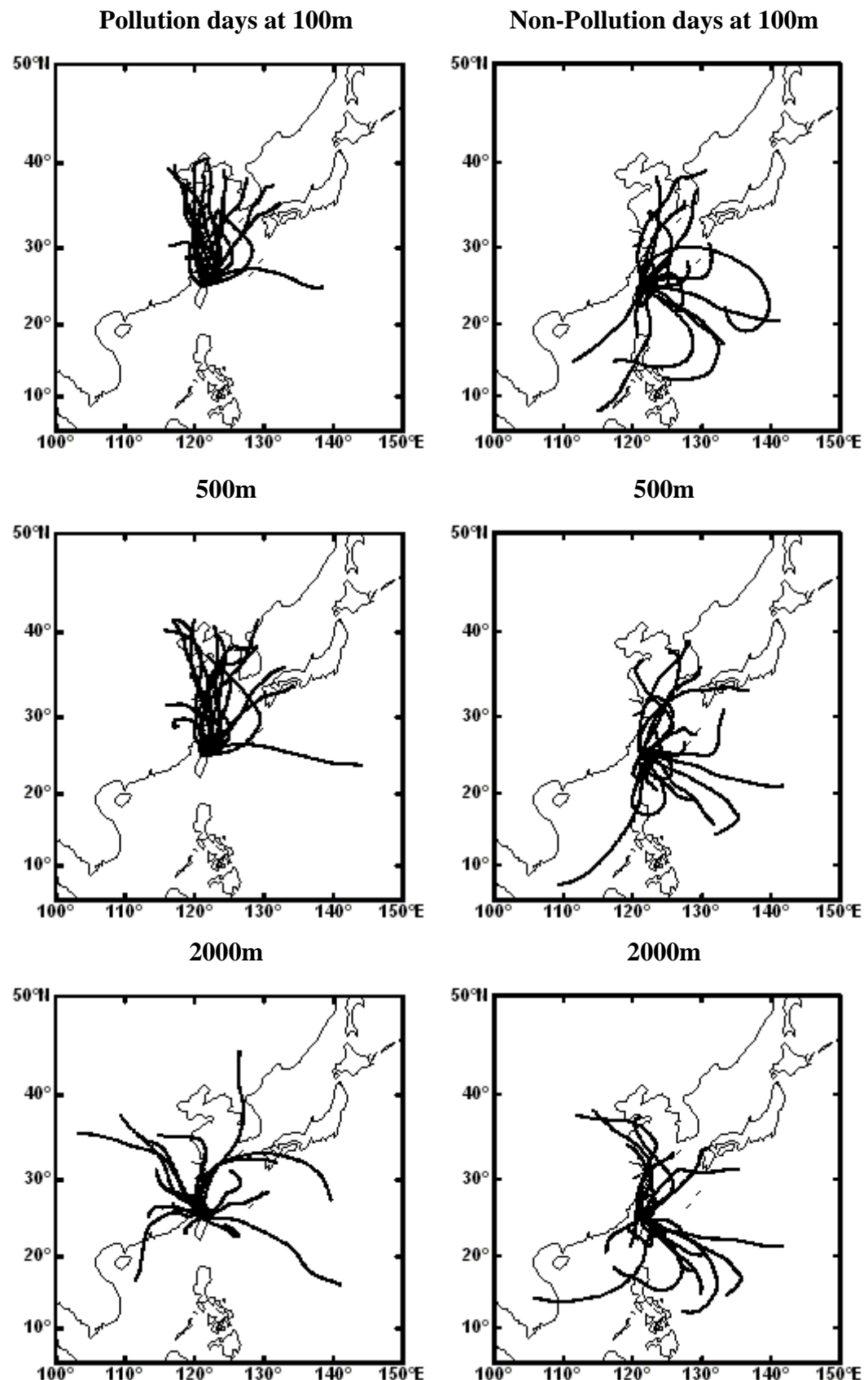
Figure 6.3(d): same as Figure 6.3 (a) but for September.

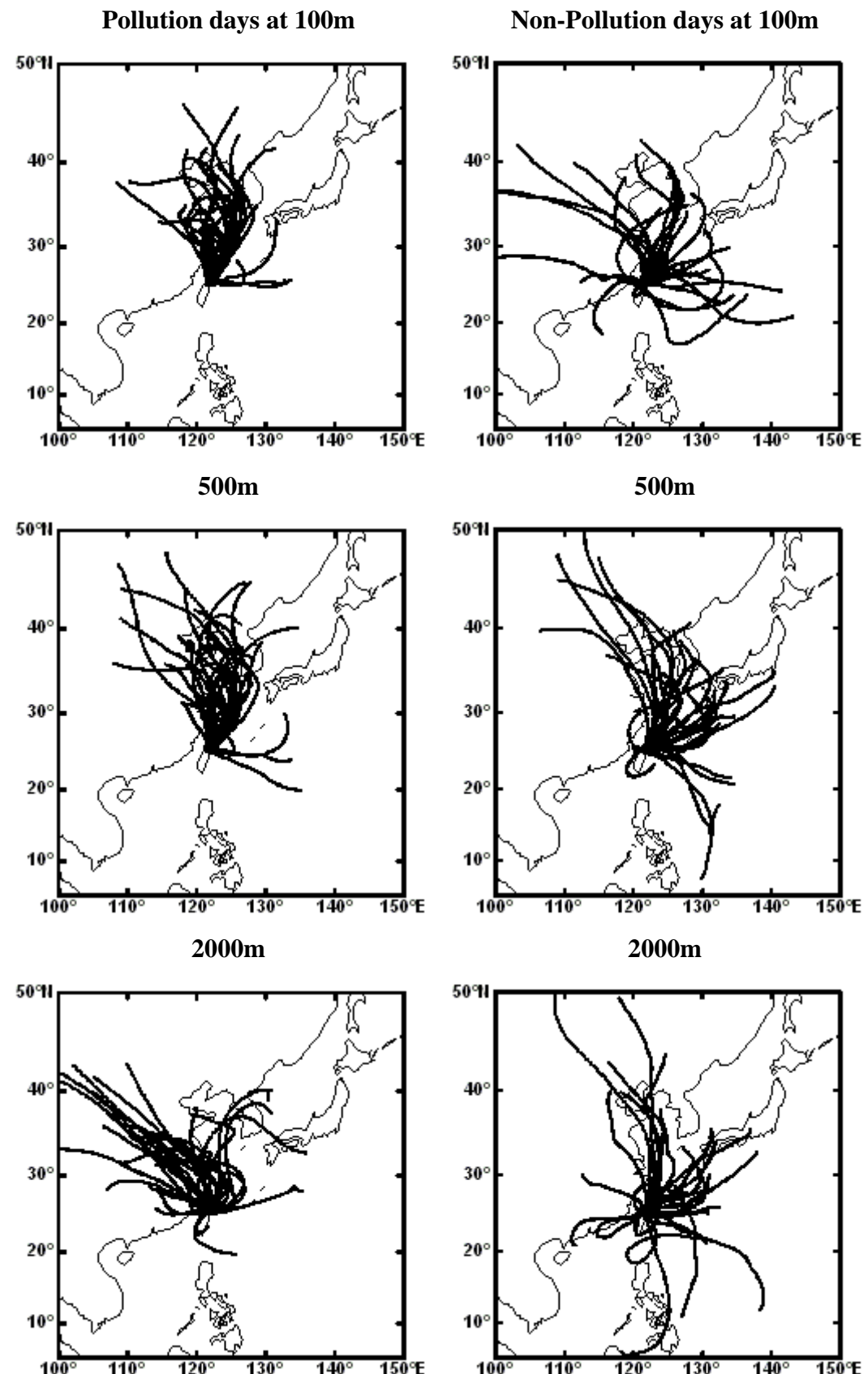
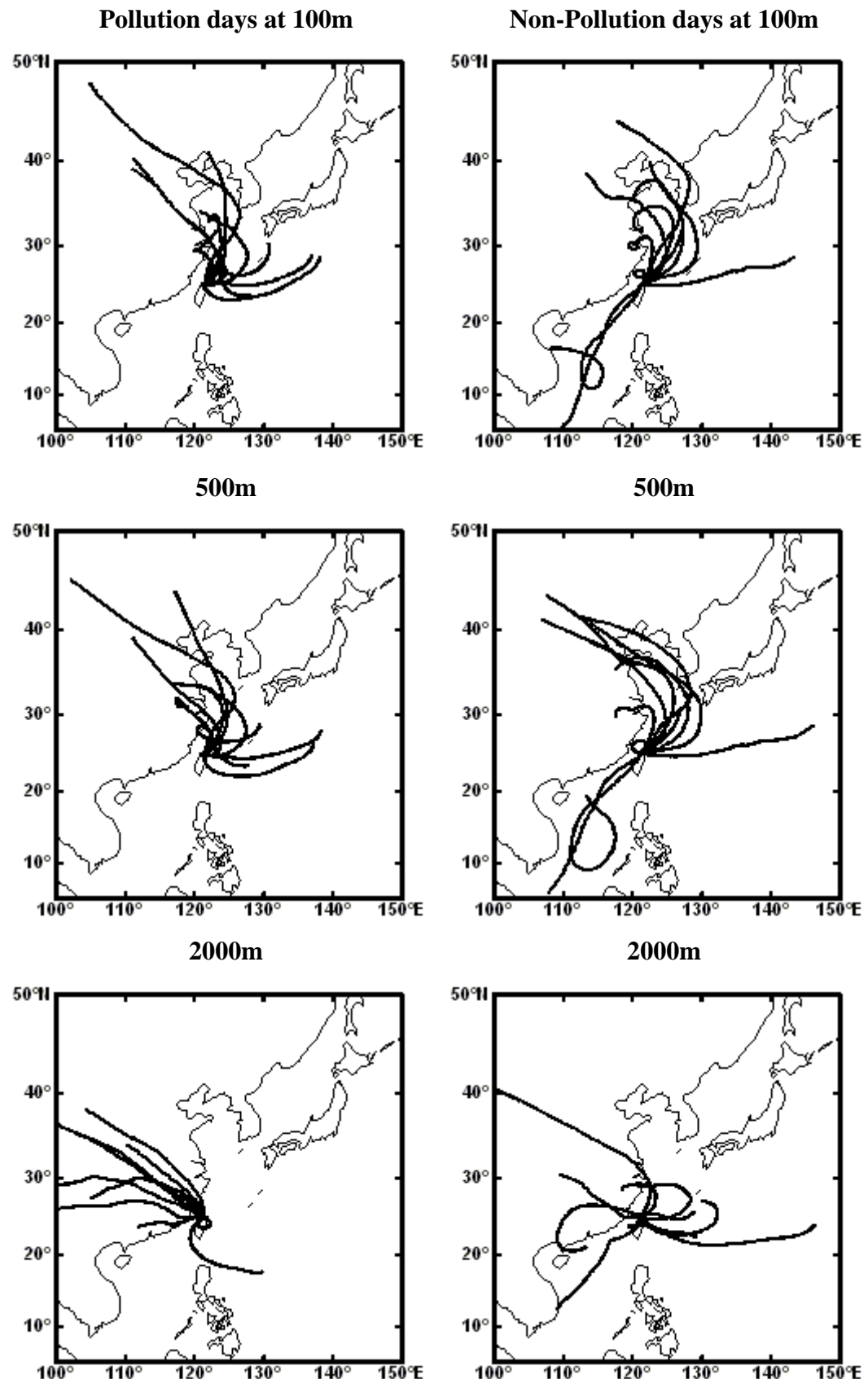
Figure 6.3(e): same as Figure 6.3 (a) but for October.

Figure 6.3(f): same as Figure 6.3 (a) but for November.

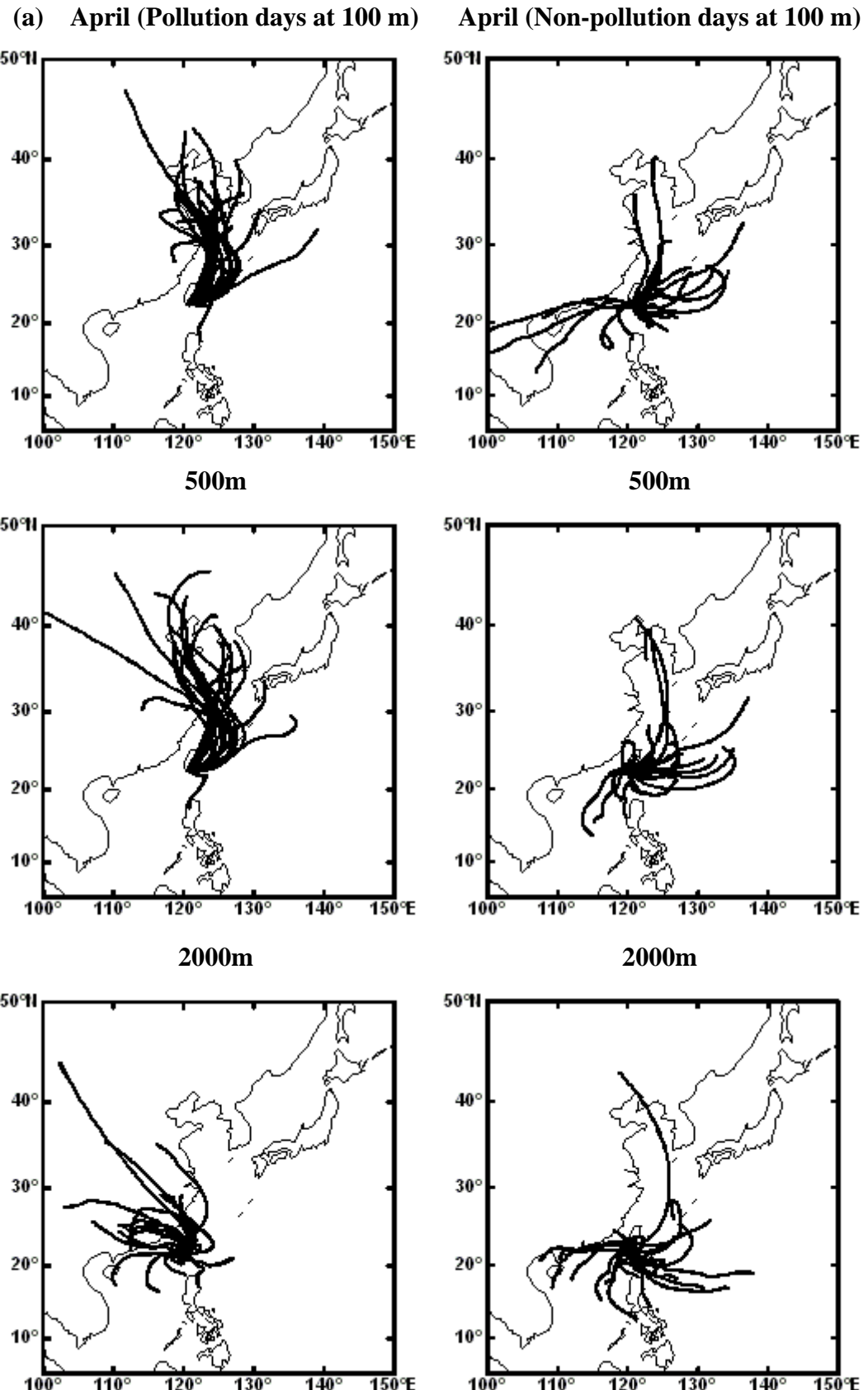


Figure 6.4: Three-day back trajectories in April (a), May (b), June (c), September (d), October (e) and November (f), Pollution days in left column and Non-pollution days in right column, at the level 100m, 500m and 2000m, for the south site.

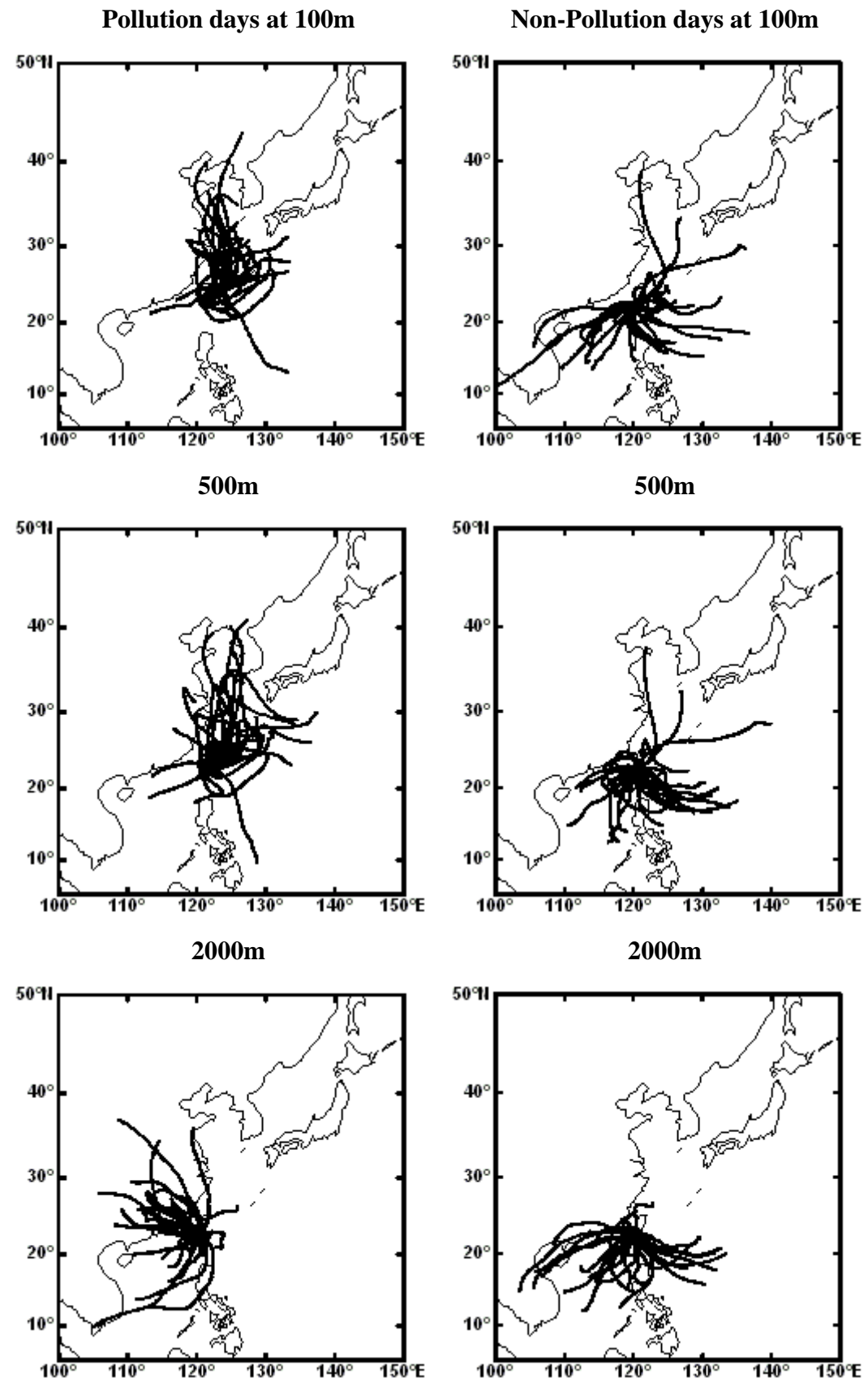
Figure 6.4(b): same as Figure 6.4(a) but for May.

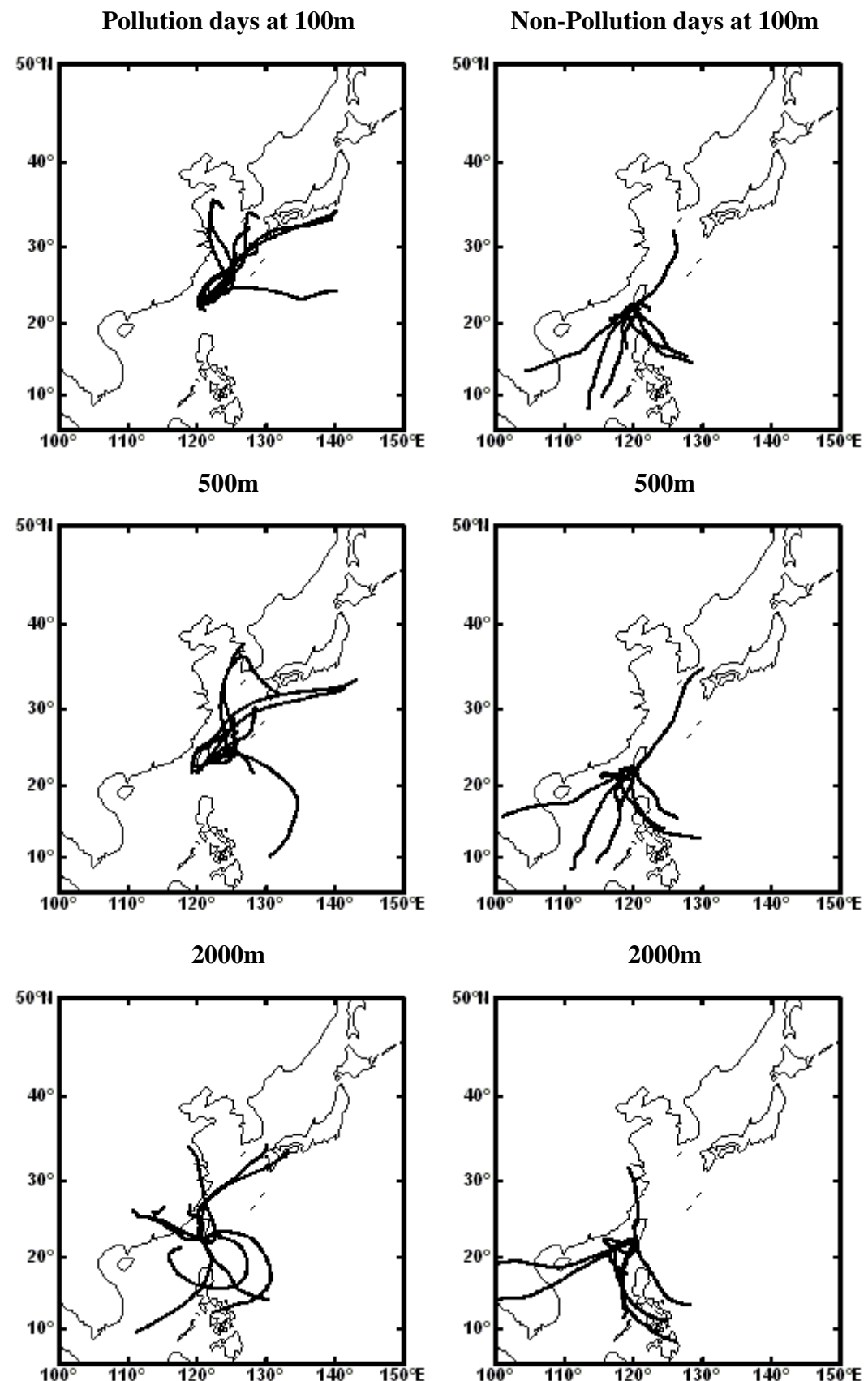
Figure 6.4(c): same as Figure 6.4 (a) but for June.

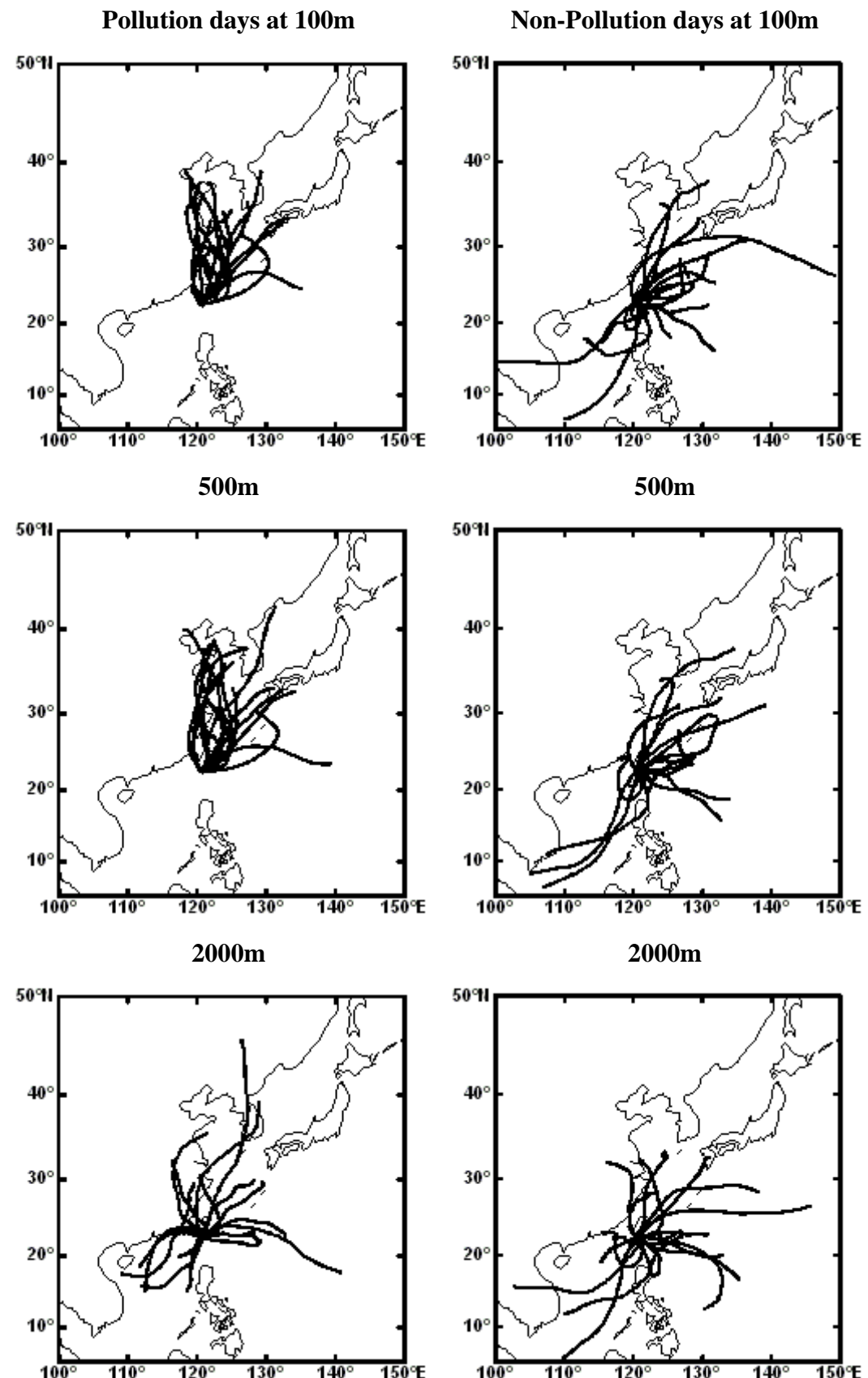
Figure 6.4(d): same as Figure 6.4 (a) but for September.

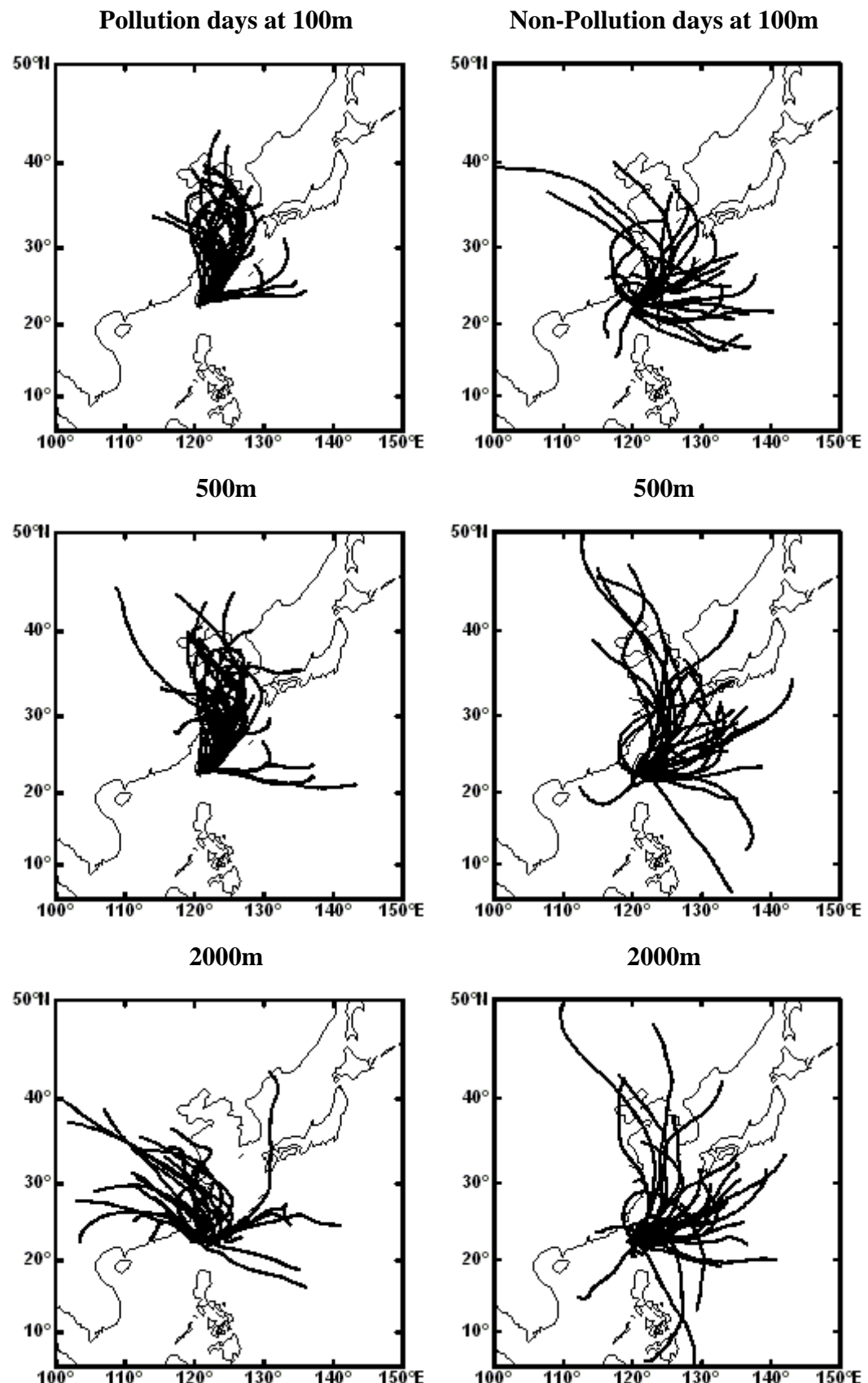
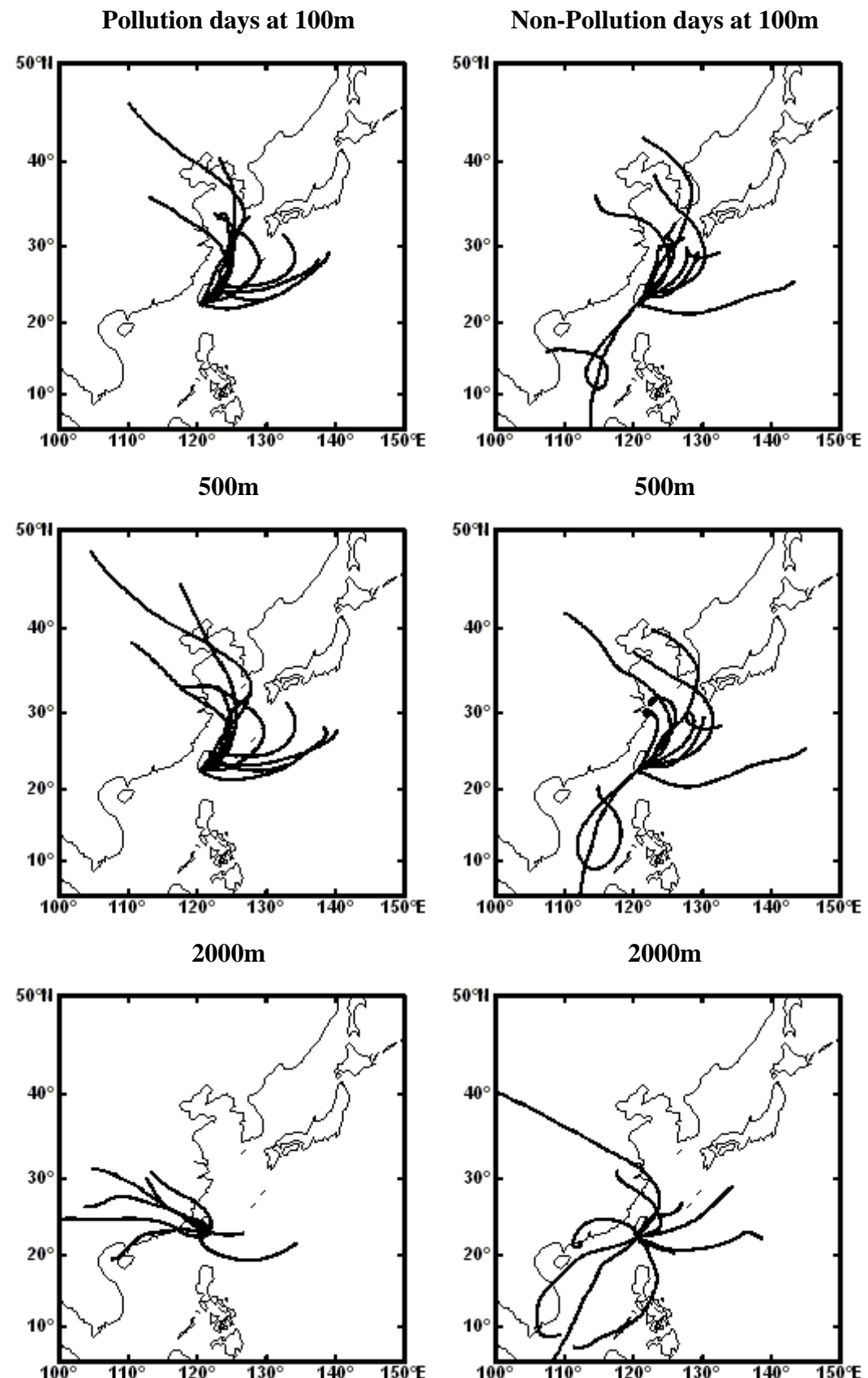
Figure 6.4(e): same as Figure 6.4 (a) but for October.

Figure 6.4(f): same as Figure 6.4 (a) but for November.

6.3 Framework for Long-Range Transport

The results of the back trajectory analysis confirm that high ozone pollution over Taiwan is contributed, at least in part, to long-range transport of ozone and its precursors from polluted areas in the region. The role of the large-scale atmospheric circulation at different times of the year can be best explained in terms of the seasonal variation in the monsoon circulation. In the following discussion, the results for pollution days are focused on except in cases where there is either little difference in the results for pollution and non pollution days (i.e. there is no clear signal) or else when the results for non pollution days are particularly relevant (i.e. in revealing clean air sources or other factors affecting ozone accumulation or loss).

During April, a transitional period, the Siberian anticyclone, which characterises the winter monsoon circulation, declines and moves eastward from mainland China with reduced pressure gradients and a trough over Japan, suppressing pollution lifetimes in the latter area (Figure 5.17). These synoptic conditions are favourable to export ozone and its precursors from the East Asian continent over Taiwan. The characteristics of transport pathways are illustrated by the anomaly pressure maps and the back trajectory analysis (Figures 5.17, 6.1a, 6.3a and 6.4a). A positive pressure anomaly located over the east coast of China indicates that heightened pressure might increase pollutant accumulation over local source areas. The adjacent anomalous northerly/northeasterly flow, confirmed by the back trajectory analysis, brings the air parcels that passed over the polluted areas, such as north China or Korea, southward to Taiwan and enhances the ozone concentration in the downwind area. The back trajectories show clear transport pathways with a northerly component at the lower levels of 100m and 500m, for both

analytical sites. The results suggest that these north and northeasterly transport pathways at lower levels provide long-range transport of ozone and its precursors in April from source areas in China and Korea.

The trajectories at 2000m may suggest transport from source areas in southern China, but this must be a secondary contribution. It is notable that the 2000m winds are weaker in the case of pollution days at the southern site.

In May, the dominant regional influence shifts from the Siberian anticyclone to the Pacific anticyclone. The pressure anomaly charts for the pollution days show a similar, but stronger, pattern to those for April (Figure 5.18). The trajectory analysis reveals weaker flows, particularly at the lower levels, with stagnation close to Taiwan, but still from a generally northerly direction (Figures 6.1b, 6.3b and 6.4b). These weak and stagnant circulations are not favourable for pollutant dispersion. In May, the trajectories at 2000m show a more marked transport from the north than was the case for April, particularly for northern Taiwan. The trajectories also illustrate more air parcels originated from the South China Sea for the south site in May than in April. In the case of non-pollution days (Figures 5.18, 6.3b and 6.4b), the pressure maps and the back trajectories indicate the strong onset of the summer monsoon which is favourable for pollutant dispersion due to convective activity. In this month, the effect of the summer monsoon is more significant than in April.

June is the month when the summer monsoon activity dominates; Taiwan is mainly affected by the interaction of air flows between the Western Pacific and the South China Sea. The average pressure maps for the non-pollution days present the characteristics of the typical synoptic circulation during this period, a clear southwesterly monsoonal flow passing over Taiwan (Figure 5.19). As noted earlier, there are fewer high ozone

episodes observed in this month due to unfavourable weather conditions associated with cyclonic circulations and short lifetime of pollutants. (Nevertheless, an increase of high ozone episodes has been observed in the recent years of the study period in this month, as discussed in Chapter 4.) In contrast, the anomaly pressure maps for the ozone pollution days show a marked anomalous, northeasterly flow over Taiwan generated by a negative pressure anomaly over the western Pacific and a positive pressure anomaly over northern China (Figure 5.19). This indicates a weakening of the dominant southwesterly monsoon flow associated with high pollution episodes. The back trajectories prove that the air parcels are travelling from a northerly or northeasterly direction to Taiwan at the lower levels (Figures 6.1c, 6.3c and 6.4 c), suggesting that ozone and its precursors may be transported from Korea and Japan southward to Taiwan.

During September, as the summer monsoon has ended and a transitional season is underway, there is a weakening of the influence of the Pacific anticyclone in Taiwan and an evolving Siberian anticyclone (Figure 5.20). The pressure anomaly charts for the pollution days show a marked strengthening of these two anticyclones, with an enhanced air flow along the east coastal region of China. The results of back trajectory analysis present similar transport pathways at the low levels, suggesting slow-moving air parcels may carry pollutants from the east coast of China, Korea and Japan and enhance local ozone concentration on the pollution days (Figures 6.3d and 6.4d). Higher pressure over the Chinese mainland may also enhance the accumulation of local pollutants over the continent, providing a steady source for advection to Taiwan. In addition, the extension of the influence of the Siberian high pressure over Taiwan would create low wind speeds, favourable for ozone formation. The back trajectories at the 2000m level show a high frequency of air parcels originating from maritime regions,

particularly for the southern site. The results suggest that the synoptic circulation at high levels may be still influenced by late summer monsoon activities or tropical depressions. In any event, the results suggest that long-range transport of ozone and its precursors is again most important at lower levels.

In October, the actual pressure maps illustrate the evolution of the winter monsoon with a dominant northeasterly wind over Taiwan (Figure 5.21). The anomaly maps show no marked pattern, but the back trajectories show similar transport pathways of air parcels as in September at the lower levels (100m and 500m), except faster moving air parcels are observed in October. Comparing the back trajectories for pollution and non-pollution days indicates a stronger contribution from the north at lower levels, but the difference is most marked at 2000m where pollution days are characterised by back trajectories from over the polluted areas of mainland China (Figures 6.1e, 6.3e and 6.4e).

In November, an intense trough from North Asia and the evolution of the Siberian anticyclone brings prevailing northeasterly winds again to Taiwan (Figure 5.22). The anomalous pressure maps show that, on pollution days, there is a stronger influence of the ridge from the Siberian anticyclone over Taiwan. This would be associated with favourable conditions for ozone formation over Taiwan, as well as greater advection towards Taiwan from the northern mainland of China. The results of the back trajectory analysis show slow-moving air parcels at the lower levels and faster-moving air parcels at altitude of 2000m, suggesting that ozone and its precursors may be accumulated in polluted source areas and transported by high level air parcels to Taiwan with central China making more of a contribution at this time of year (Figures 6.1f, 6.3f and 6.4f).

While the patterns of the back trajectories are generally similar for the northern and southern analyses, there is a suggestion that the southern site is more sensitive to changing trajectories related to monsoon strength, with the north more responsive to changes in northerly advection. In general, the back trajectories suggest faster moving air parcels at the northern site in many cases.

6.4 Summary

It is important to note that long range transport is only one factor contributing to enhanced ozone levels over Taiwan. Local sources and formation processes are of considerable importance. Nevertheless, this analysis indicates that long-range transport does play a role in increasing the severity of episodes of high ozone concentrations. This is most clear in the contrast between the atmospheric circulation for pollution and non pollution days, as evidenced by the pressure anomaly maps and the back trajectories. In general, pollution days are characterised by more frequent flows from polluted source areas to the north and west over China, Korea and, to a lesser extent, Japan, whereas non pollution days are characterised by flows from clean, maritime areas. The evolution of the winter and summer monsoons plays an influential role in determining the nature of the contribution of long-range transport and the relative importance of the different source areas. During the transition months of April, May, September and October, low level flow from a northerly direction makes a major contribution due to fluctuations in the relative strength of the Siberian and Pacific anticyclones. During the monsoon seasons (the months of June and November in this analysis), the key factor is the strength of the monsoon flow, with a weaker summer monsoon and a stronger, northeasterly monsoon in winter associated with enhanced ozone pollution. In these cases, local conditions are also strongly affected by weaker or stronger anticyclonicity as well as long range transport. At these times of year, the flow at 2000m appears more important than at the lower levels. In many months, enhanced anticyclonicity over remote source areas suggests reduced dispersal and longer pollutant lifetimes, creating a stronger source for low level long-range transport along the periphery of the region as the flow under the anomalous high pressure area diverge.

6.5 Conclusion

Back trajectory analysis has distinguished the source of ozone pollution and transport pathway in different months. A marked contrast is evident in most cases between the trajectories for pollution days and non-pollution days, confirming that the former are not spurious. The results are analogous with the findings from the weather type analysis and composite pressure maps in Chapter 5. The main findings can be summarised as follows:

Pollutants are transported to Taiwan by air parcels originating from the polluted areas of neighbouring Asia, such as mainland China, Korea and Japan. The source areas vary with month as the seasonal circulation alters.

Southern China, a rapidly developing region, is also a prominent source, particularly in May and November. The dynamic process of long-range pollutant transport from southern China is likely related to convective activity rather than advective activity.

Slow-moving air parcels from Northeast Asia and the effect of cyclones from the Southeast Asia region result in ozone pollution increasing in summer (June).

The variation of East Asian monsoon activity, such as winter monsoon and summer monsoon, affect the ozone pollution in Taiwan. Ozone pollution days are related with a weak winter monsoon activity and non-pollution days are associated with the air flow from the maritime monsoon activity (i.e. South China Sea and the Western Pacific Ocean).

Finally, it should be noted that, though ozone pollution in Taiwan may be associated with pollutants transported from distant source areas, the effect of local pollution should not be neglected, especially for south Taiwan.

Chapter 7: Conclusions

7.1 Introduction

The aim of this study has been to investigate the relationship between ozone pollution in Taiwan and the large-scale circulation, paying particular attention to the effect of the long-range transport of ozone precursors on ozone pollution. Daily ozone concentration data from the Taiwan Air Quality Monitoring Network were used to analyse annual and seasonal ozone trends. The characteristics of circulation weather types on ozone days were determined using an objective weather typing scheme with sea level pressure data from the NCEP reanalysis dataset. Spatial composite analysis and back trajectory analysis were used to characterise the signature of the large-scale circulation associated with high ozone pollution and its relation with the long-range transport of ozone precursors. The spatial composite maps were derived from the NCEP reanalysis dataset for the variables of geopotential height and sea level pressure. Back trajectories were calculated using the Hybrid Single-Particle Lagrangian Integrated Trajectory model.

This chapter focuses on concluding the findings of the study, and assess the methodology which could be improved and development. The findings are summarised by answering the specific questions identified in Chapter three as follows:

- What are the characteristics of high ozone pollution episodes and their variability over Taiwan?
- Is there evidence that regional atmospheric circulation patterns are linked to the occurrence of high ozone pollution days?
- What is the role of long-range transport and other circulation mechanisms, including the dominant monsoonal circulation of the region?

7.2 Summary of Findings

A positive trend of high ozone episodes is observed from 1994 to 2004, suggesting that the effect of moderate high ozone pollution (daily 8hrs average ozone concentration \geq 60 ppb) on Taiwan's air quality is more significant in recent years.

The spatial distribution analysis shows that the North and the Kao-Ping zones are the most polluted areas in Taiwan. The seasonal variation across Taiwan generally exhibits two peaks (with the maxima in spring and autumn), but the peak month varies with spatial distribution. For the North zone, the effect of ozone pollution is more significant in spring than in autumn, reverse in the Kao-Ping zone, corresponding to the interaction among synoptic weather patterns. The increase of high ozone days observed in summer implies that the seasonal cycle of ozone pollution may be shifting in recent years.

An integrated analysis consisting of circulation type classification, spatial composite analysis and back trajectory analysis has demonstrated that northeasterly flow over or north of Taiwan, generally associated with heightened pressure over mainland China, is typical of high ozone days. This finding suggests that the long-range transport of ozone and its precursors does influence ozone pollution in Taiwan, with air parcels originating from nearby polluted source regions such as mainland China, Korea and, at times, Japan in spring, summer and autumn. The main circulation types related to long-range transport of pollutants from Northeast Asian to Taiwan are the ANE and NE types in spring, summer and autumn, and the CNE type in autumn. It should be noted that, while long-range transport clearly plays a role, local pollution is not negligible in some areas. The SE, ASE (in spring and autumn) and the E type (in summer), for example, are characterised by small pressure gradients and maritime air flows. Ozone pollution

occurs within these types more related to local pollution than long-range transport because the circulation features are not favourable for local pollutants dispersion and the air flows of these types mainly originate from low polluted areas. The analyses have also shown that southwesterly or southerly flows related to summer monsoon are the circulation features of non-pollution days. The influence of the seasonal monsoonal circulation is evident for both high ozone pollution days and non-pollution days.

New possible source regions of ozone and its precursors have been found in this study. Ozone pollution associated with the cyclonic types (i.e. C, CNE and CE types) in different seasons suggests that pollutants may be transported from South China and Southeast Asia to Taiwan in spring or summer, which has not been noticed in the past.

The results of long-term trend analysis, between 1958 and 2004, suggest a stronger winter monsoon and a weakening summer monsoon, particularly for the regional scale. Because of the different role of the winter monsoon and summer monsoon in long-range transport, long-term trends in the frequencies of these types may, all other factors being equal, reflect trends in the frequency of high ozone episodes in Taiwan. The variation in strength of these two monsoonal circulations may have enhanced ozone pollution in Taiwan in recent years. This may explain at least part of the observed trend in ozone pollution, although, of course, the role of increased local sources of precursors and other factors should not be neglected.

7.3 Limitations of the Study

A number of limitations of the present study have been identified throughout the investigation. The main deficiencies are summarized below.

- **Data quality**

There is a need to consider further the implications of varying data quality. For example, the reanalysis data represents the best currently available observational data which provides global coverage with more than sixty years of temporal coverage. However, the homogeneity of the underlying data is subject to changes over time, especially in the late 1970s with improved satellite and aircraft data. A similar problem of data homogeneity is also considered for the ozone data, as only a short period (1993 to present) for the monitoring network, the improvement of instruments, and the change of locations etc may reduce the accuracy of ozone data. In addition, the reliability of trend analysis is affected by the shortness of the ozone pollution record available for this study.

- **The influence of meteorological conditions**

This study has not considered directly the meteorological conditions that could affect ozone pollution, such as humidity, wind speed and temperature. The identification of the relationship between ozone pollution and atmospheric circulation in this study only depends on the analysis of circulation features and the pathway of air flow; however, it may reduce the reliability of identification of relationships and mechanisms because the meteorological conditions are important factors related to ozone formation.

- **The influence of long-range transport**

This study has identified the characteristics of atmospheric circulation on high ozone days and found that long-range transport of ozone and its precursors does have an influence on ozone pollution in Taiwan. There is a need to consider the quantification of ozone precursors derived from long-range transport and to further confirm the contribution of local emissions and long-range transport to ozone pollution in Taiwan. This is necessary in order to quantify the relative role of long-range transport, variation in source strength and local factors favouring ozone formation.

- **Spatial variability**

This study has been based on the identification of ozone episodes over representative regions of Taiwan; the regions are mainly located at the western plain. The role of long-range transport and other factors may vary across the country if high spatial scales are considered. Study of the spatial distribution of these events requires further consideration of data quality across Taiwan.

7.4 Recommendations for Further Research

Based on the findings of this study, the following recommendations to extend this study can be made.

- **Relationship between meteorological conditions and circulation types**

Further work of the construction of the link between meteorological conditions (i.e. humidity/rainfall, wind speed and temperature) and circulation types is necessary. This is useful to identify the characteristics of air flow (e.g. cold or warm anticyclones), source region of air flow, to understand the weather conditions of ozone pollution days, and to improve the identification of local pollution and long-range transport of ozone pollution in Taiwan.

- **Quantification of the long-range transport contribution**

As an extension of the present study, a chemical transport model could be used to quantify the long-range transport of ozone and its precursors from the polluted areas (i.e. China, Korea and Japan) and to identify the key controlling processes of long-range transport, such as chemical production, horizontal or vertical transport, and deposition or chemical removal during transport. Model simulations could be used to compare with the results of this study and to assess the impact of ozone pollution from different source regions in high ozone pollution seasons.

- **Impact of global warming on future ozone pollution**

The relationships between ozone pollution and synoptic circulation in different seasons identified in this study suggest that ozone pollution in Taiwan may be associated with the intraseasonal variability of the East Asian monsoon over the past decade. Given that the East Asian monsoon may be affected by global warming in the future, further investigation of the influence of future changes of the East Asian monsoon in response to global warming on future ozone pollution is useful to understand the variation of future ozone pollution related to synoptic weather systems and to provide information for future air pollution control strategies in Taiwan. There are three questions which could be ideas for research design for further study as follows:

- 1) What was the long-term relationship between circulation type and the East Asian monsoon, and its link with high/low ozone pollution in Taiwan over the past decade?
- 2) How will global warming influence future climate at the regional scale (the East Asian monsoon circulation) and weather at the local scale (rainfall) for East Asia?
- 3) How will the changes of future climate at the regional scale and weather at the local scale affect future ozone pollution in Taiwan?

In order to classify both composite and meteorological features of the East Asian monsoon (winter and summer monsoons) related to circulation types, a further identification of the characteristics of the East Asian monsoon could be classified by the results of the correlation between circulation types and meteorological conditions such as rainfall and wind speed. To estimate the influence of global warming on future climate and ozone pollution, projections of future variations of the East Asian monsoons simulated by coupled atmosphere-ocean general circulation models (AOGCMs) could be analysed. Considering that the definitions of the temporal and spatial scales in the

present study are related to a shorter timescale (daily and monthly) and small region (Taiwan to East Asia), respectively; the validation of AOGCMs simulations using downscaling methods such as the circulation classification approach is necessary to improve the application of AOGCMs output for obtaining more reliable assessments of the variation of future ozone pollution in response to global warming.

7.5 Wider Implications

Ozone pollution has become an important issue of air quality control in Taiwan. The features of atmospheric circulation on ozone pollution days identified in this study have improved understanding of the relationship between ozone pollution episodes and the regional atmospheric circulation. This will assist better environmental management and pollution control.

The objective classification scheme has been applied in a low-latitude region successfully. The results of the objective classification scheme show a good agreement with the typical circulation types in Taiwan classified by subjective methods. The results could be applied in the investigation of extreme weather events such as flood and drought, to improve understanding and management of water resources in Taiwan.

References

- Abdulgith, S.S. and Harrison, R.M. 2005. The use of trajectory cluster analysis to examine the long-range transport of secondary inorganic aerosol in the UK. *Atmospheric Environment*, **39**: 6686-6695.
- Akimoto, H. 2003. Global Air Quality and Pollution. *Science*, **302**: 1716-1719.
- Akimoto, H., Mukai, H., Nishikawa, M., Murano, K., Hatakeyama, S., Liu, C.M., Buhr, M., Hsu, K.J., Jaffe, D.A., Zhang, L., Honrath, R., Merrill, J.T., and Newell, R.E. 1996. Long-range transport of ozone in the East Asian Pacific rim region. *Journal of Geophysical research*, **101**: 1999-2010.
- Allan, R. and Ansell, T. 2006. A new globally complete monthly historical gridded mean sea level pressure dataset (HadSLP2): 1850-2004. *Journal of Climate*, **19**: 5816-5842.
- Annamalai, H., Slingo, J.M., Sperber, K.R. and Hodges, K. 1999. The Mean Evolution and Variability of the Asian Summer Monsoon: Comparison of ECMWF and NCEP-NCAR Reanalyses. *Monthly Weather Review*, **127**: 1157-1186.
- Ashmore, M.R. 2005. Assessing the future global impacts of ozone on vegetation. *Plant, Cell and Environment*, **28**: 949-964.
- Aunan, K., Berntsen, T.K. and Seip, H.M. 2000. Surface Ozone in China and Its Possible Impact on Agricultural Crop Yields. *Ambio*, **29**:294-301.
- Auvray, M. and Bey, I. 2005. Long-range transport to Europe: Seasonal variations and implications for the European ozone budget. *Journal of Geophysical Research D: Atmospheres*, **110**: 1-22.
- Barkstrom, B.R., Harrison, E., Smith, G., Green, R., Kibler, J., Cess, R. and ERAB Science Team. 1989. Earth Radiation Budget Experiment (ERBE) archival and April 1985 results. *Bulletin of the American Meteorological Society*, **70**: 1254-1262.

- Barry, R.G. and Chorley, R.J. 1998. *Atmosphere, Weather and Climate*. Routledge, London.
- Barry, R.G. and Perry, A.H. 1973. *Synoptic Climatology: Methods and Applications*. Methuen & Co Ltd, London.
- Bell, M.L., Peng, R.D. and Dominici, F. 2006. The Exposure-Response Curve for Ozone and Risk of Mortality and the Adequacy of Current Ozone Regulations. *Environmental Health Perspectives*, **114**: 532-536.
- Bojkov, R.D. 1986. Surface Ozone During the Second Half of the Nineteenth Century. *Journal of Climate and Applied Meteorology*, **25**: 343-352.
- Bojkov, R.D., Fioletov, V.E. and Shalamjansky, A.M. 1994. Total ozone changes over Eurasia since 1973 based on reevaluated filter ozonometer data. *Journal of Geophysical Research D: Atmospheres*, **99**: 22,985-22,999.
- Brasseur, G.P., Hauglustaine, D.A., Walters, S., Rasch, R.J., Müller, J.-F., Granier, C. and Tie, X.X. 1998. MOZART, a global chemical transport model for ozone and related chemical tracers 1. Model description. *Journal of Geophysical Research D: Atmospheres*, **103**: 28,265-28,289.
- Brasseur, G.P., Müller, J.-F. Tie, X. and Horowitz, L. 2001. Tropospheric ozone and climate: Past, Present and Future. Present and Future of Modeling Global Environmental Change: Toward Integrated Modeling, pp. 63-75. Matsuno, T. and Kida, H. (Eds). TERRAPUB
- Briffa, K.R., Jones, P.D. and Kelly, P.M. 1990. Principal component analysis of the Lamb Catalogue of Daily Weather Types: part 2, seasonal frequencies and update to 1987. *International Journal of Climatology*, **10**: 549-563.
- Brimblecombe, P. 1996. *Air composition & chemistry*, Cambridge University Press, Cambridge.
- Bromwich, D.H. and Fogt, R.L. 2004. Strong trends in the skill of the ERA-40 and NCEP-NCAR reanalyses in the high and midlatitudes of the Southern Hemisphere, 1958-2001. *Journal of Climate*, **17**: 4603-4619.

- Bueh, C. 2003. Simulation of the future change of East Asian monsoon climate using the IPCC SRES A2 and B2 scenarios. *Chinese Science Bulletin*, **48**: 1024-1030.
- Burnett, R.T., Brook, J.R., Yung, W.T., Dales, R.E. and Krewski, D. 1997. Association between ozone and hospitalization for respiratory diseases in 16 Canadian Cities. *Environmental Research*, **72**: 24-31.
- Carslaw, D.C. 2005. On the changing seasonal cycles and trends of ozone at Mace Head, Ireland. *Atmospheric Chemistry and Physics*, **5**: 3441-3450.
- Central Weather Bureau Taiwan [online]. Available:
<http://www.cwb.gov.tw/V6/index.htm> [accessed 2006] (in Chinese)
- Chan, C.Y. and Chan, L.Y. 2000. Effect of meteorology and air pollutant transport on ozone episodes at a subtropical coastal Asian city, Hong Kong. *Journal of Geophysical Research D: Atmospheres*, **105**: 20,707-20,724.
- Chan, L.Y., Liu, H.Y., Lam, K.S., Wang, T., Oltmans, S.J. and Harris, J.M. 1998. Analysis of the seasonal behavior of tropospheric ozone at Hong Kong. *Atmospheric Environment*, **32**: 159-168.
- Chandra, S., Ziemke, J.R., Bhartia, P.K. and Martin, R.V. 2002. Tropical tropospheric ozone: Implications for dynamics and biomass burning. *Journal of Geophysical Research D: Atmospheres*, **107**: 3-1-3-17
- Chandra, S., Ziemke, J.R., Min, W. and Read, W.G. 1998. Effects of 1997-1998 El Niño on tropospheric ozone and water vapor. *Geophysical Research Letters*, **25**: 3867-3870.
- Chandra, S., Ziemke, J.R., Schoeberl, M.R., Froidevaux, L., Read, W.G., Levelt, P.F. and Bhartia, P.K. 2007. Effects of the 2004 El Niño on tropospheric ozone and water vapor. *Geophysical Research Letters*, **34**, Art. No. L06802
- Chang, C.C., Tsai, S.S., Ho, S.C. and Yang, C.Y. 2005. Air pollution and hospital admissions for cardiovascular disease in Taipei, Taiwan. *Environmental Research*, **98**: 114-119.

- Chang, S.C. and Lee, C.T. 2007. Evaluation of the trend of air quality in Taipei, Taiwan. *Environmental Monitoring and Assessment*, **127**:87-96
- Charlson, R.J., Schwartz, S.E., Hales, J.M., Cess, R.D., Coakley Jr., J.A., Hansen, J.E. and Hofmann, D.J. 1992. Climate forcing by anthropogenic aerosols, *Science*, **255**: 423-430.
- Chen, C.-S. and Chen, Y.-L. 2003. The rainfall characteristics of Taiwan. *Monthly Weather Review*, **131**: 1323-1341.
- Chen, G.T.J., Jiang, Z. and Wu, M.C. 2003. Spring heavy rain events in Taiwan during warm episodes and the associated large-scale conditions. *Monthly Weather Review*, **131**: 1173-1188.
- Chen, J.M. and Wang, F.J. 2000. The long-term variability of rainfall of Taiwan: The quasi 20-year oscillation of autumn rainfall (in Chinese). *Atmospheric Science*, **28**: 343-362.
- Chen, K.S., Ho, Y.T., Lai, C.H., Tsai, Y.A. and Chen, S.J. 2004. Trends in Concentration of Ground-Level Ozone and Meteorological Conditions during High Ozone Episodes in the Kao-Ping Airshed, Taiwan. *Journal of the Air and Waste Management Association*, **54**: 36-48.
- Chen, L.-X., Dong, M. and Shao, Y.-N. 1992. The characteristics of interannual variations on the East Asian monsoon. *Journal of the Meteorological Society of Japan*, **70**: 397-421.
- Chen, T.-C., Yen, M.-C., Hsieh, J.-C. and Arritt, R.W. 1999. Diurnal and seasonal variations of the rainfall measured by the automatic rainfall and meteorological telemetry system in Taiwan. *Bulletin of the American Meteorological Society*, **80**: 2299-2312.
- Chen, Z.H., Cheng, S.Y., Li, J.B., Guo, X.R., Wang, W.H. and Chen, D.S. 2008. Relationship between atmospheric pollution processes and synoptic pressure patterns in northern China. *Atmospheric Environment*, **42**: 6078-6087.

- Cheng, W.-L. 2001. Synoptic weather patterns and their relationship to high ozone concentrations in the Taichung Basin. *Atmospheric Environment*, **35**: 4971-4994.
- Cheng, W.-L. 2002. Ozone distribution in coastal central Taiwan under sea-breeze conditions. *Atmospheric Environment*, **36**: 3445-3459.
- Cheng, W.-L., Pai, J.-L., Tsuang, B.-J. and Chen, C.-L. 2001. Synoptic patterns in relation to ozone concentrations in west-central Taiwan. *Meteorology and Atmospheric Physics*, **78**: 11-21.
- Chou, C., Tu, J.-Y. and Yu, J.-Y. 2003. Interannual variability of the Western North Pacific summer monsoon: Differences between ENSO and non-ENSO years. *Journal of Climate*, **16**: 2275-2287.
- Chou, C.C.-K., Liu, S.C., Lin, C.-Y., Shiu, C.-J. and Chang, K.-H. 2006. The trend of surface ozone in Taipei, Taiwan, and its causes: Implications for ozone control strategies. *Atmospheric Environment*, **40**: 3898-3908.
- Christensen, J. H., Hewitson, B., Busuioc, A., Chen, A., Gao, X., Held, I., Jones, R., Kolli, R. K., Kwon, W.-T., Laprise, R., Magaña Rueda, V., Mearns, L., Menéndez, C. G., Räisänen, J., Rinke, A., Sarr, A. and Whetton, P. 2007. Regional Climate Projections. In: *Climate Change 2007: The Physical Science Basis: Contribution of Working Group I to the Fourth Assessment Report of the Intergovernmental Panel on Climate Change* [Solomon, S., D. Qin, M. Manning, Z. Chen, M. Marquis, K. M. Averyt, M. Tignor and H. L. Miller (eds)]. Cambridge University Press, Cambridge and New York.
- Collins, W.G. and Gandin, L.S. 1990. Comprehensive Hydrostatic Quality Control at the National Meteorological Center. *Monthly Weather Review*, **118**: 2752-2767.
- Comrie, A.C. 1994. A synoptic climatology of rural ozone pollution at three forest sites in Pennsylvania. *Atmospheric Environment*, **28**: 1601-1614.
- Covey, C., AchutaRao, K.M., Fiorino, M., Glecker, P.J., Taylor, K.E. and Wehner, M.F. 2002. Intercomparison of climate data sets as a measure of observational uncertainty., U.S Department of Energy , Lawrence Livermore National Laboratory. Contract No. W-745-Eng-48.

- Crawford, J.H., Davis, D.D., Chen, G., Bradshaw, J., Sandholm, S., Kondo, Y., Merrill, J., Liu, S., Browell, E., Gregory, G., Anderson, B., Sachse, G., Barrick, J., Blake, D., Talbot, R. and Pueschel, R. 1997. Implications of large scale shifts in tropospheric NO_x levels in the remote tropical Pacific. *Journal of Geophysical Research D: Atmospheres*, **102**: 28447-28468.
- Crutzen, P.J. 1970. The influence of nitrogen oxides on the atmospheric ozone content. *Quarterly Journal of the Royal Meteorological Society*, **96**:320-325
- Crutzen, P.J. 1974. Photochemical reaction initiated by and influencing ozone in unpolluted tropospheric air. *Tellus*, **26**: 45-55.
- Dai, X., Wang, P. and Chou, J. 2003. Multiscale characteristics of the rainy season rainfall and interdecadal decaying of summer monsoon in North China. *Chinese Science Bulletin*, **48**: 2730-2734.
- Daoyi, G. and Shaowu, W. 1999. Long-term variability of the siberian high and the possible connection to global warming. *Acta Geographica Sinica*, **54**: 131-133.
- D'Arrigo, R., Wilson, R., Panagiotopoulos, F. and Wu, B. 2005. On the long-term interannual variability of the east Asian winter monsoon. *Geophysical Research Letters*, **32**: 1-4.
- Davies, T.D., Kelly, P.M., Low, P.S. and Pierce, C.E. 1992. Surface ozone concentrations in Europe: links with the regional- scale atmospheric circulation. *Journal of Geophysical Research*, **97**: 9819-9832.
- Davies, T.D., Kelly, P.M., Brimblecombe, P. and Gair, A.J. 1987. Surface ozone concentrations and climate: Preliminary analysis , in Proceedings of the WMO conference on Air Pollution Modelling and Its Application. WMO/TD 187,2, 348-356, World Meteorol. Org., Geneva.
- Dentener, F., Stevenson, D., Cofala, J., Mechler, R., Amann, M., Bergamaschi, P., Raes, F. and Derwent, R. 2005. The impact of air pollutant and methane emission controls on tropospheric ozone and radiative forcing: CTM calculations for the period 1990-2030. *Atmospheric Chemistry and Physics*, **5**: 1731-1755.

- Derwent, R.G., Collins, W.J., Johnson, C.E. and Stevenson, D.S. 2001. Transient behaviour of tropospheric ozone precursors in a global 3-D CTM and their indirect greenhouse effects. *Climatic Change*, **49**: 463-487.
- Derwent, R.G., Stevenson, D.S., Collins, W.J. and Johnson, C.E. 2004. Intercontinental transport and the origins of the ozone observed at surface sites in Europe. *Atmospheric Environment*, **38**: 1891-1901
- Dessouky, T. M. and Jenkinson, A. F. 1975. An objective daily catalogue of surface pressure, flow and vorticity indices for Egypt and it's use in monthly rainfall forecasting. *Meteorological Research Bulletin, Egypt*, **11**, 1-25.
- Ding, Y. and Krishnamurti, T.N. 1987. Heat Budget of the Siberian High and the Winter Monsoon. *Monthly Weather Review*, **115**: 2428-2449.
- Draxler, R.R. 1991. The accuracy of trajectories during ANATEX calculated using dynamic model analysis versus rawinsonde observations. *Journal Applied Meteorology*. **30**: 1447-1467.
- Draxler, R.R. 1996. Boundary layer isentropic and kinematic trajectories during the August 1993 North Atlantic Regional Experiment Intensive. *Journal of Geophysical Research D: Atmospheres*, **101**: 29,255-29,268.
- Draxler, R.R. and Hess, G.D. 1997. Description of The HYSPLIT_4 Modeling System. *NOAA Technical Memorandum ERL ARL-224*.
- Draxler, R.R. and Hess, G.D. 1998. An Overview of the Hysplit-4 Modeling System for Trajectories, Dispersion, and Deposition. *Australian Meteorological Magazine*, **47**: 2458.
- Draxler, R.R. and Rolph, G.D., 2010. HYSPLIT (HYbrid Single-Particle Lagrangian Integrated Trajectory) Model access via NOAA ARL READY Website (<http://ready.arl.noaa.gov/HYSPLIT.php>). *NOAA Air Resources Laboratory*, Silver Spring, MD.
- Dueas, C., Fernández, M.C., Caete, S., Carretero, J. and Liger, E. 2002. Assessment of ozone variations and meteorological effects in an urban area in the Mediterranean Coast. *Science of the Total Environment*, **299**: 97-113.

- Dutton, J.A. 1976. *The ceaseless wind: an introduction to the theory of atmospheric motion*. McGraw-Hill, New York.
- Eck, T.F., Holben, B.N., Dubovik, O., Smirnov, A., Goloub, P., Chen, H.B., Chatenet, B., Gomes, L., Zhang, X.-Y., Tsay, S.-C., Ji, Q., Giles, D. and Slutsker, I. 2005. Columnar aerosol optical properties at AERONET sites in central eastern Asia and aerosol transport to the tropical mid-Pacific. *Journal of Geophysical Research D: Atmospheres*, **110**: 1-18.
- Ehhalt, D. H. 2001. Tropospheric ozone, chemistry and man-induced trends. *Ozone: Science and Engineering*, **23**: 445-453.
- Ehhalt, D. H., Rohrer, F. and Wahner, A. 1992. Sources and distribution of NO_x in the upper troposphere at northern mid-latitudes. *Journal of Geophysical Research*, **97**: 3725-3738.
- El-Kadi, A.K.A. and Smithson, P.A. 1992. Atmospheric classifications and synoptic climatology. *Progress in Physical Geography*, **16**: 432-455.
- EPA Taiwan 2001. The annual assessment report of the air pollution control for 2001 (in Chinese).
- EPA Taiwan 2002. The annual assessment report of the air pollution control for 2002 (in Chinese).
- EPA Taiwan 2004. The annual assessment report of the air pollution control for 2004 (in Chinese).
- EPA Taiwan 2005. The annual assessment report of the air pollution control for 2005 (in Chinese).
- EPA Taiwan 2006. The annual assessment report of the air pollution control for 2006 (in Chinese).
- Erukhimova, T. and Bowman, K.P. 2006. Role of convection in global-scale transport in the troposphere. *Journal of Geophysical Research D: Atmospheres*, **111**: Art. No.: D03105.

- Fiala, J., Cernikovsky, L., de Leeuw, F. and Kurfuerst, P. 2003. EEA Technical Report : Air pollution by ozone in Europe in summer 2003. European Environment Agency.
- Finlayson-Pitts, B.J. and Pitts, J.J.N. 2000. *Chemistry of the Upper and Lower atmosphere*. Academic Press, London.
- Fiore, A.M., Jacob, D.J., Logan, J.A. and Yin, J.H. 1998. Long-term trends in ground level ozone over the contiguous United States, 1980-1995. *Journal of Geophysical Research D: Atmospheres*, **103**: 1471-1480.
- Fuelberg, H.E., Kiley, C.M., Hannan, J.R., Westberg, D.J., Avery, M.A. and Newell, R.E. 2003. Meteorological conditions and transport pathways during the Transport and Chemical Evolution over the Pacific (TRACE-P) experiment. *Journal of Geophysical Research D: Atmospheres*, **108**: Art. No.: 8782.
- Glantz, M.H. 2002. *La Niña: An overview of the process. La Niña and Its Impacts: Facts and Speculations*. United Nations University Press, New York.
- Gandin, L.S. 1988. Complex quality control of meteorological observations. *Monthly Weather Review*, **116**: 1137-1156.
- Gong, D.-Y. and Ho, C.-H. 2002. The Siberian High and climate change over middle to high latitude Asia. *Theoretical and Applied Climatology*, **72**: 1-9.
- Gong, D.-Y., Wang, S.-W. and Zhu, J.-H. 2001. East Asian winter monsoon and Arctic Oscillation. *Geophysical Research Letters*, **28**: 2073-2076.
- Goodess, C.M. and Jones, P.D. 2002. Links between circulation and changes in the characteristics of Iberian rainfall. *International Journal of Climatology*, **22**: 1593-1615.
- Goodess, C.M. and Palutikof, J.P. 1998. Development of daily rainfall scenarios for southeast Spain using a circulation-type approach to downscaling. *International Journal of Climatology*, **18**: 1051-1083.

Gros, V., Long-term evolution of ozone at the mid-latitudes of the Northern Hemisphere [online]. Available: <http://www.atmosphere.mpg.de/enid/23a.html> [accessed January 2007]

Guicherit, R. and Roemer, M. 2000. Tropospheric ozone trends. *Chemosphere - Global Change Science*, **2**: 167-183.

Guo, Q., Cai, J., Shao, X. and Sha, W. 2003. Interdecadal variability of East-Asian summer monsoon and its impact on the climate of China. *Acta Geographica Sinica*, **58**: 576-582.

Harris, J.M., Draxler, R.R. and Oltmans, S.J. 2005. Trajectory model sensitivity to differences in input data and vertical transport method. *Journal of Geophysical Research D: Atmospheres*, **110**: 1-8.

Hauglustaine, D.A., Brasseur, G.P., Walters, S., Rasch, P.J., Muller, J.-F., Emmons, L.K. and Carroll, M.A. 1998. MOZART, a global chemical transport model for ozone and related chemical tracers 2. Model results and evaluation. *Journal of Geophysical Research D: Atmospheres*, **103**: 28,291-28,335.

Heald, C.L., Jacob, D.J., Fiore, A.M., Emmons, L.K., Gille, J.C., Deeter, M.N., Warner, J., Edwards, D.P., Crawford, J.H., Hamlin, A.J., Sachse, G.W., Browell, E.V., Avery, M.A., Vay, S.A., Westberg, D.J., Blake, D.R., Singh, H.B., Sandholm, S.T., Talbot, R.W. and Fuelberg, H.E. 2003. Asian outflow and trans-Pacific transport of carbon monoxide and ozone pollution: An integrated satellite, aircraft, and model perspective. *Journal of Geophysical Research D: Atmospheres*, **108**: ACH 25-1 - ACH 25-13.

Hoell, J.M., Davis, D.D., Liu, S.C., Newell, R., Shipham, M., Akimoto, H., McNeal, R.J., Bendura, R.J. and Drewry, J.W. 1996. Pacific Exploratory Mission-West A (PEM-West A): September-October 1991. *Journal of Geophysical Research D: Atmospheres*, **101**: 1641-1653.

Holland, M., Mills, G., Hayes, F., Buse, A., Emberson, L., Cambridge, H., Cinderby, S., Terry, A. and Ashmore, M. 2002. Economic Assessment of Crop Yield Losses from Ozone Exposure. The UNECE International Cooperative Programme on Vegetation. 1-25

Holland, M. and King, K. 1998. Economic Evaluation of Air Quality Targets for Tropospheric Ozone, Part C:Economic Benefit Assessment.

Hsu, H.-H. and Chen, C.-T. 2002. Observed and projected climate change in Taiwan. *Meteorology and Atmospheric Physics*, **79**: 87-104.

Hsu, K.-J. 2007. Relationships between ten-year trends of tropospheric ozone and temperature over Taiwan. *Science of the Total Environment*, **374**: 135-142.

Hsu, S.-C., Liu, S. C., Huang, Y.-T., Lung, S.-C. C., Tsai, F., Tu, J.-Y. and Kao, S.-J. 2008. A criterion for identifying Asian dust events based on Al concentration data collected from northern Taiwan between 2002 and early 2007. *Journal of Geophysical Research D: Atmospheres*, **113**.

Hu, Z.-Z., Bengtsson, L. and Arpe, K. 2000. Impact of global warming on the Asian winter monsoon in a coupled GCM. *Journal of Geophysical Research D: Atmospheres*, **105**: 4607-4624.

Huang, J., Minnis, P., Lin, B., Wang, T., Yi, Y., Hu, Y., Sun-Mack, S. and Ayers, K. 2006. Possible influences of Asian dust aerosols on cloud properties and radiative forcing observed from MODIS and CERES. *Geophysical Research Letters*, **33**: Art. No.: L06824.

Huang, J.-P., Fung, J. C. H. and Lau, A. K. H. 2006. Integrated processes analysis and systematic meteorological classification of ozone episodes in Hong Kong. *Journal of Geophysical Research D: Atmospheres*, **111**: Art. No. D20309.

Huang, J.-P., Fung, J. C. H., Lau, A. K. H. and Qin, Y. 2005. Numerical simulation and process analysis of typhoon-related ozone episodes in Hong Kong. *Journal of Geophysical Research D: Atmospheres*, **110**: 1-17.

Huang, R., Chen, J., Zhang, Q. and Yang, B. 2002. The ENSO Cycle in the Tropical Pacific and Its Impact on the Monsoon Rainfall Anomalies in China during 1997-2001 (in Chinese). *Jounal of Geosciences of China*, **4**: 3-4.

Hulme, M., Briffal, K.R., Jones, P.D. and Senior, C.A. 1993. Validation of GCM control simulations using indices of daily airflow types over the British Isles. *Climate Dynamics*, **9**: 95-105.

- Husar, R.B., Tratt, D.M., Schichtel, B.A., Falke, S.R., Li, F., Jaffe, D., Gassó, S., Gill, T., Laulainen, N.S., Lu, F., Reheis, M.C., Chun, Y., Westphal, D., Holben, B.N., Gueymard, C., McKendry, I., Kuring, N., Feldman, G.C., McClain, C., Frouin, R.J., Merrill, J., DuBois, D., Vignola, F., Murayama, T., Nickovic, S., Wilson, W.E., Sassen, K., Sugimoto, N. and Malm, W.C. 2001. Asian dust events of April 1998. *Journal of Geophysical Research D: Atmospheres*, **106**: 18,317-18,330.
- Inoue, T. and Matsumoto, J. 2004. A comparison of summer sea level pressure over East Eurasia between NCEP-NCAR reanalysis and ERA-40 for the period 1960-99. *Journal of the Meteorological Society of Japan*, **82**: 951-958.
- Jacob, D.J., Crawford, J.H., Kleb, M.M., Connors, V.S., Bendura, R.J., Raper, J.L., Sachse, G.W., Gille, J.C., Emmons, L. and Heald, C.L. 2003. Transport and Chemical Evolution over the Pacific (TRACE-P) aircraft mission: Design, execution, and first results. *Journal of Geophysical Research D: Atmospheres*, **108**: Art. No. 8781.
- Jenkinson, A.F. and Collison, F.P. 1977. An Initial Climatology of Gales over the North Sea. *Synoptic Climatology Branch Memorandum*, **62**: 18.
- Jhun, J.-G. and Lee, E.-J. 2004. A new East Asian winter monsoon index and associated characteristics of the winter monsoon. *Journal of Climate*, **17**: 711-726.
- Jiang, D., Wang, H. and Lang, X. 2005. Evaluation of East Asian climatology as simulated by seven coupled models. *Advances in Atmospheric Sciences*, **22**: 479-495.
- Jiang, Z., Chen, G.T.-J. and Wu, M.-C. 2003. Large-scale circulation patterns associated with heavy spring rain events over Taiwan in strong ENSO and Non-ENSO years. *Monthly Weather Review*, **131**: 1769-1782.
- Jones, P.D. and Kelly, P.M. 1982. Principal component analysis of the Lamb Catalogue of daily weather types. Part 1: annual frequencies. *Journal of Climatology*, **2**: 147-157.

- Jones, P.D., Hulme, M. and Briffa, K.R. 1993. A comparison of Lamb circulation types with an objective classification scheme. *International Journal of Climatology*, **13**: 655-663.
- Ju, J., Lü J., Cao, J. and Ren, J. 2005. Possible impacts of the Arctic Oscillation on the interdecadal variation of summer monsoon rainfall in East Asia. *Advances in Atmospheric Sciences*, **22**: 39-48.
- Kalnay, E., Kanamitsu, M., Kistler, R., Collins, W., Deaven, D., Gandin, L., Iredell, M., Saha, S., White, G., Woollen, J., Zhu, Y., Chelliah, M., Ebisuzaki, W., Higgins, W., Janowiak, J., Mo, K.C., Ropelewski, C., Wang, J., Leetmaa, A., Reynolds, R., Jenne, R. and Joseph, D. 1996. The NCEP/NCAR 40-year reanalysis project. *Bulletin of the American Meteorological Society*, **77**: 437-471.
- Kimoto, M. 2005. Simulated change of the east Asian circulation under global warming scenario. *Geophysical Research Letters*, **32**: 1-5.
- Kistler, R., Kalnay, E., Collins, W., Saha, S., White, G., Woollen, J., Chelliah, M., Ebisuzaki, W., Kanamitsu, M., Kousky, V., Van Den Dool, H., Jenne, R. and Fiorino, M. 2001. The NCEP-NCAR 50-year reanalysis: Monthly means CD-ROM and documentation. *Bulletin of the American Meteorological Society*, **82**: 247-267.
- Kley, D., Geiss, H. and Mohnen, V.A. 1994. Tropospheric ozone at elevated sites and precursor emissions in the United States and Europe. *Atmospheric Environment - Part A General Topics*, **28**: 149-158.
- Kleiman, G. and Marin, A. 2002. Trajectory Analysis of Potential Source Regions Affecting Class I Areas in the MANE-VU Region. *Technical Memorandum*.
- Knap, A.H. 1989. The long-range atmospheric transport of natural and contaminant substances. Proceedings of a NATO advanced research workshop, St. Georges, January, 1988.
- Krupa, S., McGrath, M.T., Andersen, C.P., Booker, F.L., Burkey, K.O., Chappelka, A.H., Chevone, B.I., Pell, E.J. and Zilinskas, B.A. 2001. Ambient ozone and plant health. *Plant Disease*, **85**: 4-12.

- Kuo, N.-J. and Ho, C.-R. 2004. ENSO effect on the sea surface wind and sea surface temperature in the Taiwan Strait. *Geophysical Research Letters*, **31**: L13309 1-4.
- Kurosaki, Y. and Mikami, M. 2003. Recent frequent dust events and their relation to surface wind in East Asia. *Geophysical Research Letters*, **30**: ASC 2-1 - 2-4.
- Lam, K.S., Wang, T.J., Wang, T., Tang, J., Kajii, Y., Liu, C.M. and Shim, S.G. 2004. Overview of surface ozone variability in East Asia-North Pacific region during IGAC/APARE (1994-1996). *Journal of Environmental Sciences*, **16**: 599-609.
- Lamb, H.H. 1950. Types and spells of weather around the year in the British Isles. *Quarterly Journal of the Royal Meteorological Society*, **76**: 393-438.
- Lamb, H.H. 1972. British Isles weather types and a register of the daily sequence of circulation patterns, 1861-1971. *Geophysical Memoir*, **116**: 85.
- Lee, S., Akimoto, H., Nakane, H., Kurnosenko, S. and Kinjo, Y. 1998. Lower tropospheric ozone trend observed in 1989-1997 at Okinawa, Japan. *Geophysical Research Letters*, **25**: 1637-1640.
- Lee, S.L., Wong, W.H.S. and Lau, Y.L. 2006. Association between air pollution and asthma admission among children in Hong Kong. *Clinical and Experimental Allergy*, **36**: 1138-1146.
- Lelieveld, J., Van Aardenne, J., Fischer, H., De Reus, M., Williams, J. and Winkler, P. 2004. Increasing ozone over the Atlantic Ocean. *Science*, **304**: 1483-1487.
- Lelieveld, J. and Dentener, F.J. 2000. What controls tropospheric ozone? *Journal of Geophysical Research D: Atmospheres*, **105**: 3531-3551.
- Lennartson, G.J. and Schwartz, M.D. 1999. A synoptic climatology of surface-level ozone in Eastern Wisconsin, USA. *Climate Research*, **13**: 207-220.
- Levy II, H., Mahlman, J.D., Moxim, W.J. and Liu, S.C. 1985. Tropospheric ozone: the role of transport. *Journal of Geophysical Research*, **90**: 3753-3772.

- Liang, J., Yang, S., Li, C. and Li, X. 2007. Long-term changes in the South China Sea summer monsoon revealed by station observations of the Xisha Islands. *Journal of Geophysical Research D: Atmospheres*, **112**: Art. No. D10104.
- Lin, C.-Y., Liu, S.C., Chou, C.C.-K., Huang, S.-J., Liu, C.-M., Kuo, C.-H. and Young, C.-Y. 2005. Long-range transport of aerosols and their impact on the air quality of Taiwan. *Atmospheric Environment*, **39**: 6066-6076.
- Lin, C.-Y., Liu, S.C., Chou, C. C.-K., Liu, T.H., Lee, C.-T., Yuan, C.-S., Shiu, C.-J. and Young, C.-Y. 2004. Long-range transport of Asian dust and air pollutants to Taiwan. *Terrestrial, Atmospheric and Oceanic Sciences*, **15**: 759-784.
- Lin, C.-Y., Wang, Z., Chen, W.-N., Chang, S.-Y., Chou, C.C.K., Sugimoto, N. and Zhao, X. 2007. Long-range transport of Asian dust and air pollutants to Taiwan: Observed evidence and model simulation. *Atmospheric Chemistry and Physics*, **7**: 423-434.
- Lin, J.-L., Weickman, K. M., Kiladis, G. N., Mapes, B. E., Schubert, S. D., Suarez, M. J., Bacmeister, J. T. and Lee, M.-I. 2008. Subseasonal variability associated with Asian summer monsoon simulated by 14 IPCC AR4 coupled GCMs. *Journal of Climate*, **21**: 4541-4567.
- Lin, T.-H. 2001. Long-range transport of yellow sand to Taiwan in Spring 2000: Observed evidence and simulation. *Atmospheric Environment*, **35**: 5873-5882.
- Liu, C.-M., Buhr, M. and Merrill, J.T. 1997. Ground-based observation of ozone, carbon monoxide, and sulfur dioxide at Kenting, Taiwan, during the PEM-West B campaign. *Journal of Geophysical Research D: Atmospheres*, **102**: 28,613-28,625.
- Liu, C.-M., Huang, C.-Y., Shieh, S.-L. and Wu, C.-C. 1994. Important meteorological parameters for ozone episodes experienced in the Taipei Basin. *Atmospheric Environment - Part A General Topics*, **28**: 159-173.
- Liu, C.-M., Young, C.-Y. and Lee, Y.-C. 2006. Influence of Asian dust storms on air quality in Taiwan. *Science of the Total Environment*, **368**: 884-897.

- Liu, H., Jacob, D.J., Bey, I., Yantosca, R.M., Duncan, B.N. and Sachse, G.W. 2003. Transport pathways for Asian pollution outflow over the Pacific: Interannual and seasonal variations. *Journal of Geophysical Research D: Atmospheres*, **108**: GTE 7-1 - 7-18.
- Logan, J.A. 1985. Tropospheric ozone: seasonal behavior, trends, and anthropogenic influence. *Journal of Geophysical Research*, **90**: 10,463-10,482.
- Logan, J.A., Megretskaya, I.A., Miller, A.J., Tiao, G.C., Choi, D., Zhang, L., Stolarski, R.S., Labow, G.J., Hollandsworth, S.M., Bodeker, G.E., Claude, H., De Muer, D., Kerr, J.B., Tarasick, D.W., Oltmans, S.J., Johnson, B., Schmidlin, F., Staehelin, J., Viatte, P. and Uchino, O. 1999. Trends in the vertical distribution of ozone: A comparison of two analyses of ozonesonde data. *Journal of Geophysical Research D: Atmospheres*, **104**: 26,373-26,399.
- Low, P.S., Davies, T.D., Kelly, P.M. and Farmer, G. 1990. Trends in surface ozone at Hohenpeissenberg and Arkona. *Journal of Geophysical Research*, **95**: 22,441-22,453.
- Low, P.S., Kelly, P.M. and Davies, T.D. 1992. Variations in surface ozone trends over Europe. *Geophysical Research Letters*, **19**: 1117-1120.
- Lu, M.M. 2006. The relationship between ENSO and East Asian Monsoon revealed by Taiwan climate variations. 27th Conference on Hurricanes and Tropical Meteorology.
- Lu, R. 2004. Associations among the components of the East Asian summer monsoon system in the meridional direction. *Journal of the Meteorological Society of Japan*, **82**: 155-165.
- Lund, I.A. 1963. Map-pattern classification by statistical methods. *Journal of Applied Meteorology*, **2**: 56-65.
- Luo, C., St John, J.C., Xiuji, Z., Lam, K.S., Wang, T. and Chameides, W.L. 2000. A nonurban ozone air pollution episode over eastern China: Observations and model simulations. *Journal of Geophysical Research D: Atmospheres*, **105**: 1889-1908.

- Marenco, A., Gouget, H., Nedelec, P., Pages, J.-P. and Karcher, F. 1994. Evidence of a long-term increase in tropospheric ozone from Pic du Midi data series: consequences: positive radiative forcing. *Journal of Geophysical Research*, **99**: 16,617-16,632.
- May, W. 2004. Potential future changes in the Indian summer monsoon due to greenhouse warming: Analysis of mechanisms in a global time-slice experiment. *Climate Dynamics*, **22**: 389-414.
- McPhaden, M.J. 1999. Genesis and Evolution of the 1997-98 El Nino. *Science*, **283**: 950.
- Meehl, G. A., Stocker, T. F., Collins, W. D., Friedlingstein, P., Gaye, A. T., Gregory, J. M., Kitoh, A., Knutti, R., Murphy, J. M., Noda, A., Raper, S. C. B., Watterson, I. G., Weaver, A. J. and Zhao, Z.-C. 2007. Global Climate Projections. In: *Climate Change 2007: The Physical Science Basis: Contribution of Working Group I to the Fourth Assessment Report of the Intergovernmental Panel on Climate Change* [Solomon, S., D. Qin, M. Manning, Z. Chen, M. Marquis, K. M. Averyt, M. Tignor and H. L. Miller (eds)]. Cambridge University Press, Cambridge and New York.
- Meleux, F., Solmon, F. and Giorgi, F. 2007. Increase in summer European ozone amounts due to climate change. *Atmospheric Environment*, **41**: 7577-7587.
- Milford, J. B., Gao, D. F., Sillman, S., Blossey, P. and Russell, A. G. 1994. Total Reactive Nitrogen (NOy) as an Indicator of the Sensitivity of Ozone to Reductions in Hydrocarbon and NOx Emissions. *Journal of Geophysical Research-Atmospheres*, **99**: 3533-3542.
- Millán, M., Salvador, R., Mantilla, E. and Artíñano, B. 1996. Meteorology and photochemical air pollution in Southern Europe: Experimental results from EC research projects. *Atmospheric Environment*, **30**: 1909-1924.
- Min, S.-K., Park, E.-H. and Kwon, W.-T. 2004. Future projections of East Asian climate change from multi-AOGCM ensembles of IPCC SRES scenario simulations. *Journal of the Meteorological Society of Japan*, **82**: 1187-1211.

Mitchell, J.M., Dzerdzevskii, B., Flohn, H., Hofmeyr, W.L., Lamb, H.H., Rao, K.N. and Wallen, C.C. 1966. Climate Change. *WMO Technical Note, No. 79*.

Murray, R. and Lewis, R.P.W. 1966. Some aspects of the synoptic climatology of the British Isles as measured by simple indices. *Meteorological Magazine*, **95**: 193-203.

Naja, M. and Akimoto, H. 2004. Contribution of regional pollution and long-range transport to the Asia-Pacific region: Analysis of long-term ozonesonde data over Japan. *Journal of Geophysical Research D: Atmospheres*, **109**: D21306 1-15.

Nakamura, H., Izumi, T. and Sampe, T. 2002. Interannual and decadal modulations recently observed in the Pacific storm track activity and east Asian winter monsoon. *Journal of Climate*, **15**: 1855-1874.

Nolle, M., Ellul, R., Heinrich, G. and Güsten, H. 2002. A long-term study of background ozone concentrations in the central Mediterranean - Diurnal and seasonal variations on the island of Gozo. *Atmospheric Environment*, **36**: 1391-1402.

Nolle, M., Ellul, R., Ventura, F. and Güsten, H. 2005. A study of historical surface ozone measurements (1884-1900) on the island of Gozo in the central Mediterranean. *Atmospheric Environment*, **39**: 5608-5618.

Ogunjobi, K. O., He, Z., Kim, K. W. and Kim, Y. J. 2004. Aerosol optical depth during episodes of Asian dust storms and biomass burning at Kwangju, South Korea. *Atmospheric Environment*, **38**: 1313-1323.

Ohara, T., Akimoto, H., Kurokawa, J., Horii, N., Yamaji, K., Yan, X. and Hayasaka, T. 2007. An Asian emission inventory of anthropogenic emission sources for the period 1980-2020. *Atmospheric Chemistry and Physics*, **7**: 4419-4444.

Oltmans, S.J. 1981. Surface ozone measurements in clean air. *Journal of Geophysical Research*, **86**: 1174-1180.

Oltmans, S.J., Lefohn, A.S., Harris, J.M., Galbally, I., Scheel, H.E., Bodeker, G., Brunke, E., Claude, H., Tarasick, D., Johnson, B.J., Simmonds, P., Shadwick, D., Anlauf, K., Hayden, K., Schmidlin, F., Fujimoto, T., Akagi, K., Meyer, C., Nichol, S., Davies, J., Redondas, A. and Cuevas, E. 2006. Long-term changes in tropospheric ozone. *Atmospheric Environment*, **40**: 3156-3173.

Oltmans, S.J., Johnson, B.J., Harris, J.M., Thompson, A.M., Liu, H.Y., Chan, C.Y., Vömel, H., Fujimoto, T., Brackett, V.G., Chang, W. L., Chen, J.-P., Kim, J.H., Chan, L.Y. and Chang, H.-W. 2004. Tropospheric ozone over the North Pacific from ozonesonde observations. *Journal of Geophysical Research D: Atmospheres*, **109**: D15S01 1-26.

Oltmans, S.J. and Levy II, H. 1994. Surface ozone measurements from a global network. *Atmospheric Environment - Part A General Topics*, **28**: 9-24.

Overpeck, J., Anderson, D., Trumbore, S. and Prell, W. 1996. The southwest Indian Monsoon over the last 18000 years. *Climate Dynamics*, **12**: 213-225.

Panagiotopoulos, F., Shahgedanova, M., Hannachi, A. and Stephenson, D.B. 2005. Observed trends and teleconnections of the Siberian high: A recently declining center of action. *Journal of Climate*, **18**: 1411-1422.

Prather, M., Ehhalt, D., Dentener, F., Derwent, R., Dlugokencky, E., Holland, E., Isaksen, I., Katima, J., Kitchhoff, V., Matson, P., Midgley, P. and Wang, M. 2001. Atmospheric Chemistry and Greenhouse Gases. In: *Climate Change 2001: The Scientific Basis. Contribution of Working Group I to the Third Assessment Report of the Intergovernmental Panel on Climate Change*. Cambridge University Press, Cambridge, United Kingdom and New York, NY, USA.

Penkett, S.A., Kasibhatla, P., Cox, T. and Law, K.S. 2003. "Atmospheric photooxidants." *Atmospheric chemistry in a changing world: an integration and synthesis of a decade of tropospheric chemistry research*. Brasseur, G.P., Prinn, R.G. and Pszenny, A.A.P. Springer, New York

Pierce, R.B., Al-Saadi, J.A., Schaack, T., Lenzen, A., Zapotocny, T., Johnson, D., Kittaka, C., Buker, M., Hitchman, M.H., Tripoli, G., Fairlie, T.D., Olson, J.R., Natarajan, M., Crawford, J., Fishman, J., Avery, M., Browell, E.V., Creilson, J., Kondo, Y. and Sandholm, S.T. 2003. Regional Air Quality Modeling System (RAQMS) predictions of the tropospheric ozone budget over east Asia. *Journal of Geophysical Research D: Atmospheres*, **108**: GTE 46-1 - GTE 46-17.

Pont, V. and Fontan, J. 2000. Local and regional contributions to photochemical atmospheric pollution in southern France. *Atmospheric Environment*, **34**: 5209-5223.

Quartly, G.D., Kyte, E.A., Srokosz, M.A. and Tsimplis, M. N. 2007. An intercomparison of global oceanic precipitation climatologies. *Journal of Geophysical Research D: Atmospheres*, **112**: 1361-1378.

Ramanathan, V., Chung, C., Kim, D., Bettge, T., Buja, L., Kiehl, J.T., Washington, W.M., Fu, Q., Sikka, D.R. and Wild, M. 2005. Atmospheric brown clouds: Impacts on South Asian climate and hydrological cycle. *Proceedings of the National Academy of Sciences of the United States of America*, **102**: 5326-5333.

Randall, D. A., Wood, S., Bony, R., Colman, T., Fichefet, J., Fyfe, V., Kattsov, A., Pitman, J., Shukla, J., Srinivasan, R. J., Stouffer, A., Sumi, A. and Taylor, K. E. 2007. Climate Models and Their Evaluation. In: *Climate Change 2007: The Physical Science Basis: Contribution of Working Group I to the Fourth Assessment Report of the Intergovernmental Panel on Climate Change* [Solomon, S., D. Qin, M. Manning, Z. Chen, M. Marquis, K. M. Averyt, M. Tignor and H. L. Miller (eds)]. Cambridge University Press, Cambridge and New York

Reilly, J., Paltsev, S., Felzer, B., Wang, X., Kicklighter, D., Melillo, J., Prinn, R., Sarofim, M., Sokolov, A. and Wang, C. 2007. Global Economic Effects of Changes in Crops, Pasture, and Forests due to Changing Climate, Carbon Dioxide, and Ozone. MIT Joint Program on the Science and Policy of Global Change. Report No.149

Reilly, J.M., Felzer, B.S., Paltsev, S., Melillo, J.M., Prinn, R.G., Wang, C., Sokolov, A.P. and Wang, X. 2004. The economic impact of climate, CO₂, and tropospheric ozone effects on crop yields in China, the US, and Europe. American Geophysical Union, Fall Meeting.

Richter, A., Burrows, J.P., Nüß, H., Granier, C. and Niemeier, U. 2005. Increase in tropospheric nitrogen dioxide over China observed from space. *Nature*, **437**: 129-132.

Rossow, W.B., Garder, L.C., Lu, P.J. and Walker, A.W. 1991. International satellite cloud climatology project (ISCCP) documentation of cloud data. *WMO/TD*, **No. 266**: 76pp plus appendices.

Sandroni, S. and Anfossi, D. 1994. Historical data of surface ozone at tropical latitudes. *Science of the Total Environment*, **148**: 23-29.

- Sandroni, S., Anfossi, D. and Viarengo, S. 1992. Surface ozone levels at the end of the nineteenth century in South America. *Journal of Geophysical Research*, **97**: 2535-2539.
- Schwarzhoff, P.J. and Reid, P.D. 2000. Classification of meteorological patterns associated with the ozone categories in Kelowna, British Columbia. *Journal of Applied Meteorology*, **39**: 463-470.
- Seinfeld, J.H. and Pandis, S.N. 1998. *Atmospheric Chemistry and Physics: From Air Pollution to Climate Change*. John Wiley & Sons, New York.
- Snyder, B.J. and Strawbridge, K.B. 2004. Meteorological analysis of the Pacific 2001 air quality field study. *Atmospheric Environment*, **38**: 5733-5743.
- Spellman, G. 2000. The use of an index-based regression model for precipitation analysis on the Iberian peninsula. *Theoretical and Applied Climatology*, **66**: 229-239
- Staehelin, J., Thudium, J., Buehler, R., Volz-Thomas, A. and Graber, W. 1994. Trends in surface ozone concentrations at Arosa (Switzerland). *Atmospheric Environment - Part A General Topics*, **28**: 75-87.
- Sterl, A. 2004. On the (in)homogeneity of reanalysis products. *Journal of Climate*, **17**: 3866-3873.
- Stern, A. C. 1968. Classification and Extent of Air Pollution Problems. *Air Pollution, Second Edition*. Academic Press, INC., London.
- Stevenson, D.S., Dentener, F.J., Schultz, M.G., Ellingsen, K., van Noije, T.P.C., Wild, O., Zeng, G., Amann, M., Atherton, C.S., Bell, N., Bergmann, D.J., Bey, I., Butler, T., Cofala, J., Collins, W.J., Derwent, R.G., Doherty, R.M., Drevet, J., Eskes, H.J., Fiore, A.M., Gauss, M., Hauglustaine, D.A., Horowitz, L.W., Isaksen, I.S.A., Krol, M.C., Lamarque, J.-F., Lawrence, M.G., Montanaro, V., Müller, J.-F., Pitari, G., Prather, M.J., Pyle, J.A., Rast, S., Rodriquez, J.M., Sanderson, M.G., Savage, N.H., Shindell, D.T., Strahan, S.E., Sudo, K. and Szopa, S. 2006. Multimodel ensemble simulations of present-day and near-future tropospheric ozone. *Journal of Geophysical Research D: Atmospheres*, **111**: Art. No. D08301.

- Stohl, A. 1998. Computation, accuracy and applications of trajectories - A review and bibliography. *Atmospheric Environment*, **32**: 947-966.
- Stohl, A. 1999. A textbook example of long-range transport: Simultaneous observation of ozone maxima of stratospheric and North American origin in the free troposphere over Europe. *Journal of Geophysical Research D: Atmospheres*, **104**: 30,445-30,462.
- Streets, D.G. and Waldhoff, S.T. 2000. Present and future emissions of air pollutants in China: SO₂, NO(x), and CO. *Atmospheric Environment*, **34**: 363-374.
- Stunder, B.J.B. 1996. An assessment of the quality of forecast trajectories. *Journal of Applied Meteorology*, **35**: 1319-1331.
- Sudo, K. and Takahashi, M. 2001. Simulation of tropospheric ozone changes during 1997-1998 El Niño: Meteorological impact on tropospheric photochemistry. *Geophysical Research Letters*, **28**: 4091-4094.
- Sun, J., Zhang, M. and Liu, T. 2001. Spatial and temporal characteristics of dust storms in China and its surrounding regions, 1960-1999: Relations to source area and climate. *Journal of Geophysical Research D: Atmospheres*, **106**: 10325-10333.
- Sunwoo, Y., Carmichael, G.R. and Ueda, H. 1994. Characteristics of background surface ozone in Japan. *Atmospheric Environment - Part A General Topics*, **28**: 25-37.
- Tanaka, M. 1997. Interannual and interdecadal variations of the Western North Pacific Monsoon and Baiu rainfall and their relationship to the ENSO cycles. *Journal of the Meteorological Society of Japan*, **75**: 1109-1123.
- Tanimoto, H., Furutani, H., Kato, S., Matsumoto, J., Makide, Y. and Akimoto, H. 2002. Seasonal cycles of ozone and oxidized nitrogen species in northeast Asia 1. Impact of regional climatology and photochemistry observed during RISOTTO 1999-2000. *Journal of Geophysical Research D: Atmospheres*, **107**: Art. No. 4747.
- Tie, X., Chandra, S., Ziemke, J.R., Granier, C. and Brasseur, G.P. 2007. Satellite measurements of tropospheric column O₃ and NO₂ in eastern and southeastern asia: Comparison with a global model (MOZART-2). *Journal of Atmospheric Chemistry*, **56**: 105-125.

- Tomás, C., De Pablo, F. and Soriano, L.R. 2004. Circulation weather types and cloud-to-ground flash density over the Iberian Peninsula. *International Journal of Climatology*, **24**: 109-123.
- Tomita, T. and Yasunari, T. 1996. Role of the northeast winter monsoon on the biennial oscillation of the ENSO/monsoon system. *Journal of the Meteorological Society of Japan*, **74**: 399-413.
- Trenberth, K.E. and Guillemot, C.J. 1998. Evaluation of the atmospheric moisture and hydrological cycle in the NCEP/NCAR reanalyses. *Climate Dynamics*, **14**: 213-231.
- Trenberth, K.E. and Paolino, D.A. 1980. The Northern Hemisphere sea level pressure data set -trends, errors and discussions. *Monthly Weather Review*, **108**: 855-872.
- Trenberth, K.E., Stepaniak, D.P., Hurrell, J.W. and Fiorino, M. 2001. Quality of reanalyses in the tropics. *Journal of Climate*, **14**: 1499-1510.
- Trigo, R.M. and DaCamara, C.C. 2000. Circulation weather types and their influence on the precipitation regime in Portugal. *International Journal of Climatology*, **20**: 1559-1581.
- Tsai, S.-S., Goggins, W.B., Chiu, H.-F. and Yang, C.-Y. 2003a. Evidence for an association between air pollution and daily stroke admissions in Kaohsiung, Taiwan. *Stroke*, **34**: 2612-2616.
- Tsai, S.-S., Huang, C.-H., Goggins, W.B., Wu, T.-N. and Yang, C.-Y. 2003b. Relationship between air pollution and daily mortality in a tropical city: Kaohsiung, Taiwan. *Journal of Toxicology and Environmental Health - Part A*, **66**: 1341-1349.
- Tu, J.-Y., Yu, J.Y. and Chou, C. 2003. *Climate in Taiwan (in Chinese)*. Sino cultural enterprise Ltd. Co., Taipei.
- Ueda, H., Iwai, A., Kuwako, K. and Hori, M.E. 2006. Impact of anthropogenic forcing on the Asian summer monsoon as simulated by eight GCMs. *Geophysical Research Letters*, **33**: Art. No.: L06703.

United Nation Development Programme (UNDP) 2009. *Human Development Report*, Palgrave Macmillan, New York.

Vingarzan, R. 2004. A review of surface ozone background levels and trends. *Atmospheric Environment*, **38**: 3431-3442.

Volz, A. and Kley, D. 1988. Evaluation of the Montsouris series of ozone measurements made in the nineteenth century. *332*: 240-242.

Vukovich, F. M. 1994. Boundary layer ozone variations in the eastern United States and their association with meteorological variations: long-term variations. *Journal of Geophysical Research*, **99**: 16,839-16,850.

Wai, K.M. and Tanner, P.A. 2005. Extreme particulate levels at a Western Pacific Coastal City: The influence of meteorological factors and the contribution of long-range transport. *Journal of Atmospheric Chemistry*, **50**: 103-120.

Wang, B., Wu, R. and Fu, X. 2000. Pacific-East Asian Teleconnection: How Does ENSO Affect East Asian Climate? *Journal of Climate*, **13**: 1517.

Wang, K.-Y. 2005. A 9-year climatology of airstreams in East Asia and implications for the transport of pollutants and downstream impacts. *Journal of Geophysical Research D: Atmospheres*, **110**: 1-21.

Wang, T., Cheung, V.T.F., Anson, M. and Li, Y.S. 2001. Ozone and related gaseous pollutants in the boundary layer of eastern China: Overview of the recent measurements at a rural site. *Geophysical Research Letters*, **28**: 2373-2376.

Wang, X., Huang, J., Ji, M. and Higuchi, K. 2008. Variability of East Asia dust events and their long-term trend. *Atmospheric Environment*, **42**: 3156-3165.

Wang, X. and Mauzerall, D.L. 2004. Characterizing distributions of surface ozone and its impact on grain production in China, Japan and South Korea: 1990 and 2020. *Atmospheric Environment*, **38**: 4383-4402.

Watanabe, M. and Nitta, T. 1999. Decadal changes in the atmospheric circulation and associated surface climate variations in the Northern Hemisphere winter. *Journal of Climate*, **12**: 494-510.

- Wayne, R.P. 2000. *Chemistry of Atmospheres*. Oxford University Press, Oxford.
- Wild, O. and Akimoto, H. 2001. Intercontinental transport of ozone and its precursors in a three-dimensional global CTM. *Journal of Geophysical Research D: Atmospheres*, **106**: 27,729-27,744.
- Wild, O., Prather, M.J., Akimoto, H., Sundet, J.K., Isaksen, I.S.A., Crawford, J.H., Davis, D.D., Avery, M.A., Kondo, Y., Sachse, G.W. and Sandholm, S.T. 2004. Chemical transport model ozone simulations for spring 2001 over the western Pacific: Regional ozone production and its global impacts. *Journal of Geophysical Research D: Atmospheres*, **109**: D15S02 1-14.
- Woollen, J.S., Gandin, L., Collins, W., Saha, S., Kistler, R., Kanamitsu, M. and Chelliah, M. 1994. Quality control in the reanalysis system, Perprints, 10th Conference on Numerical Weather Prediction13 -14, Portland, OR, American Meteorological Society.
- World Health Organization (WHO), Regional Office for Europe. 2003. Health aspects of air pollution with particulate matter, ozone and nitrogen dioxide. *Copenhagen: Report of a WHO Working Group, Bonn, Germany 13-15 January*.
- Wu, B. and Wang, J. 2002. Winter Arctic Oscillation, Siberian High and East Asian Winter Monsoon. *Geophysical Research Letters*, **29**: 3-1.
- Wu, M.C. and Chan, J.C.L. 2005. Observational relationships between summer and winter monsoons over East Asia. Part II: Results. *International Journal of Climatology*, **25**: 453-468.
- Wu, M.C. and Chen, Y.L. 1993. The classification of the climate in Taiwan.(in Chinese). *Atmospheric Sciences*, **21**: 55-66.
- Xie, P. and Arkin, P.A. 1996. Analyses of global monthly precipitation using gauge observations, satellite estimates, and numerical model predictions. *Journal of Climate*, **9**: 840-858.
- Xie, S., Yu, T., Zhang, Y., Zeng, L., Qi, L. and Tang, X. 2005. Characteristics of PM10, SO₂, NO_x and O₃ in ambient air during the dust storm period in Beijing. *Science of the Total Environment*, **345**: 153-164.

- Yamaji, K., Ohara, T., Uno, I., Tanimoto, H., Kurokawa, J.-i. and Akimoto, H. 2006. Analysis of the seasonal variation of ozone in the boundary layer in East Asia using the Community Multi-scale Air Quality model: What controls surface ozone levels over Japan? *Atmospheric Environment*, **40**: 1856-1868.
- Yang, K.-L., Ting, C.-C., Wang, J.-L., Wingenter, O. W. and Chan, C.-C. 2005. Diurnal and seasonal cycles of ozone precursors observed from continuous measurement at an urban site in Taiwan. *Atmospheric Environment*, **39**: 3221-3230.
- Yang, S., Lau, K.-M. and Kim, K.-M. 2002. Variations of the East Asian jet stream and Asian-Pacific-American winter climate anomalies. *Journal of Climate*, **15**: 306-325.
- Yarnal, B. 1984. The effect of weather map scale on the results of a synoptic climatology. *Journal of Climatology*, **4**, 481.
- Yarnal, B. 1985. A 500 mb synoptic climatology of pacific north-west coast winters in relation to climatic variability, 1948-1949 to 1977-1978. *International Journal of Climatology*, **5**: 237-252.
- Yarnal, B. and White, D.A. 1987. Subjectivity in a computer-assisted synoptic climatology I: classification results. *Journal of Climatology*, **7**: 119-128.
- Yeh, H.-C. and Chen, Y.-L. 1998. Characteristics of rainfall distributions over Taiwan during the Taiwan area mesoscale experiment (TAMEX). *Journal of Applied Meteorology*, **37**: 1457-1469.
- Yen, M.-C. and Chen, T.-C. 2000. Seasonal variation of the rainfall over Taiwan. *International Journal of Climatology*, **20**: 803-809.
- Yim, S.-Y., Yeh, S.-W., Wu, R. and Jhun, J.-G. 2008. The Influence of ENSO on Decadal Variations in the Relationship between the East Asian and Western North Pacific Summer Monsoons. *Journal of Climate*, **21**: 3165-3179.
- Yu, T.-Y. and Chang, I.-C. 2006. Spatiotemporal features of severe air pollution in Northern Taiwan. *Environmental Science and Pollution Research*, **13**: 268-275.

- Zhang, R., Sumi, A. and Kimoto, M. 1996. Impact of El Niño on the East Asian Monsoon: A diagnostic study of the '86/87 and '91/92 events. *Journal of the Meteorological Society of Japan*, **74**: 49-62
- Zhang, Y., Huang, W., London, S.J., Song, G., Chen, G., Jiang, L., Zhao, N., Chen, B. and Kan, H. 2006. Ozone and daily mortality in Shanghai, China. *Environmental Health Perspectives*, **114**: 1227-1232.
- Zhao, P., Chen, L., Zhou, X., Gong, Y. and Han, Y. 2003. Modeling the East Asian climate during the last glacial maximum. *Science in China, Series D: Earth Sciences*, **46**: 1060-1068.
- Ziemke, J. R. and Chandra, S. 1999. Seasonal and interannual variabilities in tropical tropospheric ozone. *Journal of Geophysical Research D: Atmospheres*, **104**: 21,425-21,442.

Appendix

1. The calculation of the flow and vorticity parameters for the grid is shown for the regional area:

- westerly flow (W): the westerly component of geostrophic surface wind calculated from the pressure gradient between 13.75° N and 33.75° N;
- southerly flow (S): the southerly component of geostrophic surface wind calculated from the pressure gradient between 110° E and 130° E;
- resultant flow (F): total resultant westerly and southerly flow;
- direction (dir): in degree (0 to 360°) of the resultant surface wind obtained from w and s , the directional category is calculated on a eight-point compass with a resolution of 45° (e.g. NE occurs between 22.5° and 67.5°);
- westerly shear vorticity (ZW): difference of the westerly flow between 3.75° N and 23.75° N minus that between 23.75° N and 43.75° N;
- southerly shear vorticity (ZS): difference of the southerly flow between 23.75° N and 150° E minus that between 23.75° N and 90° E;
- total shear vorticity (Z): the sum of westerly and southerly shear vorticity.

All the indices, listed above, are calculated from the grid-point values using the following equations (adapted from Jenkinson and Collison, 1997; Jones *et al.*, 1993):

$$W = 0.5(12+13)-0.5(4+5) \quad (1)$$

$$S = 1.09 [0.25(5+2x9+13)-0.25(2+2x8+12)] \quad (2)$$

$$F = (S^2 + W^2)^{1/2} \quad (3)$$

$$ZW = 1.72 [0.5(15+16)-0.5(8+9)]-0.73[0.5(8+9)-0.5(1+2)] \quad (4)$$

$$ZS = 0.6 [0.25(6+2x10+14)-0.25(5+2x9+13)-0.25(4+2x8+12)+0.25(3+2x7+11)] \quad (5)$$

$$Z = ZW + ZS \quad (6)$$

2. The list of all ozone pollution days (HOD₃) for the period 1994-2004

YEAR	DAY(dd/mo)	YEAR	DAY(dd/mo)	YEAR	DAY(dd/mo)	YEAR	DAY(dd/mo)
1994	01/10	1999	15/04	2002	28/02	2003	01/06
1995	26/09		27/04		12/03		02/06
1996	20/04		28/04		24/05		04/06
	21/04		29/04		25/05		05/06
	25/04		08/05		26/05		26/09
	12/05		13/05		27/05		04/10
	13/05		14/05		28/05		22/10
	18/05		21/05		29/05		23/10
	29/10		29/05		30/08		27/10
	30/10		31/05		21/09		29/10
1997	24/04		05/06		22/09	2004	06/04
	25/04		24/09		29/09		21/04
	29/05		24/10		30/09		28/04
	12/11		27/10		01/10		29/04
1998	04/04	2000	18/04		02/10		11/05
	18/04		09/05		04/10		05/06
	19/09		18/09		05/10		06/06
	20/09		20/09		09/10		12/06
	22/09	2001	23/03		10/10		13/06
	23/09		13/05		08/11		30/06
	24/09		24/05		13/11		30/09
	25/09		25/05		17/12		08/10
	27/09		26/05	2003	20/02		09/10
	01/10		04/07		05/04		10/10
	02/10		10/09		09/04		20/10
	03/10		11/09		10/05		21/10
	18/10		05/10		20/05		23/10
	12/11		06/10		21/05		02/11
			11/10		26/05		03/11
			12/10		27/05		05/11
	07/04		13/10		30/05		10/11
	08/04		14/10		31/05		20/11